THE ROLE OF SPLEEN TYROSINE KINASE IN GLOMERULONEPHRITIS

A thesis submitted to Imperial College London in candidature for the degree of Doctor of Philosophy by

Stephen McAdoo

June 2014

Renal and Vascular Inflammation Section
Department of Medicine
Imperial College London
Commonwealth Building
Hammersmith Hospital
Du Cane Road
LONDON W12 0NN

ABSTRACT

Spleen tyrosine kinase (SYK) is a non-receptor tyrosine kinase that has an important role in immunoreceptor signalling, including for the B cell receptor and activatory Fc receptors. SYK inhibition has shown efficacy in animal models of non-renal autoimmune disease. The role of SYK in experimental and clinical renal disease, however, is not well defined.

I have studied the effects of SYK inhibition using a specific small molecule inhibitor (R788; fostamatinib) in two distinct experimental models of glomerulonephritis in the rat. In experimental autoimmune glomerulonephritis (EAG; a model of anti-glomerular basement membrane disease), I have shown that SYK inhibition with fostamatinib both prevents and treats established disease. Significant attenuation of humoral autoimmune responses was observed, and ELISpot and flow cytometric analysis suggests that this was due to a direct inhibitory effect on B cell activity, rather than overall B cell survival. In addition, SYK inhibition appeared to inhibit antibody-dependent, Fc receptor-mediated pro-inflammatory responses, particularly within glomerular macrophages, in EAG. In experimental autoimmune vasculitis (EAV; a model of anti-neutrophil cytoplasm antibody [ANCA] associated vasculitis), SYK inhibition was an effective treatment for life-threatening manifestations of disease, including glomerulonephritis and lung haemorrhage.

I have also examined the pattern of SYK expression by immunohistochemistry in clinical renal biopsy specimens from approximately 100 patients with a spectrum of glomerular pathologies. I found that SYK is expressed and activated in proliferative types of glomerulonephritis, and that expression levels correlate with disease activity in anti-GBM disease, ANCA-associated vasculitis, lupus nephritis and IgA nephropathy.

These data suggest that SYK is important in the pathogenesis of proliferative glomerulonephritis. SYK inhibition is an effective treatment strategy for the organ-threatening manifestations of disease in two experimental models, and SYK inhibition therefore warrants further investigation in human renal disease.

Et á quoi bon exécuter des projets, puisque le projet est en lui-même une jouissance suffisante? (What good is it to accomplish projects, when the project itself is enjoyment enough?)

Charles Baudelaire
Le Spleen de Paris, 1862

STATEMENT OF CONTRIBUTION

I, Stephen Paul McAdoo, confirm that this thesis is composed of my own original work. Where work was performed in collaboration with other persons, or where information has been derived from other sources, I confirm that this has been indicated in the thesis.

COPYRIGHT DECLARATION

ACKNOWLEDGEMENTS

I am very grateful to the UK Medical Research Council for awarding the Clinical Research Training Fellowship that enabled me to undertake this project.

I would like to thank Esteban Masuda at Rigel Pharmaceuticals for providing the SYK inhibitors used in these studies, and for his support in abstract and manuscript preparation.

I would like to thank all my colleagues in the renal laboratory at the Hammersmith; for their initial patience and good will in sharing their expertise with a laboratory newcomer, and for the affability and humour that meant coming to the lab each day rarely felt like 'work'. In particular, I would like thank Jenny Smith for teaching me how to handle the 'beasts'; John Reynolds for his advice on many aspects of the EAG work; Gurjeet Bhangal for instruction in the 'dark art' of immunohistochemistry; Anisha Tanna for her collaboration on EAV (and the alarm clock); John McDaid for his work on EAV; John Booth for his assistance in the animal house; Theresa Page for teaching me how to do a proper Western; Will Jackson for his patience on the flow cytometer; and Sharron Stubbs and Anjli Jagpal for generally keeping the show on the road.

Finally, I would like to acknowledge my supervisors, Terry, Fred and Charles, for giving me the opportunity to work on such a strong project, and for their tremendous support and direction throughout.

TABLE OF CONTENTS

LIST OF FIGURES

LIST OF TABLES

LIST OF ABBREVIATIONS

α3(IV)NC1	non-collagenous (NC1) domain of the alpha-3 chain of type IV collagen
AAV	anti-neutrophil cytoplasm antibody-associated vasculitis
ACR	American College Rheumatology
ADP	adenosine diphosphate
AHR	airway hyper-responsiveness
AIDS	acquired immunodeficiency syndrome
ALP	alkaline phosphatase
AML	acute myeloid leukaemia
ANCA	anti-neutrophil cytoplasm antibody
ANOVA	analysis of variance
ASO	antisense oligonucleotides
ATG	anti-thymocyte globulin
ATP	adenosine triphosphate
AUC	area under curve
BCIT-NBT	5-bromo-4-chloro-3-indolyl phosphate/nitro blue tetrazolium
BCR	B cell receptor
bd	twice daily
BLyS	B lymphocyte stimulator
BMDM	bone marrow derived macrophage
BP	blood pressure
BSA	bovine serum albumin
CFA	complete Freund's adjuvant
CIA	collagen antibody-induced arthritis
CLEC	C-type lectin
CLL	chronic lymphocytic leukaemia
C_{max}	peak concentration
CMV	cytomegalovirus
CrCl	creatinine clearance
CRP	C reactive protein
DAB	3,3’-diaminobenzidine
DAP12	DNAX activation protein of 12kDa
DAS	disease activity score
DMARD	disease modifying anti-rheumatic drug
DMEM	Dulbecco’s modified Eagle medium
DMSO	dimethyl sulphoxide
DPIGN	diffuse proliferative post-infectious glomerulonephritis
DTH	delayed-type hypersensitivity
EAG	experimental autoimmune glomerulonephritis
EAV	experimental autoimmune vasculitis
EBV	Epstein Barr virus
EC_{50}	half maximal effective concentration
ECL	enhanced chemiluminescence
eGPA	eosinophilic granulomatosis with polyangiitis

ELISA	enzyme linked immunosorbent assay
ELISpot	enzyme linked immunosorbent spot assay
ESR	erythrocyte sedimentation rate
EULAR	European League Against Rheumatism
Fc	fragment, crystallisable
FcR	Fc receptor
FCS	foetal calf serum
FDA	Food and Drug Administration (USA)
FITC	fluorescein isothiocyanate
Fosta	fostamatinib
GAD	glutamate decarboxylase
GBM	glomerular basement membrane
GCS	glomerular cross section
GEC	glomerular endothelial cell
GN	glomerulonephritis
GPA	granulomatosis with polyangiitis
GWAS	genome wide association study
H&E	haematoxylin and eosin
HBSS	Hank's balanced salt solution
HEK	human embryonic kidney
HEPES	hydroxyethyl piperazineethanesulfonic acid
HLA	human leucocyte antigen
HRP	horse-radish peroxidase
IC_{50}	half maximal inhibitory concentration
IFN	interferon
IHC	immunohistochemistry
IL	interleukin
iMN	idiopathic membranous nephropathy
ITAM	immunoreceptor tyrosine-based activation motif
ITP	idiopathic thrombocytopaenic purpura
IVIG	intravenous immunoglobulin
JNK	c-Jun N-terminal kinase
K_i	inhibition constant
LAMP-2	lysosome-associated membrane protein 2
LAT	linker of activated T cells
LEW	Lewis rat
LH	lung haemorrhage
LMP2A	latent membrane protein 2A
LN	lupus nephritis
LPS	lipopolysaccharide
MAPK	mitogen activated protein kinase
MCD	minimal change disease
MCP-1	monocyte chemoattractant protein 1
M-CSF	macrophage-colony stimulating factor
MFI	mean fluorescence intensity
MHC	major histocompatibility complex

miRNA	micro RNA
MMF	mycophenolate mofetil
MPA	microscopic polyangiitis
MPO	myeloperoxidase
MRI	magnetic resonance imaging
MTT	3-(4,5-dimethylthiazol-2-yl)-2,5 diphenyl tetrazolium bromide
NC1	non-collagenous (NC1) domain
NET	neutrophil extracellular trap
NHL	non-Hodgkin's lymphoma
NK	natural killer
NOD	non-obese diabetic
NTN	nephrotoxic nephritis
NTS	nephrotoxic serum
OCT	optimal cutting temperature
od	once daily
OVA	ovalbumin
PAMP	pathogen-associated molecular pattern
PAS	periodic acid-Schiff
PBS; PBS/T	phosphate buffered saline; PBS-Tween
PE	phycoerythrin
PFA	paraformaldehyde
PI3K	phosphoinositide 3-kinase
PK	pharmacokinetic
PLC	phospholipase C
PRR	pathogen recognition receptor
PR3	proteinase 3
P-SYK	phosphorylated spleen tyrosine kinase
PTLD	post-transplant lymphoproliferative disorder
RA	rheumatoid arthritis
RISC	RNA-induced silencing complex
RNAi	RNA interference
rpm	revolutions per minute
RPMI	Roswell Memorial Park Institute
RTX	rituximab
SCID	severe combined immunodeficiency
SDS-PAGE	sodium dodecylsulphate-polyacramide gel electrophoresis
SH2	Src Homology 2
siRNA	small interfering RNA
SLE	systemic lupus erythematosus
SLP-76	SH2 domain containing leukocyte protein of 76kDa
SYK	spleen tyrosine kinase
$t_{½}$	half life
TBM	thin basement membrane
TBS; TBS/T	Tris-buffered saline; TBS-Tween
TCL1	T cell leukaemia 1
TCR	T cell receptor

TEMED	tetramethylethylenediamine
TLR	toll-like receptor
TMB	3,3’,5,5’-tetramethylbenzidine
TNF-α	tumour necrosis factor alpha
T-SYK	total spleen tyrosine kinase
uPCR	urinary protein:creatinine ratio
UrCl	urea clearance
WBC	white blood cell
WKY	Wistar Kyoto
ZAP-70	ζ-chain-associated protein kinase 70

PRIZES, PUBLICATIONS AND PRESENTATIONS ARISING FROM THIS WORK

PRIZES

Best Poster Selection, Academy of Medical Sciences Spring Meeting 2014

Fokko van der Woude Award, 16th International Vasculitis and ANCA Workshop 2013

Best Oral Presentation Prize, Imperial College Clinical Academic Trainees Event 2013

Highly Commended Poster Selection, Imperial College Graduate School Summer Symposium 2013

Top Oral Abstract by a Trainee selection, American Society of Nephrology 2012

Stewart Cameron Renal Clinical Scientist Prize, Royal Society of Medicine 2012

PUBLICATIONS

Glomerular Spleen Tyrosine Kinase Expression Correlates with Disease Activity and Outcome in Proliferative Glomerulonephritis
SP McAdoo, G Bhangal, HT Cook, CD Pusey, FWK Tam
(under revision)

Spleen Tyrosine Kinase Inhibition Attenuates Autoantibody Production and Reverses Experimental Autoimmune GN
SP McAdoo, J Reynolds, G Bhangal, J Smith, J McDaid, A Tanna, WD Jackson, ES Masuda, HT Cook, CD Pusey, FWK Tam
Journal of the American Society of Nephrology 2014 (in press)

Anti-glomerular basement membrane disease.
SP McAdoo, CD Pusey
Encyclopaedia of Medical Immunology. Springer 2014 (Textbook Chapter; in Press)

SYK Inhibition in Experimental Autoimmune Vasculitis and its Glomerular Expression in ANCA-Associated Vasculitis
SP McAdoo, A Tanna, J McDaid, G Bhangal, ES Masuda, HT Cook, CD Pusey, FWK Tam
The Lancet 2014; S72: 383

Experimental crescentic glomerulonephritis: a new bicongenic rat model
Z D'Souza, SP McAdoo, J Smith, CD Pusey, HT Cook, J Behmoaras, TJ Aitman
Disease models & mechanisms 2013; 6: 1477-86

Novel forms of clinical vasculitis: Anti-GBM vasculitis (Goodpasture's disease)
SP McAdoo, CD Pusey
Presse Medicale 2013; 42: 625-8

Spleen Tyrosine Kinase is important in the production of proinflammatory cytokines and cell proliferation in human mesangial cells following stimulation with IgA1 isolated from IgA nephropathy patients
MJ Kim, JP McDaid, SP McAdoo, J Barratt, K Molyneux, ES Masuda, CD Pusey, FW Tam
Journal of Immunology 2012; 189(7): 3751-8

Spleen Tyrosine Kinase: A Novel Target in Autoimmunity
SP McAdoo, FWK Tam
Immunosuppression. S Kapur (Ed) & MB Portela (Ed). InTech 2012; 41-56

Fostamatinib Disodium
SP McAdoo, F Tam
Drugs of the Future 2011; 36(4): 273-80

Experimental Models of Rapidly Progressive Glomerulonephritis
SP McAdoo, F Tam, C Pusey
Drug Discovery Today: Disease Models 2010; 7(1-2): 43-50

CONFERENCE ABSTRACTS: ORAL COMMUNICATIONS

Treatment of Experimental Autoimmune Vasculitis with a SYK inhibitor

SP McAdoo, A Tanna, J McDaid, G Bhangal, ES Masuda, HT Cook, FWK Tam, CD Pusey.

UK Renal Association Annual Conference 2014

Glomerular Spleen Tyrosine Kinase (SYK) expression correlates with disease activity and outcome in proliferative glomerulonephritis

SP McAdoo, G Bhangal, HT Cook, CD Pusey, FWK Tam.

UK Renal Association Annual Conference 2014

Expression of Spleen Tyrosine Kinase (SYK) in Human ANCA-Associated Glomerulonephritis and Treatment of Experimental Autoimmune Vasculitis with a SYK inhibitor

SP McAdoo, A Tanna, J McDaid, G Bhangal, ES Masuda, HT Cook, FWK Tam, CD Pusey.

European Renal Cell Study Group Meeting 2014

Spleen tyrosine kinase (SYK) inhibition in Experimental Autoimmune Glomerulonephritis (EAG).

SP McAdoo, J Reynolds, J Smith, G Bhangal, J McDaid, E Masuda, T Cook, C Pusey, F Tam.

16th International ANCA and Vasculitis Workshop 2013

SYK inhibition reduces autoantibody production and abrogates crescentic glomerulonephritis and lung haemorrhage in Experimental Autoimmune Glomerulonephritis.

SP McAdoo, J Reynolds, J Smith, G Bhangal, J McDaid, E Masuda, T Cook, C Pusey, F Tam.

American Society of Nephrology Renal Week 2012

SYK inhibition reduces autoantibody production and is an effective treatment for crescentic glomerulonephritis and lung haemorrhage in Experimental Autoimmune Glomerulonephritis.

SP McAdoo, J Reynolds, J Smith, G Bhangal, J McDaid, E Masuda, T Cook, C Pusey, F Tam.

UK Renal Association Annual Conference 2012

CONFERENCE ABSTRACTS: POSTER PRESENTATIONS

Genetic Susceptibility to Experimental Autoimmune Glomerulonephritis

SP McAdoo, Z D'souza, J Behmoaras, FWK Tam, HT Cook and CD Pusey.

American Society of Nephrology Renal Week 2013

Spleen Tyrosine Kinase (SYK) expression correlates with Disease Activity and Outcome in Glomerulonephritis

SP McAdoo, G Bhangal, A Tanna, L Lightstone, HT Cook, CD Pusey and FWK Tam

American Society of Nephrology Renal Week 2013

Spleen Tyrosine Kinase (SYK) expression in Renal Allograft Rejection

SP McAdoo, G Bhangal, J Smith, D Taube, CD Pusey, FWK Tam and HT Cook.

American Society of Nephrology Renal Week 2013

CHAPTER ONE - INTRODUCTION AND BACKGROUND

The glomerulonephritides are a common cause of end-stage renal disease that result in significant morbidity and mortality[1,2]. Whilst they represent a heterogeneous group of clinical diagnoses, it is believed that, in common, they share an immune-mediated mechanism of renal injury, with both innate and adaptive, and cellular and humoral components of the immune system contributing to the pathogenesis of disease[3]. Current treatments rely on the use of non-specific immunosuppression with corticosteroids and often cytotoxic agents, which are not always effective and often associated with significant adverse effects. For this reason, there is a need to identify alternative specific therapies to treat glomerulonephritis. To achieve this we need a greater understanding of the underlying mechanisms of disease.

Spleen tyrosine kinase (SYK) is a non-receptor tyrosine kinase that has an important role in the intracellular signalling pathway for immunoreceptors such as the B cell receptor (BCR) and the Fc receptor (FcR). As such, it has emerged as a potential therapeutic target in autoimmune disease. The potential role of SYK in the pathogenesis of glomerulonephritis, however, is not clearly defined. I have examined the role of SYK in the induction of autoimmune responses and immune-mediated tissue damage in rodent models of anti-glomerular basement membrane (GBM) disease and anti-neutrophil cytoplasm antibody (ANCA) associated vasculitis (AAV). I have also sought to demonstrate the presence of activated SYK in human glomerulonephritis (GN).

SYK has been subject of many original research papers (and several excellent reviews[4-6]) in recent years. In this introductory chapter, I therefore aim to concisely summarise (i) the current understanding of SYK structure and function as it relates to this project, (ii) the details of the SYK inhibitors that I have used, and (iii) the details of the animal models which I have used for *in vivo* studies. Since the majority of this work was in rodent models of anti-

GBM disease and AAV, I have also described he immunologic, pathologic and clinical features of these conditions in detail.

1.1 Spleen tyrosine kinase (SYK)

1.1.1 Discovery of SYK

SYK was identified in the early 1990s in the cytostolic fractions of lysates from porcine spleen and bovine thymus as a 40kDa protein with intrinsic kinase activity[7,8]. This 40kDa protein was subsequently shown to be a fragment, containing only the catalytic domain, of a larger 72kDa protein that was identified from a porcine spleen cDNA library (from whence it gained its name) using oligonucleotides designed according to the partial sequence of the purified 40kDa fragment[9]. The *SYK* gene was subsequently mapped to chromosome 9q22 in humans, and chromosome 13 in mice[10].

To the best of my knowledge, there are no reports of disease causing somatic mutations in *SYK* that result in either immunodeficiency or autoimmunity. Genetic polymorphisms have been reported in association with differences in Toll-like receptor (TLR)-induced cytokine production in neonates, though not with any specific immune diathesis[11]. Epigenetic modifications of the *SYK* gene have been associated, both positively and negatively, with some tumours[12,13], but not with any state of immune deregulation. As alluded to, SYK has been implicated in the pathogenesis of some tumours, and in particular the development of haematological malignancy. Since this project examines the role of SYK in inflammatory and autoimmune disease, I will not, however, discuss the role of SYK in oncogenesis in detail.

1.1.2 Basic structure and function

The SYK molecule has a multi-domain structure (Figure 1A) containing two N-terminal tandem Src Homology 2 (SH2) domains and a C-terminal kinase domain[4]. Interdomains A and B connect the SH2-SH2 and SH2-kinase domains, respectively. At least ten major phosphorylation sites have been identified within the molecule[14] – one located in interdomain A, five within interdomain B, two within the kinase domain, and two near the extreme C-terminus. An alternatively spliced form of SYK - SYKB – lacks a 23 amino acid sequence in interdomain B, and in this respect is similar to ZAP-70, the only other member of the SYK family of kinases. ZAP-70 (ζ-chain-associated protein kinase 70) has approximately 60% overall homology to SYK and its expression appears to be more restricted, in particular to T lymphocytes and natural killer (NK) cells[15].

In the resting state, it is thought that SYK assumes a closed, auto-inhibited structure (Figure 1B), wherein interdomain A and interdomain B bind to the C-terminal kinase domain, preventing its interaction with potential substrates, in what is termed a 'linker-kinase sandwich'[16,17]. Upon activation, structural changes within the molecule result in an open conformation that allows the exposed catalytic kinase domain to interact with downstream targets.

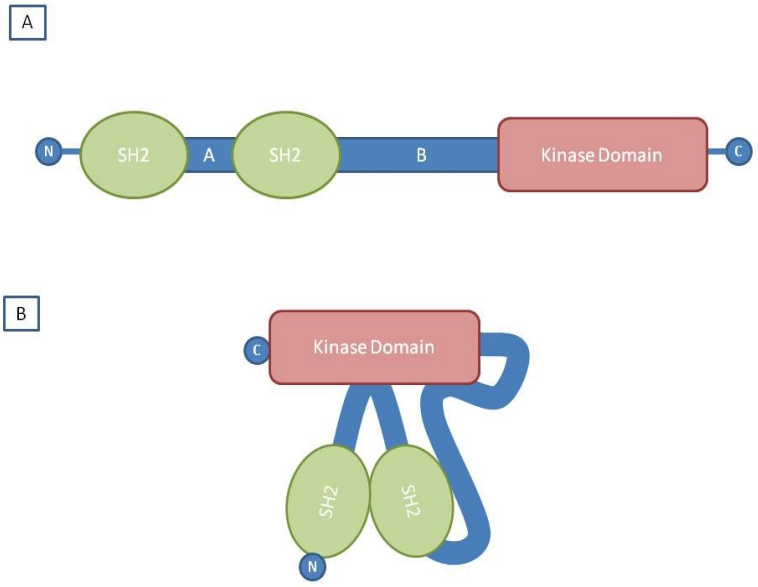

Figure 1.1: Basic Structure of SYK.
(A) Schematic diagram showing the multi-domain structure of SYK, including two N-terminal SH2-domains, a C-terminal kinase domain, and interdomains A and B. (B) Schematic diagram of the 'linker-kinase sandwich' conformation that has been suggested for resting SYK.

The canonical mechanism of SYK activation is via its interaction with immunoreceptor tyrosine-based activation motifs (ITAMs)[18]. ITAMs are short peptide sequences characterised by a consensus sequence that contains two tyrosine residues 6-12 amino acids apart. As their name suggests, they are found in association with the cytoplasmic components of classical immunoreceptors, including the T-cell receptor (TCR), BCR and FcR for immunoglobulins, either as an associated adaptor protein, or within the cytoplasmic region of the receptor itself.

Upon receptor engagement, the tyrosine residues on ITAMs are rapidly phosphorylated, primarily by Lyn and other members of the Src family of kinases (Figure 1.2). The phosphorylated ITAM can now act as a docking site for the SH2 domains of SYK, resulting in conformational changes, exposure of the kinase domain, autophosphorylation and propagation of downstream signalling. In addition, disruption of the 'linker-kinase sandwich' may occur upon phosphorylation of tyrosine residues alone, particularly those within

interdomain B. This may occur by autophosphorylation following ITAM-mediated activation or by transphosphorylation by other kinases, such as Lyn or other Src family kinases that are often co-localised with ITAMs at the cell membrane. As a consequence, positive feedback and sustained SYK activity is possible in the absence of phosphorylated ITAMs. This 'dual' mechanism of activation has recently lead to the proposal of SYK as an 'OR' gate in signalling pathways[19,20]. This may explain why SYKB, which lacks interdomain B, is reported to be less efficient at coupling stimulation of FcR to cellular activation[21].

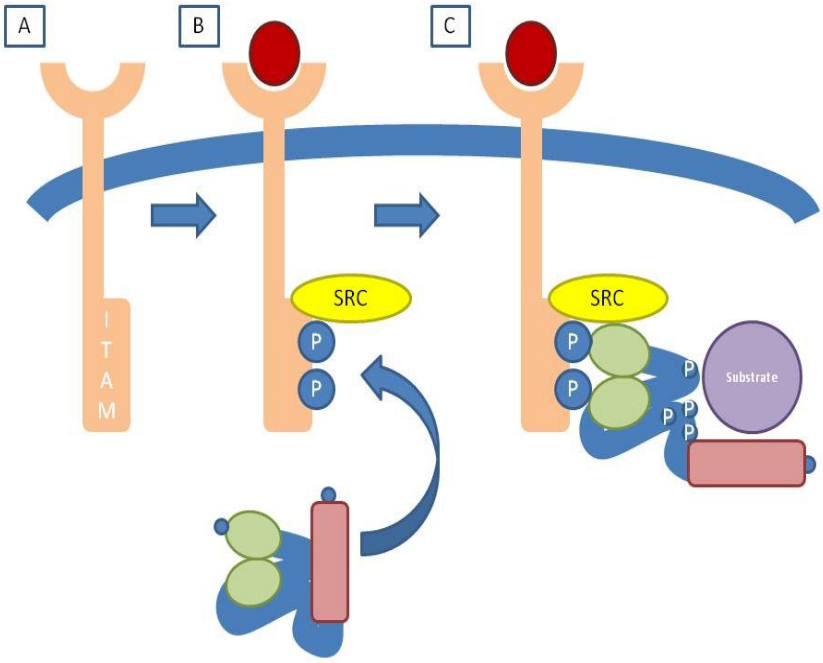

Figure 1.2: SYK activation following interaction with ITAM.
(A) Unengaged receptor bearing non-phosphorylated ITAM motif within its cytoplasmic tail. (B) Upon receptor engagement Src family kinases (SRC) phosphorylate (P) tyrosine residues within the ITAM motif. (C) Phosphorylated ITAM motif acts as a docking site for the SH2 domains of SYK, resulting in conformational changes, auto- and transphosphorylation of tyrosine residues within SYK, thus resulting in activation and phosphorylation of downstream targets.

In addition to releasing the enzymatic domain of the protein from the 'linker-kinase sandwich', these changes in structure and phosphorylation, particularly within the tyrosine-rich interdomain B, create docking sites for downstream targets of SYK, for which it can perform both enzymatic and adaptor functions[17]. These downstream targets include a host of adaptor proteins and other enzyme targets (including LAT, SLP76, Vav1, PLC-γ, PI3K and other MAPK) that are the able to effect complex cellular responses including proliferation, differentiation, phagocytosis and cytokine production[5].

1.1.3 *SYK* knockout

Two groups simultaneously reported the effects of targeted disruption of the *SYK* gene in mice in the mid-90s[22,23]. *SYK* knockout resulted in perinatal death with a severe haemorrhagic phenotype. This was subsequently shown to be due to a failure of communication between developing vasculature and lymphatics during embryogenesis[24]. Analysis of SYK-deficient lymphoid cells derived from these knock-out animals was critical in developing our early understanding of the functional role of SYK in immunoreceptor signalling in various cell types.

Bone marrow chimera animals, reconstituted with haematopoietic stem cells from SYK-deficient mice, showed no reduction in the numbers of circulating erythrocytes, platelets and total leucocytes. These animals had relatively normal reconstitution of T cells, however detailed analysis revealed impaired differentiation of the B cell lineage, with development arrested at the pro-B to pre-B cell stage, consistent with a role for SYK in pre-BCR signalling[22,23]. Subsequent *in vitro* work, using a variety of deficient cell lines, targeted mutagenesis and cell-based reconstitution systems, has defined a clear role for SYK in initiating downstream signalling following engagement of the BCR[25].

Analysis of myeloid cells, such as macrophages and neutrophils, from *SYK* knockout bone marrow chimeras showed ablation of FcR-mediated responses including phagocytosis and the generation of reactive oxygen intermediates[26,27]. The role of SYK in signal transduction for activatory FcR in these and a variety of other cell types is now well established, including mast cells bearing FcεR[28]. A critical role for SYK in FcγR-mediated antigen internalisation and maturation by dendritic cells was also described in these chimeras[29], and is notable given

the important role of dendritic cells in initiating adaptive immune responses. In addition to FcR-mediated responses, SYK has been implicated in integrin signalling in myeloid cells[30,31]. Integrins are transmembrane receptors that have a critical role in cell adhesion and migration, via their interaction with adhesion molecules expressed on other cells, particularly the vascular endothelium. SYK deficient myeloid cells show impaired integrin-mediated responses, thought to be dependent on the association of integrins with ITAM-containing adaptor proteins such as FcRγ-chain and DAP12, as myeloid cells deficient in these adaptor proteins show similar defects.

The first *in vivo* disease model study using bone marrow chimeras generated using SYK deficient progenitor cells was published in 2010, and confirmed that SYK deficiency in the haematopoietic cell compartment conferred resistance to a passively-transferred antibody-dependent model of inflammatory arthritis[32]. A number of targeted genetic techniques have allowed more specific analysis of SYK functions in fully differentiated cells and in *in vivo* models, as well as potential therapeutic targeting of SYK in disease states.

1.1.4 Antisense oligonucleotides (ASO)

ASO are short, single stranded nucleic acid sequences that bind sense mRNA via complementary base-pairing, and thus inhibit the translation of the corresponding protein. ASO directed against SYK have shown activity in a variety of cell types *in vitro*, including inhibitory effects on FcγR-mediated signalling in monocytes[33]. Published *in vivo* studies using *SYK* ASO are limited to animal models of allergic inflammation[34,35]. These have shown that aerosolised *SYK* ASO, delivered in a liposomal complex, suppress SYK expression in, and inflammatory mediator release from, alveolar macrophages. In addition, markers of

pulmonary inflammation were reduced in two distinct animal models. Whilst there have been no *in vivo* studies in autoimmune models, the proposed mechanism of action in these allergic models is via inhibition of activatory FcR-mediated responses, suggesting similar approaches may be effective in autoimmune disease. However, progress in the clinical use of ASO based therapy has been slow since the introduction of Fomivirsen, the first antisense therapy to be licensed by the Food and Drug Administration (FDA), being approved for use in AIDS-related cytomegalovirus (CMV) retinitis over ten years ago. This is due, in part, to the difficulty of producing reliable delivery systems to target the cells, tissues or organs of choice[36] – a not insignificant problem given the multi-system nature of many autoimmune diseases. In addition, there has been concern regarding the specificity of effects exerted by ASO.

1.1.5 RNA interference (RNAi)

RNAi is an innate cellular process that is thought to regulate endogenous gene expression and protect against viral infection. A variety of small RNA molecules, such as endogenous, genetically encoded microRNA (miRNA) or exogenous small interfering RNA (siRNA), may bind target mRNA via Watson-Crick complementary base pairing, and then direct this target mRNA into an RNA-induced silencing complex (RISC), a natural degradation pathway, thus effecting gene silencing prior to translation. Since the first description of RNAi in 1998, advance in the field has been rapid, and there have been promising early phase clinical studies in a number of conditions, including retinal diseases, malignancies and viral infections. The most commonly used technique to harness RNAi for therapy has been to transfect siRNA into target cells. siRNA specific to *SYK*, for example, have been shown to inhibit antibody-mediated phagocytosis by human macrophages[37]. Again, *in vivo* studies in

this field are limited to models of allergic inflammation, and to date are only reported in international patent applications. Aerosolised delivery of *SYK* siRNA, using similar methods as used for ASO delivery, resulted in decreased pulmonary inflammation, as determined by recruitment of cells to broncho-alveolar lavage fluid, in a rat model of ovalbumin-induced asthma. Again, these finding augur well for the translation and use of RNAi in autoimmune disease. As with antisense therapy, outstanding challenges for harnessing RNAi include the development of effective delivery systems, escape of the innate 'interferon' response directed against foreign nucleic acids, and avoidance of 'off-target' gene silencing[38].

1.1.6 Conditional *SYK* knockout

The development of inducible or conditional genetic knockout techniques has allowed more detailed analysis of SYK functions *in vivo*. Two groups, for example, have reported studies in mice harbouring a floxed *SYK* gene and a tamoxifen-inducible Cre recombinase under the control of the ubiquitous Rosa26 promoter[39,40]. Short term *SYK* deletion did not appear to have adverse effects on the well-being of these mice, and they were resistant to mast cell and myeloid cell dependent models of inflammation and allergy. *In vitro* analysis of myeloid cells derived from these mice confirmed attenuation of FcR-mediated responses, but not of FcR-independent processes, such as chemotaxis and migration.

Using a similar system, inducible deletion of *SYK* in B lymphocytes resulted in loss of follicular B cells after a period of 5-8 weeks[41]. Notably, this effect is thought to be mediated by loss of BLyS (B Lymphocyte Stimulator) induced signalling, the authors suggesting that the BLyS receptor recruits the Igα subunit of the BCR as an adaptor protein in a signalling

pathway that activates SYK. To date, there are no other published studies on the role of SYK in mature B cells using targeted genetic techniques.

The collective data suggests, therefore, that SYK is important for B cell maturation beyond the pro-B cells stage and for prolonged follicular B cell survival. *In vitro* data also suggests that SYK is also activated upon BCR ligation, resulting in the activation of downstream intracellular signalling pathways. However, the role of SYK in mature B cell functions *in vivo*, such as antibody production, cytokine production, antigen presentation, and provision of co-stimulation, is not clearly defined.

1.1.7 Pharmacological SYK inhibition

A number of biotechnology and pharmaceutical companies are working to develop compounds to inhibit SYK for use in allergic, autoimmune and haematological disease[6,42,43]. A small number of these compounds have progressed to clinical studies, although to date published results are available for only two such inhibitors, both developed by Rigel Pharmaceuticals – initially R112, and more recently the related compound, R406 (and its respective prodrug, R788; fostamatinib). These are the compounds are discussed in detail in section 1.2.

The majority of the other small molecule inhibitors in development, like R112 and R406, are competitive inhibitors for the ATP binding site of the catalytic domain of SYK, based on the same di-substituted pyrimidine scaffold. Bayer, for example, has developed the imidazo-pyrimidine analogue BAY 61-3606, which inhibits SYK-mediated responses *in vitro* and which has demonstrated efficacy in animal models of allergy *in vivo*[44]. However, the

published selectivity profile is limited to only six other kinases, and comparison with genetic knockdown suggests that BAY 61-3606 may have significant off-target effects[45].

Other groups have chosen to target the non-kinase domains of the SYK molecule. By inhibiting the interaction of the SH2-domains with their docking proteins, it has been proposed that SYK inhibition may be achieved whilst avoiding off-target effects on other kinases, and one such approach has been shown to inhibit IgE-mediated responses *in vitro* and *in vivo*[46]. Whilst the precise molecular mechanism of the inhibitory effects of this molecule are yet to be definitively described, it should be noted that the SH2-domain is a highly conserved motif found in a large number of proteins involved in signal transduction, and targeting this molecule may in turn have diverse off target effects.

1.2 Fostamatinib

Fostamatinib (also referred to as R788) is the orally bioavailable prodrug of R406, an ATP-competitive small molecule SYK inhibitor developed by Rigel Pharmaceuticals.

1.2.1 Pre-clinical pharmacology

Cell based high-throughput screening of small molecules initially identified R112 as a potent inhibitor of SYK activity, as assayed by production and release of inflammatory mediators following FcεR crosslinking by anti-IgE on mast cells[47]. Subsequent characterisation showed that R112 is an ATP-competitive inhibitor of SYK activity – that is, it binds competitively to the ATP binding pocket that is exposed upon SYK activation. Thus, it does not inhibit the phosphorylation of SYK itself; rather it inhibits the activity of phosphorylated SYK on its downstream targets. *In vitro* kinase assays using R112 demonstrated an IC_{50} of 226nmol/l. These assays also showed activity against other kinases such as Lyn (IC_{50} = 300nmol/l) and Lck (IC_{50} =645nmol/l). However, when tested in cell-based assays, R112 was shown to be relatively selective for SYK as determined by phosphorylation of target proteins, despite the similar IC_{50} values in the *in vitro* assays.

Based on R112, Rigel subsequently developed the related compound R406, another competitive inhibitor for ATP binding to the SYK catalytic domain (K_i = 30nM), that inhibits SYK kinase activity *in vitro* with an IC_{50} of 41nM[48]. Selectivity assessments using a panel of over 90 *in vitro* kinase assays showed that R406, whilst relatively specific for SYK, did demonstrate inhibitory activity on other kinases, including Flt3, Lyn (IC_{50} 63nM) and Lck (IC_{50} 37nM)[49]. When tested in cell-based assays, however, R406 inhibited all other kinases

tested at 5- to 100-fold less potency than SYK as judged by phosphorylation of target proteins, despite the similar IC_{50} values on isolated kinase assays.

As expected, R406 inhibits BCR-mediated responses *in vitro*. In primary human B cells, for example, it inhibits CD69 up-regulation in response to anti-IgM with an EC_{50} of 48nM[48]. BCR-mediated signalling has been implicated as an important survival signal in haematological malignancies of B cell origin, and accordingly R406 has shown anti-proliferative and pro-apoptotic activity in a variety of B cell lymphoma and chronic lymphocytic leukaemia (CLL) cell lines and primary tumour cells *in vitro*[50-52]. These effects are most likely due to the effects of inhibited BCR-induced signalling in these cells, although BCR-independent mechanisms such as disrupted chemokine and integrin signalling have also been implicated[53].

R406 has been shown to inhibit FcR-mediated responses (such as degranulation, cytokine production and FcR-mediated antigen internalisation) in a variety of cell types *in vitro*, including mast cells, macrophages, neutrophils and dendritic cells[48,54,55] (EC_{50} for IgE-induced degranulation of primary human mast cells *in vitro* is 56nM). These effects occur in association with inhibition of intracellular phosphorylation events downstream of SYK. R406 did not demonstrate a significant effect on SYK-independent signalling pathways in these cells; for example, significantly higher levels of R406 were required to inhibit monocyte tumour necrosis factor alpha (TNF-α) production induced by LPS (EC_{50} 2.1μM). Conditional knock-out of the *SYK* gene and siRNA knock-down in rodent cells bearing the FcR, have a similar phenotypic effect as treatment with R788/406, further evidence of drug specificity for SYK as its primary target[56,57].

Apart from its anticipated effects on BCR- and FcR-mediated functions, R406 has shown activity in other cell types and signalling pathways. To what extent these effects are due to the biological role of SYK in these pathways, rather than off-target effects of R406, is not definitively established. For example, in T cells from patients with systemic lupus erythematosus (SLE), R406 inhibited T cell receptor (TCR) induced signalling[58]. An altered TCR in which TCR-ζ is replaced by FcR-γ, allowing it to signal through SYK, has been described in many patients with SLE[59,60], and this may be the mechanism of inhibition in this case. R406 has been shown to promote cell death of Flt3-mutant acute myeloid leukaemia (AML) cells *in vivo*, although it has been suggested that this effect may be attributable to its off-target activity on Flt3 rather than SYK inhibition *per se* [61]. Other pathways in which R406 has shown an inhibitory effect include (TNF-α-induced signalling in fibroblast-like synoviocytes [49], and integrin- and lectin-induced signalling in platelets[62].

1.2.2 *In vivo* studies

Building on the *in vitro* evidence, fostamatinib (R788) has been shown to be highly active in two animal models of CLL – adoptively transferred T cell leukaemia 1 (TCL1) leukaemias and leukaemias that spontaneously develop in Emu-TCL1 transgenic mice[63]. In addition, it has shown efficacy in murine models of non-Hodgkin's lymphoma (NHL), reducing tumour burden and prolonging survival in treated mice[64]. Notably, this effect was not seen in tumours lacking surface expression of the BCR, in keeping with the drugs proposed mechanism of action.

The effects of fostamatinib (as either R788 or R406) have been more extensively studied *in vivo* in a diverse range of animal models of allergy, autoimmunity and inflammation, where

its inhibitory action on FcR-mediated signalling is thought to be the key mechanism of action. For example, treatment with fostamatinib effectively prevents the development of thrombocytopenia and haemolytic anaemia induced by the passive transfer of anti-platelet and anti-red cell antibodies, respectively, to mice[65]. In rodent models of asthma, R406 reduced airway hyper-responsiveness (AHR) and markers of airway inflammation following antigen challenge in sensitised mice, in two distinct models[55,66]. Similarly, in mice passively sensitised with anti-OVA IgE, R406 treatment prevented the development of AHR[66].

Treatment with R406 reduced joint inflammation in two passive transfer models of antibody-induced arthritis (the passive anti-collagen antibody-induced arthritis (passive anti-CIA) and K/BxN serum transfer models)[48]. In addition, treatment with either R406 or R788 in Louvain and Lewis rats reduced clinical, histological and radiographic evidence of joint inflammation following active induction of collagen-induced arthritis (CIA)[67]. These improvements were associated with a reduction in pro-inflammatory cytokine and chemokine expression in synovial tissue and fluid.

Fostamatinib has also shown efficacy in animal models of SLE. In the lupus-prone NZB/NZW mouse strain, treatment was effective in both preventing and ameliorating established disease, the treated animals showing reduced proteinuria with improved renal function, improved renal histology, improved platelet counts and prolonged survival[68]. In the MRL/lpr strain, fostamatinib suppressed both established renal and skin disease, and reduced lymphadenopathy[69]. Notably, this study demonstrated a sustained benefit from fostamatinib in the period after drug cessation, suggesting a possible immunomodulatory effect of treatment, although this was not investigated further. Treatment with fostamatinib also

prevented lupus-like skin disease and reduced lymphadenopathy in the BAK/BAX knockout mouse[69].

Finally, fostamatinib significantly delayed the onset of insulinitis and spontaneous diabetes in non-obese diabetic (NOD) mice, and also delayed progression of early established diabetes even when treatment was initiated after the development of glucose intolerance[56]. These findings, in an autoimmune model that is critically T cell-dependent, suggest that SYK inhibition with fostamatinib may have broader therapeutic potential in autoimmune disease beyond its established role in effector processes mediated by the FcR. The authors suggest that, via its effects on antigen internalisation (and thus antigen presentation) by B cells and dendritic cells, treatment may prevent T cell priming and the development of T cell effector responses, suggesting that SYK inhibition may be a useful target in both antibody-mediated and cellular autoimmune responses. In addition, a window study showed a sustained benefit up to 11 weeks after withdrawal of treatment in NOD mice (similar to the effects seen in the MRL/lpr lupus-prone strain), again suggesting the possible induction of immunomodulatory or tolerogenic mechanisms. Notably, an increase in the proportion of interleukin-10 (IL-10) secreting B cells (which have putative regulatory and suppressive function) was seen, and transfer of splenic B cell populations from treated to untreated mice protected from disease. These results suggest that sustained treatment with fostamatinib may not be necessary in autoimmune disease.

1.2.3 Clinical studies

R112 was the first SYK inhibitor treatment to be assessed in clinical studies, where it showed benefit in relieving symptoms of allergic rhinitis when delivered as an intranasal

preparation[70]. Subsequent work focused on R406/R788. Early phase studies in over 100 normal human volunteers in single and multiple dose pharmacokinetic-safety-pharmacodynamic studies showed that R788/R406 was well tolerated and highly bioavailable following oral administration, with an effective concentration for SYK inhibition of approximately 0.5-1.0μM[48,71,72]. For example, R406 administered orally to human volunteers inhibited human basophil activation in response to anti-IgE *ex vivo*, with an IC_{50} of 1.06μM (corresponding plasma concentration 496 ± 42ng/ml). These concentrations were achievable within the dose range (75-150 mg bd) that was well tolerated by volunteers. The disparity between the cell-based and *in vivo* IC_{50} values is attributed to the high protein binding of R406 in human plasma (>98%).

To date there have been six phase II clinical studies, recruiting over 1000 patients, using Fostamatinib.

One of the earliest, and smallest, studies was an open-label, single-arm cohort dose escalation trial in 16 patients with idiopathic thrombocytopaenic purpura (ITP), with an average follow-up time of 36 weeks, which showed that fostamatinib 75-175mg bd induced a sustained improvement in platelet count in 50% of patients[65]. Those who had a sustained response tended to have an early response, with improvements seen in the first few weeks of treatment. Four patients (25%) had transient responses and improved in other clinical parameters such as fewer bleeding episodes, avoidance of rescue mediations and tapering of steroids. Although four patients did not respond, it should be noted that the majority of patients in the study had refractory disease, with a mean number of previous ITP treatments of five. Over two thirds of patients had been treated previously with steroids, intravenous immunoglobulin,

rituximab, and splenectomy. As such, the results of this study are encouraging and larger studies in ITP are planned (NCT02077192).

Three clinical studies investigating the use of fostamatinib in rheumatoid arthritis (RA) have been published (summarised in Table 1.1). The first enrolled 189 patients with active RA despite methotrexate therapy, who were randomised (3:1 ratio) to receive fostamatinib in an ascending-dose manner or placebo in a double-blind trial[73]. The study included a significant proportion of patients who had received multiple previous therapies: more than 50% of the patients were receiving concomitant steroid therapy, approximately one third were receiving other disease-modifying anti-rheumatic drugs (DMARDS) in addition to methotrexate, and 28% had received biologic response modifiers in the past. The primary end-point was the American College of Rheumatology 20% improvement criteria (ACR20) response rate at 12 weeks. This was achieved in 72% and 65% of patients receiving fostamatinib 150mg bd and 100mg bd respectively, significantly greater response rates than seen with 50mg bd (32%) or placebo (38%) ($p < 0.01$). Improvements in a number of secondary end-points (including ACR50, ACR70 and disease activity score (DAS)-28 assessments) were noted. These clinical responses were rapid, with effects noted within one week of treatment, and were associated with reduced levels of circulating pro-inflammatory cytokines such as IL-6.

A second double-blind, placebo-controlled study enrolled 457 patients with active RA despite long-term (i.e. greater than three months) methotrexate therapy, who were randomised (1:1:1) to receive fostamatinib 100mg bd, fostamatinib 150mg od, or placebo[74]. 67% and 57% of the patients in the respective treatment groups achieved the primary end-point of an ACR20 response after six months, versus 35% of patients receiving placebo ($p<0.001$). In keeping with the findings of the earlier study, treatment with both dosing schedules also had a

significant impact on ACR50, ACR70, and DAS-28 remission. Again, clinical responses were seen as early as one week and the majority of patients in whom there was a response at six months had already demonstrated a response at two months, suggesting that an early response may identify those patients who are likely to benefit from ongoing therapy. These patients also had improved patient reported quality of life outcomes[75]. Fewer patients in this study (15%) had failed previous biologic therapy than in the first RA trial. Although overall response rates in this subgroup were lower than for the whole study population, the ACR20 response was achieved in 43% and 46% of patients receiving fostamatinib 100mg bd or 150mg od respectively, versus 14% in the placebo group (p=0.04 and p=0.02 respectively).

These encouraging results, however, must be tempered with the findings of the latest study in RA, which aimed to look specifically at this population – 229 patients with RA who had failed at least one prior biologic therapy were enrolled to receive fostamatinib 100mg bd or placebo (2:1 ratio)[76]. There was no difference between groups in the rate of ACR 20/50/70 or DAS-28 response (38% vs 37% for primary endpoint of ACR20 at three months, p = 0.84). There were, however, statistically significant improvements in synovitis scores as judged by MRI, and inflammatory markers (ESR and CRP), in the treatment group. Despite randomisation, there were baseline differences in steroid use, prior biologic use, and synovitis scores that the investigators suggest may account in part for the lack of efficacy seen in this trial.

REFERENCE	N	ENTRY CRITERIA	FOLLOW UP	ENDPOINT	OUTCOMES	COMMENTS
Weinblatt, Kavanaugh et al. 2008)	189	Active RA (≥ 12 months from diagnosis) despite ≥ 6 months methotrexate therapy	12 weeks	ACR20 response rate (ACR50, ACR70, DAS28 response rates)	Significant benefits in all disease activity scores in patients treated with fostamatinib 100-150mg bd. Clinical responses noted as early as one week after initiation of treatment.	Approximately 1/3 of patients continued to receive other DMARDs during the study; Approximately 20% had received prior biologic therapy (with appropriate washout period before entering study).
Weinblatt, Kavanaugh et al. 2010)	457	Active RA (≥ 6 months from diagnosis) despite ≥ 3 months methotrexate therapy	6 months	ACR20 response rate (ACR50, ACR70, DAS28 response rates)	Significant benefits in all disease activity scores in patients with treated fostamatinib 100-150mg bd. Again, responses noted as early as one week.	15% of patients in this study had received prior biologic therapy. Although overall response rates were lower in this subgroup, still significantly more patients demonstrated responses than the equivalent placebo group.
Genovese, Kavanaugh et al. 2011)	229	Active RA (≥ 12 months from diagnosis) with disease unresponsive to current or previous biologic therapy	3 months	ACR20 response rate (ACR50, ACR70, DAS28 response rates; synovitis scores on MRI,)	No difference in disease activity scores across treatment and placebo groups. Significant improvements in circulating inflammatory markers and synovitis scores on MRI noted in treatment groups.	Despite randomisation, baseline differences in steroid dose, previous biologic exposure and synovitis scores were noted between groups, which authors suggest may account for lack of efficacy.

Table 1.1: Summary of Phase II trials with fostamatinib in patients with rheu

ACR20/50/70, American College of Rheumatology 20/50/70% improvement criteria; DAS
joint counts; MRI, magnetic resonance imaging; DMARD, disease modifying anti-rheumatic

Three phase III trials in RA have been completed (NCT01197521, NCT01197534, NCT01197755) although the results of these studies are not formally published.

In addition to these studies in autoimmune disease, there have been two phase II trials using fostamatinib in patients with haematological and solid tissue malignancies. These suggested significant biological activity in patients with NHL and CLL, but limited activity in advanced, refractory solid organ malignancies[77,78].

1.2.4 Pharmacokinetics and metabolism

R788 was developed as the methylene phosphate prodrug of R406, which exhibits low aqueous solubility, to improve its bioavailability and potential for oral dosage development.

Pre-clinical pharmacokinetic (PK) studies with fostamatinib in Louvain rats confirmed that it is highly bioavailable, rapidly absorbed, and that systemic exposure is proportional to dose[67]. C_{max} was observed at approximately one hour, and $t_{½}$ was 4.2 hours. The prodrug was not detected in plasma suggesting R788 is completely converted to R406.

Phase I studies in humans similarly showed a C_{max} for R406 of 1-1.5 hours and $t_{½}$ of 13-21 hours following single dose exposure to R788[72]. The was a dose-related increase in exposure (C_{max} and AUC) when the dose increased from 80 to 400mg, however exposure was essentially unchanged from 400 to 600mg doses of fostamatinib. Following seven days of multiple dosing of fostamatinib at 160mg, there was an approximate 2-2.5 fold increase in exposure to R406 on day 7 compared to day 1, with steady state being achieved following 3-4 days of twice daily dosing.

A detailed assessment of the pharmacokinetics and metabolic fate of fostamatinib using a combination of *in vitro* intestinal and hepatic microsomes and human mass balance studies has also been conducted[79]. This suggests that R788 is rapidly hydrolysed to R406 by intestinal alkaline phosphatases, after which the more hydrophobic R406 is rapidly absorbed. R406 was the major drug-related product observed in plasma, with peak levels observed at one hour after dosing, and $t_{½}$ ranging from 10.8 to 15.7 hours in this study. Only small amounts of the parent compound R788 were detected in the plasma at early time-points, consistent with rapid intestinal conversion to R406. Elimination of drug-related material in the urine accounted for 19% of the administered dose (the major urinary metabolite in urine being the lactam *N*-glucuronide of R406) and on average 80% was recovered in faeces. It appears that R406 undergoes both direct glucuronidation and a CYP3A4-mediated *para*-*O*-demethylation to R529 in the liver. Conjugates of R529 secreted in bile are hydrolysed back to R529 which, the authors suggest, is subsequently *O*-demethylated and dehydroxylated by anaerobic gut bacteria to a unique 3,5-benzene-diol metabolite, the major drug-related compound detected in faeces.

It is notable that in a trial of fostamatinib in patients with ITP, similar levels of SYK inhibition (as assessed by basophil activation assay) at peak and trough times (2 and 12 hours post-dose respectively) were associated with better platelet responses, although the numbers in this study were small and no other PK parameters were reported[65]. In RA, total exposure (as determined by AUC) was related to adverse outcomes and study withdrawal[73]. Conversely, in the phase I NHL study, there was no correlation between clinical outcomes and measured PK parameters[77]. Future studies will assess more precisely the relationship

between pharmacokinetics and clinical outcomes in order to establish the most effective and tolerable dosing regimens.

1.2.5 Safety

The results of detailed toxicity and immunotoxicology assessments in rats have been reported[80]. Animals were treated with R406 at doses up to 100mg/kg/day for 28 days, achieving average plasma concentrations of approximately 2280ng/ml, in excess of those needed to achieve inhibition of SYK-mediated signalling in clinical studies. Consistent with the reported observations of the cited studies using animal disease models, there were no R406-related changes in appearance, behaviour, food consumption, ophthalmoscopy, coagulation or urinalysis seen in normal animals. At high doses (100mg/kg/day) there was a reduction in circulating lymphocyte count, thymic and spleen weight and bone marrow cellularity. These effects generally resolved during a 14 day recovery period. In host-resistance mouse models of viral and both intracellular and capsulated bacterial infection, treatment with fostamatinib at doses up to 80 mg/kg/day did not impair the ability to clear influenza, listeria or streptococcal infection, consistent with previous *in vitro* observations that R406 had negligible effects on phagocytosis, oxidative burst, chemotaxis, or microbicidal activity of human leucocytes[48], suggesting that fostamatinib does not adversely affect innate immune responses.

In phase I studies, fostamatinib was well tolerated and no serious adverse events were encountered[72]. Neutropenia was a common adverse event in the phase II clinical studies to date, occurring in up to 30% of patients receiving the highest doses in the RA and NHL trials[73,77]. Co-administration of methotrexate, previous immunosuppressant therapy and

underlying bone marrow disease may have been contributing to these rates. Neutrophil counts recovered with temporary withdrawal or dose reduction of fostamatinib. In the second phase II study in RA[74], there was increase in the incidence of upper respiratory tract infection (14.5% in 100 mg bd group versus 7.1% in placebo group; $p < 0.05$), however none of the infections seen were associated with neutropenia. To date, there are no reports of opportunistic or atypical infection in clinical studies.

The most common adverse event seen in clinical studies with fostamatinib was gastro-intestinal toxicity. Diarrhoea was reported at rates of up 45% in some groups[73]. This is a common side effect of other kinase inhibitors, and symptoms appeared to be dose-related and responsive to temporary withdrawal or dose reduction. Nausea and diarrhoea were, however, the most common reasons for patient withdrawal from the treatment groups in larger RA studies[74,76].

Modest but significant elevations in blood pressure (BP) were noted in all the large clinical studies. In the largest RA trial, for example, the incidence of hypertension (systolic BP >140 or diastolic BP >90) was 29% in treatment groups versus 17% in the control group ($p = 0.006$) at one month follow-up. Increases in blood pressure were seen most frequently in those with pre-existing hypertension or who were already on treatment at enrolment. It has been suggested that off-target effects of R406 on vascular endothelial growth factor receptor 2 may account for this phenomenon[81]. In general, hypertension responded to conventional antihypertensive therapy or dose-reduction of fostamatinib.

Moderate elevation in transaminase enzymes were reported in all the clinical studies. Transaminitis was also reported in the pre-clinical toxicity studies, where it was not

associated with any histopathological changes in the liver. In both pre-clinical and clinical studies, liver function normalised with dose-reduction or withdrawal of fostamatinib. In the phase II oncology study, it was noted that pre-existing abnormalities of liver function at baseline increased the risk of developing drug-related hepatotoxicity[78].

Clinical studies with fostamatinib have not, to date, identified any effect of treatment on lipid metabolism, renal function or other biochemical parameters. There was one episode of unexplained acute-on-chronic renal injury in a patient receiving fostamatinib in the NHL study; the role of the drug in this case is unclear.

Developmental toxicity studies in gravid rabbits and rats showed a dose-dependent increase in foetal malformations, including renal and ureteric agenesis and a specific major vessel anomaly – retro-oesophageal right subclavian artery – a phenotype similar to that seen in *c-Ret* knockout mice[82]. The *c-Ret* gene encodes a receptor tyrosine kinase that has a critical role in renal and ureteric development and, strikingly, R406 has been shown to inhibit Ret kinase in *in vitro* and cell-based assays (IC_{50} 5nM and 80nM respectively). Off target effects on this protein may account for some of the developmental anomalies seen. In addition, *SYK* knockout mice show perinatal lethality with petechial haemorrhage, a consequence of the failure to separate developing lymphatic and blood vessels, and so disruption of SYK signalling *in utero* may account for the vascular anomalies seen.

1.2.6 Drug interactions

Hepatic microsome studies show that R406 is extensively metabolised by expressed human CYP3A4 enzymes *in vitro*, and that this is inhibited by cytochrome P450 inhibitors, such as ketoconazole, by up to 90%[79]. These interactions have not been explored in published *in vivo* or clinical studies**.**

The effects of fostamatinib on the metabolism of methotrexate, the most commonly used disease modifying drug used in RA, have been examined in a small phase I study, where no significant pharmacokinetic interaction between the two drugs was reported[83]. Notwithstanding, neutropenia was observed more frequently in the RA trials, where it was co-administered with methotrexate, than in the ITP trial, suggesting a possible synergistic effect on the bone marrow beyond their individual PK parameters.

A potential and important, though as yet unexplored, interaction is that of fostamatinib with monoclonal antibody therapies such as rituximab, which may rely on FcR-mediated processes such as antibody-dependent cell-mediated cytotoxicity, for their effects[84].

1.3 Anti-Glomerular Basement Membrane (GBM) Disease

Anti-GBM disease, also known as Goodpasture's disease, is a rare but life-threatening condition that is characterised by circulating and deposited antibody directed against the GBM, which presents with features of crescentic glomerulonephritis (GN), with or without concomitant pulmonary haemorrhage[85]. It is widely recognised to represent the most severe form of GN, usually presenting with a rapidly progressive renal failure[86], and is regarded as a 'prototypic' autoimmune disease, in which pathologic autoantibodies directed against a well-defined autoantigen are key mediators of tissue injury.

1.3.1 History

The eponymous term 'Goodpasture's Syndrome' was first used by Australians Stanton and Tange[87] in their 1958 article describing nine cases of glomerulonephritis in association with pulmonary haemorrhage, in which they acknowledge the American pathologist Ernest Goodpasture with the first description of the syndrome in his 1919 paper on the aetiology of influenza[88]. However, it is not known whether any of these cases had anti-GBM antibodies, as it was not until the development of immunofluorescence techniques in the 1960s that Sheer and Grossman first described the typical linear staining pattern for immunoglobulins in renal tissue seen in this disease[89]. In 1967, Lerner and colleagues showed that these antibodies, eluted from the kidneys of patients, were reactive with normal kidney tissue, and subsequently demonstrated their pathogenic potential by administration to non-human primates[90]. Circulating anti-GBM antibodies were first detected in the sera of patients by indirect immunofluorescence on normal kidney, though more sensitive immunoassays using

collagenase-solubilised partially-purified GBM were rapidly developed[91]. The first comprehensive clinical report of 'anti-GBM disease' was by Wilson and Dixon in 1973[92].

The term 'Goodpasture's Disease' is now generally reserved for those patients with detectable anti-GBM antibodies in association with renal or pulmonary disease, whereas 'Goodpasture's *Syndrome'* may refer less specifically to any similar reno-pulmonary presentation, such as that seen in small vessel vasculitis associated ANCA.

1.3.2 Epidemiology and associations

Goodpasture's Disease is a rare disorder, with an approximate incidence of one per million population per year[93]. There is a slight male preponderance and bimodal age distribution, with peak incidence in the third and sixth decades. The disease is more common in Caucasian populations, is well represented in Asians, and thought to be rare in those of African origin.

Reported environmental associations include cigarette smoking[94] and exposure to hydrocarbons and industrial solvents[95]. Associations with other diseases include membranous nephropathy[96], AAV[97], and renal stone disease treated with lithotripsy[98-100].

In common with other autoimmune diseases, genetic predisposition is believed to be an important determinant of disease development[101], and there is a strong association with human leucocyte antigen (HLA) genes in particular, with approximately 80% of patients inheriting an HLA-DR2 haplotype. Genotyping studies have revealed a hierarchy of associations with particular DRB1 alleles: DRB1*1501, DRB1*03 and DRB1*04 are positivity associated with disease, whereas there is a negative association with DRB1*01 and

DRB1*07[102]. The molecular basis of these HLA associations is not defined, although the observation that the DRB1*01 and DRB1*07 alleles appear to confer a dominant negative effect, and that these protective alleles bind peptides from the Goodpasture autoantigen with greater affinity than the positively associated alleles, suggests that they might compete for peptide epitopes with the susceptibility alleles.

A link to major histocompatibility complex (MHC) Class II genes has also been reported in murine strains susceptible to experimental disease, although non-MHC genes are also involved since both resistant and susceptible rat strains have been shown to share the same MHC type. In addition, the susceptibility alleles in humans are common in the general population, yet the disease remains exceedingly rare. These observations demonstrate the importance of other, as yet undefined, genetic and environmental factors in the development of disease.

1.3.3 Pathogenesis

Lerner's classic transfer experiments (since repeated in a number of different species) were the first demonstration that autoantibodies could directly cause disease, and the role of humoral immunity and the nature of the target autoantigen have been the predominant focus of historical research interest in this condition. More recent observations, and in particular studies of animal models that manifest a similar pathology, also confirm an important role for cellular immunity, both as orchestrator of the autoimmune response, and direct effector of tissue injury (Section 1.4).

.

1.3.3.1 The Goodpasture autoantigen

The Goodpasture autoantigen has been defined as the non-collagenous (NC1) domain of the alpha-3 chain of type IV collagen (α3(IV)NC1)[103-105], and the clinical pattern of reno-pulmonary disease reflects the restricted expression of this antigen to the basement membranes of glomerular and alveolar capillaries (and to a lesser extent the retina, choroid plexus and cochlea, where it is generally not associated with clinical disease[106]). Immunisation with either collagenase-solubilised or recombinant forms of the protein from various species induces disease in a number of animal models, confirming the universal antigenicity of this protein.

In its native form, the collagen IV network in the GBM consists of triple-helical protomers of α3, α4 and α5 chains[107,108] (Figure 1.3). The carboxyl-terminal domains of these α3α4α5 protomers form a trimeric 'cap', end-to-end association of which results in the formation of the hexameric NC1 domain. The quaternary structure of this hexamer is stabilised by hydrophobic and hydrophilic interactions across the planar surfaces of opposing trimers, and reinforced by sulphilimine bonds cross-linking opposing NC1 domains. Two key autoantibody epitopes within α3(IV)NC1 have been described, designated E_A (incorporating residues 17-31 towards the amino-terminus) and E_B (residues 127-141 towards the carboxyl-terminus), which in the native form are sequestered at the junction with α4 and α5 chains within the triple helical structure[104,109].

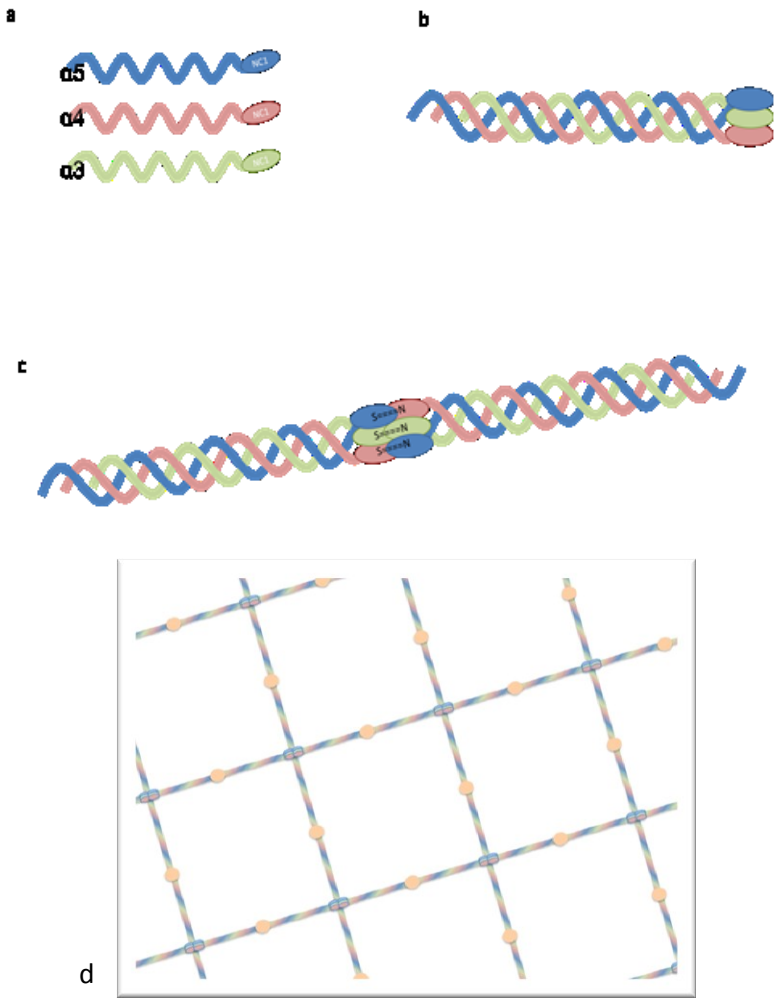

Figure 1.3: Collagen IV in the glomerular basement membrane.

(A) Individual α3, α4 and α5 chains of Type IV collagen with carboxyl terminal non-collagenous (NC1) domains.(B) Association of α3, α4 and α5 chains to form triple-helical trimer, with NC1 domain 'cap'. (C) Type IV collagen molecule, showing end-to-end association of NC1 trimers to form NC1 hexamers, with sulphilimine crosslinks(S=N), and resultant sequestration of α3 chain epitopes. (D) Binding through 7s domains (shown in orange) completes the lattice-like structure of the Type IV collagen network.

1.3.3.2 Humoral immunity

Sera from all patients with anti-GBM disease appear to recognise α3(IV)NC1 (both epitopes E_A and E_B), although sera from a proportion of patients may also recognise other collagen chains. Approximately 70%, for example, will have both circulating and deposited antibodies to the α5(IV)NC1 domain, suggested to arise through a process of 'epitope spreading' following primary disease initiation by autoantibodies to α3(IV)NC1[104].

In addition to the passive transfer models of Lerner and others, several clinical observations support a directly pathogenic role for these autoantibodies in anti-GBM disease. Antibody titre, immunoglobulin subclass and, in at least one study, antibody avidity have each been correlated with disease outcome in patient cohorts[110-113]. Rapid removal of circulating antibodies by plasmapheresis is associated with better clinical outcomes[114], and disease recurs rapidly in renal allografts if circulating antibodies are present at the time of transplantation[92]. In addition, copy number variation of activatory FcγIIIA genes is found at higher frequency in patients compared with healthy controls[115], and certain FcγIIB receptor polymorphisms are also present at higher frequency in diseased patients[116], implicating antibody-dependent responses in disease susceptibility.

The presence of low titre 'natural' autoantibodies to GBM has been reported in normal populations[117]. These antibodies recognise the same epitopes as antibodies from patients, although their presence does not result in disease. This may be due to differences in the titre or predominant subclasses of these natural autoantibodies (IgG2 and IgG4 versus IgG1 and IgG3 in disease) or the role of other regulatory factors. The presence of circulating antibody has been reported to predate the onset of clinical disease by several years[118] (although

antibody subclass and epitope specificity was not reported in this study), an observation that suggests the involvement of other factors in the development of disease.

1.3.3.3 Cellular immunity

In addition to the experimental data discussed below, several clinical observations support a role for cell-mediated immunity in the pathogenesis of anti-GBM disease. CD4+ and CD8+ T cells can be demonstrated in diseased glomeruli in humans, and the presence of class-switched, high-affinity autoantibody, along with a strong HLA-association, implies a requisite for T cell-mediated help. Mononuclear cells from patients have also been shown to proliferate in response to α3(IV)NC1 (as do cells from healthy individuals, though at much lower frequency), and the frequency of autoreactive CD4+ T cells has been shown to correlate with disease activity[119-121]. The pathogenic T cell epitopes in humans, however, have not been consistently defined.

1.3.3.4 Tolerance and autoimmunity to α3(IV)NC1

α3(IV)NC1 is expressed in human thymus[122], although the finding of natural autoantibodies and T cells reactive to α3(IV)NC1 in normal individuals suggests some failure to achieve central tolerance to this antigen during immunological development. It has been suggested that certain autoreactive T cell peptides are sensitive to rapid enzymatic degradation during antigen processing, limiting the exposure of autoreactive cells to their corresponding antigens, and thus allowing them to escape negative selection[123]. The additional factors that result in further breakdown of tolerance and development of clinical disease are not clear, though may include the need to expose sequestered epitopes within the Goodpasture antigen.

Notably, the cross-linked native hexameric NC1 domain does not bind antibody, and it is thought that disruption of its quaternary structure, with rupture of the sulphilimine cross-links and dissociation of the hexamer, is required to expose the pathogenic epitopes required for autoantibody binding. Both cross-linked and non-cross-linked forms of the hexamer exist in humans and other primates, but only the cross-linked form in mice, perhaps explaining the resistance of some mouse strains to passive transfer models of disease. This requirement for 'conformational transition'[104] of the autoantigen may also explain the association of anti-GBM disease with other processes that may damage the basement membrane in the kidney (such as membranous nephropathy, AAV, or lithotripsy) or the lung (such as smoking and inhalation of hydrocarbons), resulting in exposure of usually sequestered epitopes.

The recovery phase of this condition is associated with a progressive fall in autoantibody titre (even in the absence of immunosuppressant treatment) and a lower frequency of CD4+ T cells reactive to α3(IV)NC1, along with development of a regulatory CD25+ T cell subset that may suppress responses to α3(IV)NC1[124]. This suggests the re-emergence of immunological tolerance, which may be reflected by the rarity of clinical relapses in this condition.

1.3.4 Clinical considerations

The great majority of patients will present with features of rapidly progressive glomerulonephritis, which is characterised by an abrupt decline in renal function and an 'active' or 'nephritic' urinary sediment containing protein and red cell casts. There are a small number of reported cases, however, presenting with only mild renal impairment[125]. Approximately 50% of patients will have co-existent pulmonary haemorrhage, which may

present with haemoptysis and be seen as alveolar shadowing on chest radiography, or detected by the finding of an increased carbon monoxide transfer factor. A small number of patients may present with isolated lung disease in the absence of overt renal pathology. Strictly, the diagnosis of anti-GBM disease rests on the demonstration of:

(i) Circulating anti-GBM antibodies – these are detectable in the majority of patients by conventional techniques such as enzyme-linked immunosorbent assay (ELISA) and Western blotting using purified human or animal GBM preparations. In the small proportion of patients who do not have detectable antibodies using these methods, more sensitive techniques such as biosensor assay using recombinant antigen have been reported to detect circulating antibody[126].

(ii) Deposited anti-GBM antibodies – seen as linear deposits of IgG along the GBM by immunofluorescence techniques. The majority of patients will also demonstrate linear staining for complement C3, and some for other antibody isotypes, such as IgA and IgM.

(iii) Crescentic glomerulonephritis – seen on standard light microscopy of renal tissue. Fibrinoid necrosis may be present. The finding of 'synchronous' injury, where all glomeruli show lesions of similar acuity, is typical.

Standard treatment for anti-GBM disease, first introduced in the 1970s[127], consists of plasmapheresis, to rapidly remove the pathogenic antibody (and possibly other pro-inflammatory mediators) from the circulation, and immunosuppression with cyclophosphamide and corticosteroids, which inhibit the production of further autoantibody and reduce end-organ tissue inflammation and damage. Retrospective series suggest this combination of treatment is effective in most patients with serum creatinine <500μmol/l at

presentation, and one large study showed it can be successful even in patients who present with severe renal injury (creatinine > 500μmol/l) but not yet on dialysis[128]. In the same study, lung haemorrhage responded to treatment in 90% of patients. One small trial suggested better recovery of renal function when plasmapheresis was used in addition to drug therapy[114]; however given its rarity (and the efficacy of accepted treatments) there are no large randomised controlled trials in this disease. The use of alternative immunosuppressant agents (such as cyclosporine, mycophenolate mofetil or rituximab) has been reported in small series and individual cases, although there is insufficient evidence to support their use as first-line treatment at present. Poor prognostic features include dialysis-dependency at diagnosis and 100% crescents on renal biopsy, which suggest the patient will not recover independent renal function.

1.4 Experimental models of anti-GBM disease

1.4.1 Nephrotoxic nephritis

The nephrotoxic nephritis (NTN) model is the best known animal model of crescentic glomerulonephritis. First described at the beginning of the 20th Century by Lindemann[129], who injected rabbits with heterologous antiserum to rabbit kidney raised in guinea pigs, NTN has since been reproduced in a variety of species including dog, rabbit, mouse, rat and hamster, the rodent models being the most extensively studied. Disease is initiated by administering nephrotoxic serum (NTS) raised in sheep or rabbits immunised with rodent glomeruli. The animals then develop an inflammatory renal lesion that is initiated by the co-localisation of alloantibody against kidney antigens (heterologous phase) and the host response to this foreign antibody (autologous phase). Accelerated NTN involves pre-immunisation with sheep or rabbit immunoglobulin. NTN is characterised by a rapid onset of disease, with early leucocyte infiltration and subsequent mesangial proliferation, crescent formation, fibrin deposition, tissue destruction and progression to scarring and renal failure[130]. It histologically resembles anti-GBM disease and has the typical linear staining pattern for IgG on immunofluorescence. Studies in NTN have shed light on the role of various immune effectors in glomerulonephritis, including antibodies, complement, infiltrating lymphocytes and resident renal cells. Historically, it has been ascribed a Th1 dependent delayed-type hypersensitivity (DTH) reaction phenotype, characterised by macrophage infiltration, under the influence of key cytokines such as interferon gamma (IFN-γ) and IL-12[131].

Studies of NTN in rats, using the genetically susceptible Wistar Kyoto (WKY) strain in particular, have been used to test an extensive number of therapeutic approaches for crescentic GN, and have simultaneously contributed to the understanding of the underlying pathogenic processes.

Various approaches aimed at manipulating cytokine activity have been used in NTN, including antagonism of pro-inflammatory cytokines such as TNF-α[132]. Administration of 'anti-inflammatory' cytokines including IL-4[133] and IL-11[134] can attenuate disease, in keeping with the DTH phenotype of the model. Targeting of the intracellular signalling pathways involved in promoting inflammation, such as the p38 MAPK pathway, have also been effective[135]. Notably, in each of these intervention studies, no significant effects were reported on circulating or deposited autologous rat anti-rabbit antibody levels, suggesting that the intervention was predominantly acting on effector phase of renal injury.

In work previously reported by our laboratory, SYK inhibition with fostamatinib was shown to both prevent and treat established disease in this model[136]. As shown in figure 1.4, for example, when treatment was started at either day 0 or day 4 after disease induction, there was complete protection from the development of glomerular crescents at day 10. In this study, pre-treatment (from day 0) with fostamatinib reduced the production of autologous rat anti-rabbit antibody, although there was no effect on circulating antibody levels if treatment was delayed until disease was established (from day 4).

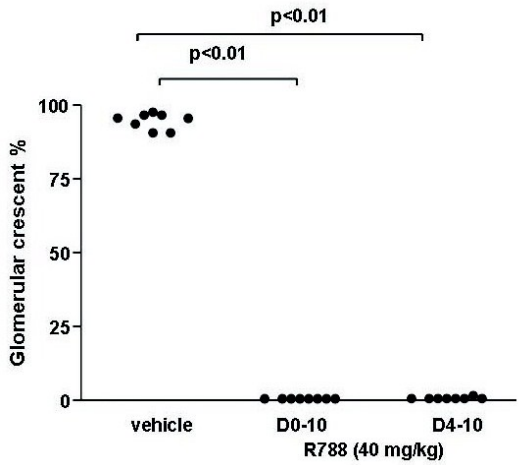

Figure 1.4: Reduction in glomerular crescents following treatment with fostamatinib in rat nephrotoxic nephritis (NTN).
Treatment with fostamatinib from day 0 or from day 4 after disease induction resulted in complete protection from the development of glomerular crescents in rat NTN. (From Smith *et al,* 2010).

Attempts to determine the genetic basis of the unique susceptibility of the WKY rat strain to NTN has provided a further means of identifying important factors in the pathogenesis of crescentic GN. A genome wide linkage analysis, for example, of F2 offspring derived from WKY and NTN-resistant Lewis rats identified seven significant quantitative trait loci for crescentic GN, with two major loci (lod score >8) on rat chromosomes 13 (*Crgn1*) and 16 (*Crgn2*). Deletion of the rat *Fcgr3-rs* gene was identified as the molecular basis of *Crgn1*, and recent work has shown that the AP-1 transcription factor JunD in an important determinant of macrophage activity, and that *JunD* is located at the *Crgn2* peak of linkage.

NTN in mice is more variable and often has a more thrombotic pathological phenotype than in rats, which may limit its relevance to translation in humans. Studies in mice, however, have the obvious advantage of allowing investigation of a multitude of genetically altered strains, and have made a significant contribution to the understanding of the underlying disease processes and key immune effectors in crescentic GN. Disease appears to be critically

dependent on CD4+ T cells, since CD4 deficient mice do not deposit autologous anti-sheep IgG and are protected from disease, whereas CD8 deficiency appears to exacerbate antibody deposition and nephritis in a non-accelerated model[137]. Similarly, administration of anti-CD4 antibody (prior to anti-GBM serum in an accelerated model) prevented disease in antibody-deficient mice[138]. The importance of T cell co-stimulation pathways has been shown in NTN, as mice deficient in CD40 do not produce nephritogenic humoral immune responses and fail to develop disease in accelerated NTN[139]. Conversely, if an anti-CD40L blocking antibody was administered prior to injection of anti-GBM serum, humoral immune responses were not affected, although disease was attenuated, implicating CD40-mediated co-stimulation in the effector phase of renal injury. A possible role for regulatory T cells in disease suppression has also been demonstrated[140] – administration of CD4+CD25+ T regulatory cells before injection of anti-GBM serum attenuated disease in accelerated NTN, without affecting deposition of immune complexes, suggesting that T regulatory cells suppress cell-mediated organ damage rather than priming of the immune response.

Studies in knockout and bone marrow chimeric animals have provided information on the relative contribution of infiltrating and resident cells in disease initiation. It appears, for example, that renal mesangial cells are not mere bystanders in the disease process, but rather that they have an important role in the production of pro-inflammatory cytokines such as TNF-α and IL-12 necessary for full expression of disease[141,142]. The identification of the IL-17 secreting CD4+ T cell subset, termed Th17, has modified the traditional Th1/Th2 paradigm. The presence of this subset has been demonstrated in NTN, and studies in *IL-23 p19* knockout mice (which have reduced numbers of Th17 cells) and *IL-17* knockout mice has shown that the IL-17 pathway makes a significant contribution to renal inflammation in glomerulonephritis[143]. It is also interesting, given its cell-mediated phenotype, that disease is

critically dependent on expression of receptors for the Fc portion of IgG (FcR). In particular, the expression of activatory FcγRI and FcγRIII on infiltrating leucocytes is key in disease initiation[144,145]. Finally, there has been an increasing interest in the role of innate immune elements in this model, with recent studies in knockout mice showing potential roles for TLR[146] and the mannose receptor[147]. In each of these studies, no significant effect on mouse anti-sheep humoral immunity was observed suggesting that these elements were important in effecting tissue injury, rather than in priming the humoral response (except in the case of LPS-induced TLR signalling at the time of pre-immunisation in an accelerated model, which augmented circulating antibody responses)[146].

1.4.2 Experimental autoimmune glomerulonephritis

Studies by Steblay in 1962[148] demonstrated that sheep immunised with human collagenase-solubilised GBM in complete Freund's adjuvant (CFA) developed crescentic glomerulonephritis. This model, now termed experimental autoimmune glomerulonephritis (EAG), has since been reproduced in several species including rodents, using collagenase-solubilised fractions of bovine, rat or human GBM and latterly recombinant mouse, rat or human α3(IV)NC1, confirming the universal antigenicity of this protein.

Induction of EAG in the Brown Norway or the particularly susceptible WKY rat strains has provided a good model of human disease. WKY rats develop circulating and deposited anti-GBM antibodies in association with a reproducible crescentic glomerulonephritis. Studies in these rat models have confirmed that disease can be adoptively transferred by antibodies[149,150]. They have also demonstrated a critical role for T cells in disease initiation. Renal immunohistology in EAG has shown that T cell influx precedes macrophage

infiltration and glomerular injury. T cells from WKY rats with EAG proliferate in response to NC1 domains of rat GBM. The transfer of splenic CD4+ T cells from EAG rats can prime naïve recipients for disease[151]. More recently, it has been shown that transfer of *in vitro* activated CD4+ T cells from immunised rats can result in crescentic GN in the absence of IgG binding to the GBM or C3 deposition in recipients[152], suggesting a directly injurious T cell response.

These findings have led to a number of T cell directed therapies being studied in EAG in the rat. Cyclosporin A[153] and monoclonal therapies against CD4[154] and CD8[155] have shown efficacy in preventing or ameliorating established experimental disease. Similarly, approaches aimed at interrupting T-cell co-stimulation pathways, such as monoclonal antibody blockade of CD40-CD40L[156] and CD28-B7[157] interactions have also been effective. Approaches based on inducing tolerance by mucosal administration of antigen have also shown promise in these models. For example, oral administration of GBM antigen, nasal administration of recombinant α3(IV)NC1, and more recently nasal administration of an immunodominant peptide, pCol (24-38), from α3(IV)C1[158], have been shown to be effective in preventing or treating established EAG. The underlying mechanism of mucosal tolerance has not been firmly established, but likely reflects the induction of regulatory T cells. In each of these studies, it is difficult to assess the relative contribution of reduced antibody production and attenuated effector responses, due to differences in the timings of intervention during the natural history of disease.

Several mouse strains are susceptible to EAG, although disease in mice is less severe, less reproducible and consequently less extensively studied than in the rat. Studies of EAG in mice have confirmed dependency on T cells. Mice that do not express a functional T cell

receptor, for example, are protected from disease induction, even after passive transfer of anti-GBM antibodies[159]. Splenocytes from EAG mice proliferate in response to α3(IV)NC1 and have a Th1-biased secretory phenotype, producing high levels of IFN-γ and low amounts of the anti-inflammatory cytokine IL-10, suggesting that antigen-specific Th1 effector cells make a significant contribution to the tissue damage seen in this model[160]. Finally, it is noteworthy that mice deficient in the type IIB inhibitory Fc receptor for IgG (FcγRIIB) have increased susceptibility to EAG, suggesting a possible role for this receptor in maintaining immunological tolerance[161].

1.5 ANCA-associated vasculitis (AAV) and glomerulonephritis (AAGN)

The association of pauci-immune crescentic glomerulonephritis with circulating autoantibodies directed against antigens in neutrophil cytoplasm (ANCA) was first reported in 1985[162]. The two major ANCA antigens were subsequently shown to be myeloperoxidase (MPO) and proteinase 3 (PR3)[163-165]. The clinical syndromes now associated with ANCA include granulomatosis with polyangiitis (GPA; formerly Wegener's Granulomatosis), microscopic polyangiitis (MPA), eosinophilic GPA (formerly Churg-Strauss Syndrome) and renal limited vasculitis[85,166]. These are generally multi-system diseases characterised by necrotising inflammation of small blood vessels, complicated by life-threatening features of crescentic GN and alveolar haemorrhage in their most severe forms.

1.5.1 Pathogenicity of ANCA in AAV

Several clinical observations suggest that ANCA are pathogenic in these conditions. They are specific and relatively sensitive markers of disease, and ANCA target specificity correlates with disease phenotype[167]. ANCA titre has been reported to correlate with disease severity and, in some series, rising titres predicted disease relapse[168-171]. There is also a reported case of maternal-foetal transfer of ANCA resulting in disease in a neonate[172,173]. Removal of antibodies by plasmapheresis has been associated with improved clinical outcomes[174], and recently B cell targeted therapies have been shown to be effective treatments AAV[175,176]. Finally, a recent genome-wide association study (GWAS) identified the strongest genetic associations with antigenic specificity of ANCA, rather than the clinical syndrome[177]. In anti-PR3 vasculitis, strong associations with HLA-DP, the gene encoding proteinase 3 (*PRTN3*;

the autoantigen) and α_1-antitrypsin (*SERPINA1*; the circulating inhibitor of the autoantigen) were identified, implicating the autoimmune response to PR3 in the pathogenesis of disease.

A number of experimental observations also suggest that ANCA are pathogenic. *In vitro* analyses of human autoantibody-autoantigen interactions and the effects of these autoantibodies on leucocyte behaviour, have critically informed the understanding of ANCA-related disease pathogenesis. Both MPO- and PR3-ANCA are able to activate cytokine-primed leucocytes *in vitro*, resulting in damage of endothelial cells in culture[178,179]. In flow conditions, using chambers lined with activated platelets or endothelial cells, treatment of rolling neutrophils with ANCA-IgG resulted in adhesion and transmigration of neutrophils[180,181], suggesting that ANCA may participate directly in vascular inflammation by promoting neutrophil adhesion to the vascular endothelium where they can then initiate tissue damage. Notably, SYK phosphorylation has been implicated in the activation of primed neutrophils by ANCA *in vitro*[182]. It has also been reported that MPO-ANCA may activate murine glomerular endothelial cells (mGEC) directly[183]. Notably, mGEC lack expression of MPO, and it is suggested that moesin, a protein with partial amino-acid sequence homology to MPO, is the target of MPO-ANCA on mGEC in this case.

A recently identified mechanism via which ANCA may initiate and perpetuate disease in AAV is through the enhanced formation and disordered regulation of neutrophil extracellular traps (NETs). NETs are chromatin-based structures containing antimicrobial molecules (including MPO and PR3) that are released during a cell death process unique to neutrophils ('NETosis'), thought to represent an important innate defence mechanism that may trap and destroy invading microbes[184,185]. However, inappropriate exposure of the vascular endothelium to NETs may result in local host damage. Both MPO- and PR3-ANCA have

been shown to stimulate the formation of autoantigen-containing NETs by primed neutrophils *in vitro*[186,187]. In addition, DNase I activity (an important negative regulator of NETs) in sera from patients with anti-MPO vasculitis is reduced, perhaps accounting for the decreased rates of NET degradation seen in these patients. Finally, NETs have been identified using immunofluorescence methods in renal biopsy specimens from patients with AAGN[186].

Studies in animal models (Section 1.5.3) provide further evidence of the pathogenicity of ANCA in AAV.

1.5.2 Generation of the autoimmune ANCA response

Whilst the reported data suggest that ANCA contribute to the pathogenesis of AAV, the mechanisms underlying the immunogenesis of ANCA are less clear, though likely to be multi-factorial and involving both host and environmental factors. The genetic associations identified in a large GWAS have already been discussed. Environmental associations include exposure to air pollutants such as silica[188,189], drugs[190], and bacterial infections.

Postulated mechanisms of bacterial infection-induced ANCA production include direct stimulation of autoreactive T or B cells by bacterial superantigens[191]. A process of 'molecular mimicry', whereby the immune response directed against microbial antigens 'cross-reacts' to self-antigens that bear homology to the microbial peptides has also be proposed. This is perhaps best illustrated by the example of anti-human lysosome-associated membrane protein-2 (anti-LAMP-2) antibodies, a non-classic ANCA first identified in patients with pauci-immune necrotising GN in 1995[192]. LAMP-2 demonstrates 100% homology to the adhesin FimH, expressed on gram-negative bacteria. Infections with fimbriated bacteria are

reported to be common prior to the onset of necrotising GN, and notably susceptible rat strains immunised with FimH develop nephritis and antibodies that react to rat and human LAMP-2[193]. The clinical relevance of anti-LAMP2 antibodies in human AAGN, however, remains controversial[194,195].

A related, though distinct, mechanism that has been proposed for the development of infection-induced ANCA is that of 'antigen-autoantigen complementarity'. This theory suggests that ANCA arise through anti-idiotype interactions with antibodies directed against peptides that are complementary to the autoantigen epitopes on ANCA. The presence of antibodies and CD4+ T cells that recognise complementary PR3 (cPR3) have been demonstrated in patients with PR3-AAV (but not in MPO-AAV patients)[196,197]. Again, studies in rodents have demonstrated that immunisation of mice with cPR3 results in production of antibodies not only to cPR-3, but also to the sense counterpart, PR3, and that both human and mouse antibodies to PR3 and cPR3 bind to each other, indicating idiotypic relationships[196]. It is of interest that cPR3 is reported to have high homology to *Staphylococcus aureus* peptides. The association *of Staphylococcus aureus* carriage and GPA relapse is well recognised[198], and this may account for the efficacy of some anti-microbial treatments in the preventing relapse in GPA[199,200].

Disordered T cell responses may also contribute to (or fail to suppress) the generation of circulating ANCA. Patients with GPA, for example, have a relative deficiency in Foxp3-positive T regulatory cells, that also appear to be functionally impaired[201], although the same may not be true of patients with MPO-AAV[202]. A recent study also suggested that AAV patients have a suppressor-resistant CD4+ effector T cell population that produces pro-inflammatory cytokines (and is antigen experienced)[203]. In addition, the IL-17 axis may

contribute to the development of ANCA – serum IL-23 (which induces the differentiation of Th17 cells) and IL-17A (produced by Th17 cells) levels are elevated in patients with acute AAV[204]. IL-23 levels appeared to correlate with ANCA titres, suggesting that it might have a role in maintaining ANCA production. Finally, the role of regulatory B cells in the pathogenesis of AAV has been the subject of two recent studies, with reduced regulatory B cell number associated with active disease, remission-status, and frequency of relapse after B cell depletion[205,206].

1.5.3 Animal models of ANCA-associated vasculitis

1.5.3.1 Mouse anti-MPO glomerulonephritis

Whilst longstanding *in vitro* observations have suggested a pathogenic role for ANCA in clinical disease, a convincing *in vivo* model of systemic vasculitis or pauci-immune GN has been unavailable until relatively recently. One such model was developed by Xiao *et al* in 2002[207]. *MPO* knockout mice immunised with mouse MPO in CFA develop high-titre anti-MPO antibodies. When splenocytes from these immunised mice are transferred to lymphocyte-deficient recipients, the recipients subsequently develop crescentic GN and pulmonary haemorrhage. Purified anti-MPO antibodies from the immunised mice, when delivered to wild-type mice, were also capable of inducing a crescentic GN in the absence of significant glomerular immunoglobulin deposition. This was the first convincing *in vivo* data supporting the hypothesis that ANCA have a directly pathogenic role. This model, however, is not strictly a model of autoimmunity, given that MPO is a novel antigen for the knockout mouse, and so the ANCA may have different characteristics to the autoantibodies seen in human disease. Study of the model has nonetheless provided useful insights into the

pathogenic mechanisms at work in vasculitis and pauci-immune GN, with roles for complement[208], TNF-α[209] and, critically, primed neutrophils being demonstrated. Depletion of neutrophils before induction with MPO-ANCA prevented disease[210], and administration of MPO-ANCA to *MPO* knockouts with transplanted circulating *MPO* +/+ neutrophils resulted in glomerulonephritis[211].

1.5.3.2 Experimental autoimmune vasculitis in the WKY rat

Our laboratory has developed a model termed 'Experimental Autoimmune Vasculitis' (EAV)[212]. Disease is induced by immunisation of WKY rats with human MPO in CFA. The rats develop polyclonal anti-MPO antibodies, along with evidence of small vessel vasculitis, pauci-immune glomerulonephritis and pulmonary haemorrhage. Of note, intra-vital microscopy demonstrates enhanced leucocyte-endothelial cell adhesion and transmigration in response to an inflammatory stimulus (CXCL1) in the immunised animals, and in naïve animals following passive transfer of ANCA-rich immunoglobulin. This is the first direct *in vivo* evidence for pathogenicity of *auto*antibodies to MPO supporting previous *in vitro* observations. The initial model has been optimised to produce a reliable, reproducible system that results in crescentic GN and pulmonary haemorrhage in all animals[213] and study in this model has demonstrated a potential therapeutic role for anti-TNF-α directed therapies[214].

1.5.3.3 Animal models of PR3-ANCA vasculitis

Whilst the *in vitro* evidence suggests PR3-ANCA can activate leucocytes in a similar manner to MPO-ANCA, a reliable animal model of PR3-ANCA induced glomerulonephritis has not yet been developed – immunisation of rodents with PR3 or passive transfer of PR3-ANCA

does not reproducibly result in renal or pulmonary disease[215,216]. The reasons for this are not clear, but may include insufficient surface expression of PR3 on murine neutrophils. Primo and colleagues showed that splenocyte transfer from NOD mice immunised with recombinant murine PR3 to NOD-SCID (non-obese diabetic, severe combined immunodeficiency) mice resulted in the development of vasculitis and necrotising GN[217]. However, this model is limited by the development of significant glomerular immune complex deposition after splenocyte transfer. Notably, it was recently shown that in mice reconstituted with a humanised immune system, administration of human ANCA could result in renal and lung injury[218].

1.5.4 Treatment and prognosis of AAV

Current guidelines, based largely on the findings of several randomised controlled trials, suggest that medical therapy in AAV should be tailored according to the extent of disease activity and the disease phase[219,220]. The 2008 European League Against Rheumatism (EULAR) guidelines are summarised in Table 1.2.

STAGE	DESCRIPTION	SUGGESTED TREATMENT
REMISSION INDUCTION		
• **Localised**	Upper and/or lower respiratory tract disease without any other systemic involvement or constitutional symptoms	Methotrexate & Glucocorticoids
• **Early Systemic**	Any, without organ-threatening or life-threatening disease	Methotrexate & Glucocorticoids
• **Generalised**	Renal or other organ-threatening disease, serum creatinine <500μmol/l	Cyclophosphamide & Glucocorticoids
• **Severe Systemic**	Renal or other vital organ failure, serum creatinine >500μmol/l	Cyclophosphamide & Glucocorticoids, with the addition of plasma exchange
• **Refractory**	Progressive disease unresponsive to glucocorticoids and cyclophosphamide	Consider IVIG, 15-deoxyspergualin, ATG, Infliximab, MMF or RTX.
MAINTENANCE	Controlled disease activity after remission-induction, where therapeutic aim is to prevent disease relapse	Low-dose Glucocorticoids & Azathioprine Or Leflunomide Or Methotrexate

Table 1.2: 2008 EULAR guidelines for the treatment of ANCA-associated vasculitis.
Modified from Mukhtyar *et al*, 2010. IVIG, intravenous immunoglobulin; ATG, anti-thymocyte globulin; MMF, mycophenolate mofetil; RTX, rituximab.

Since the publication of these guidelines, two randomised controlled trials have demonstrated that rituximab, a chimeric monoclonal antibody directed against CD20 that results in depletion of peripheral blood B lymphocytes, is as effective as cyclophosphamide for inducing remission in generalised AAV, and may even be superior in patients presenting with relapsing disease[175,176,221]. Uncontrolled series also suggest that rituximab may be effective in maintaining remission and preventing relapse[222,223]. Notably, the therapeutic effect seen following rituximab treatment is not only dependent upon elimination of circulating ANCA, since a significant proportion of patients remain ANCA-positive despite achieving clinical remission. This observation suggests that B cell functions other than autoantibody production (such as antigen presentation, cytokine production, and provision of co-stimulation) may be important in the pathogenesis of AAV.

Analysis of patient outcomes in four randomised controlled trials in AAV show that survival has improved dramatically with the introduction of effective immunosuppressive treatments (11.2% mortality at one year)[224]. However, the majority of early deaths were caused by treatment side effects (59%) rather than active vasculitis (15%), highlighting the ongoing need for more targeted therapies in AAV.

1.6 Experimental questions and study aims

Given its well defined role in BCR and FcR mediated signalling, it is likely that SYK activity contributes to the pathogenesis of autoimmune conditions, including immune-mediated glomerular diseases. Indeed, as I have described, SYK inhibition with fostamatinib has been shown to attenuate several experimental models of autoimmune disease, including murine lupus and nephrotoxic nephritis. However, the pathology of murine lupus nephritis poorly replicates that of human of disease, and nephrotoxic nephritis, whilst histologically resembling human crescentic GN, relies on the alloimmune response to a planted foreign antigen, so cannot be regarded as a true model of autoimmune glomerulonephritis. In addition, whilst inhibition of antibody-dependent FcR-mediated responses has been shown to contribute to the reduction in injury seen with fostamatinib in the various models, the specific impact of SYK inhibition on autoantibody production remains unclear. No effect on circulating autoantibody levels was observed in CIA or murine lupus. Conversely, in NTN, there was a significant reduction in autologous rat anti-rabbit antibody titre in animals pre-treated with fostamatinib. In NOD mice, treatment resulted in a reduction in anti-glutamate decarboxylase (GAD) antibodies, but not anti-insulin antibodies. These conflicting results are of particular interest given that the role of SYK in antibody production in mature B cells and plasma cells is not defined, since constitutively SYK deficient B cells arrest at the pro-B cell stage. Several factors may account for these discrepancies, such as timing and duration of SYK inhibitor exposure, and potential differences in response to auto- or alloantigens. Notably, all of the reported non-spontaneous models, like NTN, rely on immunisation with alloantigen, or passive transfer of antibody that acts as planted alloantigen in target tissue, and so their translation to clinical autoimmunity is limited.

(i) SYK inhibition in EAG

To address these questions, I have studied the effects of SYK inhibition in EAG, the rodent model that most closely recapitulates the immunobiology and pathology of anti-GBM disease. In our laboratory, it is induced by immunising susceptible rat strains with a well-defined recombinant rat protein (α3(IV)NC1)[225], the universal Goodpasture autoantigen that is germane to human disease. Both the model and clinical disease are critically dependent on the development of autoantibodies directed against this autoantigen, and both manifest features of crescentic glomerulonephritis and alveolar haemorrhage[93,226]. EAG, therefore, can be regarded as a genuine model of autoimmunity, and since it is characterised by the ongoing production of a directly pathogenic, disease-relevant autoantibody, it more accurately reproduces clinical disease than our previous studies in NTN, and in particular allows for study of pathogenic humoral responses, in addition to renal and lung end-organ damage.

(ii) SYK inhibition in EAV

B cell depletion is an effective treatment in AAV, with effects on autoantibody production and other B cell functions likely contributing. In addition, SYK phosphorylation has been implicated in the activation of primed neutrophils by ANCA *in vitro*[182]. SYK inhibition may be an effective therapeutic strategy in AAV by inhibiting these B cell and ANCA-mediated functions. However, the role of SYK in an *in vivo* model of vasculitis has not been examined. I have therefore studied the effects of SYK inhibition using fostamatinib in experimental autoimmune vasculitis, in collaboration with Dr Anisha Tanna and Dr John McDaid.

(iii) SYK expression in human glomerular disease

Finally, there is limited direct evidence implicating SYK in the pathogenesis of human glomerulonephritis. I have therefore used an immunohistochemistry based approach on clinical biopsy specimens, to establish if SYK is expressed and activated in these diseases, and to correlate the presence of SYK staining to features of disease severity.

CHAPTER TWO - MATERIALS AND METHODS

2.1 General reagents and buffers

Unless otherwise stated, laboratory chemicals were purchased from Sigma-Aldrich (Poole, UK), plastic consumables from Becton Dickenson (BD) Biosciences (Oxford, UK), tissue culture plastic-ware from Corning (Corning, New York) and tissue culture media from Gibco, Life Technologies (Paisley, UK). Microcentrifuge tubes were supplied by Eppendorf (Hamburg, Germany). Specific materials and their source are described in the relevant sections below. Table 2.1 summarises the constituents of commonly used buffers and reagents.

Phosphate Buffered Saline (PBS)		**Cell lysis buffer**	
NaCl	8g/l	NP40 detergent	1%
KCL	0.2g/l	Tris pH 7.5	25mM
$Na_2HPO_4.2H_2O$	1.44g/l	NaCl	150mM
$K(HPO_4)_2$	0.2g/l		
Tri-Buffered Saline (TBS)		**Running buffer for SDS-PAGE**	
Tris-HCl	7.88g/l	Tris-base	3.03g/l
NaCl	8.76g/l	Glycine	14.4g/l
Adjust pH	7.4	SDS	1g/l
Acid elution buffer		**Transfer buffer**	
Glycine HCl	11.1g/l	Tris-Base	3.03g/l
Adjust pH	3.5	Glycine	14.4g/l
Carbonate Buffer		**5X Sample Buffer for SDS-PAGE**	
Na_2C0_3	1.59g/l	1M Tris-HCl pH 6.8	5ml
$NaHCO_3$	2.93 g/l	Sodium Dodecylsulphate (SDS)	2g
Adjust pH	9.6	dH_2O	2.5ml
		Glycerol	10ml
Rat Red Cell Lysis Buffer		Bromophenol blue 0.2%	0.1ml
NH_4Cl	8.34mg/l	±β-mercaptoethanol	2.5ml
EDTA	3.7mg/l		
$NaHCO_3$	1g/l		

Table 2.1: Constituents of commonly used buffers.

2.2 SYK inhibitors

R406, the active small molecule inhibitor of SYK, and its oral prodrug, fostamatinib disodium (R788), were provided by Rigel Pharmaceuticals (South San Francisco, California) and AstraZeneca (UK). The details of these molecules are discussed extensively in Chapter One. For clarity in reporting of results in Chapters Four and Five, the truncation 'Fosta' has been used. This is the current preferred abbreviation for publication purposes at Rigel Pharmaceuticals.

2.3 Production of α3(IV)NC1

2.3.1 Expression of α3(IV)NC1-FLAG fusion protein

Recombinant rat α3(IV)NC1 was prepared from a HEK (Human Embryonic Kidney) 293 cell line stably transfected with genes encoding the amino-terminal fragment of rat α3(IV)NC1 and the FLAG signal peptide. The FLAG signal peptide is a synthetic octapeptide of molecular weight 1013 and amino acid sequence N-Asp-Tyr-Lys-Asp-Asp-Asp-Asp-Lys-C, which allows affinity isolation of expressed fusion proteins. This cell line is co-transfected with a neomycin phosphotransferase antibiotic resistance gene, such that when it is grown in the presence of G418 disulphate, an aminoglycoside antibiotic that demonstrates toxicity to eukaryotic cells, selective growth of cells transfected with the α3(IV)NC1 construct is ensured[227]. This cell line was kindly provided by Dr John Reynolds.

'Complete' medium for HEK 293 cell line was prepared by supplementing Dulbecco's modified Eagle medium with 4500mg/l glucose and L-glutamine 580mg/ml (DMEM) with 10% foetal calf serum (FCS; Sigma), 2% penicillin and streptomycin (Gibco, Life Technologies) and G418 disulphate 600mg/l (Sigma). 'Serum-free' medium for HEK 293 cell line was prepared by supplementing DMEM with 2% penicillin and streptomycin only.

Cells were grown continuously in 15 x 2.5cm cell culture treated plastic Petri dishes for a period of approximately three months. Cells were grown to confluence in complete cell culture medium. Once confluent, the medium was aspirated, discarded (since serum-

containing medium could not be efficiently passed through affinity columns) and replaced with serum-free medium for five days, or until significant loss of confluent growth was observed. The serum-free supernatant was then collected and stored at -20°C until required for use, and the cells returned to complete medium until confluent again, and the cycle repeated.

2.3.2 Purification of α3(IV)NC1

Purification of α3(IV)NC1 was performed by running the collected supernatant through an anti-FLAG affinity column, prepared according to manufacturer instructions, and maintained at 4°C throughout. A 10ml polypropylene column (ThermoFisher Scientific, Waltham, Massachusetts) was mounted securely on a retort stand, filled with Tris-buffered saline (TBS; Table 2.1), and a porous disc floated on top of the liquid within the column. Using the reverse end of a serum separator (ThermoFisher Scientific) the disc was pushed evenly to the bottom of the column. The column was then rinsed with 0.5% Triton X-100 Surfactant-Amps Solution (ThermoFisher Scientific) in TBS; I found that the addition of surfactant was essential to remove air bubbles and thus enable efficient passage of medium through the column. After rinsing thrice in 10ml TBS, 5ml of anti-FLAG affinity gel (Sigma), provided in 50% glycerol, was mixed by gentle inversion, and added to the column and allowed to settle. The column was washed in three column volumes of TBS to remove the 50% glycerol buffer, then further washed in three column volumes of acid elution buffer (Table 2.1), with care being taken to avoid leaving the column in acid for longer than 20 minutes. Five further column volumes of TBS were then passed through the column to equilibrate for use.

500 ml of serum-free cell culture supernatant was pooled (after centrifugation at 1500 revolutions per minute [rpm] for five minutes at 4°C to remove cellular debris) and diluted 2:1 in TBS (to a final volume of 750ml). This solution was passed through the affinity column at a rate of 1-2 ml/minute, using a peristaltic pump (Masterflex, Oldham, UK), typically overnight, whilst being maintained at 4°C. The column was then washed as before with five column volumes of TBS. The bound FLAG-α3(IV)NC1 protein was then eluted in 1 ml fractions using acid elution buffer and collected in vials containing 50µl of 1M Tris-base neutralising buffer, pH 9. The concentration of the eluted fractions was measured by a spectrophotometer (Cecil Instruments, Cambridge, UK) at 280nm. Eluted fractions were stored at -20°C until required for further use.

After characterisation (see 2.3.3), pooled fractions of the α3(IV)NC1 preparation were placed in a dialysis cassette (membrane molecular weight cut-off 10,000 Daltons; ThermoFisher Scientific) and left in sterile water overnight at 4ºC to remove contaminating reagents present as a result of the purification process. The dialysis cassette was then immersed in sterile phosphate buffered saline (PBS; Table 2.1) for eight hours at 4ºC, and protein content quantified again by spectrophotometry at 280nm. The purified antigen was then aliquoted into 5ml volumes and stored at -20ºC until use.

2.3.3 Characterisation of α3(IV)NC1

Sodium Dodecylsulphate-Polyacramide Gel Electrophoresis (SDS-PAGE) and Western blotting were used to characterise recombinant rat α3(IV)NC1 antigenicity and specificity.

The collected fractions were run on a Phastsystem according to manufacturer's instructions. (General Electric [GE] Healthcare, Amersham, UK). Briefly, samples were diluted 5:1 in 5x sample buffer without β-mercaptoethanol (Table 2.1) and electrophoresed on a pre-made 12.5% polyacramide gel containing SDS (GE Healthcare). Non-reducing conditions were used in order to preserve the dimerised form of the α3(IV)NC1 peptide. Samples were then transferred onto a nitrocellulose membrane (Hybond-N, GE Healthcare) by pressing under lead overnight. The blot was then blocked with 5% milk powder (Marvel; Premier International Foods, St Albans, UK) in 0.1% Tween in PBS (PBS/T) for 30 minutes. Subsequently the blot was washed with 0.1% PBS/T three times. The blot was then incubated with an anti-FLAG M2 monoclonal antibody (Sigma) at a dilution of 1:1000 for one hour, then washed again three times in 0.1% PBS/T, then incubated with an alkaline phosphatase (ALP) conjugated anti-mouse IgG antibody (Sigma) at a dilution of 1:1000 for one hour, then washed three times in 0.1% PBS/Tween. A tablet of 5-bromo-4-chloro-3-indolyl phosphate/nitro blue tetrazolium (Sigma) dissolved in 10ml of distilled water was then used to develop the blot.

α3(IV)NC1 was also blotted with either serum from a historical EAG animal immunised with rat recombinant α3(IV)NC1 (provided by Dr John Reynolds) at a dilution of 1:10, or with serum from a patient with anti-GBM disease at a dilution of 1:100. After three washes with 0.1% PBS/T, either ALP-conjugated anti-rat IgG (Sigma) or ALP-conjugated anti-human IgG (Sigma), respectively, was added at a dilution of 1:1000 for one hour. The blot was then developed using the method above.

2.4 Animal methods

2.4.1 Animal study approval

All animal procedures were licensed by the Home Office Science Unit (personal license 70/23027 and project license 70/7104 [Prof Charles Pusey]) and conducted in accordance with the UK Animals (Scientific Procedures Act) 1986.

2.4.2 Animal husbandry

Rats were purchased from Charles River (Margate, UK) and maintained in a pathogen-free animal facility at the Central Biomedical Services Unit, Imperial College London, Hammersmith Hospital campus, in individually-ventilated cages with free access to water and standard laboratory diet. Cage occupancy varied between two to five rats per cage, depending on body weight. Table 2.2 summarises animal use for the *in vivo* studies reported in this thesis. Additional animals were used for the derivation of nephritic glomeruli, bone marrow cells and peripheral blood leucocyte preparations for *in vitro* studies as needed.

EXPERIMENT	N	STRAIN	SEX	APPROXIMATE AGE	MEDIAN WEIGHT, g (RANGE)	DURATION
EAG 1: Immunogenicity of α3(IV)NC1	11	WKY	Female	5 weeks	97g (81-108)	28 days (8 animals) 42 days (3 animals)
EAG 2: Dose response and disease beyond day 28	24	WKY	Female	7 weeks	154g (120-171)	56 days
EAG 3: Early disease in young male and female rats	16	WKY=8 LEW=8	Female=8 Male=8	4 weeks	85g (70-103)	21 days (8 animals) 28 days (8 animals)
EAG 4: SYK inhibition in EAG, Prevention study	16	WKY	Female	6 weeks	127g (107-156)	36 days
EAG 5: SYK inhibition in EAG, Established disease	16	WKY	Female	6 weeks	130g (112-155)	36 days
SYK inhibition in EAV	24	WKY	Female	5-6 weeks	118g (89-144)	42 days

Table 2.2: Summary of animals used for *in vivo* studies.

2.4.3 Induction of EAG

Disease was induced by immunising rats with recombinant rat α3I(IV)NC1 dissolved in PBS, in an equal volume of complete Freund's adjuvant (CFA; Sigma). Unless otherwise stated, a dose of 100µg α3(IV)NC1 per animal was generally used, with a maximum injection volume of 200µl, administered as 2 x 100µl injections to each thigh.

For the emulsification procedure, equal volumes of α3(IV)NC1 in the aqueous buffer and CFA were placed in a glass vial, then aspirated from the interface using an 20 gauge needle, rapidly re-expelled and re-aspirated from the interface. I found this method resulted in a rapid and reliable emulsification. To ensure the formation of an emulsion, I confirmed that a drop of the mixture remained globular when placed in water (as opposed to spreading across the surface of the water).

2.4.4 Induction of EAV

Disease was induced by immunising rats with purified human myeloperoxidase (MPO; Calbiochem, Merck Millipore, Darmstadt, Germany) reconstituted in sterile water for injection. A dose of 1600µg/kg was administered, emulsified with an equal volume of CFA (with addition of killed *Mycobacterium butyricum*, to a final concentration of 4mg/ml) as described above, with a maximum injection volume of 200µl administered as 2 x 100µl injections to each thigh. Immunised animals also received 500ng of pertussis toxin (Invitrogen, Life Technologies) in PBS intraperitoneally on day zero and day two.

2.4.5 Preparation and administration of SYK inhibitor for *in vivo* experiments

Fostamatinib was provided as the disodium salt. For *in vivo* experiments, it was reconstituted in vehicle formulation (0.1% carboxymethylcellulose, 0.1% methylparaben sodium, 0.02% propylparaben sodium, in distilled water, pH 6.5) to a concentration of 8mg/ml, sonicated for 15-20 minutes until dissolved, and then pH re-adjusted to 6.5 with 0.1M HCl. This preparation was stored at 4°C for a maximum of seven days prior to use.

Based on a previous dose-ranging study in NTN in WKY rats[136], treated animals received 20mg/kg, 30mg/kg or 40mg/kg body weight, administered by twice daily oral gavage. Control animals received an equivalent volume and schedule of vehicle formulation. Whilst undergoing gavage, animals were provided with wet laboratory diet in case of oesophageal irritation.

2.4.6 Collection of biological specimens from rats

2.4.6.1 Urine collection

For collection of urine samples, rats were housed overnight, with free access to water and standard laboratory diet, in individual metabolism cages. At the end of the collection, total urine volume was measured, and aliquots were centrifuged at 1500rpm for five minutes to sediment macroscopic debris, and stored at -80°C until use. There was a minimum 48 hour interval between urine collections, in accordance with the terms of the project license.

2.4.6.2 Serum collection

For collection of serum samples at non-terminal time-points, rats were placed in a warming chamber at 30°C to promote vasodilation, then placed under isofluorane anaesthesia on a warming mat. Whole blood (maximum volume 0.5ml) was collected by superficial tail vessel puncture using a 23 gauge needle. Samples were centrifuged at 1500rpm for five minutes, serum removed and stored at -80°C until use.

2.4.6.3 Terminal processing of blood and tissues

At the end of the study protocol, animals were placed under isofluorane anaesthesia for final collection of blood and tissues. Blood was obtained either by cardiac puncture using a 10ml pre-heparinised syringe and a 23 gauge needle, or by transection of the great vessels and exsanguination into both plain and heparinised collection tubes.

Tissues were dissected out after the animal had been sacrificed by exsanguination. When necessary, lung haemorrhage score (section 2.5.6) was documented by inspection of the lung surfaces before dissection of these organs. For each animal, a coronal mid-pole section of kidney, and a sample of lung, spleen and liver tissue was placed in a histology cassette and transferred to 10% neutral buffered formalin for fixation. A remaining kidney pole was placed in OCT (optimal cutting temperature compound) embedding matrix (ThermoFisher Scientific) on a cork disc, immersed in isopentane and then snap frozen in liquid nitrogen,

and stored at -80°C until use. The remaining kidney material, and a sample of lung tissue and spleen tissue were snap frozen in individual cryovials and stored at -80°C until use.

2.5 Analysis of renal and lung injury in EAG and EAV

2.5.1 Haematuria analysis

Haematuria was quantified by dipstick analysis (Multistix 8 SG, Siemens Healthcare Diagnostics, Tarrytown, New York), and expressed as 0 (negative), 0.5 (trace), 1+, 2+ or 3+ for each animal.

2.5.2 Biochemical analysis of serum and urine

Concentrations of urea and creatinine in serum and urine samples were kindly measured by Dr Olatunji Rowland and Dr John Morris in the Department of Clinical Biochemistry, Hammersmith Hospital UK, using an AU700 analyser (Olympus, Southend, UK). Urinary clearance of each marker was calculated using the following equation: urinary clearance per unit time = (urine concentration x urine volume per unit time)/serum concentration.

Proteinuria was quantified using sulphosalicylic acid method. Urine samples, diluted between 1:3 and 1:100 in water, were added to a 96-well microtitre plate in triplicate, to which 10µl of 25% sulphosalacylic acid was added to two of three replicates, and 10µl of water to the third replicate (providing a 'blank' reading for that sample). Known quantities of bovine serum albumin (BSA; Sigma) in water were used to define a standard curve, and absorbance read at 450nm on microplate reader and dedicated software (Biotek EL800; Gen5 Analysis Software; both Biotek Instruments Ltd, Potton, UK). The protein concentration in each sample was

calculated from a regression equation described by the standard curve, and the 24 hour protein excretion rate was calculated by multiplying by the total urine volume. Urinary protein creatinine ratio was calculated by dividing the urinary protein concentration by the urinary creatinine concentration.

2.5.3 Haematological analysis

Haemoglobin concentrations and white blood cell and platelet counts were measured in heparinised whole blood samples using an automated analyser (XE-2100, Sysmex, Milton Keynes, UK) in the Department of Clinical Haematology, Hammersmith Hospital UK.

2.5.4 Renal histology

Kidney tissue collected at the time of sacrifice was fixed in 10% neutral buffered formalin overnight, then transferred to 70% ethanol and processed to paraffin blocks. 4μm sections were cut on a rotary microtome and stained with haematoxylin and eosin (H&E), periodic acid Schiff (PAS), and Jones methanamine silver stain, for assessment of renal injury. Sectioning and staining was performed by Ms Lorraine Lawrence, Department of Leucocyte Biology, Imperial College London (except Silver stain, performed by Dr Donna Horncastle, Department of Histopathology, Hammersmith Hospital).

For quantification of renal histology in EAG, 50 consecutive glomeruli were assessed by light microscopy in a blinded fashion, and graded as severely abnormal (>50% of the glomerular tuft affected by necrosis, crescent formation or sclerosis), abnormal (any abnormality not meeting the criteria for 'severe') or normal. Results are expressed either as the percentage of severely affected glomeruli per animal, or as the mean percentage of normal, abnormal and severely abnormal glomeruli per group.

For quantification of renal injury in EAV, 50 consecutive glomeruli were assessed by light microscopy in a blinded fashion, and graded as normal or abnormal. Results are expressed as the percentage of abnormal glomeruli per animal.

2.5.5 Immunohistochemistry for leucocyte markers

Immunostaining for ED1 and CD8 positive cells was performed on formalin-fixed paraffin embedded kidney sections. For details of immunostaining methods, see section 2.10.

CD8 positive cell infiltrate was quantified in a blinded fashion by counting the number of CD8 positive cells in 50 consecutive glomeruli in each section, and expressed as the mean number of cells per glomerular cross section (GCS) for each animal. ED1 positive cell infiltrate was quantified in a blinded fashion using automated image analysis software (ImagePro Plus, Media Cybernetics, Rockville, Maryland) to measure the percentage of glomerular staining in 20 consecutive glomeruli in each section, and expressed as the mean percentage stain per GCS for each animal.

2.5.6 Macroscopic assessment of lung injury

Based on observations in preliminary experiments in EAG, I developed a semi-quantitative scoring system that could be used to grade the severity of lung haemorrhage by visual inspection at the time of cull. Lungs were graded as follows: 0 points – normal macroscopic lung appearances; one point if fewer than ten petechiae were visible; two points if ten to 20 petechiae were visible; three points if more than 20 petechiae were visible; four points if large areas of infarction or haemorrhage were evident. Representative lung appearances are shown in Figure 2.1. The same scoring system was used for assessment of lung injury in EAV.

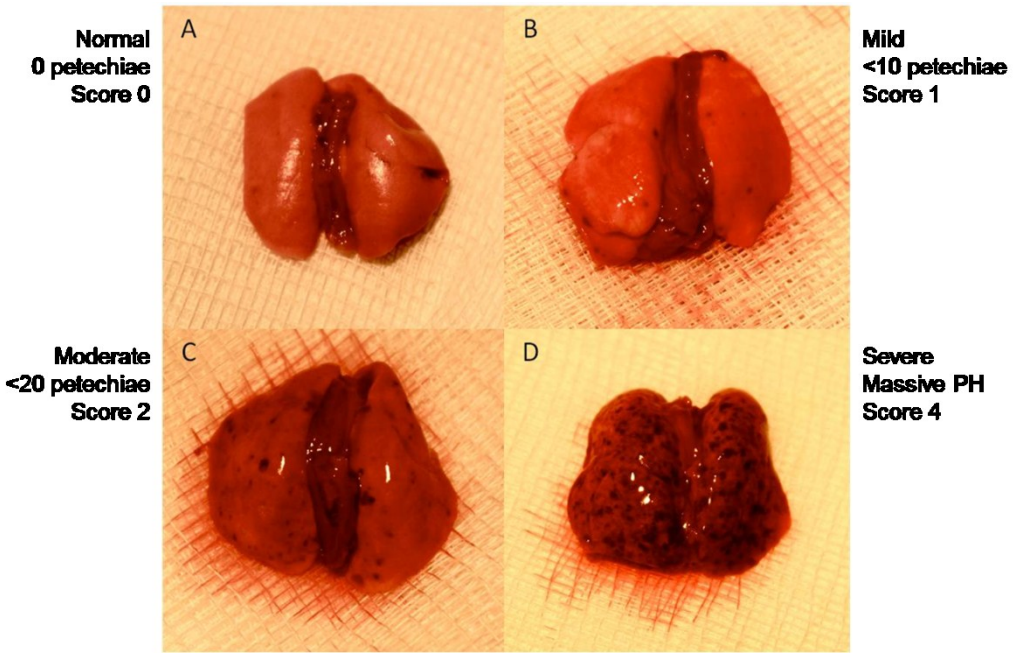

Figure 2.1: Scoring system to quantify lung haemorrhage (LH) severity.
The lungs surfaces were inspected at the time of sacrifice, and scored in accordance with the number of visible petechiae on the lung surface: zero points – normal macroscopic lung appearances (Panel A); one point if fewer than ten visible petechiae (Panel B); two points if ten to 20 visible petechiae (Panel C); three points if more than 20 visible petechiae (not shown); four points if large areas of infarction or haemorrhage were evident (Panel D).

2.5.7 Microscopic scoring of lung injury

Lung tissue was collected for histological analysis and processed as per kidney tissue (section 2.5.4). 4μm paraffin-embedded sections were stained with Perls' Prussian blue (by Ms L Lawrence) without counterstain, to enable identification of haemosiderin-laden cells. These were quantified by a blinded observer using automated image analysis software (ImagePro Plus) to measure the proportion of Perls' stained cells across five random high-power fields of lung sections from each animal, and expressed as the mean proportion per high power field per animal.

2.6 Assessment of humoral responses

2.6.1 ELISA for α3(IV)NC1 antibodies in EAG

The concentration of anti-α3(IV)NC1 antibodies in rat sera was measured by direct enzyme linked immunosorbent assay (ELISA)[225,226]. Recombinant rat α3(IV)NC1 was diluted in carbonate buffer and coated onto 96 well ELISA plates (Nunc, Roskilde, Denmark) at a concentration of 5µg/well (with one uncoated well per two coated wells to provide a 'blank' reading for each sample duplicate). The plates were left overnight at 4ºC, and then washed with 0.1% PBS/T three times. 3% BSA was then applied and the plate incubated for one hour at 37ºC, in order to block non-specific binding sites, followed by another series of washing. Rat sera were diluted in PBS, and added to wells in triplicate. The plate was incubated for one hour at 37ºC, followed by a series of washing. An ALP-conjugated goat anti-rat IgG (Sigma) diluted 1:1000 in PBS was added to each well, and the plate incubated for one hour at 37ºC, followed by a series of washing. The plate was then developed using p-nitrophenyl phosphate solution (Sigma) and read at 405nm using a microplate reader. In initial experiments, results are reported as optical density at 405nm. For subsequent experiments, sera from preliminary experiments with a high titre of anti-α3(IV)NC1 antibodies were pooled, and serial dilutions used to develop a one-site binding hyperbole standard curve, from which subsequent results were interpolated using the regression equation described by the curve, and expressed in arbitrary units. An example curve is shown in Figure 2.2. A co-efficient of variance of 10% between sample replicates was accepted. The pooled sera were stored at -80°C in 10-20µl aliquots and each aliquot was used once to avoid repeated freeze-thaw cycles.

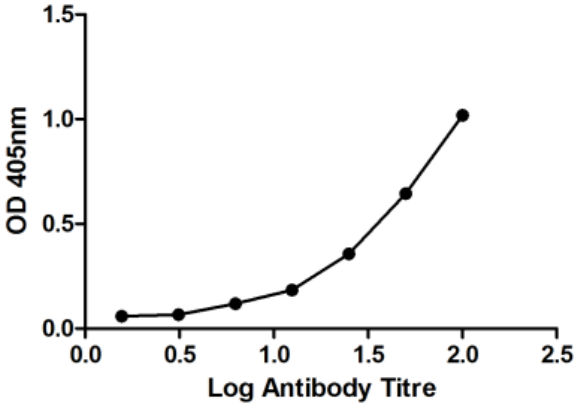

Figure 2.2: Representative standard curve for anti-α3(IV)NC1 antibody ELISA..

2.6.2 Bead-based assay for anti-glomerular basement membrane (GBM) antibodies

Reactivity of sera from α3(IV)NC1-immunised rats to GBM was confirmed by using a commercially available bead-based assay, usually intended for use on clinical samples, but modified for detection of rat IgG (FIDIS Vasculitis Luminex panel, Theradiag, Marne La Vallee, France). This assay uses fluorescently labelled beads coated with bovine GBM, which serve to 'capture' anti-GBM antibodies in serum samples. A secondary antibody, labelled with a distinct fluorochrome, is then used to detect and quantify bound sample by flow cytometry. Since the α3(IV)NC1 'universal' Goodpasture epitope is highly conserved between species, rat anti-α3(IV)NC1 antibodies should recognise this epitope in bovine GBM. The standard kit uses a phycoerythrin- (PE-) labelled anti-human IgG secondary antibody, which I substituted with a PE-labelled anti-rat antibody (Miltenyi Biotech, Cologne, Germany). The kit also includes beads coated in the anti-neutrophil cytoplasm antibody (ANCA) target antigens, MPO and proteinase-3 (PR3). These served as negative control assays for rat samples, to confirm that binding of rat anti-α3(IV)NC1 antibodies was

specific, and not due to non-specific binding of rat IgG to the beads. Rat serum samples were diluted 1:100 in the provided assay diluent, and 100µl added to 50µl of bead mix (including GBM, MPO and PR3 coated beads) in wells of 96-well filter plate, and incubated for one hour at room temperature. Excess diluent and sample was removed from the wells by vacuum suctioning, and 300µl of the provided wash buffer added to each well, then removed by vacuum suctioning. 100µl of secondary antibody (PE-labelled goat anti-rat IgG diluted 1:50 in assay diluent) was then added to each well for one hour. The beads were washed as before, resuspended in 200µl assay diluent, and data acquired on a dedicated flow cytometer (Luminex 200, LuminexCorp, Austin, Texas). Data are reported as the mean fluorescence intensity (MFI) for PE detection per sample. This work was conducted in the Clinical Immunology laboratory at Charing Cross Hospital, London UK, with the assistance of Dr Angela Hall and Dr Dipti Patel.

2.6.3 Direct immunofluorescence for deposited antibodies and complement in EAG

IgG and C3 deposited in the glomeruli were assessed by direct immunofluorescence using snap frozen renal tissue obtained at the time of cull. Frozen kidney sections were cut on a cryostat at 5µm thickness and placed on poly-L-Lysine coated slides (Leica Biosystems, Milton Keynes, UK). After fixation in acetone for ten minutes, the slides were air dried. If not used immediately, the slides were stored at -80°C in sealed boxes containing silica crystals. The slides were blocked with 20% normal rabbit serum (Dako, Ely, UK) for 30 minutes at room temperature. After washing in PBS, the slides were incubated with FITC (fluorescein isothiocyanate)-conjugated rabbit anti-rat IgG (Sigma) at 1:100 dilution in PBS, or with FITC-conjugated goat anti-rat C3 (Nordic MUbio, Susteren, The Netherlands) at 1:10

dilution, for one hour at room temperature in a humidified chamber. Following two ten minute washes in PBS, the sections were mounted in PBS/Glycerol (Citifluor, London, UK). For quantification, 20 consecutive glomeruli on each section were inspected by fluorescence microscopy in a blinded fashion. For deposited IgG and C3 in EAG, the degree of immunofluorescence was graded from 0 to 3+, with results expressed as the mean intensity per glomerulus for each animal. For deposited IgG in EAV, automated image analysis was used to calculate fluorescence intensity throughout each glomerulus, in arbitrary units, and expressed as the mean intensity per glomerulus for each animal. Automated image analysis was used in EAV since the granular pattern of pauci-immune deposition was difficult to quantify by visual inspection alone (unlike the clearly linear pattern observed in EAG).

2.6.4 B cell ELISpot assays in EAG

The B cell ELISpot assay provides a method to enumerate antigen-specific antibody-producing cells. Filter-plate wells are coated in the antigen of interest, to which a cell suspension is added. Antibodies produced by antigen-specific cells in this suspension bind to antigen in the region of the cell, and are then detected using a labelled-secondary system. This method was adapted from the protocol for a commercially available kit designed for use in mice (Mabtech AB, Nacka Strand, Sweden).

After sacrifice of animals, spleens were harvested, kept on ice-cold Hank's balanced salt solution (HBSS; Gibco, Life Technologies) and transferred to the tissue culture hood. Splenocytes were obtained by passing whole spleen tissue through 100µm filters (BD

Biosciences) in cold sterile PBS. Following red blood cell lysis in buffer (Table 2.1) and three washing-resuspension cycles in sterile PBS (centrifuged at 1500rpm for five minutes at 4°C) cells were divided for use either in B cell ELISpot assays or for flow cytometry (section 2.6.5).

For B cell ELISpot assays, the cells were resuspended in Roswell Park Memorial Institute medium (RPMI) supplemented with 10% FCS, 2% penicillin and streptomycin, 2mM L-glutamine (Invitrogen, Life Technologies), to a final concentration of 1-10 million cells/ml. 100µl of cell suspension (containing 10^5 to 10^6 cells; eight replicates per animal) was then added to wells of ELISpot plates (Multiscreen HTS 96 well filter plates; Merck Millipore) that had previously been coated with recombinant rat α3(IV)NC1 by incubating at a concentration of 50µg/ml in sterile PBS at 4°C overnight, and blocked with 10% FCS in RMPI for one hour at 37°C. Cells were then incubated at 37ºC in 5% CO_2 for 12-48 hours *without moving*. After five washes in PBS (*no* Tween), the ELISpot plates were incubated with a biotinylated polyclonal rabbit anti-rat immunoglobulin secondary antibody (Dako; dilution 1:250) at room temperature for two hours. Following a further wash cycle, the plates were incubated with an Extravadin-ALP conjugate (Sigma; dilution 1:1000) for one hour at room temperature, washed again, and finally developed in 5-bromo-4-chloro-3-indolyl phosphate/nitro blue tetrazolium (BCIP-NBT) solution (Sigma). Membranes were dried, and the number of spots in each well, corresponding to antigen-specific antibody producing cells, was quantified using an ELISpot plate reader and dedicated software (ELISpot 4.0, Autoimmun Diagnostika, Strassberg, Germany).

For inhibitor studies, splenocytes were incubated with R406, prepared as described in section 2.7.1, for 30 minutes prior to plating into ELISpot wells. For assessment of cell viability at the end of inhibitor studies, splenocytes were incubated under identical conditions in standard 96 well culture dishes (since cells could not be retrieved from ELISpot plates), then counted using trypan blue exclusion method on a haemocytometer at the end of the experiment.

2.6.5 Flow cytometry

Splenocytes were obtained as above, resuspended in PBS to a concentration of 10^6 cells per 100µl in wells of a 96-well round-bottomed microtitre plate, and stained with the following antibodies with a volume of 1µl per 10^6 cells, for 30 minutes in the dark: CD45RA-PE (OX-33; BD Biosciences); CD8-PECy7 (OX8; eBiosciences, Hatfield, UK); CD4-FITC (W3/25; eBiosciences). Cells were washed in PBS and centrifuged at 2000rpm for five minutes at 4°C, twice, and fixed with 100µl 3% paraformaldehyde (PFA) in PBS for 30 minutes. Cell suspensions were then passed through a 70um cell strainer into polypropylene tubes, centrifuged at 2000rpm for five minutes, resuspended in 100µl PBS, and run on a BD Accuri C6 flow cytometer (BD Biosciences). Analysis was performed on FlowJo X software (Tree Star, Olten, Switzerland).

2.6.6 ELISA for MPO antibodies in EAV

Anti-MPO antibody levels in rat sera were measured using direct ELISA[212,213], using a method similar to that used to detect anti-α3(IV)NC1 antibodies in EAG. Wells were coated

with purified human MPO (Calbiochem) at a concentration of 1.33µg/ml in carbonate buffer and stored at 4°C overnight. The following day, plates were washed three times in 0.1% PBS/T, and non-specific binding sites blocked by incubating the wells with 1% BSA in 0.1% PBS/T for one hour. After three washes in 0.1% PBS/T, 100µl of serum samples (diluted 1:100 to 1:100000 in PBS/T plus 1% BSA) were applied in duplicate, with a negative control 'blank' that did not contain serum. Plates were incubated at 37°C for one hour and then washed three times in 0.1% PBS/T. 100µl of rabbit anti-rat IgG with ALP conjugate in 0.1% PBS/T plus 1% BSA (dilution 1:1000) was then added for one hour at 37°C. After a wash cycle in 0.1% PBS/T, 100µl of p-nitrophenyl phosphate was applied to each well. The colour change was monitored, and then quantified on a microplate reader at 405nm. A co-efficient of variance of 10% between sample replicates was accepted. As before, istorical pooled sera were used to develop a standard curve from which subsequent samples could be assigned an interpolated value in arbitrary units,

2.6.7 Indirect immunofluorescence for anti-MPO antibodies

Rat red cell lysis buffer (Table 2.1), filtered and centrifuged at 2400rpm for five minutes to remove particles, was added to whole rat peripheral blood at a ratio of 2:1 (buffer:blood) and incubated for ten minutes on ice, with intermittent mixing, then centrifuged at 1500rpm for five minutes. Cells were resuspended in PBS to a concentration of 50 000 cells/ml, and 100µl of cell suspension applied to coated slides (Leica) using a cytospin centrifuge (450rpm for six minutes; Cytospin 2, Shandon, ThermoFisher Scientific). After drying, slides were fixed in 100% acetone, dried, then stored in sealed boxes with silica crystals at -80°C until use.

For indirect immunofluorescence, slides were thawed and rinsed in PBS, then blocked in 20% rabbit serum (Dako) for 30 minutes. Rabbit serum was tapped off, and serum from EAV and control rats (1:20 dilution in PBS) applied for 30 minutes in a covered humidified chamber. Slides were washed thrice in PBS, then incubated with a secondary rabbit anti-rat IgG FITC (1:100) for 30 minutes, washed again, mounted in PBS/Glycerol (Citifluor) and inspected immediately by fluorescence microscopy.

2.7 *In vitro* methods

2.7.1 Preparation of SYK inhibitor for *in vitro* studies

R406 was provided at the besylate salt. This was dissolved in sterile-filtered DMSO (dimethyl sulphoxide; Sigma) to a stock concentration of 10mM and stored in 10-100µl aliquots at 4°C until use. For cell culture experiments, the stock solution was serially diluted in cell culture medium, to avoid precipitation, to the desired concentration of R406 in a final concentration of 0.1% DMSO.

2.7.2 Nephritic glomeruli *ex vivo*

Glomeruli were extracted from untreated animals 28 days after induction of EAG, using a variation of the method described by Krakower and Greenspon in 1951[228,229]. After sacrifice, kidneys were harvested, kept in ice-cold sterile HBSS and taken to the tissue culture hood. The kidney capsule was removed and the kidney dissected into pieces, then passed through a 250µm stainless steel sieve using the plunger from a 10ml syringe. The sieved material was then passed sequentially through 125µm and 75µm sieves using ice-cold PBS. With this process, connective tissue and tubular fragments are retained by the first two sieves, whereas glomeruli are retained by the final sieve. Using a Pasteur pipette and small volumes of PBS, glomeruli were rinsed from the final sieve into a 50ml centrifuge tube. After three wash-resuspension cycles in ice-cold PBS (centrifuged at 500rpm for five minutes at 4°C), glomeruli were resuspended in complete cell culture medium (RPMI supplemented with 10%

FCS, 2% penicillin and streptomycin, 2mM L-glutamine). All glomeruli obtained from a single rat were then divided in equal proportion to wells of 24-well cell culture dishes in the following conditions at a final volume of 500µl: vehicle (0.1% DMSO in complete culture medium), and 0.2µM, 1µM and 2µM R406 in vehicle. Glomeruli were incubated for 48 hours and culture media collected for analysis of cytokine levels, as described below (section 2.9). Since the yield of glomeruli from each rat was variable, results were normalised to vehicle conditions, to allow comparison of each biological replicate.

2.7.3 Culture of L929 cell line

L929-conditioned medium, rich in macrophage colony stimulating factor (M-CSF) that can be used to drive differentiation of rat bone marrow cells[230], was prepared by growing a murine fibroblast cell line, available in our laboratory, in DMEM supplemented with 10% FCS, 2mM L-glutamine, and 2% penicillin and streptomycin. Once cells were confluent, the medium was collected and stored at -20°C until use.

2.7.4 Culture of bone marrow derived macrophages (BMDM)

After sacrifice, rat femurs were isolated and transferred to the tissue culture hood in ice-cold sterile HBSS solution. The bones were cleaned of hair and soft tissue, washed twice in 70% ethanol, and rinsed again in HBSS. Both ends of the cleaned bones were then cut, and bone marrow cells flushed out with a 20 gauge needle using 10ml of cold HBSS per bone, and collected into a 50ml centrifuge tube. Cells were then centrifuged at 1500rpm for five

minutes at 4°C, and re-suspended in 10ml HBSS buffer. The 50ml centrifuge tube was then placed in the CO_2 incubator in a horizontal position for 10min to hypotonically lyse red blood cells. The cells were then centrifuged at 1500rpm for five minutes at 4°C, the supernatant aspirated, and the cell pellet re-suspended in DMEM containing 25mM HEPES (hydroxyethyl piperazineethanesulfonic acid), 25% L929 cell line conditioned medium, 25% FCS, 2mM L-glutamine, and 2% penicillin and streptomycin. The bone marrow cells were cultured in 15cm non-treated cell culture Petri dishes (Sterilin, Newport, UK) for seven days. Following dissociation (using non-enzymatic buffer for 30 minutes; Biological Industries, Kibbutz Beit-Haemek, Israel), cells were counted on a haemocytometer and re-plated either (i) to 96-well culture dishes at a density of 10^5 cells per well, to obtain cell culture supernatants for analysis of secreted cytokines by ELISA, or (ii) to 6-well culture dishes at a density of 10^6 cells per well, to obtain cell lysates for analysis of intra-cellular proteins by Western blot. After re-plating, cells were left to adhere overnight in full culture medium. The following evening (day 8), cells were serum-starved overnight prior to any stimulation (on day 9).

2.7.5 Stimulation of BMDM

For SYK inhibitor studies, cells were pre-incubated with vehicle (0.1% DMSO in serum-free culture medium) or 0.2μM, 1μM and 2μM R406 in vehicle for 30 minutes. For stimulation, whole rat IgG (Sigma) was dissolved in sterile saline, heat-aggregated by placing in a heating block at 63°C precisely for 20mins, and centrifuged at 135 000rpm for five minutes (a method modified from that originally described by Hora *et al*, and previously used in our laboratory[136,231,232]). The supernatant was removed and reconstituted to a final concentration

of 250μg/ml in serum-free cell culture medium, and used to stimulate BMDM. For analysis of secreted cytokines, experiments were conducted in technical (cell culture) triplicate and (at least) biological duplicate. Supernatants were collected after 24 hours and cytokine levels assayed as described below (section 2.9). For analysis of intra-cellular proteins by Western blot, biological duplicate experiments were performed, and cells lysates were collected 0-30 minutes after stimulation as described below (section 2.8).

2.7.6 MTT assay

MTT (3-[4,5-dimethylthiazol-2-yl]-2,5 diphenyl tetrazolium bromide) assays were performed to assess cell viability at the end of cell stimulation experiments. Viable and metabolically active cells reduce MTT, a yellow tetrazole dye, to a coloured soluble formazan (purple) product, the absorbance of which at 550nm is directly proportional to the number of living cells present in the culture system. It can thus be employed to assess viability or proliferative responses to substances under test[233]. After medium was collected for cytokine analysis, fresh medium containing 0.5mg/ml MTT was added to each well, and cells incubated overnight. The following day, the media were removed and the remaining crystals dissolved in isopropanol with 0.1% Triton, and absorbance read at 550nm.

2.8 Western blot

2.8.1 Cell lysate preparation

At the defined time-points after cell stimulation with heat-aggregated IgG, the cell culture plate was transferred to ice, the culture medium removed, and the cell monolayer was washed in ice-cold PBS. 150µl of cell lysis buffer (Table 2.1; supplemented immediately before used with protease inhibitor cocktail [ThermoFisher Scientific] and 1mM sodium vanadate) was added to each well, and the plate kept on ice and agitated for 20 minutes to ensure complete lysis. Lysates were transferred to microcentrifuge tubes and clarified by centrifugation (135 000rpm for seven minutes at 4°C). The supernatants were transferred to fresh tubes, diluted in 5x sample buffer with β-mercaptoethanol (Table 2.1) and boiled for five minutes on a heating block at 95°C, then rapidly cooled and stored at -80°C until use.

2.8.2 SDS-PAGE

Samples were resolved by SDS-PAGE. Resolving and stacking gels were prepared as summarised in Table 2.3. Electrophoresis was performed using the Hoefer SE 600 Ruby Vertical Electrophoresis Unit (GE Healthcare). Two clean glass plates were opposed in a casting block, separated by 1.5mm diameter spacers. The resolving gel (activated immediately before pouring by addition of TEMED [Tetramethylethylenediamine]) was poured between the plates and left for 20 minutes to set. Immediately after pouring, the gel was covered by a shallow depth of water- to exclude air and level the surface. Once set, the

water layer was poured off and the gel surface blotted dry, and stacking gel added (activated immediately before pouring by addition of TEMED). A 1.5mm 14 well comb was carefully inserted into the stacking gel before leaving to set for one hour. Once polymerised, the stacking gel has a large pore size allowing proteins to concentrate rapidly at the stacking gel–resolving gel interface, allowing proteins to separate by size in the resolving gel. The comb was then removed, excess gel carefully cleaned away with a needle and the casting block placed into the gel electrophoresis tank submerged in running buffer.

	10% Resolving Gel	**5% Stacking Gel**
30% acrylamide-bisacrylamide	3.4ml	1.7ml
1M Tris pH 8.8 0.1% SDS	3.75ml	-
1M Tris pH 6.8 0.1% SDS	-	1.25ml
dH_2O	2.8ml	6.9ml
10% APS (ammonium persulfate)	100ul	100ul
TEMED* (Tetramethylethylenediamine)	10ul	10ul
Volumes given to prepare 10ml of gel *added immediately before pouring		

Table 2.3: Preparation of resolving and stacking gels for SDS-PAGE.

2.8.3 Sample preparation and electrophoresis

Samples were thawed and boiled again for five minutes on a heating block at 95°C. Heating, in tandem with β-mercaptoethanol in the sample buffer, acts as a potent reducing agent,

breaking disulphide bonds and linearising proteins so that subsequent electrophoretic separation is governed by molecular weight alone. Samples and a marker protein ladder (Kaleidoscope Pre-stained Standards; BioRad, Hercules, California) were loaded onto the gel taking care not to cross-contaminate between lanes. The gel tank was connected to a power supply and the gel run at 100 volts for approximately ten hours.

2.8.4 Transfer to nitrocellulose membrane

Adequate separation of proteins was confirmed by inspection of the coloured ladder markers before halting electrophoresis. The Transphor-4 Cassettes and Cooler system (GE Healthcare) was used for transfer of proteins to nitrocellulose. The glass plates were removed from the casting block and immediately submerged in transfer buffer. A sheet of nitrocellulose membrane (Hybond-N; GE Healthcare) was cut to size and soaked in transfer buffer. Four sheets of filter paper, cut to the size of the gel, were also soaked in transfer buffer. The stacking gel was discarded and a 'sandwich' formed within the gel-holder cassette comprising: one foam pad, two sheets of filter paper, the nitrocellulose membrane, resolving gel, two sheets of filter paper, one foam pad. Any trapped air bubbles were removed by rolling with a plastic pipette.

The cassette was then inserted into the transfer tank adjacent to a cooling unit, the tank filled with transfer buffer, and a charge of 80 volts applied for 1.5 hours. The membrane was removed and transferred to wash buffer solution (0.1% Tween in TBS; TBS/T). Adequate transfer of protein was confirmed by visual inspection of coloured ladder protein transfer.

2.8.5 Blocking and antibody application

For detection of phospho-proteins, the membrane was transferred to a solution of 2% BSA in 0.1% TBS/T and placed on a rocker for one hour in order to block non-specific protein binding sites. The blocking solution was poured off and the membrane washed briefly with wash buffer before adding the relevant primary antibody (Table 2.4) and placing on a rocker either for one hour at room temperature or overnight at 4°C. The membrane was then washed three times (1 x 15 minutes, 2 x 5 minutes) in wash buffer before incubating with a species-specific horse-radish peroxidase (HRP)-linked secondary antibody (Table 2.4) for one hour. The membrane was then washed three times, as before, in preparation for the detection step.

For detection of the corresponding total proteins, the membrane previously immuno-probed for the phospho-protein was incubated in stripping buffer (Western blot Re-probe Reagent; Calbiochem) for 30 minutes at room temperature on a rocker, then washed thrice as before in 0.1% TBS/T. The membrane was then blocked (in 5% dry milk powder in 0.1% TBS/T) and incubated with the relevant primary and secondary antibodies (Table 2.4) as above.

TARGET	PRIMARY ANTIBODY	SECONDARY ANTIBODY	BLOCKING SOLUTION/ANTIBODY DILUENT
Phosphorylated SYK	P-SYK Try525/526 Cell Signaling #2711 Rabbit polyclonal 1:1000	Goat anti-rabbit IgG-HRP BioRad 1:5000	2% BSA in 0.1% TBS/T
Phosphorylated JNK	Clone JNK-PT48 Sigma Mouse monoclonal 1:1000	Goat anti-mouse IgG-HRP BioRad 1:5000	2% BSA in 0.1% TBS/T
Phosphorylated p38	Clone P38-TY Sigma Mouse Monoclonal 1:1000	Goat anti-mouse IgG-HRP BioRad 1:5000	2% BSA in 0.1% TBS/T
Total SYK	SYK-N19 Santa Cruz #1077 Rabbit polyclonal 1:1000	Goat anti-rabbit IgG-HRP BioRad 1:5000	5% milk powder in 0.1% TBS/T
Total JNK	Clone JNK-FL Santa Cruz Rabbit polyclonal 1:1000	Goat anti-rabbit IgG-HRP BioRad 1:5000	5% milk powder in 0.1% TBS/T
Total p38	Clone C-20 Santa Cruz Rabbit polyclonal 1:1000	Goat anti-rabbit IgG-HRP BioRad 1:5000	5% milk powder in 0.1% TBS/T

Table 2.4: Summary of antibodies used for Western blot.

2.8.6 Chemiluminescence and signal detection

The chemiluminescence reaction was used for detection of bound antibody. The enhanced chemiluminescence kit (ECL; GE Healthcare) used in this step consists of two reagents: hydrogen peroxide and luminol. These were mixed in a 1:1 ratio prior to use and applied directly to the membrane lying on a cellophane sheet. The membrane was incubated in ECL

medium for approximately one minute before gently tapping off and wrapping the membrane in the cellophane sheet. The membrane was placed in a photographic cassette and transferred to the dark room where it was exposed against x-ray film (Hyperfilm ECL; GE Healthcare) and developed using an automatic film processor (SRX-101A, Konica Minolta, Osaka, Japan).

In the presence of an oxidising agent (produced by decomposition of hydrogen peroxide by HRP), luminol is converted to an excited state and chemiluminesces as this species decays. This chemiluminescence is proportional to the amount of HRP present, and consequently the abundance of target protein, and can be detected with great sensitivity using high performance x-ray film. After development of the exposed x-ray film, the target protein(s) can be seen as discrete bands and the identity confirmed by comparing the molecular weight with those of the marker ladder proteins. Relative abundance of protein between samples was assessed by visual comparison of band size and density, and by densitometry using image analysis software (ImageJ) on scanned immunoblot images (acquired using a Desktop Scanner; AOI 922, Dell, Round Rock, Texas).

2.9 Analysis of cytokines

2.9.1 Monocyte chemoattractant protein 1 (MCP-1)

MCP-1 concentrations in cell culture supernatants were measured using a commercially available sandwich ELISA development kit (OptEIA Rat MCP-1 ELISA Set, BD Biosciences) used according to the manufacturer's instructions. A 96-well ELISA plate (Nunc) was coated with 100µl of capture antibody at a dilution of 1:250 in carbonate buffer, sealed and stored overnight at 4°C (or for a maximum of four days) until use. For use, the capture antibody solution was removed, wells washed thrice in 0.1% PBS/T, and 200µl of assay diluent (10% FCS in PBS) was added to each well for one hour at room temperature to block non-specific binding sites on the surface of the plate. After three washes in 0.1% PBS/T, 100µl of samples (neat or diluted up to 1:5000 in assay diluent, as necessary), known standards and negative control samples (containing assay diluent alone) were added to wells in duplicate and incubated for one hour at room temperature. After three further washes in 0.1% PBS/T, 100µl of assay diluent containing biotinylated detection antibody (1:500) and streptavidin-HRP conjugate (1:250) was added to each well for one hour, and wells washed five times. A solution of 3,3',5,5'-tetramethylbenzidine (TMB; Cambridge Bioscience, Cambridge UK) and hydrogen peroxide was prepared, and 100µl added to each well. TMB is colourless in solution in basal conditions but forms a blue product when oxidised by HRP in the presence of hydrogen peroxide, the colour intensity of which is proportional to the degree of HRP activity and, in turn, the amount of bound secondary antibody. The plate was incubated in the dark for approximately ten minutes before stopping the reaction by adding 50µl of 2M sulphuric acid. This final step yields a yellow colour change, proportionally

identical in intensity to its blue counterpart. The absorbance was measured at 450nm on a microplate reader. Adjusted absorbance was calculated by subtracting the background absorbance of the 'blank' sample. A best-fit standard curve was generated from the absorbances of the recombinant MCP-1 reference series using four variable non-parametric regression modelling. Concentrations of MCP-1 in samples could then be calculated from the raw blank-subtracted absorbances using the resultant regression equation. A co-efficient of variance of <10% between sample replicates was accepted.

2.9.2 Interleukin 12 (IL-12)

Concentrations of IL-12 in cell culture supernatants were measured using a commercially available sandwich ELISA kit (Rat IL-12+p40 ELISA Kit, Invitrogen, Life Technologies) used according to the manufacturer's instructions. 100µl of samples (neat), known standards and negative control samples were added in duplicate to 8-well strips pre-coated with capture antibody. 50µl of the provided incubation buffer was added to standards and control sample wells, 50µl of the provided assay diluent was added to sample wells, then the strips were sealed and incubated for two hours at room temperature. Standards and samples were expelled and the wells washed thrice in the provided wash buffer. 100µl of the provided biotinylated anti-IL-12 solution was added to each well and incubated for one hour at room temperature. The wells were washed a further three times and 100µl of streptavidin-HRP added to each well for 30 minutes at room temperature. After five washes, 100µl of the provided chromagen solution was added to each well. This solution is equivalent to TMB and hydrogen peroxide in the MCP-1 ELISA process, and the wells were processed and read in an identical manner from this point forward.

2.9.3 Tumour necrosis factor alpha (TNF-α)

TNF-α concentrations in cell culture supernatant were assayed using a commercially available fluorescent bead-based assay, used according to the manufacturer's instructions (Cytometric Bead Array Rat TNF-α Flex Set, BD Biosciences). This assay system provides a method of capturing soluble analyte with coated beads of known size and specific fluorescence. It is then possible to detect and quantify the bound analyte using flow cytometry, using a detection reagent that provides a second, distinct fluorescent signal in proportion to the amount of bound analyte. Briefly, 50µl of sample or known standards were incubated with 50µl of capture bead mix for two hours at room temperature. 50µl of detection reagent, containing a PE-labelled anti-TNF-α antibody was then added, and samples incubated for a further one hour at room temperature. 1ml of wash buffer was then added, and samples centrifuged at 1200rpm for five minutes. The supernatant was carefully removed, and the pellet of beads resuspended in 300µl of wash buffer. Samples were acquired on a flow cytometer (BD Accuri, BD Biosciences) and data analysed using the automated FCAP array software (BD Bioscience).

2.10 Immunohistochemistry (IHC)

2.10.1 Study Approval for use of human tissue

Human renal tissue samples were obtained from patients under local ethics committee approval (04/Q0406/25 Hammersmith and Queen Charlotte's & Chelsea Hospitals Research Ethics Committee). Lymph node samples were provided by the Imperial College Healthcare NHS Trust Tissue Bank (Application R10015).

2.10.2 Pre-treatment of paraffin sections

All IHC in this study was performed on formalin-fixed paraffin embedded tissue sections. Paraffin wax embedding and sectioning of formalin-fixed animal tissues was performed by Ms Lorraine Lawrence (Department of Leukocyte Biology, Imperial College London). Sections were cut on a rotary microtome to a thickness of 4μm. Human renal biopsy specimens were spare paraffin sections, surplus to clinical need, retrieved from the histology archive at Hammersmith Hospital, or provided by Kay Dawson (on behalf of the Imperial College Healthcare NHS Trust Tissue Bank).

Sections were placed in two sequential baths of xylene, to remove wax, before passage through graded ethanol concentrations and finally water. The latter steps serve to remove xylene and rehydrate the tissue.

Formaldehyde preserves tissues by cross-linking amino groups in proteins with other nearby nitrogen atoms in protein or DNA, producing methylene bridges and other types of bridging links. These cross-links must usually be broken either by thermal or enzymatic means ('epitope retrieval') to enable the primary antibody to recognise its target epitope. De-waxed sections therefore underwent heat-induced epitope retrieval in 0.1M sodium citrate buffer, pH 6.0. The sections were then sequentially blocked for endogenous peroxidase activity by submerging in 0.3% hydrogen peroxide from ten minutes, and rinsed in PBS. A wax pen (Dako) was used to encircle tissue sections on the slide to minimise 'run-off' when subsequent solutions were applied. A 20% serum solution was applied for 30 minutes (See Table 2.5 for details) to block non-specific binding of subsequent antibodies.

2.10.3 Primary antibodies

The blocking antibody was tapped off, and primary antibodies added at the appropriate dilution in sufficient volume to cover the tissue section, typically 50-200µl. Slides were placed in a covered, humidified staining chamber to minimise evaporation and left to incubate for the appropriate duration (Table 2.5). For exploratory SYK IHC, negative controls comprised omission of primary antibody and, where available, use of primary antibody pre-incubated with the cognate immunising peptide at a 1:1 ratio. Omission of primary antibody was used for IHC protocols that were already established in our laboratory (e.g. CD68).

2.10.4 Detection

Two methods were used for detection of primary antibodies in tissue sections:

(i) A commercial secondary antibody detection system (EnVision, Dako) was used for the detection of the majority of primary antibodies (Table 2.5). The EnVision reagent consists of a peroxidase-conjugated polymer backbone which carries secondary antibody molecules raised in goat and directed against rabbit or mouse immunoglobulins. Primary antibody was tapped off and slides washed two times for five minutes in PBS. Sufficient EnVision reagent was then added to completely cover the tissue section and the slide placed in the humidified incubation chamber for 30 minutes. The reagent was then tapped off and a further two PBS washes performed.

(ii) For rat ED1 and CD8 staining in rat tissue, excessive non-specific background staining within glomeruli was observed using the EnVision system. In these instances, a biotinylated rabbit anti-mouse secondary antibody (as detailed in Table 2.5) was incubated with the sections for one hour. The sections were then washed twice in PBS, and incubated with an Extravadin-HRP conjugate (Sigma) at a dilution of 1:100 for 30 minutes, then washed thrice in PBS.

A 3,3'-diaminobenzidine (DAB) chromagen solution was prepared by mixing DAB+ chromagen with DAB+ substrate buffer in a ratio of 1:50 (Dako). This was applied to tissue sections for 30 seconds to five minutes depending on the primary antibody; oxidation of DAB

by peroxidase/H_2O_2 yields a dark brown pigment signifying positive staining. Reaction was terminated by placing slides in PBS. Slides were then rinsed in water and counterstained by immersion for 30 seconds in filtered Harris haematoxylin (CellPath, Powys, UK). After rinsing, excess stain was removed by brief (<1 second) immersion in acid-alcohol solution (1% HCl in 70% ethanol). Sections were then washed in water and dehydrated by sequential passage through ascending alcohol concentrations to xylene. Slides were then mounted with DPX (Distrene, Plasticiser, Xylene; VWR International, Lutterworth, UK) and glass coverslips and allowed to dry before examination.

2.10.5 Double staining

For double staining for phosphorylated SYK and CD68, in both rat and human tissue, sections were first stained for phosphorylated SYK as described above. Following development in DAB, the sections were sequentially rinsed, re-subjected to heat-induced antigen retrieval (0.1M citrate buffer, pH 6.0), blocked with 20% rabbit or goat serum (Dako), incubated with mouse anti-rat ED1 primary antibody (Serotec, Oxford UK; dilution 1:500) or mouse anti-human CD68 (Dako; dilution 1:50) at room temperature for one hour, washed, then incubated with a biotinylated rabbit or goat anti-mouse immunoglobulin secondary antibody (Sigma; dilution 1:100) for one hour, then ALP-conjugated streptavidin (Roche Diagnostics; dilution 1:100) for 30 minutes, before final development using the Vector Blue ALP Substrate Kit III (Vector Labs, Peterborough, UK) according to manufacturer's specifications. Slides were mounted in AquaPerm (ThermoFisher Scientific) without counterstaining, and coverslips placed.

2.10.6 Quantification of total SYK staining in human biopsies

Automated image analysis software (ImagePro Plus) was used, in a blinded fashion, to quantify the percentage of glomerular staining in all glomeruli in each biopsy section, and expressed as the mean percentage stain per GCS for each case.

TARGET PROTEIN (SPECIES)	BLOCKING SOLUTION	PRIMARY ANTIBODY	PRIMARY ANTIBODY DILUTION AND INCUBATION	SECONDARY ANTIBODY (FOR SINGLE STAINING)
Total SYK (Human, Rat)	20% Goat Serum (Dako)	SYK-N19 Santa-Cruz #1077 Rabbit polyclonal	1:300 (Human) 1:1000 (Rat) 1h, room temperature	Dako-EnVision HRP-linked polymer anti-rabbit
Phosphorylated SYK (Human)	20% Goat Serum (Dako)	P-SYK Try525/526 Cell Signaling #2711 Rabbit polyclonal	1:25 2h, room temperature Or overnight 4°C	Dako-EnVision HRP-linked polymer anti-rabbit
Phosphorylated SYK (Rat)	20% Goat Serum (Dako)	P-SYK Tyr323 Abcam #63515 Rabbit polyclonal	1:50 2h, room temperature Or overnight, 4°C	Dako-EnVision HRP-linked polymer anti-rabbit
CD68 (Human)	20% Goat Serum (Dako)	Clone PGM1 Dako Mouse monoclonal	1:50 1h, room temperature	Dako-EnVision HRP linked polymer anti- mouse
CD15 (Human)	20% Goat Serum (Dako)	Clone Carb-3 Dako Mouse monoclonal	1:50 1h, room temperature	Dako-EnVision HRP linked polymer anti-mouse
CD68 (Rat)	20% Rabbit Serum (Dako)	Clone ED1 Serotec Mouse monoclonal	1:500 1h, room temperature	Biotinylated rabbit anti-mouse immunoglobulin (Sigma; dilution 1:100); Followed by Extravadin-HRP (Sigma; dilution 1:100)
CD8 (Rat)	20% Rabbit Serum (Dako)	Clone MCA48R Serotec Mouse Monoclonal	1:100 1h, room temperature	Biotinylated rabbit anti-mouse immunoglobulin (Sigma; dilution 1:100); Followed by Extravadin-HRP (Sigma; dilution 1:100)

Table 2.5: Summary of antibodies used for immunohistochemistry.

2.11 Statistics

Graphs were constructed and statistical analysis conducted using Prism 5.0 (GraphPad Software Inc., San Diego, California). Whenever a statistical test was used, this is indicated in the text. The means of two or more normally distributed variables were compared with a t-test or analysis of variance (ANOVA) respectively, with Bonferroni post-hoc test to compare individual groups. Most biological data are not, however, normally distributed. For non-parametric datasets, or where <8 samples were available, Mann-Whitney U, Kruskal-Wallis or Friedman tests were used to assess the difference between 2, >2 and >2 (repeated measures) groups respectively, with Dunn's post-hoc test to compare individual groups. All tests were two-tailed.

CHAPTER THREE – DEVELOPMENT OF METHODS AND PRELIMINARY INVESTIGATIONS

3.1 Production, purification and characterisation of recombinant rat α3(IV)NC1

The HEK 293 cell line with stable transfection of the rat α3(IV)NC1-FLAG construct, kindly provided by Dr John Reynolds, was grown continuously for a period of three months, during which approximately 20mg of purified antigen was isolated for use. Seven purification procedures were undertaken using the anti-FLAG epitope affinity column. Fractions were collected in 1ml volumes and protein concentration was quantified by measuring optical density (OD) at 280nm. A representative example of an elution is shown in Figure 3.1.

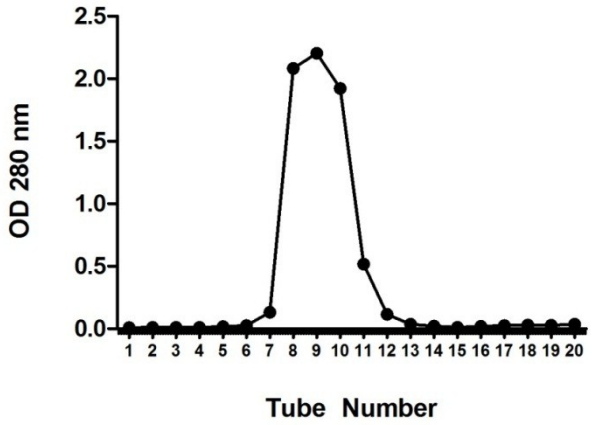

Figure 3.1: Representative elution of α3(IV)NC1 from anti-FLAG affinity column.
Protein content measured at 280nm in serial fractions purified from supernatant collected from α3(IV)NC1 transfected HEK 293 cells, using anti-FLAG affinity chromatography column.

The recombinant α3(IV)NC1 eluted from the anti-FLAG column was characterised by SDS-PAGE and Western blotting. Serial fractions were run on a gel for protein separation. A Western blot of the eluted fractions was blotted with a monoclonal antibody specific for the FLAG signal peptide included in the recombinant α3(IV)NC1 construct. Two bands were evident between the 30 and 45kDa molecular weight markers, signalling the isoforms of the recombinant antigen. The dimer form appears at 67kDa (Figure 3.2).

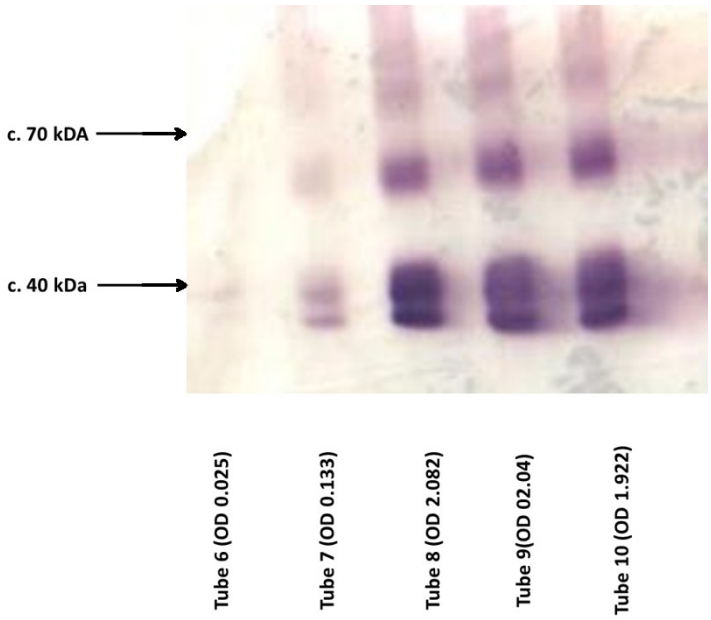

Figure 3.2: Western blot for FLAG signal protein.

Western blot using anti-FLAG monoclonal antibody on serial fractions of affinity column eluent, demonstrating the two isoforms of the recombinant antigen at c.35kDA, and the dimerised form of the antigen at c.70kDa.

While the anti-FLAG Western blot confirmed the presence of the FLAG epitope, it was necessary to demonstrate that the recombinant α3(IV)NC1 was also intact and functionally active as an antigen. Serial fractions were blotted with serum from a patient with anti-GBM disease and a rat with EAG. The α3(IV)NC1 antibodies in these two sera samples revealed banding at the same molecular weight as did the control anti-FLAG antibody (not shown).

3.2 EAG Experiment 1: Induction of EAG in WKY rats by immunisation with α3(IV)NC1

The purpose of experiment 1 was to confirm the immunogenicity of the purified recombinant rat α3(IV)NC1 in WKY rats, and to establish that disease could be induced 'in my hands' with this antigen preparation. Female animals, aged five weeks with body weight approximately100g (n=3-4 per group), were immunised with either 100μg α3(IV)NC1 emulsified in an equal volume of CFA, or an equivalent volume of buffer and CFA alone (negative control), administered by intramuscular injection to the thighs. This dose was chosen based on Dr Reynolds' previous characterisation of this model[225]. Urine and serum were collected weekly for either 28 or 42 days (with an additional urine collection on day 18, the time-point when disease onset is typically observed by Dr Reynolds) before being culled for tissue analysis. The severity of glomerular injury was assessed by (1) serial measurement of proteinuria, (2) quantification of histological injury and degree of inflammatory cell infiltrate, and (3) measurement of biochemical renal function. The humoral immune response was assessed by serial measurement of circulating anti-α3(IV)NC1 antibodies, and glomerular antibody deposition at the end of the experiment.

3.2.1 Proteinuria

Proteinuria was quantified both as total urinary protein loss per day, and as the urinary protein:creatinine ratio (uPCR), which aims to correct urinary protein concentrations for the differences in total urine volume and concentration. Negative control animals did not develop detectable proteinuria for the duration of the experiment. Positive control animals had

detectable proteinuria by day 18, consistent with Dr Reynolds' previous observations. The degree of proteinuria increased consistently for the duration of the experiment (Figure 3.3).

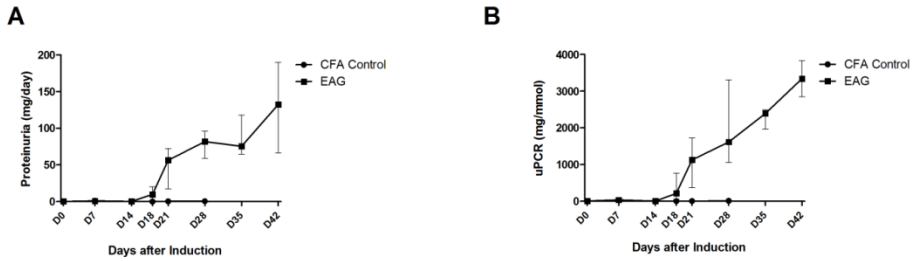

Figure 3.3: Development of proteinuria following immunisation with α3(IV)NC1.
Proteinuria expressed (A) as total urinary protein loss per day, and (B) as urinary protein:creatinine ratio (uPCR), in CFA control and EAG animals following immunisation with α3(IV)NC1 at day 0. Data are shown as median ±IQR.

3.2.2 Histological Injury

Negative control animals had normal glomerular histology when assessed at day 28, by which point positive controls had developed significant glomerular injury, with approximately 70% of glomeruli severely affected by crescent formation or necrosis. By day 42, over 90% of glomeruli were severely affected (Figure 3.4).

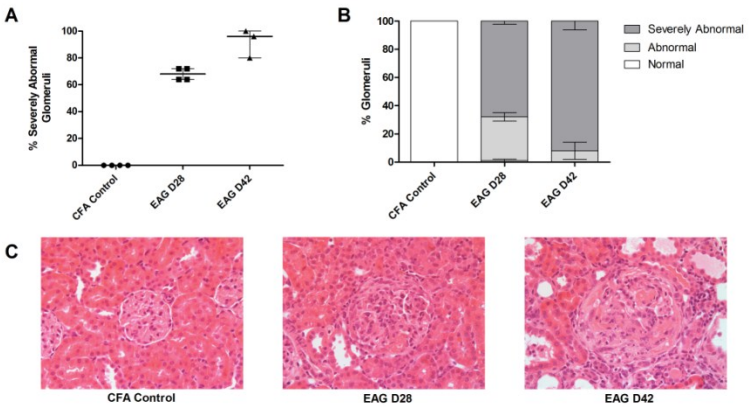

Figure 3.4: Renal histology following immunisation with α3(IV)NC1.
(A) Proportion of severely abnormal glomeruli in CFA Control and EAG animals 28 and 42 days following immunisation, shown as median ±IQR. (B) The range of glomerular abnormalities (normal, abnormal or severely abnormal) in each group, shown as mean ±SEM. (C) Photomicrographs showing representative histology in each group. H&E stain, x400 magnification.

3.2.3 Infiltrating leucocytes

The extent of inflammatory cell infiltrate into glomeruli was assessed by immunohistochemical staining for ED1, a rat macrophage specific marker, and CD8. These markers were chosen based on previous descriptions of the natural history of this model[226]. Negative control animals had no evidence of ED1+ or CD8+ cells within glomeruli at day 28. In the positive control animals, there was a marked ED1+ inflammatory infiltrate by day 28 that had decreased by day 42, suggesting a peak in inflammatory cell infiltrate before this time point. There was a similar pattern of CD8+ cell infiltration, although absolute numbers of CD8+ cells were much lower (Figure 3.5).

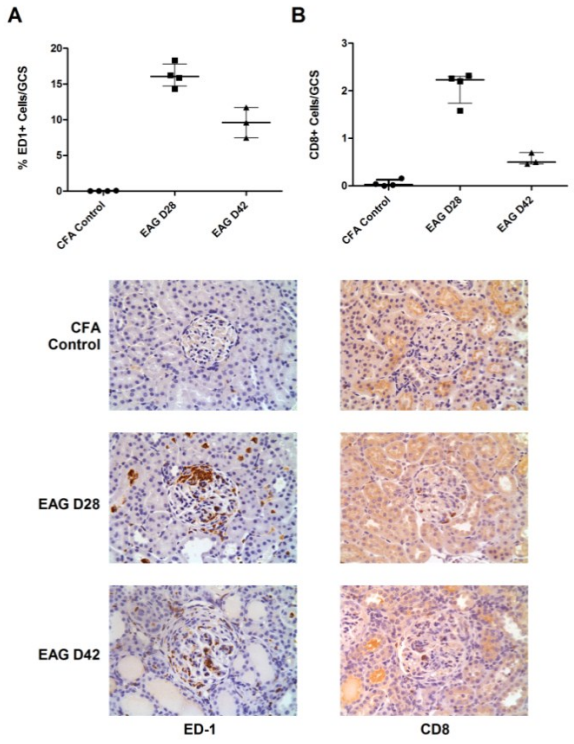

Figure 3.5: Glomerular inflammatory cell infiltration following immunisation with α3(IV)NC1.
(A) Macrophage infiltration, expressed as the mean percentage of ED1+ cells per glomerular cross section (GCS), in CFA control and EAG animals 28 and 42 days after immunisation. Lower panel photomicrographs show representative staining images. (B) CD8+ leucocyte infiltration, expressed at the mean number of CD8+ cells per GCS in each group, with representative photomicrographs. All data shown as median ±IQR. Images are immunoperoxidase stains with haematoxylin counterstain, x400 magnification.

3.2.4 Renal function

Biochemical renal function was assessed by measuring serum urea and creatinine concentrations, and the respective renal clearance of each substance (Figure 3.6). There was minimal change in serum concentrations of urea and creatinine at day 28 after disease induction. By day 42, there was clear evidence of impaired renal function, although there was high variability, with one animal having very severe renal failure (despite appearing well on inspection prior to culling).

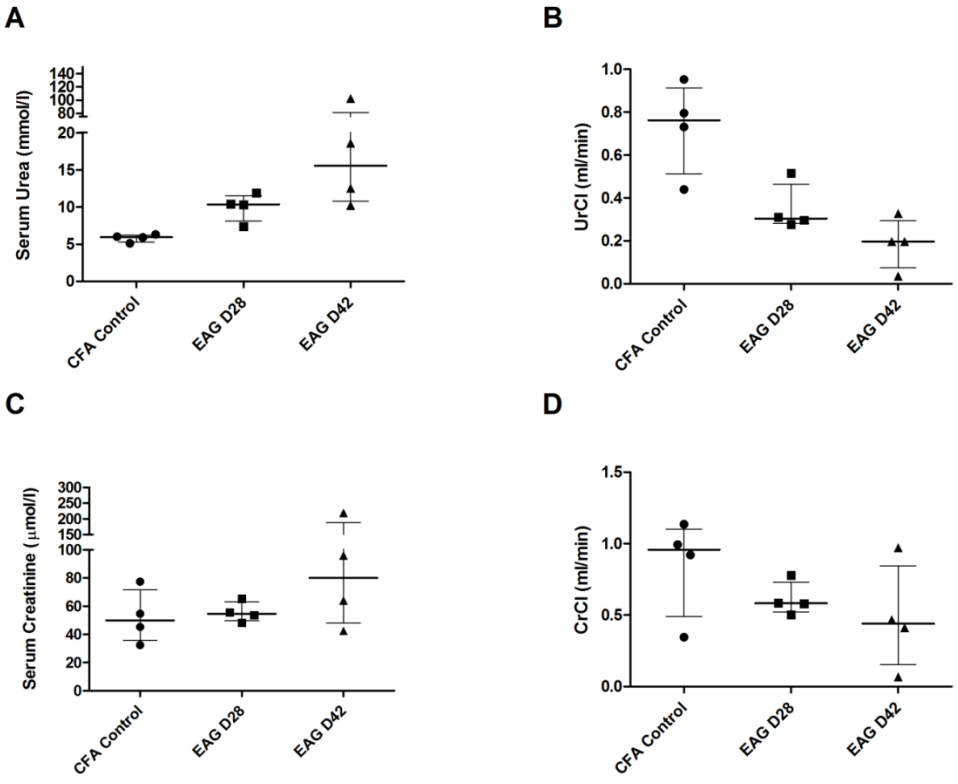

Figure 3.6: Assessments of renal function following immunisation with α3(IV)NC1.
(A) Serum urea, (B) Urea clearance, UrCl, (C) Serum creatinine, and (D) Creatinine clearance, CrCl, in CFA control and EAG animals 28 and 42 days after immunisation. Data are shown as median ±IQR.

3.2.5 Circulating and deposited α3(IV)NC1 antibodies

CFA negative control animals did not have detectable antibodies to α3(IV)NC1 by day 28. Positive control animals had detectable circulating antibody by day 7. The titre of antibody rose progressively until day 21 and then appeared to plateau (Figure 3.7), although serial dilutions were not performed. In keeping with the development of circulating autoantibodies, the α3(IV)NC1 immunised animals had intense linear deposits of IgG within glomeruli at day 28, as detected by direct immunofluorescence, whereas no antibody was observed in negative control animals.

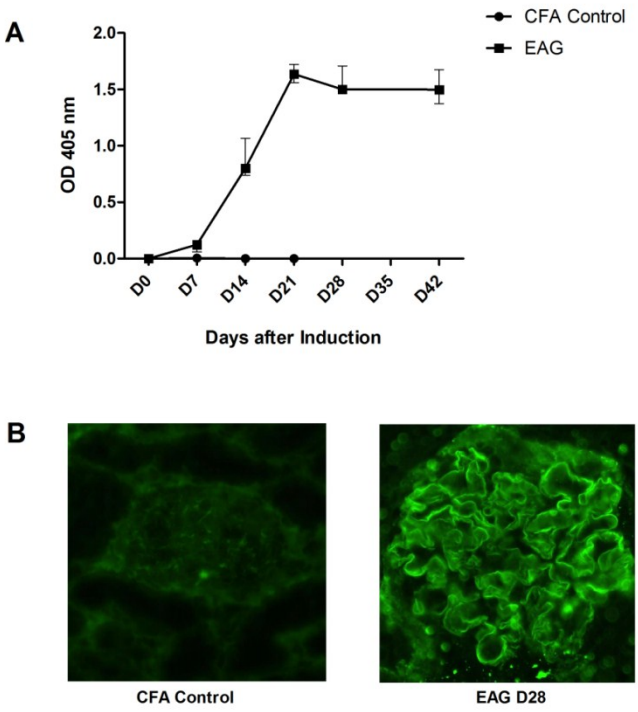

Figure 3.7: Humoral responses following immunisation with α3(IV)NC1.
(A) Circulating anti-α3(IV)NC1 antibody levels, reported as mean optical density at 405nm (OD 405) per group, in CFA control and EAG animals following immunisation with α3(IV)NC1 at day 0. Data are shown at median ±IQR. (B) Direct immunofluorescence for deposited rat IgG in CFA control and EAG animals 28 days after immunisation. All EAG animals had strong linear deposits of IgG along the glomerular basement membrane. Anti-rat IgG FITC, x400 magnification.

3.3 EAG Experiment 2: Dose-response and disease beyond day 28

In the previous experiment, I established that the α3(IV)NC1 antigen I had purified was immunogenic and could induce renal disease comparable to that observed in this model in our laboratory previously. Since the production of the antigen was labour and time intensive, I wanted to test if lower doses could be used to induce similar levels of disease. In addition, despite having histopathological evidence of severe renal disease at day 28, the animals had minimal disturbance of their renal biochemistry, and I was keen to describe the natural history of disease beyond 28 days. I therefore conducted a dose-response experiment (using 100μg, 50μg, 25μg and 12.5μg α3(IVI)NC1) and assessed the animals at 4, 6 and 8 weeks after immunisation. Female rats, aged seven weeks, with average body weight 150g were used. Between week 7 and week 8, three of the animals became unwell and demonstrated >10% loss of body weight, thus reaching the pre-defined limits of our Home Office licence (two animals in the 100μg group and one animal in the 25μg group). These animals were therefore culled immediately, without a final urine collection, and the results are reported accordingly.

3.3.1 Proteinuria

Twenty-four hour urinary protein loss and uPCR are summarised in Figure 3.8. At all time points, animals in the 25μg, 50μg and 100μg groups had comparable degrees of proteinuria. Animals in the 12.5μg group tended to have less proteinuria, although the difference was statistically significant at week 4 only. In addition, correlation analysis of all data pairs suggested that measures of uPCR and 24 hour urinary protein loss provided comparable information in this model (Pearson correlation coefficient 0.84, $p<0.0001$; Figure 3.9).

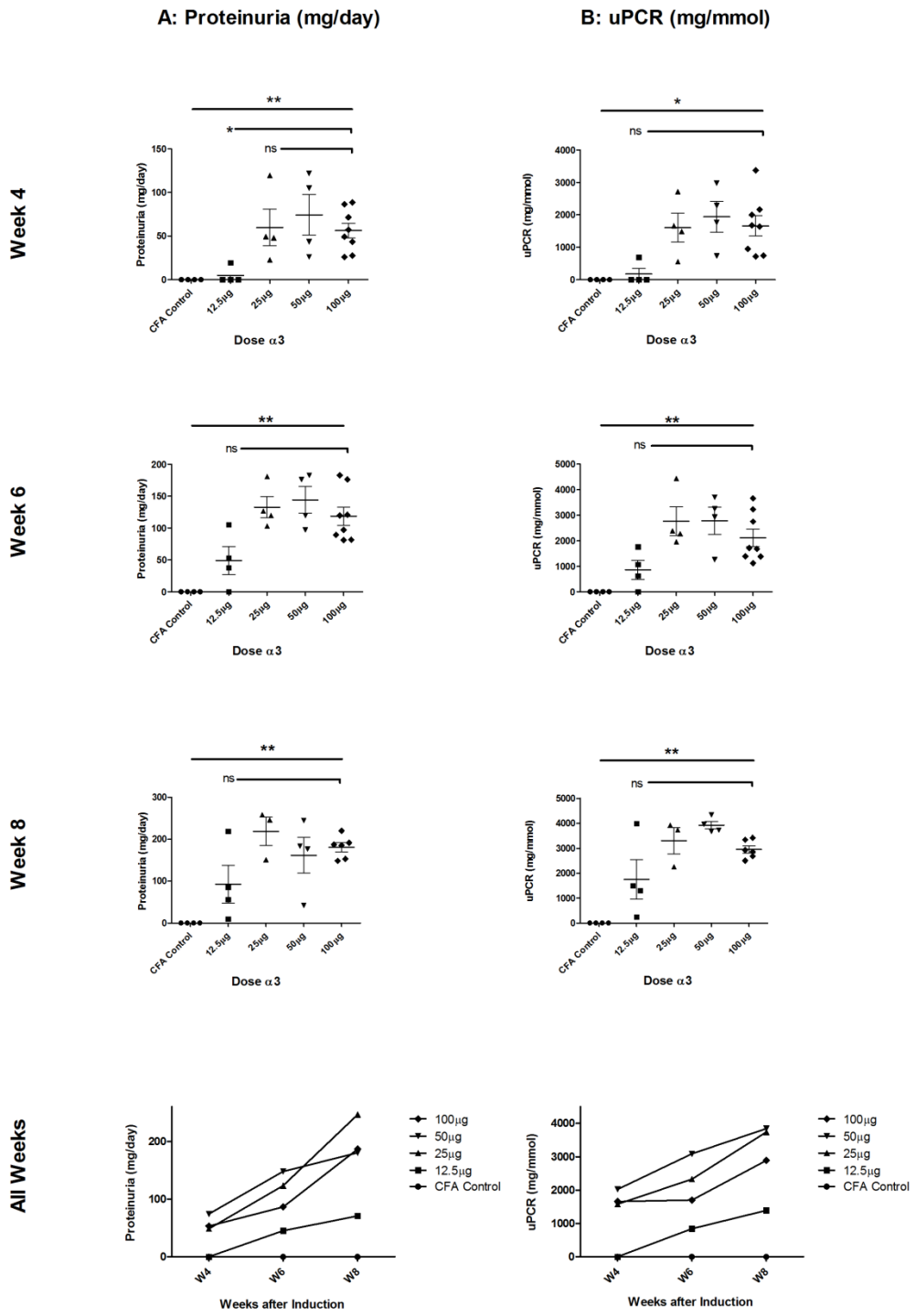

Figure 3.8: Proteinuria 4 to 8 weeks after Induction of EAG.

(A) 24 hour urinary protein, and (B) Urinary protein:creatinine ratio (uPCR) at week 4, 6 and 8 after induction of EAG with varying doses of α3(IV)NC1. Animals immunised with 12.5mcg α3(IV)NC1 tended to have lesser degrees of proteinuria, though this was statistically significant at week 4 only. Data are shown as median ±IQR. Lower summary plots reported as median only, without error, for clarity. Week 8 data not available for 3 rats culled early. ns – not significant, *p<0.05, **p<0.01, by Kruskall Wallis test (overall significance indicated by upper symbol) with Dunn's post-test comparison to 100µg dose group (significance indicated by lower symbols).

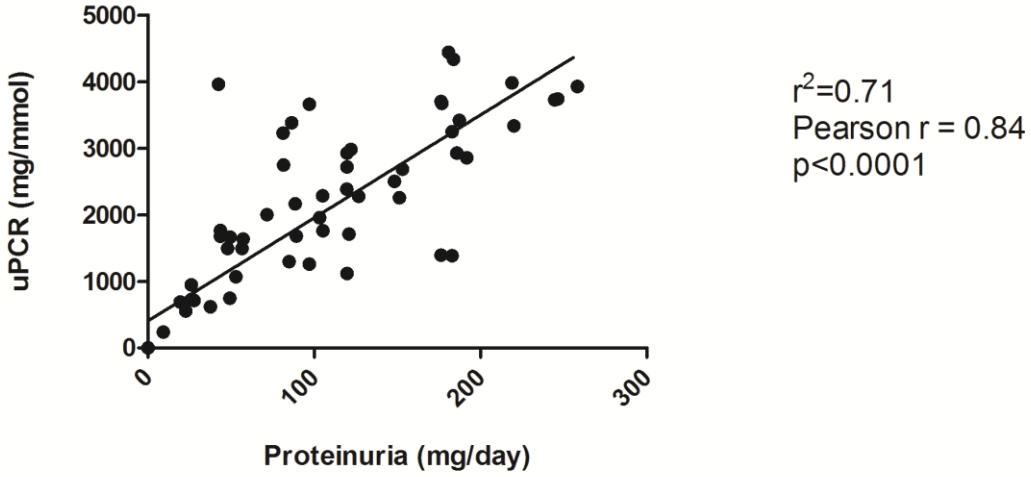

Figure 3.9: Correlation of uPCR with 24 hour urinary protein in EAG.
Correlation analysis suggests that measures of urinary protein:creatinine ratio (uPCR) and 24 hour urinary protein loss provide equivalent information in EAG.

3.3.2 Histological Injury

At week 8, animals in the 25µg, 50µg and 100µg groups had comparable renal histology, with the almost all glomeruli affected by disease. Significant tubular atrophy and interstitial fibrosis was also observed, though not formally quantified. Animals in the 12.5µg group tended to have less renal injury, although this trend was not statistically significant (Figure 3.10).

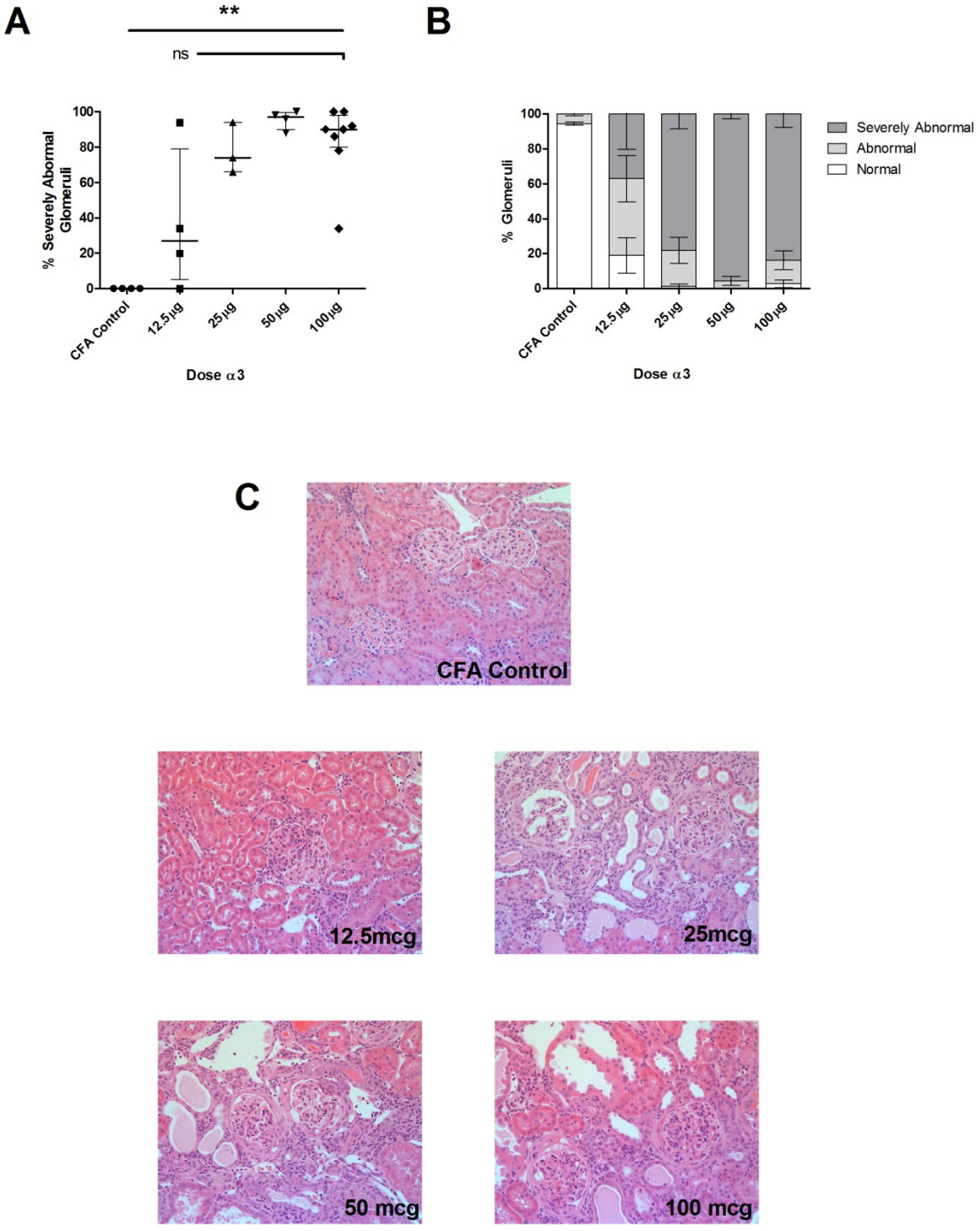

Figure 3.10: Renal histology 8 weeks after Induction of EAG.

(A) Proportion of severely abnormal glomeruli 8 weeks following immunisation with varying doses of α3(IV)NC1, shown as median ±IQR. ns – not significant, *p<0.05, **p<0.01, by Kruskall Wallis test (overall significance indicated by upper symbol) with Dunn's post-test comparison to 100µg dose group (significance indicated by lower symbols). (B) The range of glomerular abnormalities (normal, abnormal or severely abnormal) in each group, shown as mean ±SEM. (C) Photomicrographs showing representative histology, including significant degrees of tubular atrophy, in each group. H&E stain, x200 magnification.

3.3.3 Renal function

The various measurements of renal function at week 8 are shown in Figure 3.11. The outlier data points represent the animals which were culled early (assigned a clearance of 0ml/min since urine collection was not possible; serum measurements were made). There was a trend, in all parameters, towards more severe renal impairment with increasing dose of α3(IV)NC1, although this was not statistically significant with measures of creatinine concentration or clearance.

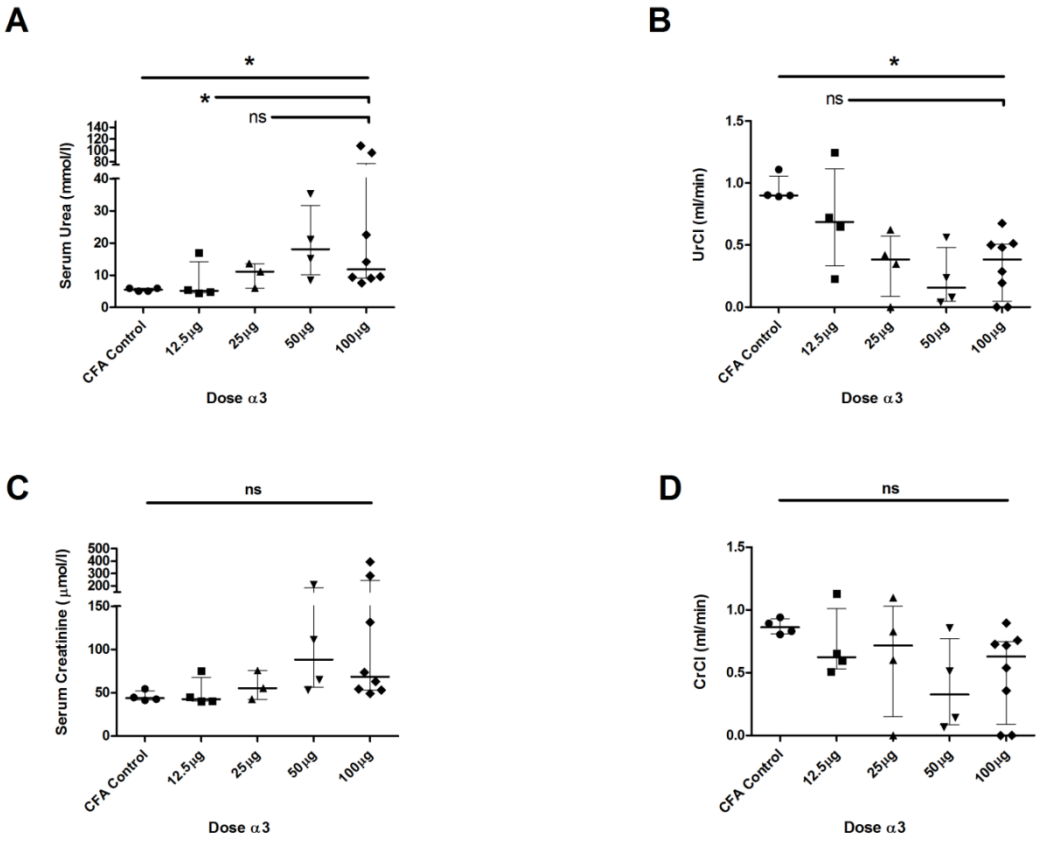

Figure 3.11: Renal function 8 weeks after induction of EAG.

(A) Serum urea, (B) Urea clearance, UrCl, (C) Serum creatinine, and (D) Creatinine clearance, CrCl, 8 weeks after immunisation with varying doses of α3(IV)NC1. Data are shown as median ±IQR. Serum measurements include animals culled early at week 7; these animals were assigned clearance of 0ml/min at week 8. ns – not significant, *p<0.05, **p<0.01, by Kruskall Wallis test (overall significance indicated by upper symbol) with Dunn's post-test comparison to 100µg dose group (significance indicated by lower symbols).

Notably, serial measurements of urea and creatinine clearance between week 4 and 6 provided discordant results compared to serum measurements of each (Figure 3.12). Whilst serum levels of both substances tended to rise between week 4 and 6, there was an increase in their urinary clearance, particularly noted in CFA control animals. This may reflect, in part, the physiological changes in glomerular filtration and muscle mass that were occurring in the young (and thus rapidly growing) rats used in these studies. Direct measurement of serum urea and creatinine may thus be a more reliable marker of renal function in these animals.

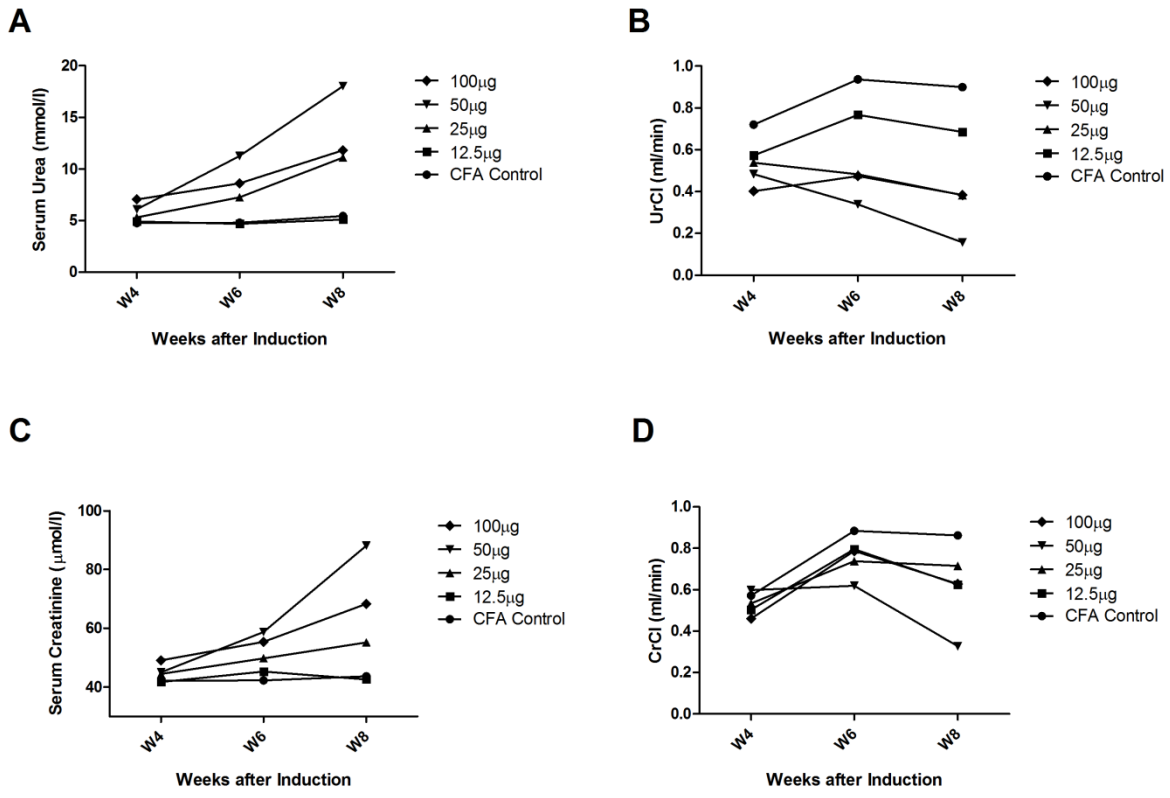

Figure 3.12: Renal function 4 to 8 weeks after induction of EAG.
(A) Serum urea, (B) Urea clearance, UrCl, (C) Serum creatinine, and (D) Creatinine clearance, CrCl, 4 to 8 weeks after immunisation with varying doses of α3(IV)NC1. Data are shown as median only, without error, for clarity. Serum measurements include animals culled early at week 7; these animals were assigned clearance of 0ml/min at week 8.

3.3.4 Lung haemorrhage

Based on initial observations of pulmonary disease in EAG Experiment 1, I developed a semi-quantitative scoring system to assess the severity of lung haemorrhage in this model. As shown in Figure 3.13, lung haemorrhage was consistently observed only in the 100µg dose group.

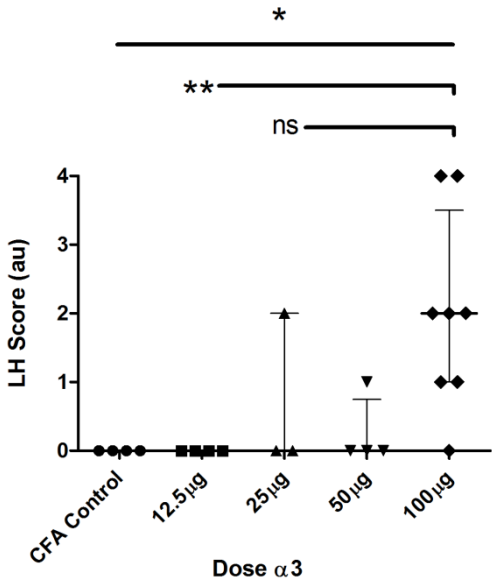

Figure 3.13: Lung haemorrhage 8 weeks after induction of EAG.
Semi-quantitative lung haemorrhage (LH) score 8 weeks after immunisation with varying doses of α3(IV)NC1. Data are shown as median ±IQR. ns - not significant, *p<0.05, **p<0.01, by Kruskall-Wallis test (overall significance indicated by upper symbol) with Dunn's post-test comparison to 100µg dose group (significance indicated by lower symbols).

3.3.5 Circulating anti-GBM antibodies

Since the direct α3(IV)NC1 ELISA method used elsewhere is this project uses the recombinant rat α3(IV)NC1 protein that is also used for immunisation, it is possible that the ELISA may detect antibodies made to other components of the antigen preparation (such as the FLAG construct or contaminants) rather than anti-GBM antibodies. In order to confirm

that the animals were making anti-α3(IV)NC1 antibodies, I used a bead-based assay, using commercially available, fluorescently-labelled beads coated with bovine GBM, to quantify circulating antibody levels in this experiment. This assay confirmed that the rats made antibodies directed against the 'universal' Goodpasture epitope. It also showed that highest levels of circulating antibody were consistently observed in the 100µg dose group (Figure 3.14).

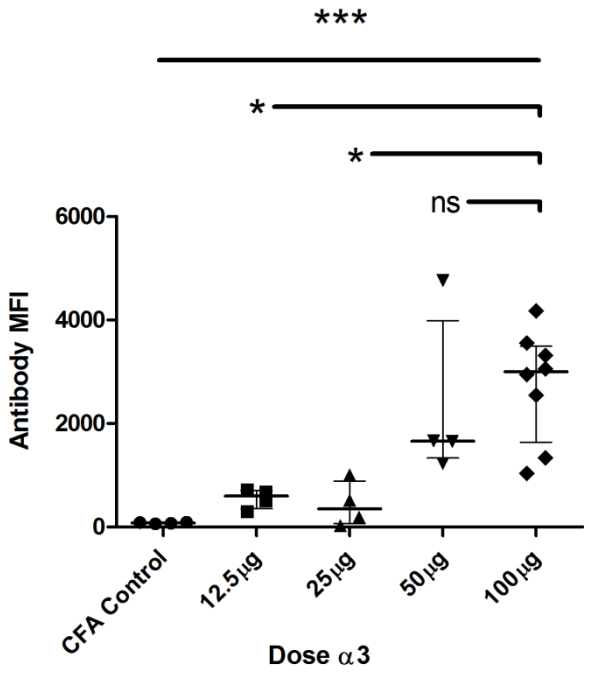

Figure 3.14: Anti-GBM antibody levels 8 weeks after induction of EAG.
Mean fluorescence intensity (MFI) of anti-GBM antibodies 8 weeks after immunisation with varying doses of α3(IV)NC1. This assay confirms that rats are making antibodies directed against the 'universal' Goodpasture epitope. Data are shown as median ±IQR. ns - not significant, *p<0.05, **p<0.01, ***p<0.001 by Kruskall Wallis test (overall significance indicated by upper symbol) with Dunn's post-test comparison to 100µg dose group (significance indicated by lower symbols).

3.4 EAG Experiment 3: Early disease in young male and female rats

In a subsequent experiment, I characterised further the pattern of early disease in EAG (at day 21 and day 28) and directly compared the susceptibility of male and female rats at these time points. Notably, whilst both male and female WKY rats develop disease after immunisation with α3(IV)NC1, I could not find any data from our laboratory that directly compared susceptibility between rat sexes. This experiment was conducted with Ms Zelpha D'Souza, from the Physiological Genomics and Medicine Group at the Medical Research Council Clinical Sciences Centre, and the preliminary results generated here were also used to inform the design of our parallel collaborative project investigating the genetic susceptibility of the WKY rat to experimental models of glomerulonephritis[234]. As such, this experiment included groups of Lewis (LEW) rats, the resistant rat strain used as a negative control in the genetic studies, which I have included here for completeness. Four week old rats (2-4 per group) with average body weight 85g were used in this experiment, immunised with a dose of 50μg of α3(IV)NC1. Since individual group numbers are small, I have not conducted formal statistical analysis.

3.4.1 Proteinuria

As expected, Lewis rats were resistant to the development of proteinuria following immunisation with α3(IV)NC1 (Figure 3.15). WKY rats had developed proteinuria by day 21, consistent with the findings of EAG Experiment 1 where disease onset was confirmed by day 18, and had progressed in severity by day 28. There was a trend for more proteinuria in female WKY rats at day 21, although male and female rats were comparable at day 28.

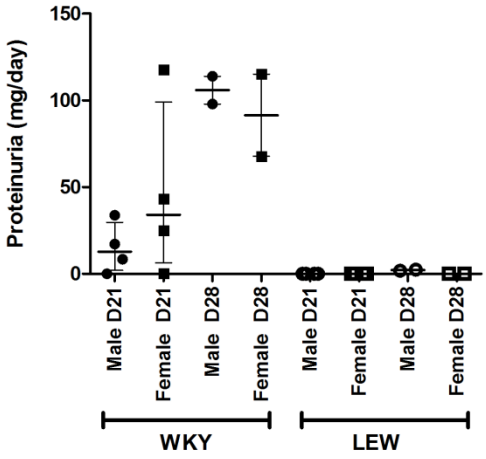

Figure 3.15: Proteinuria in WKY and Lewis rats 21 and 28 days after immunisation with α3(IV)NC1.
Lewis (LEW) rats were resistant to the development of proteinuria, whilst both male and female WKY rats developed proteinuria by day 21, that progressed by day 28. Data shown as median ±IQR.

3.4.2 Histological injury and infiltrating leucocytes

Lewis rats were similarly resistant to severe glomerular injury and leucocyte infiltration (Figure 3.16). There was a trend for female WKY rats to have more severe glomerular injury and leucocyte infiltration at day 21, but male and female rats were comparable at day 28.

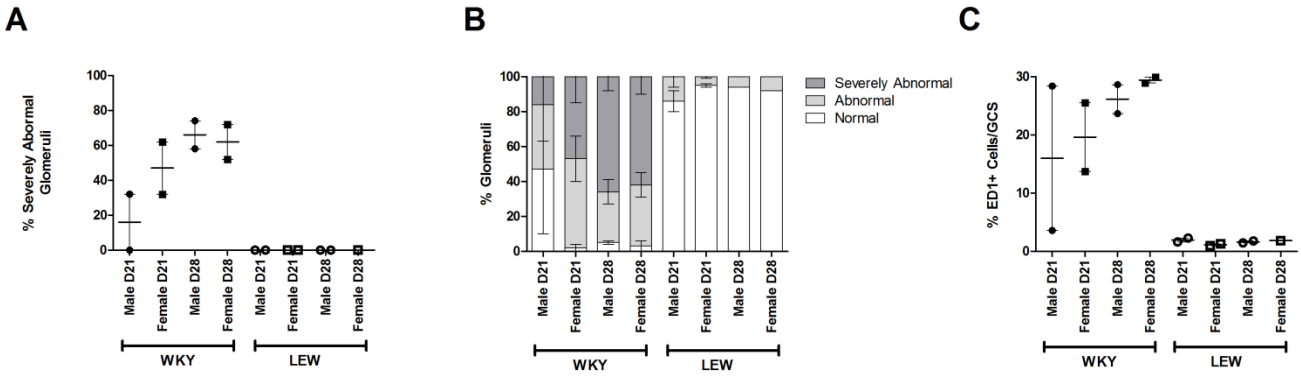

Figure 3.16: Glomerular histology and leucocyte infiltration in WKY and Lewis rats 21 and 28 days after immunisation with α3(IV)NC1.
(A) Severe glomerular abnormalities, shown as median ±IQR, (B) All glomerular abnormalities, shown as mean ±SEM, and (C) Infiltrating ED1+ cells, shown as median ±IQR. Lewis (LEW) rats were resistant to all parameters, whilst both female and male WKY rats developed glomerular abnormalities and macrophage infiltration by day 21 that progressed by day 28.

3.4.3 Deposited glomerular antibodies

As shown in Figure 3.17, Lewis rats did not deposit significant amounts of IgG within glomeruli by day 21 or day 28. There was a trend for female WKY rats to have more intense fluorescence for glomerular IgG at day 21 compared to male WKY rats, though fluorescence was equivalent by day 28.

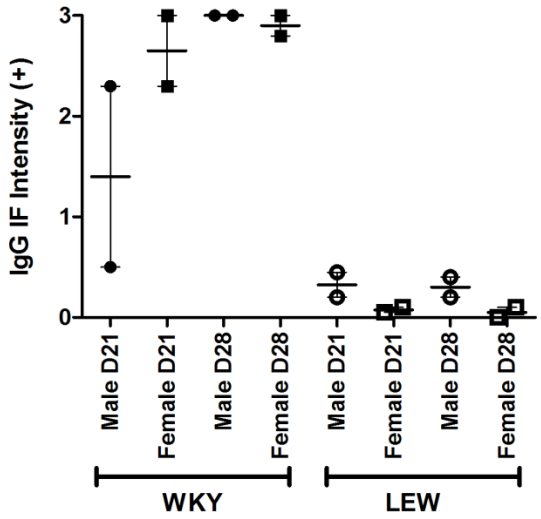

Figure 3.17: Deposited glomerular antibody in WKY and Lewis rats 21 and 28 days after immunisation with α3(IV)NC1.

Lewis (LEW) rats did not deposit glomerular IgG, whilst both male and female WKY rats developed deposits by day 21, that progressed by day 28. Data shown as median ±IQR.

3.5 Development of an ELISpot assay for detection of α3(IV)NC1-specific splenic B cells

Since I later wanted to study the effects of SYK inhibition on humoral immune function, I developed a B cell ELISpot assay to enable enumeration of α3(IV)NC1-specific antibody-producing splenocytes from EAG rats. The protocol was adapted from a commercially available kit for use in mice. Since this was a novel procedure in our laboratory, a series of method development experiments were necessary to optimise the assay. Cell concentration was varied between 10^5 and 10^6 per well, and incubation time between 12 and 48 hours. Results were acquired on an automated ELISpot plate reader, and reported as either the absolute number of α3(IV)NC1-specific cells per million splenocytes, or the amount of anti-α3(IV)NC1-specific 'activity' (a composite of spot number, size and intensity). Example read-outs using a number of example incubation protocols are shown in Figure 3.18.

As illustrated in Figure 3.18, cell concentrations greater than $5x10^5$ per well resulted in excessive 'background' detection in non-α3(IV)NC1 immune rats, and prolonged incubation (of 48 hours) increased the detection of cells and activity in α3(IV)NC1 immunised rats, without resulting in significantly more 'background' detection in non-immune animals, and so these parameters were used for subsequent studies. It was not possible to completely eliminate 'background' detection in non-immune rats, however, so in subsequent *in vivo* studies splenocytes from a non-immune rat were included on all plates to provide an appropriate control comparator. There was also significant variation in the number of cells detected in replicate wells from the same animal, so the assay was repeated in at least eight replicate wells to provide an accurate estimation of α3(IV)NC1-specific cell number.

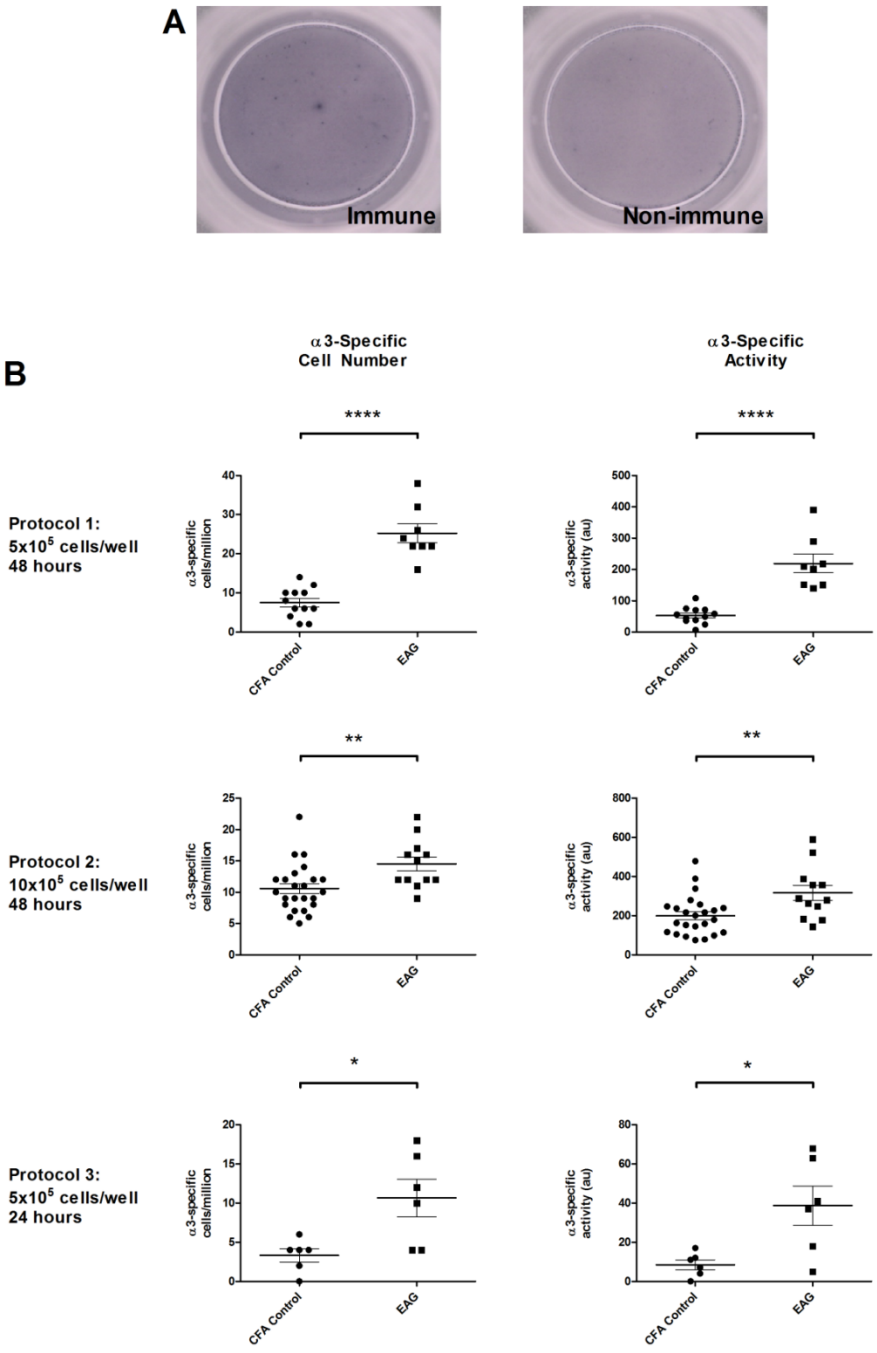

Figure 3.18: Development of an ELISpot assay to detect α3(IV)NC1-specific splenic B cells.
(A) Representative images of ELISpot wells using α3(IV)NC1-immune (EAG) and non-immune (CFA Control) WKY rats, showing 'spots' that indicate anti-α3(IV)NC1 antibody production by splenocytes *in vitro*. (B) Quantification of ELISpot readings as both absolute number of α3(IV)NC1-specific cells and overall α3(IV)NC1-specific 'activity' (a composite of spot number, size and intensity). Results using three examples of different incubation protocols, as indicated, are shown for comparison. Protocol 1 was the protocol used in subsequent studies. All data shown as mean ±SEM. *p<0.05, **p<0.01, ***p<0.001, ****p<0.0001, by unpaired t-test.

3.6 SYK expression in EAG

In subsequent experiments I will study the effects of SYK inhibition using fostamatinib, a small molecule kinase inhibitor with selectivity for SYK, in EAG. However, I felt it was first important to confirm that SYK in expressed and/or activated in this model. I therefore conducted immunohistochemical analysis for total (T-SYK) and phosphorylated (P-SYK) in rat tissue.

3.6.1 Choice of primary antibodies

For T-SYK staining, I used a commercially available rabbit polyclonal antibody raised against a 19 amino acid sequence at the N-terminus of human SYK, which is also reported to react to rat SYK. Rat and human SYK share overall 95% amino-acid sequence homology, and this region is reported to be 100% homologous. I have also shown that this antibody is reactive to rat SYK by Western blot (Chapter Four). Negative control stains were performed by pre-incubating the primary antibody with the immunising peptide, sourced from the antibody manufacturer.

For P-SYK staining, I tested a variety of commercially available antibodies directed against various phosphorylated tyrosine residues within the SYK molecule. The most reproducible staining in rat tissue was achieved with a rabbit polyclonal directed against a phospho-tyrosine 323 in interdomain B of SYK. Notably, it has been shown that phosphorylation of Tyr323 creates a binding site for CBL, a negative regulator of SYK signal transduction in B cells and mast cells[235-237]. However the demonstration of phosphorylation at this tyrosine residue is consistent with the hypothesis that SYK is in an activated state, prior to it

processing towards a negative regulation pathway. This antibody has also been used by other investigators to demonstrate the presence of activated SYK in mouse intestinal and lung tissue[238]. Since the immunising peptide for this antibody was not readily available, negative control studies were performed by omitting the primary antibody (and using buffer alone) for this step of the staining procedure.

3.6.2 Total and phosphorylated SYK detection in rat spleen tissue

Staining for both T-SYK and P-SYK was positive in spleen tissue taken from rats with EAG at all time points examined (18, 28, 36, 42 days after disease induction; day 28 shown in Figure 3.19). Staining was strongest within the germinal centres and marginal zones of lymphoid follicles, consistent with an important role for SYK in the generation of adaptive immune responses.

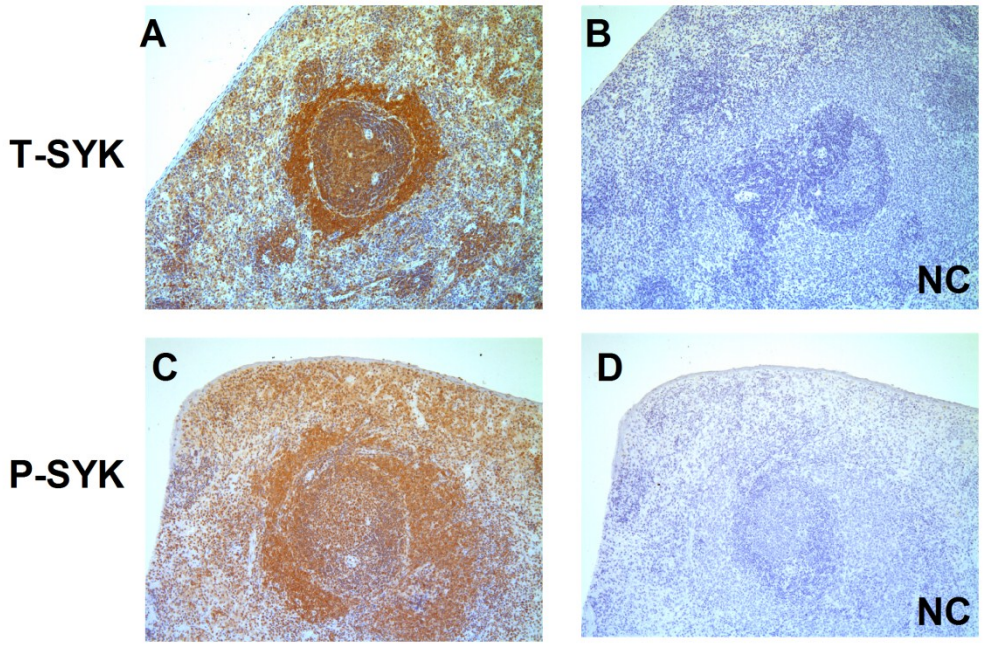

Figure 3.19: Total (T-SYK) and phosphorylated SYK (P-SYK) detection in rat spleen.
Positive and negative control (NC) staining on paired sections of rat spleen for (A) & (B) T-SYK and (C) & (D) P-SYK. In both cases, SYK staining is strongest within germinal centres and marginal zones of lymphoid follicles. Immunoperoxidase stains with haematoxylin counterstain, x100 magnification.

3.6.3 Total and phosphorylated SYK detection in normal rat kidney tissue

In normal rat kidney tissue, T-SYK staining was intermittently positive within distal tubular epithelial cells, but consistently negative within glomeruli (Figure 3.20). Detection of P-SYK was negative in both glomeruli and distal tubular epithelial cells, suggesting that SYK may be expressed but not activated within the latter cell type. A similar pattern of both T-SYK and P-SYK detection was subsequently observed in human renal tissue (Chapter Six).

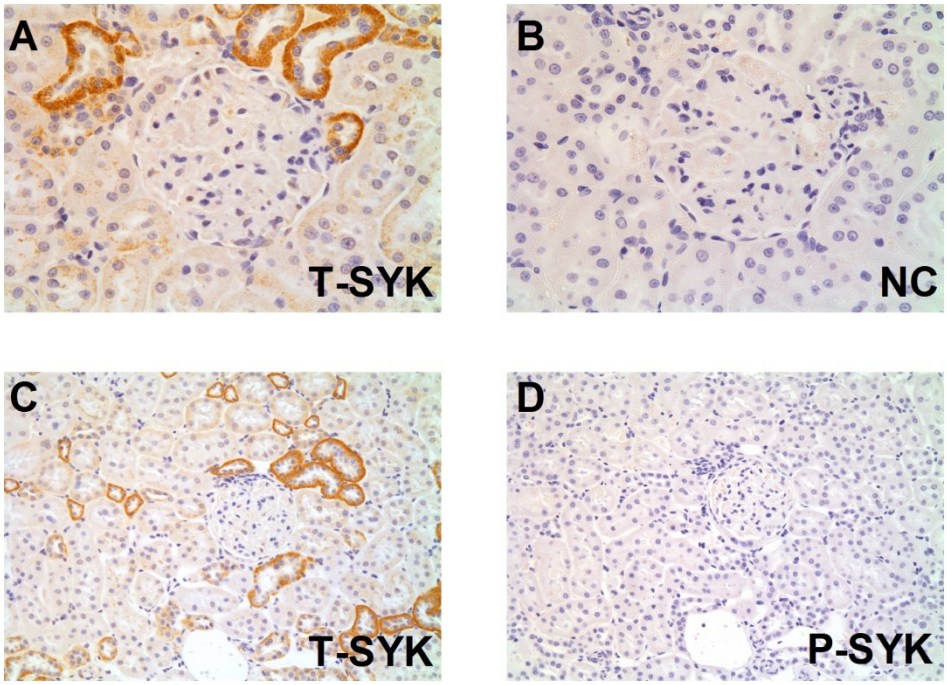

Figure 3.20: Total (T-SYK) and phosphorylated SYK (P-SYK) detection by in normal rat kidney.
(A) & (B) Positive and negative control (NC) staining for T-SYK on paired sections of normal rat kidney, showing intermittent distal tubular epithelial cell staining but no glomerular staining. (C) & (D) Paired sections of T-SYK and P-SYK staining in normal rat kidney, showing negative staining for P-SYK in both tubules and glomeruli. Immunoperoxidase stains with haematoxylin counterstain, x200-400 magnification.

3.6.4 Total and phosphorylated SYK detection in nephritic rat kidney tissue

In nephritic rat tissue, taken from animals 18 days after induction of EAG (Figure 3.21), staining for T-SYK was again positive in the same pattern within distal tubular epithelial cells, but also within glomeruli, and appeared to localise to areas of proliferation or crescent formation. P-SYK expression remained predominantly negative within distal tubular epithelial cells, but was positive within glomeruli in a similar pattern to that observed for T-SYK.

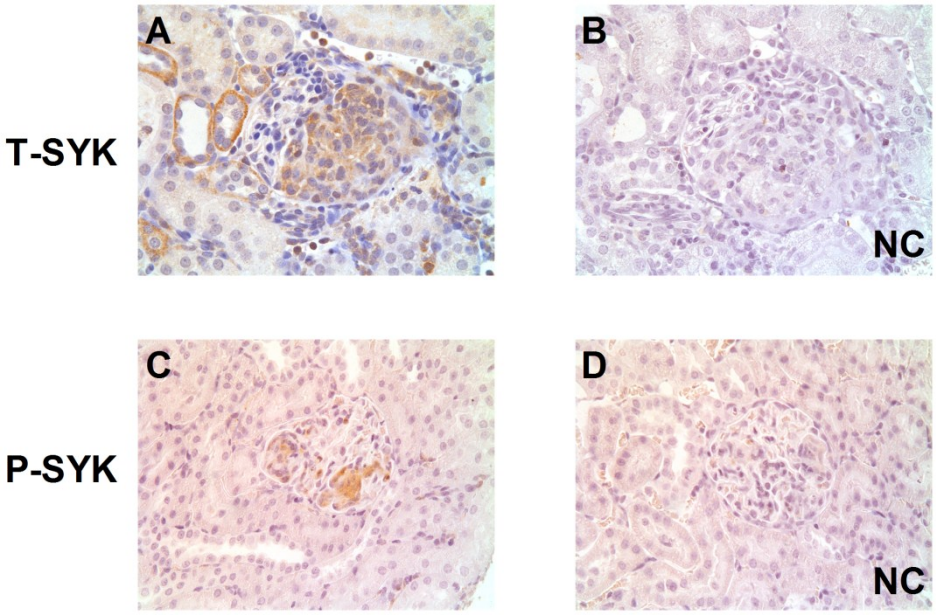

Figure 3.21: Total (T-SYK) and phosphorylated SYK (P-SYK) detection in nephritic rat kidney.
(A) & (B) Positive and negative control (NC) staining for T-SYK on paired sections of nephritic rat kidney (day 18 after induction of EAG), showing intermittent distal tubular epithelial cell staining and also strong glomerular staining within an area of proliferation. (C) & (D) Positive and negative control (NC) staining for P-SYK on sections of nephritic rat kidney, showing negative staining for P-SYK in tubular cells, but positive staining within a glomerulus localised to an area of proliferation. Immunoperoxidase stains with haematoxylin counterstain, x400 magnification.

To identify the cellular localisation of SYK within diseased glomeruli, I went on to perform double staining for P-SYK and ED1 (Figure 3.22) on tissue taken from rats 28 days after disease induction. This suggested that SYK was predominantly found within ED1+

macrophages within diseased glomeruli. However, there were a small number of cells that were P-SYK+ and ED1-, implying that other cells types may also express SYK, such as resident renal cells or other types of infiltrating leucocyte.

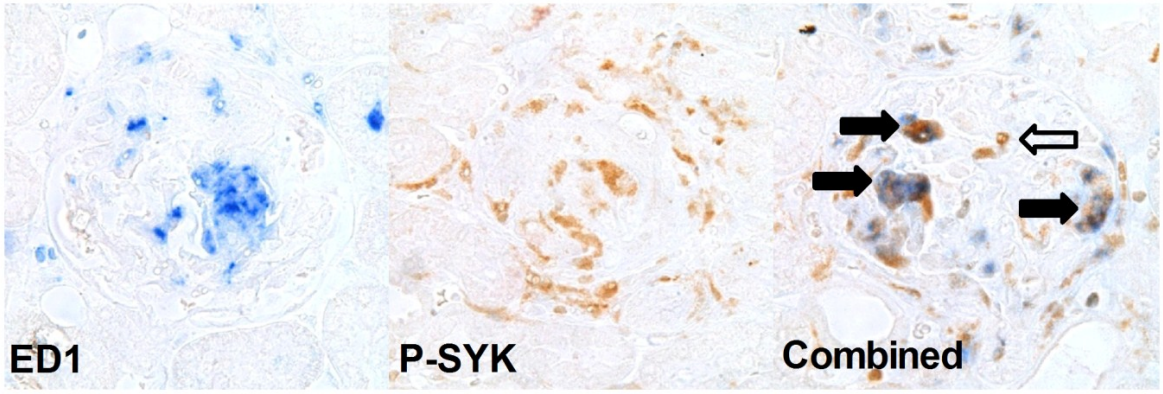

Figure 3.22: Double staining for ED1 and phosphorylated SYK (P-SYK) in nephritic rat kidney.
ED1 (immunophosphatase; blue) and P-SYK (immunoperoxidase; brown) staining within glomeruli of rats 28 days after induction of EAG. Combined staining suggests significant co-localisation of P-SYK to ED1+ macrophages (solid arrows), although there are a small number of P-SYK+ cells that are not ED1+ (hollow arrows). No counterstain, x400 magnification.

3.7 Chapter Three: Summary and discussion of results

This chapter summarises the preparatory work and development of the model and methods that were used in the subsequent investigational experiments described in Chapters Four, Five and Six.

This work included the production and purification sufficient α3(IV)NC1 to conduct subsequent *in vivo* and *in vitro* experiments. I have shown that my protein preparation is both antigenic (by Western blot) and immunogenic *in vivo*, resulting in the induction of anti-GBM antibodies along with end-organ renal and lung damage in WKY rats. Dose-response studies showed that, while α3(IV)NC1 doses of 25-100μg appeared to induce similar degrees of renal injury, use of a 100μg dose resulted in more robust antibody responses and lung damage, and so this dose was used for subsequent intervention studies. Male and female WKY rats are susceptible to EAG, though female rats may develop earlier deposited antibody and glomerular inflammation. Female rats were therefore used in subsequent studies. As anticipated, Lewis rats are resistant to disease induction using this antigen.

Changes in renal biochemistry were not consistently observed until after day 28 post-immunisation. However, after week 6 animals were at risk of severe renal failure and exceeding limits of the home office licence. This suggests an end-point between 4-6 weeks is optimal for assessing changes in renal function in this model; day 36 was used at the end-point in subsequent experiments.

Changes in urea and creatinine clearance may be difficult to interpret in these young, rapidly growing rats. Direct serum urea and creatinine measurements may be adequately reliable

markers of renal dysfunction in these cases. Quantification of proteinuria using 24 hour urinary protein and uPCR measurements provide equivalent information this model.

In addition to refining the *in vivo* EAG model, I have used this antigen preparation to develop a B cell ELISpot assay that allows enumeration of α3(IV)NC1-specific splenic B cells *in vitro*. The incubation conditions for this assay have been optimised.

Finally, I have shown that SYK is expressed and activated (i.e. phosphorylated) within nephritic glomeruli in EAG, and appears to localise significantly (though not exclusively) to infiltrating ED1+ macrophages, a key mediator of injury in this model, strongly implicating SYK activity in the pathogenesis of EAG and supporting my rationale for pharmacologic inhibition of this kinase in future studies. As described in Chapter One, SYK inhibition using fostamatinib or other small molecule inhibitors has been studied in other *in vivo* models of immune-mediated injury. However, confirmation of SYK expression by IHC in these models is limited. T-SYK expression has been described in the skin lesions of MRL/lpr lupus-prone mice[69] and in the synovium of CIA rats[67], although the identification of SYK in its activated, phosphorylated state is limited to the alloimmune heterologous phase of rat nephrotoxic nephritis[239]. This is therefore the first report of P-SYK detection by IHC in an autoimmune model of renal injury. In addition to SYK expression in diseased end-organ renal tissue, I observed strong staining for both T-SYK and P-SYK in the lymphoid tissue, consistent with a well characterised role for SYK in the generation of adaptive immune responses, which supports the rationale for investigating the role of SYK in the development of humoral immunity. The technical strengths and limitations of the immunohistochemical methods I have used are discussed in more detail in Chapter Six.

CHAPTER FOUR - SPLEEN TYROSINE KINASE INHIBITION IN EXPERIMENTAL AUTOIMMUNE GLOMERULONEPHRITIS

4.1 Introduction and experimental design

The aim of the following studies in EAG was to examine the effects of SYK inhibition using fostamatinib on both humoral immune responses and end-organ damage in a pre-clinical model that is relevant to human renal disease (Section 1.6).

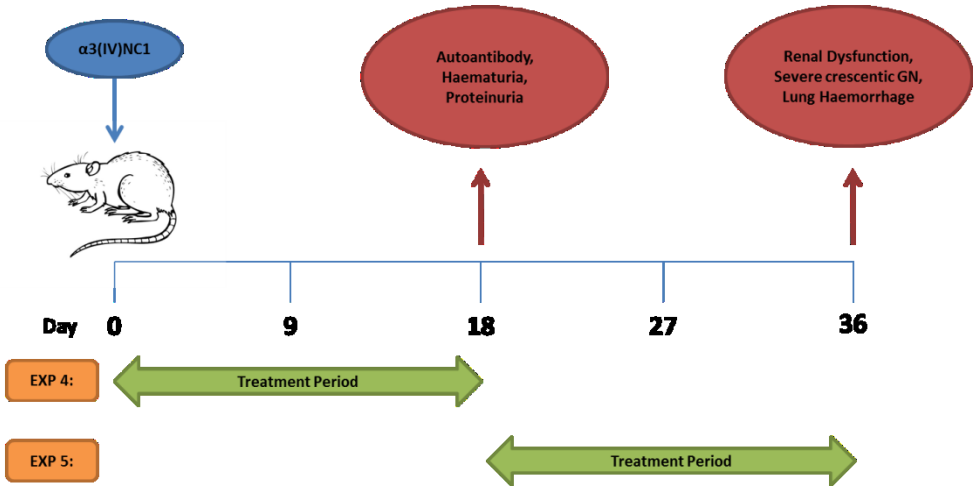

Figure 4.1: Experimental design for SYK inhibition studies in EAG.
Experiment 4 was a preventive study to examine the effects of SYK inhibition on the induction of autoimmunity in EAG. Experiment 5 was to examine the effects of SYK inhibition in established disease, to more accurately reflect the potential clinical use of this strategy.

I have conducted two separate experiments using fostamatinib in the model (Figure 4.1). The purpose of the first study (EAG Experiment 4) was to establish if SYK has a role in the pathogenesis of autoimmunity in EAG - animals were treated from one hour prior to immunisation with α3(IVI)NC1 until day 18. This time point was chosen based on the results of the preliminary experiments in Chapter One which confirmed that immunised animals have both circulating antibodies and early renal injury by this time point, so the effects of SYK inhibition on induction of the autoimmune response should be maximally observed before day 18. From day 18 onwards, treatment was discontinued and animals were monitored for progression of disease after treatment withdrawal. The animals were observed

for a further 18 day period (until day 36) as this provided a sufficient time period for disease to develop after treatment withdrawal, and created overall 'symmetry' in the experimental protocol.

In a second study (EAG Experiment 5), I examined the effects of SYK inhibition in established EAG, to more accurately reflect the potential effect of treatment in clinical practice. In this experiment, initiation of treatment was delayed until 18, at which point the onset of disease was confirmed by the development of haematuria and proteinuria. The animals were then followed until day 36, as the findings of the preliminary studies suggested that severe renal injury (accompanied by biochemical abnormalities) would be observed at this time point before development of symptoms or significant mortality from renal failure.

In both intervention studies, female rats (eight per group) were used since preliminary experiment 3 suggested that females mount earlier immune responses. To obtain comparative histology in treated and untreated animals at day 18, an additional two groups (n=4) were used. A dose of 100μg α3(IVI)NC1 was used since preliminary experiment 2 showed this resulted in more robust humoral responses and reproducible lung injury.

A dose of fostamatinib 40mg/kg twice daily was chosen based on our laboratory's previous dose-response study in NTN that demonstrated maximal biological effect without toxicity, and is consistent with the dose used in murine lupus studies.[68,136] One animal in the preventive study was sacrificed early due to an immediate complication of oral gavage; results for seven animals in the fostamatinib group are therefore reported.

4.2. EAG Experiment 4: Prevention Study

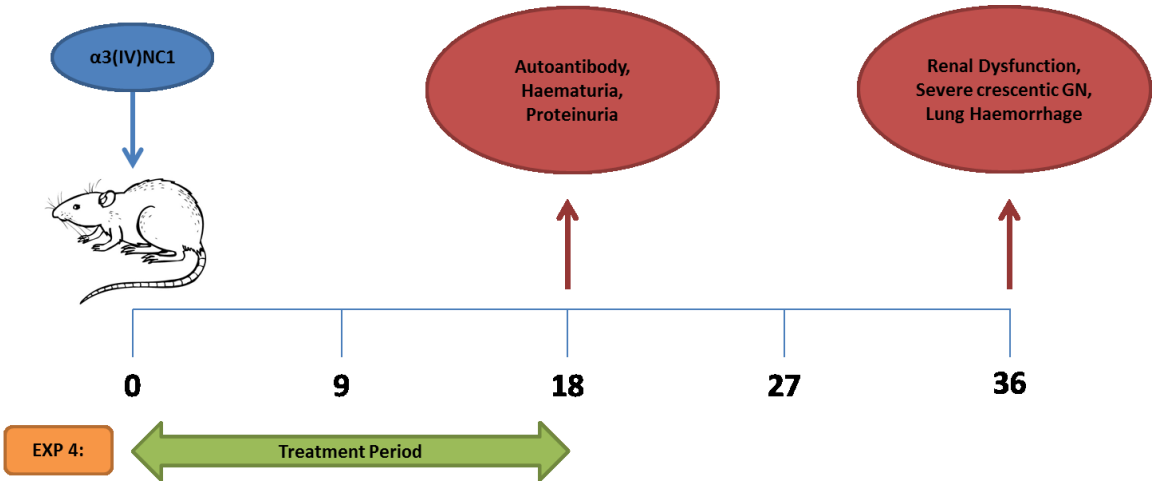

4.2.1 Haematuria and proteinuria

During the treatment period, fostamatinib-treated rats were completely protected from haematuria and proteinuria. When treatment was withdrawn after day 18, animals subsequently developed both urinary abnormalities, though with sustained protection compared to vehicle-treated controls at day 36 (Figure 4.2).

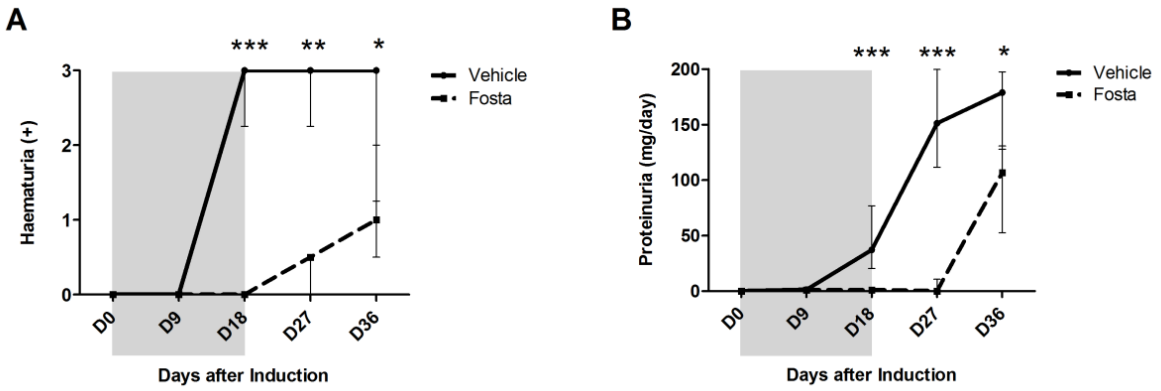

Figure 4.2: Urinary findings in EAG Experiment 4: Prevention Study (Day 0-18).
(A) Haematuria and (B) Proteinuria in fostamatinib and vehicle-treated animals during the 18 day treatment period (shaded) and the 18 day treatment withdrawal period (unshaded), showing complete protection from these urinary abnormalities during fostamatinib treatment. Data shown as median ±IQR. *p<0.05, **p<0.01, ***p<0.001, Mann Whitney U test.

4.2.2 Histological injury

Fostamatinib-treated animals had entirely normal renal histology at day 18, whereas vehicle-treated animals had severe pathology affecting 26% of glomeruli (Figure 4.3). Glomeruli had acute crescent formation, characterised by rupture of the glomerular basement membrane and extravasation of fibrin and cells into Bowman's space (Figure 4.4). By day 36, these had progressed to large, circumferential, fibrocellular crescents in the vehicle-treated group, whereas fostamatinib-treated animals had earlier lesions, similar to those seen in untreated animals at day 18, which were also fewer in number (38% reduction; p=0.0014) compared to vehicle-treated controls.

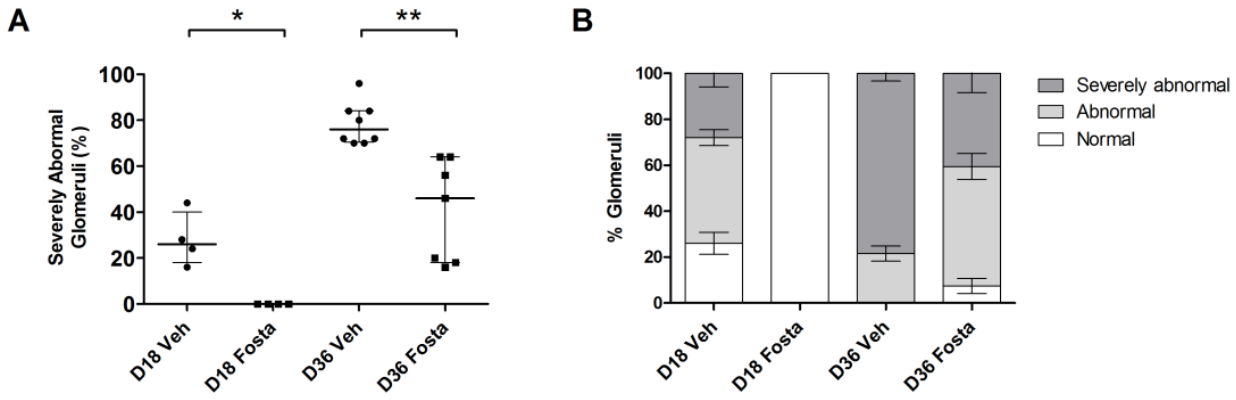

Figure 4.3: Histological injury in EAG Experiment 4: Prevention Study (Day 0-18).
(A) Proportion of severely abnormal glomeruli in fostamatinib and vehicle-treated animals at day 18 and day 36, shown as median ±IQR. *p<0.05, **p<0.01, Mann Whitney U test. (B) The range of glomerular abnormalities (normal, abnormal or severely abnormal) in each group, shown as mean ±SEM.

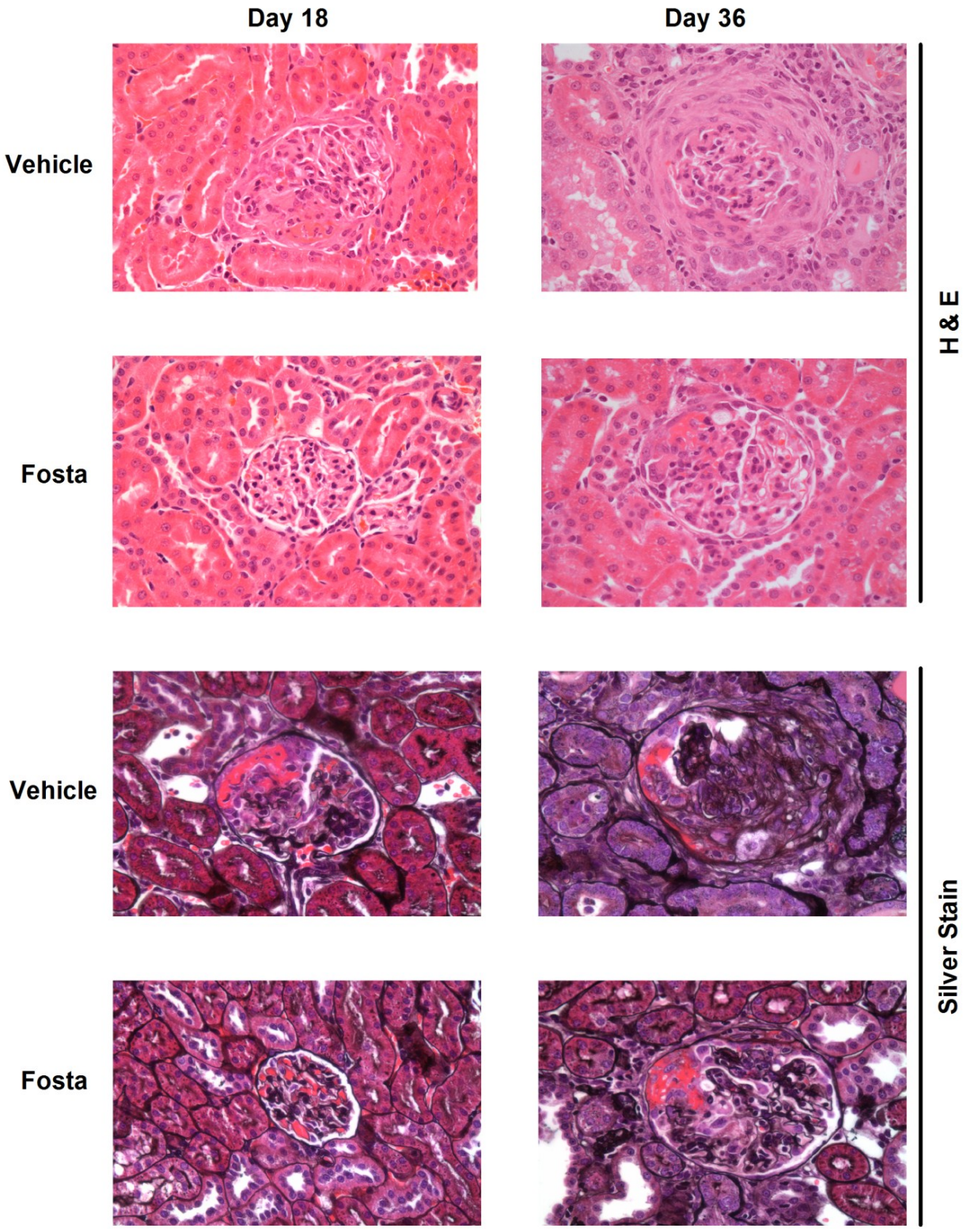

Figure 4.4: Representative histological injury in EAG Experiment 4: Prevention Study (Day 0-18). Photomicrographs showing representative glomerular histology in fostamatinib and vehicle-treated animals at day 18 and day 36. H&E and Jones methanamine silver stains as indicated, x400 magnification.

4.2.3 Infiltrating leucocytes

The histopathological findings were closely mirrored by leucocyte infiltration (Figure 4.5). At day 18, fostamatinib-treated animals had no evidence of ED1+ or CD8+ cells within glomeruli, whereas vehicle-treated controls had demonstrable leucocyte infiltration. After treatment withdrawal, animals developed an influx of both cell types, and by day 36 there was a trend towards higher numbers of both ED1+ and CD8+ cells in the fostamatinib group (though not statistically significant, $p=0.12$ for both parameters). The lower number of glomerular leucocytes in vehicle-treated animals at this time point is in keeping with the observations of preliminary experiment 1 that suggested glomerular leucocyte number falls between day 28 and day 42, possibly as the peak inflammatory phase of disease has been passed.

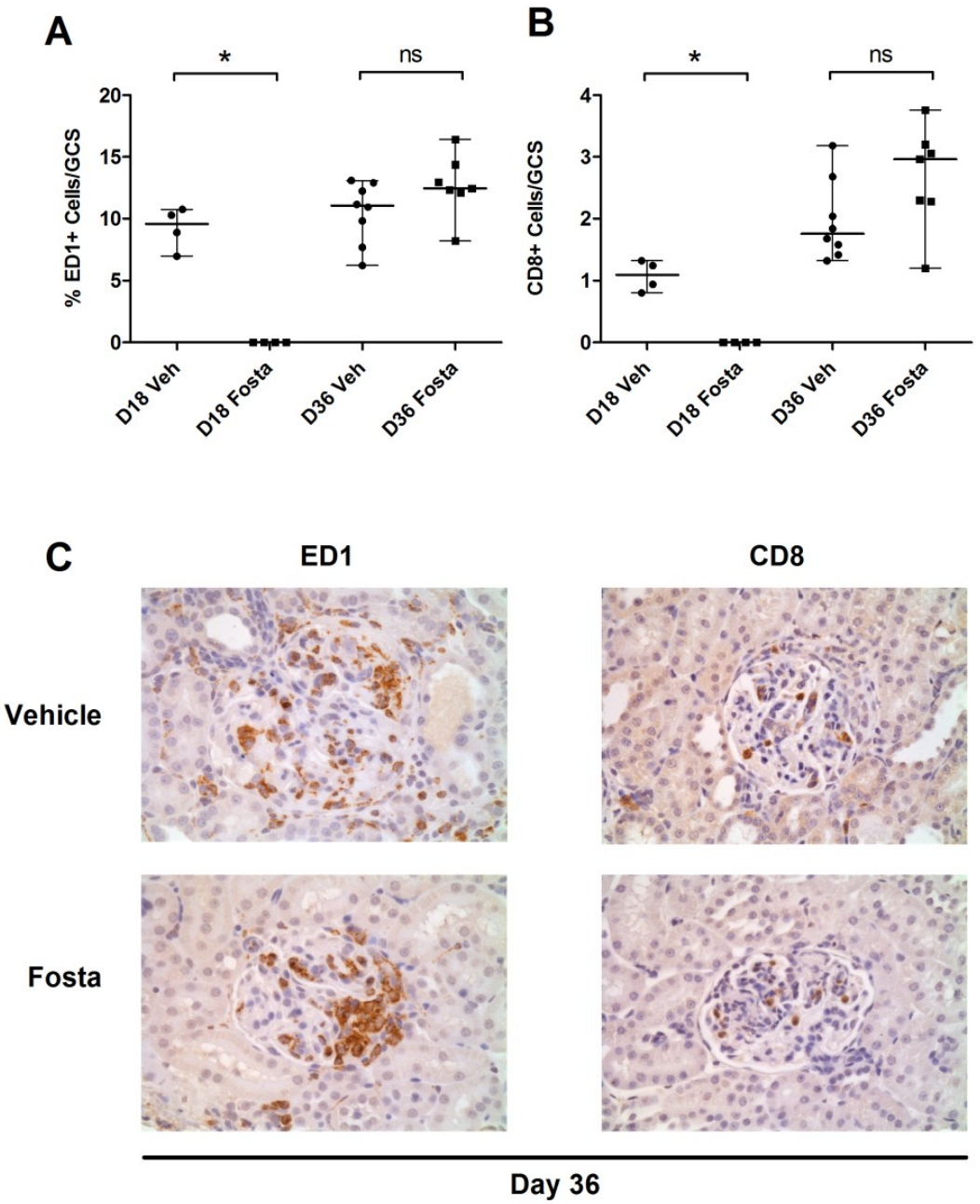

Figure 4.5: Glomerular leucocyte infiltration in EAG Experiment 4: Prevention Study (Day 0-18).
(A) Macrophage infiltration, expressed as the mean percentage of ED1+ cells per glomerular cross section (GCS), and (B) CD8+ leucocyte infiltration, expressed as the mean number of CD8+ cells per GCS, in fostamatinib and vehicle-treated animals at day 18 and day 36. Data shown as median ±IQR, ns – not significant, *p<0.05, Mann Whitney U test. (C) Photomicrographs showing representative immunoperoxidase stains for ED1+ and CD8+ cells in both groups at day 36, with haematoxylin counterstain, x400 magnification.

4.2.4 Renal function

As shown in Figure 4.6, fostamatinib-treated animals had lower serum urea and serum creatinine concentrations compared to vehicle-treated controls at day 36, in keeping with preservation of excretory renal function.

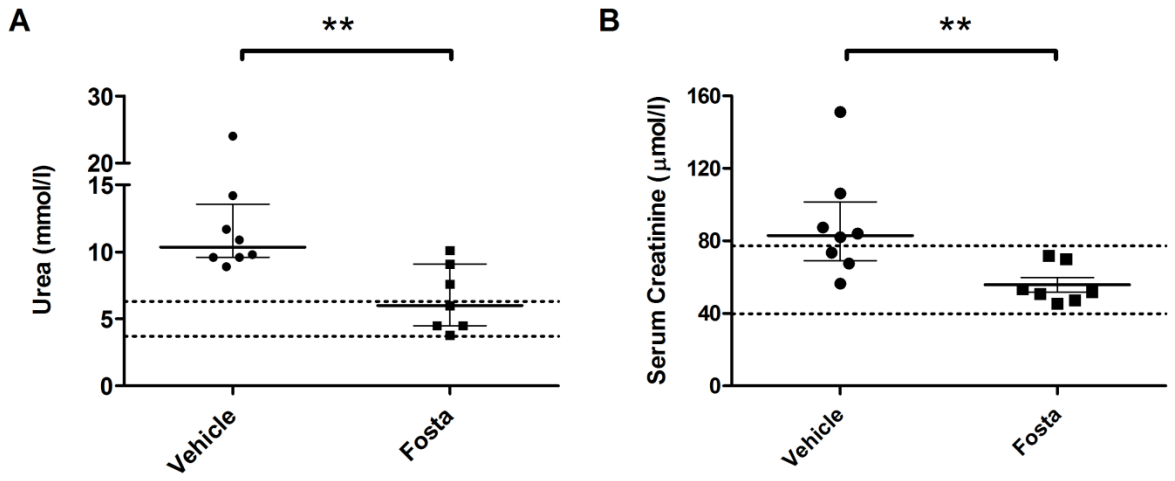

Figure 4.6: Renal function in EAG Experiment 4: Prevention Study (Day 0-18).
(A) Serum urea, and (B) Serum creatinine concentrations in fostamatinib and vehicle-treated control animals at day 36, showing preservation of renal function with fostamatinib treatment. Normal ranges, determined from all CFA control animals in preliminary experiments 1 & 2 are shown by horizontal dotted lines. Data shown as median ±IQR. *p<0.05, **p<0.001, Mann Whitney U Test.

4.2.5 Lung haemorrhage

At day 36, fostamatinib-treated animals had less severe lung disease, whether quantified by macroscopic inspection of the lung surfaces at the time or cull, or microscopic inspection for haemosiderin-laden cells (Figure 4.7).

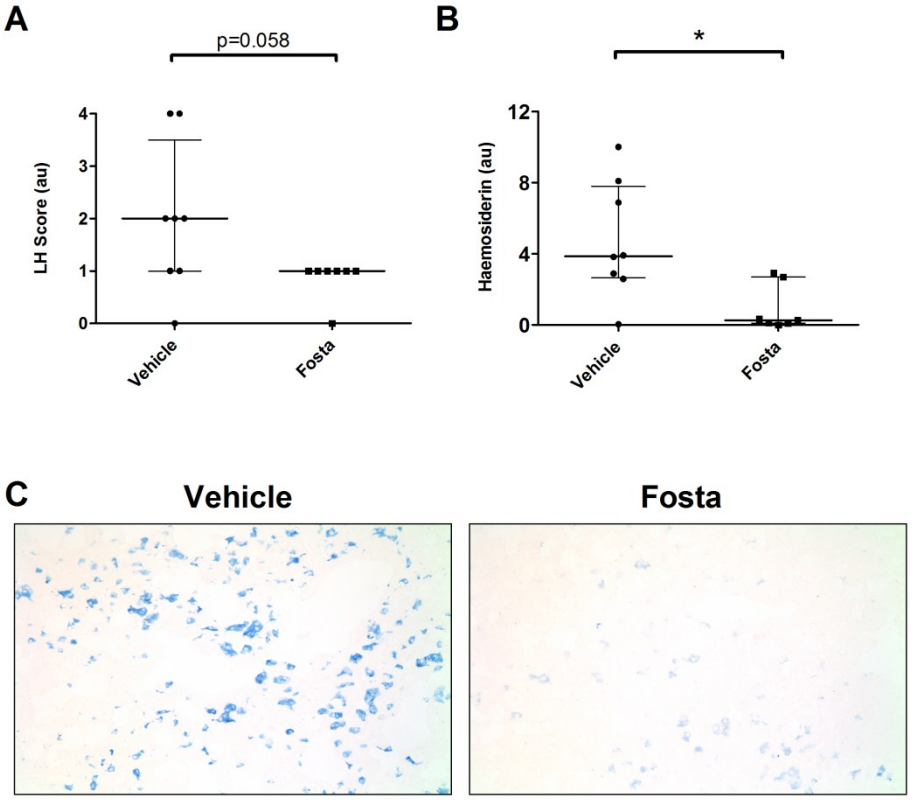

Figure 4.7: Lung haemorrhage in EAG Experiment 4: Prevention Study (Day 0-18).
(A) Macroscopic lung haemorrhage score, and (B) Quantification of haemosiderin-laden cells in lung tissue, in vehicle and fostamatinib-treated animals at day 36. Data shown as median ±IQR, *p<0.05, Mann Whitney U test. (C) Photomicrographs showing representative staining for haemosiderin-positive cells in lung sections, using Perls' Prussian Blue, without counterstain to facilitate accurate counting, x200 magnification.

4.2.6 Humoral autoimmune response

During the 18 day treatment period, fostamatinib-treated animals had minimal serological evidence of autoimmunity, with barely detectable circulating anti-α3(IV)NC1 antibodies (Figure 4.8A). When treatment was withdrawn, antibody levels rose, but reached a lower plateau level than vehicle-treated control animals at day 36. (51% reduction; p=0.021). In keeping with lower levels of circulating autoantibodies, there was less deposited antibody detected in the glomeruli of fostamatinib-treated animals at day 36 (Figure 4.8B).

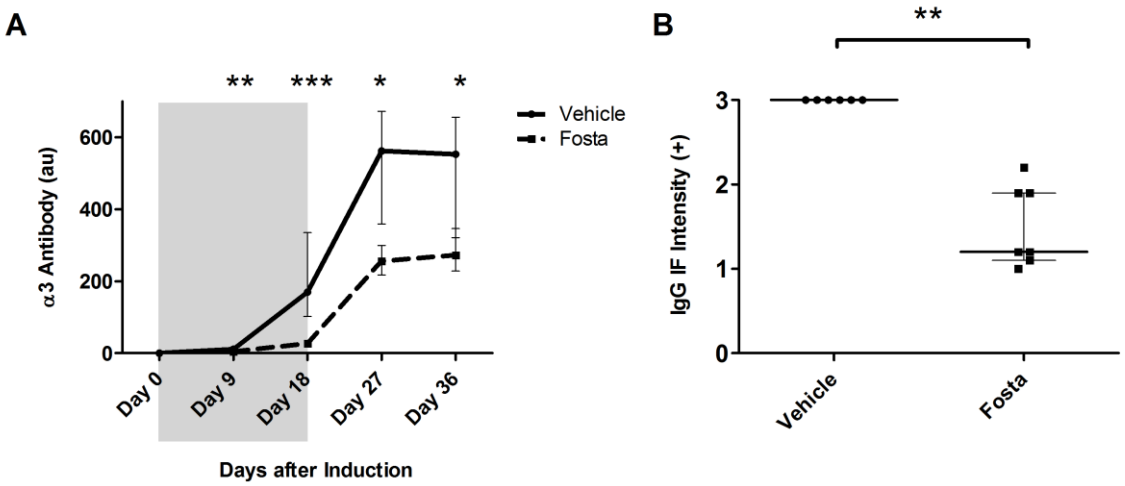

Figure 4.8: Humoral responses in EAG Experiment 4: Prevention Study (Day 0-18).
(A) Circulating anti-α3(IV)NC1 antibodies during the 18 treatment period (shaded) and the 18 day treatment withdrawal period (unshaded), showing minimal antibody responses during fostamatinib treatment, and a lower plateau response after treatment withdrawal. (B) Quantification of direct immunofluorescence for deposited IgG at day 36, showing reduced glomerular antibody deposition in fostamatinib-treated animals. All data shown as median ±IQR, *p<0.05, **p<0.01, ***p<0.001, Mann Whitney U test.

4.2.7 EAG Experiment 4: Prevention Study summary

In this study, fostamatinib treatment completely protected from the development of key disease phenotypes during the initial 18 day treatment period – animals did not develop circulating antibodies, urinary abnormalities, histological renal injury or glomerular inflammatory cell infiltrates. This observation suggests that SYK activity is an absolute requirement for the induction of autoimmunity in this model. When treatment was withdrawn at day 18, animals subsequently developed typical features of disease, and at day 36 each of these disease parameters was comparable to those in untreated animals at day 18, suggesting that SYK 'disinhibition' by treatment withdrawal allowed the natural history of the model to be restored.

4.3 EAG Experiment 5: Established Disease Study

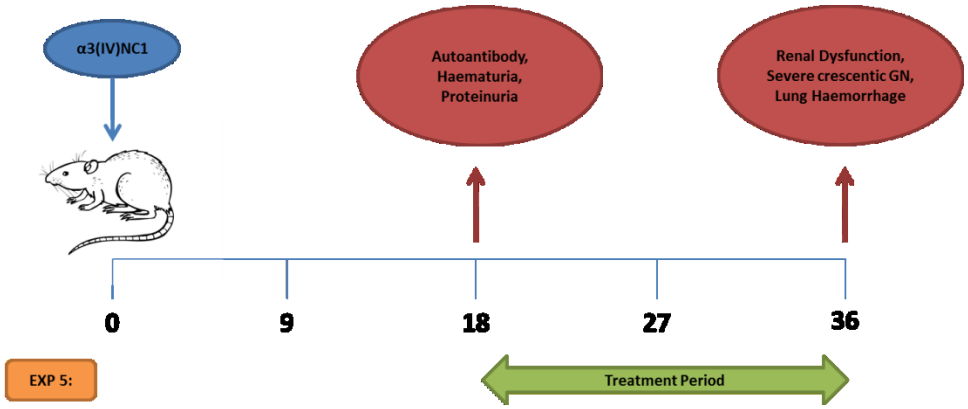

4.3.1 Haematuria and proteinuria

At day 18, disease was confirmed in all animals by the onset of haematuria and proteinuria. The introduction of fostamatinib treatment at day 18 resulted in a complete and rapid resolution of these urinary abnormalities that was sustained until day 36 (Figure 4.9), whereas vehicle-treated controls had progression in both parameters.

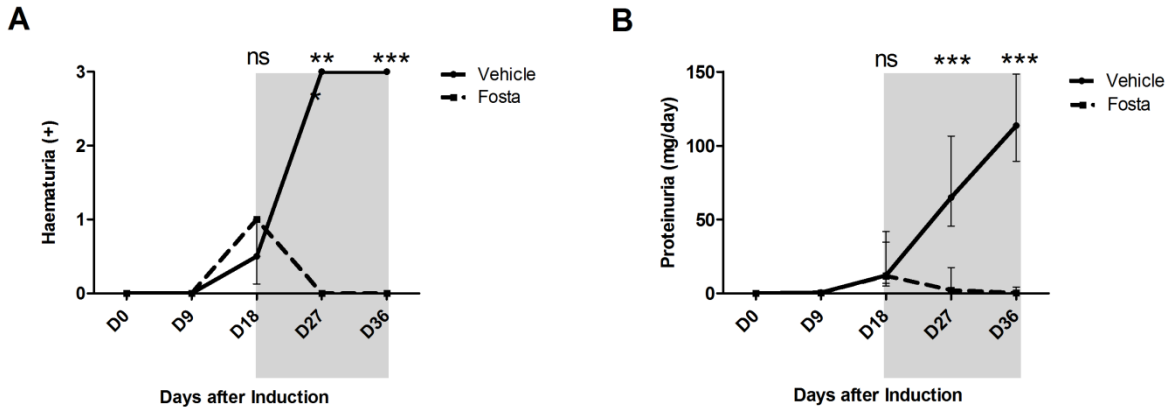

Figure 4.9: Urinary findings in EAG Experiment 5: Established Disease Study (Day 18-36).
(A) Haematuria and (B) Proteinuria in fostamatinib and vehicle-treated animals during the 18 day treatment free period (unshaded) and the 18 day treatment period (shaded), showing complete resolution of urinary abnormalities with fostamatinib treatment. Data shown as median ±IQR. *p<0.05, **p<0.01, ***p<0.001, Mann Whitney U test.

4.3.2 Histological injury

As described in section 4.2.2, vehicle-treated animals had severe abnormalities in 26% of glomeruli at day 18. Following treatment from day 18 to 36, the fostamatinib group had almost entirely normal glomerular histology (Figure 4.10) whereas vehicle-treated animals had progression to >70% severe glomerular abnormalities. Representative histology is shown in Figure 4.11. This striking observation suggests that introduction of fostamatinib treatment lead to reversal of glomerular necrosis and crescents during the course of the 18 day treatment exposure.

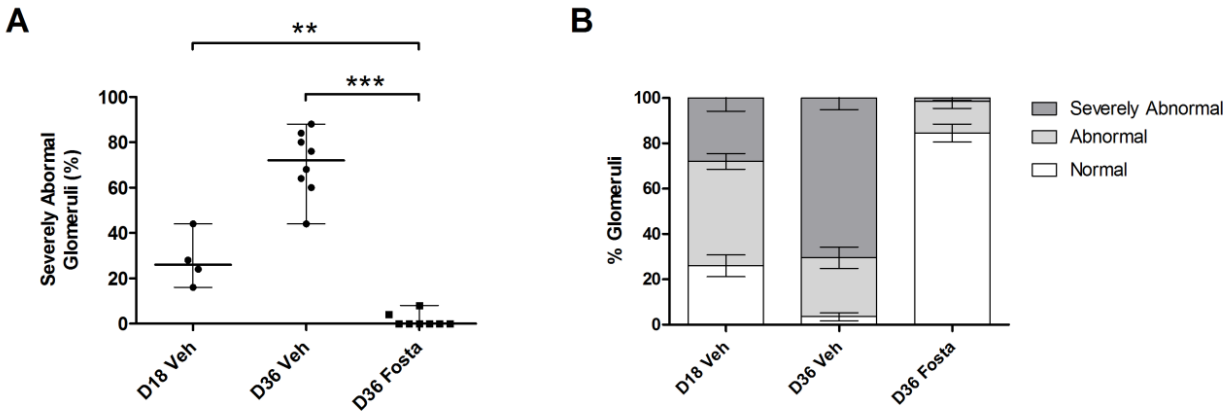

Figure 4.10: Histological injury in EAG Experiment 5: Established Disease (Day 18-36).
(A) Proportion of severely abnormal glomeruli in fostamatinib and vehicle-treated animals at day 18 and day 36, with day 18 vehicle-treated controls repeated from Figure 4.3 for comparison. Data shown as median ±IQR. *p<0.05, **p<0.01, ***<0.001, Mann Whitney U test. (B) The range of glomerular abnormalities (normal, abnormal or severely abnormal) in each group, shown as mean ±SEM.

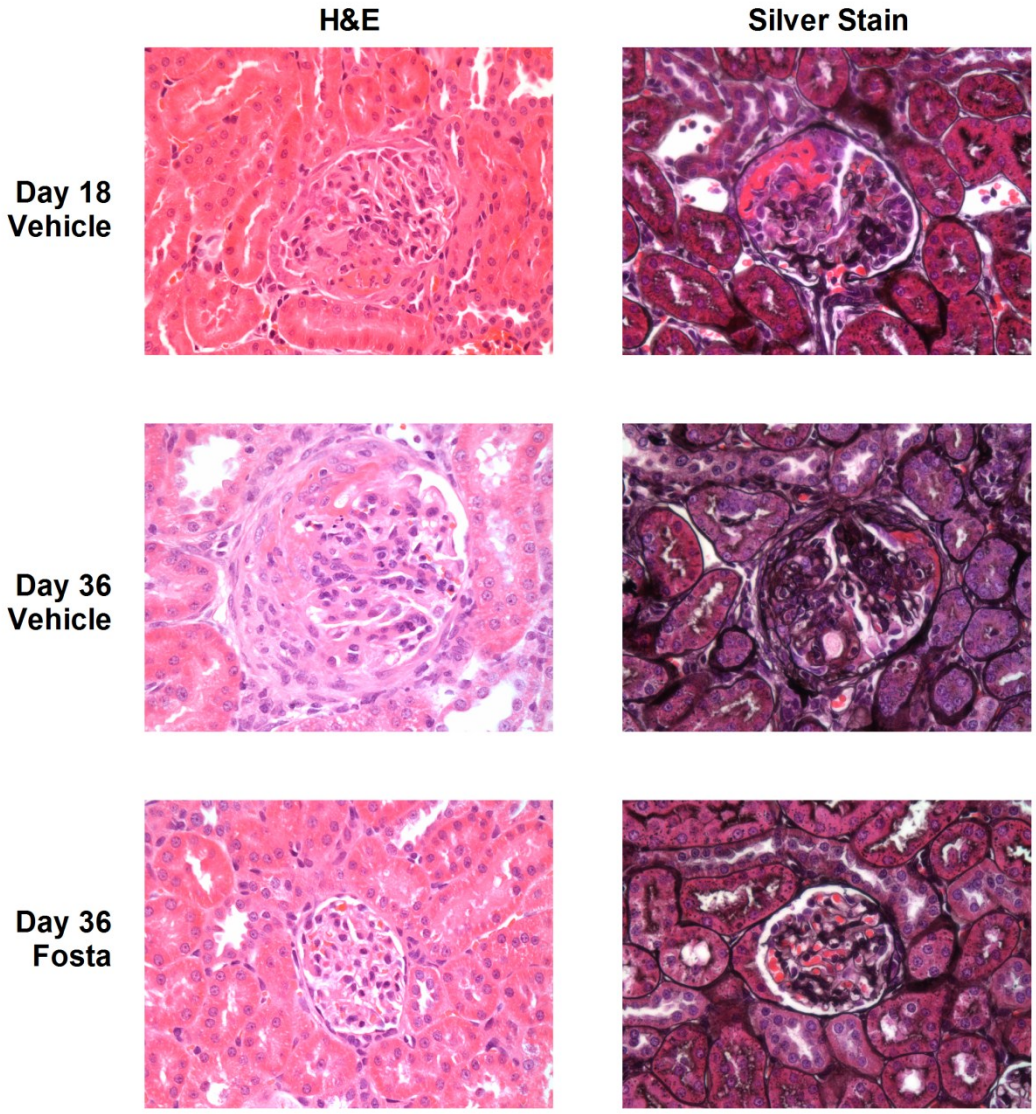

Figure 4.11: Representative histological injury in EAG Experiment 5: Established Disease (Day 18-36). Photomicrographs showing representative glomerular histology in fostamatinib and vehicle-treated animals at day 36, with day 18 histology in vehicle-treated animals repeated from figure 4.4 for comparison. At day 18, vehicle treated animals had early crescents, characterised by rupture of the glomerular basement membrane and extravasation of fibrin and cells into Bowman's space. By day 36, in vehicle treated animals, these had progressed to large circumferential fibrocellular crescents. In fostamatinib treated animals, early crescentic changes had resolved and glomeruli had essentially normal histological appearances by day 36. H&E and Jones methanamine silver stains as indicated, x400 magnification.

4.3.3 Infiltrating leucocytes

At the end of the 18 day treatment period, fostamatinib-treated animals had minimal evidence of ED1+ or CD8+ cell infiltration into glomeruli. Again, when compared to day 18 vehicle-treated control animals, this suggested significant efflux during treatment from day 18 to 36 (Figure 4.12).

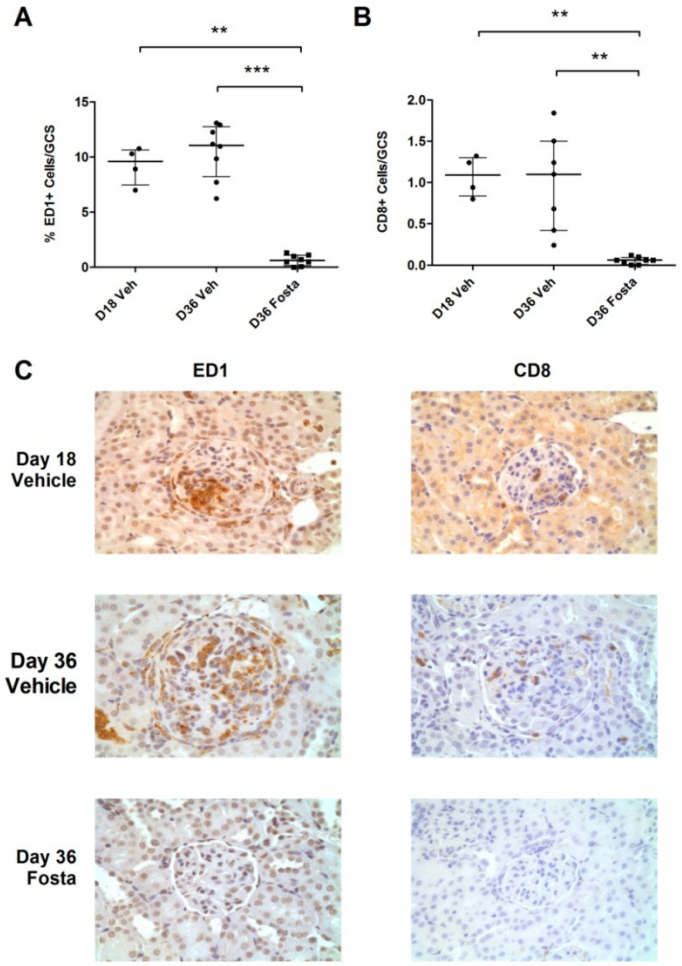

Figure 4.12: Glomerular leucocyte infiltration in EAG Experiment 5: Established Disease (Day 18-36).
(A) Macrophage infiltration, expressed as the mean percentage of ED1+ cells per glomerular cross section (GCS), and (B) CD8+ leucocyte infiltration, expressed as the mean number of CD8+ cells per GCS, in fostamatinib and vehicle-treated animals at 36, with day 18 data repeated from Figure 4.5 for comparison. Introduction of fostamatinib treatment at day 18 lead to reversal of inflammatory cell infiltration. Data shown as median ±IQR, *p<0.05, **p<0.01, Mann Whitney U test. (C) Photomicrographs showing representative immunoperoxidase stains for ED1+ and CD8+ cells at day 18 and day 36 as indicated, with haematoxylin counterstain, x400 magnification.

4.3.4 Renal function

As shown in Figure 4.13, vehicle-treated animals had significantly elevated serum urea concentrations compared to the fostamatinib group, implying loss of excretory renal function. In this experiment, however, I did not observe a significant change in serum creatinine levels (or creatinine clearance; data not shown), possibly reflecting the inadequacy of this marker as an indicator of renal function in young rats with low muscle mass.

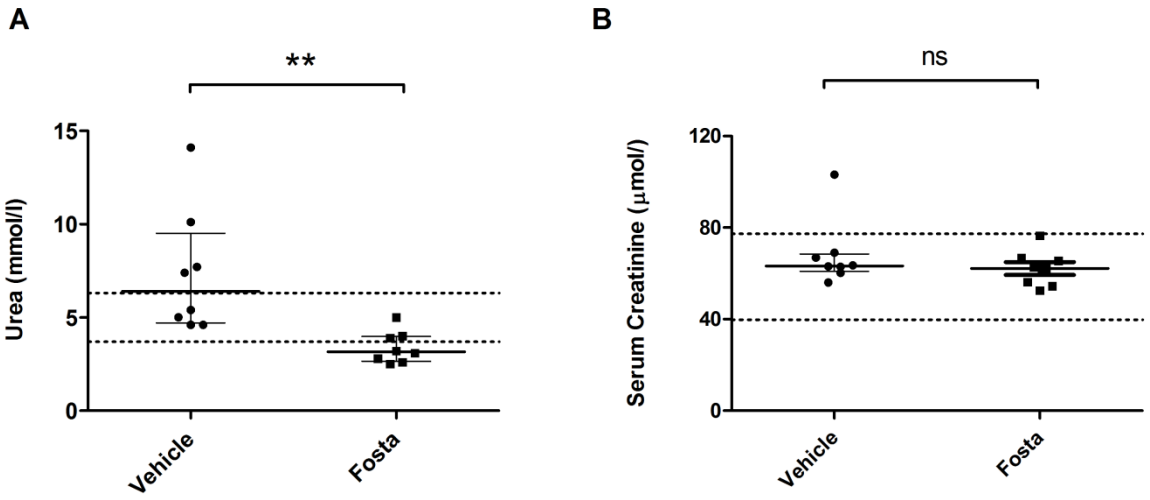

Figure 4.13: Renal function in EAG Experiment 5: Established Disease (Day 18-36).
(A) Serum urea, and (B) Serum creatinine concentrations in fostamatinib and vehicle-treated control animals at day 36. Normal ranges, determined from all CFA control animals in preliminary experiments 1 & 2 are shown by horizontal dotted lines. Data shown as median ±IQR.*p<0.05, **p<0.01, Mann Whitney U Test.

4.3.5 Lung haemorrhage

In this experiment, fostamatinib-treated animals were completely protected from macroscopic evidence of lung injury, and had minimal evidence of haemosiderin-laden cells in the lung on microscopic examination (Figure 4.14).

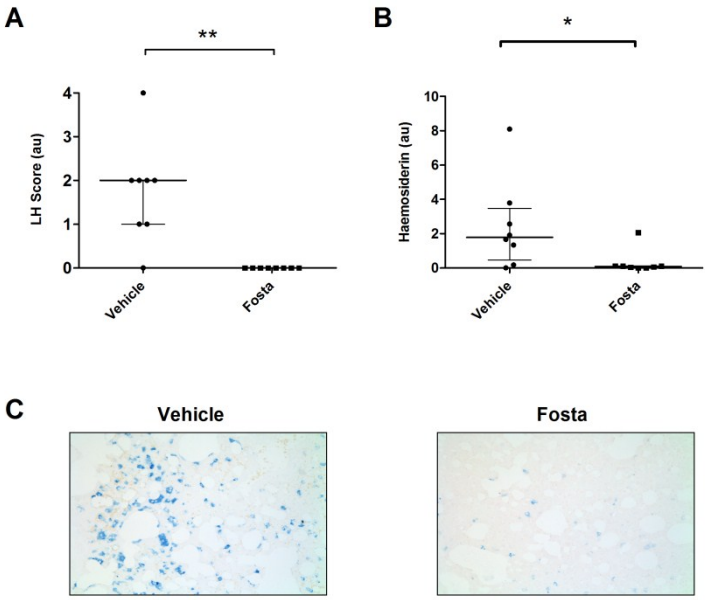

Figure 4.14: Lung haemorrhage in EAG Experiment 5: Established Disease (Day 18-36).
(A) Macroscopic lung haemorrhage score, and (B) Quantification of haemosiderin-laden cells in lung tissue, in vehicle and fostamatinib-treated animals at day 36. Data shown as median ±IQR, *p<0.05, **p<0.01, Mann Whitney U test. (C) Photomicrographs showing representative staining for haemosiderin-positive cells in lung sections, using Perls' Prussian Blue, without counterstain to facilitate accurate counting, x200 Magnification.

4.3.6 Humoral autoimmune response

The introduction of fostamatinib treatment at day 18 caused circulating autoantibody levels to plateau, at a time when levels were rising rapidly in the vehicle treated group (Figure 4.15A). Since the half-life of these autoantibodies exceeds 2-3 weeks, this suggests that there was no ongoing antibody production after the introduction of treatment, implying possible effects of SYK inhibition on mature, antibody secreting B cells or plasma cells. At the end of the treatment period, there was a 75% reduction in circulating antibody levels (p=0.0006) with a concomitant decrease in the amount of deposited antibody (Figure 4.15B). There was also a decrease in deposited complement component C3 (Figure 14.5C), in keeping with reduced activation of the classical complement pathway. The intensity of complement staining was,

however, much less than for deposited IgG, in keeping with Dr Reynolds previous observations in this model (personal communication).

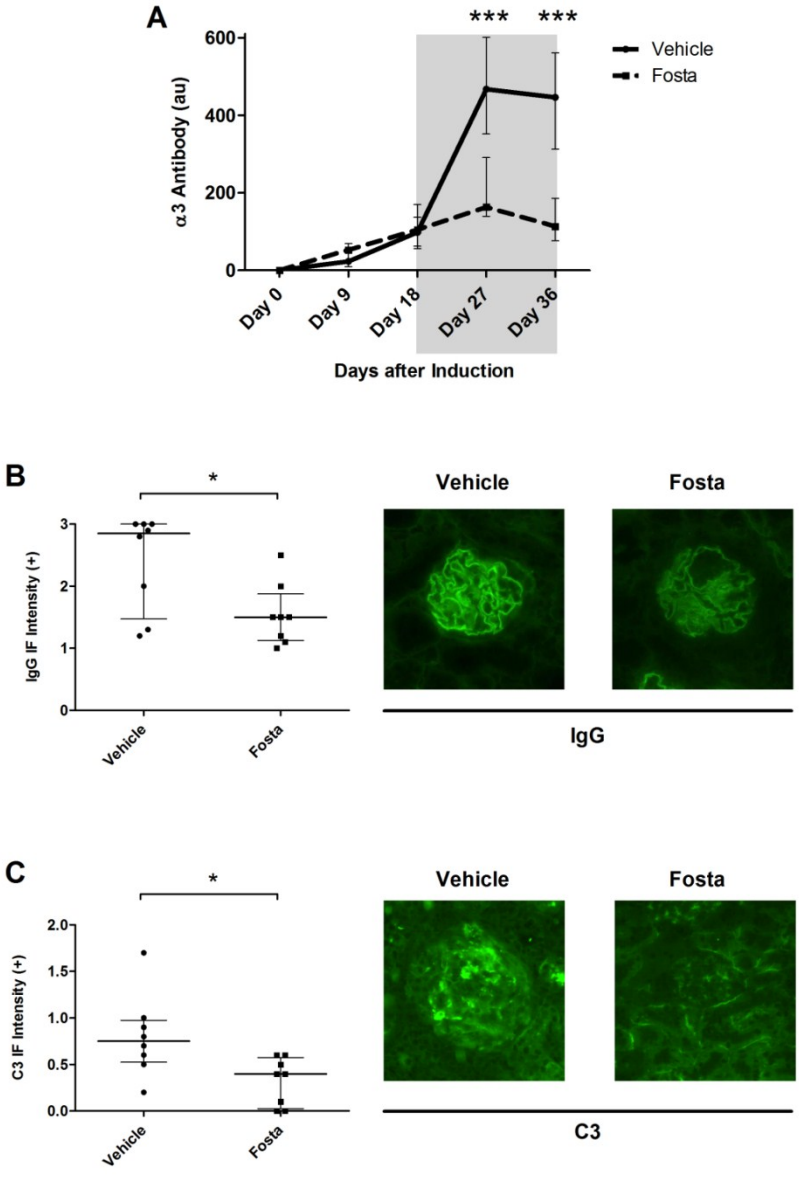

Figure 4.15: Humoral responses in EAG Experiment 5: Established Disease (Day 18-36).
(A) Circulating anti-α3(IV)NC1 antibodies during the 18 treatment free period (unshaded) and the 18 day treatment period (shaded), showing cessation of autoantibody production following the introduction of fostamatinib treatment. (B) & (C) Quantification of direct immunofluorescence for IgG and complement C3 at day 36, showing reduced glomerular antibody and complement deposition in fostamatinib-treated animals, with representative fluorescence images. Anti-rat IgG FITC and anti-rat C3 FITC as indicated, x400 magnification. All data shown as median ±IQR, *p<0.05, **p<0.01, ***p<0.001, Mann Whitney U test.

4.3.7 Haematological indices

In this experiment, I had the opportunity to measure haemoglobin, white cell and platelet counts at day 36, following 18 days treatment with fostamatinib (Figure 4.16). There was a modest but significant decline in both haemoglobin concentrations and white cell count following fostamatinib treatment. There was also a moderate thrombocytosis. These observations are consistent with previously reported immunotoxicity assessments in Sprague-Dawley rats[80]. In these studies, full recovery of peripheral blood counts was observed following a 14 day 'wash-out' period.

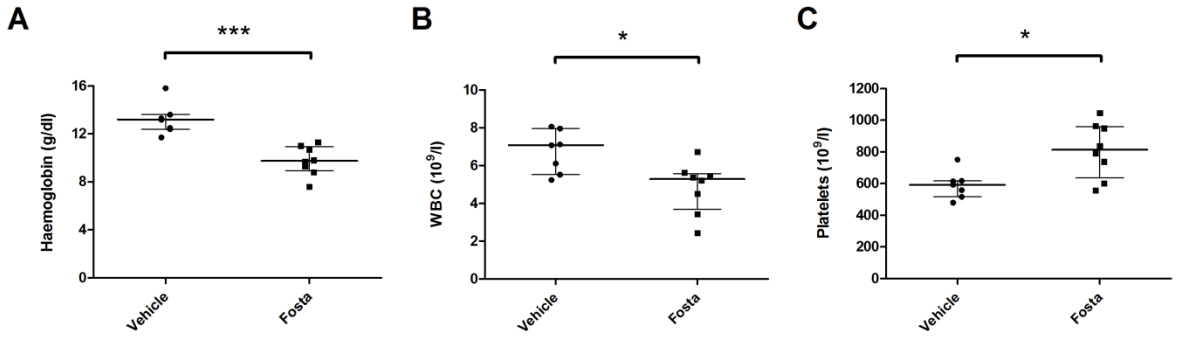

Figure 4.16: Haematological indices in EAG Experiment 5: Established Disease (Day 18-36).
(A) Haemoglobin concentration, (B) White blood cell (WBC) count, and (C) Platelet count in fostamatinib and vehicle-treated animals at day 36. Data shown as median ±IQR, *p<0.05, **p<0.01, ***p<0.001, Mann Whitney U test.

4.3.8 EAG Experiment 5: Established Disease Study summary

This experiment has shown that SYK inhibition with fostamatinib is an effective treatment for established disease in EAG. Introduction of treatment at day 18 resulted in reversal of severe glomerular pathology, preservation of renal function, and protection from lung haemorrhage. It also resulted in cessation of antibody production, suggesting a direct

inhibitory effect on mature, antibody producing B cells or plasma cells. These dramatic effects were observed without disproportionate bone marrow suppression.

4.4 B cell ELISpot and flow cytometric analysis

Since I observed significant effects of SYK inhibition on humoral immune responses in both *in vivo* studies, I went on to enumerate antigen-specific splenic B cells using the B-cell ELISpot assays described in Chapter Two. Fostamatinib treatment from days 0 to 18 after disease induction resulted in a significant reduction in the generation of α3(IV)NC1 specific splenic B cells, when measured at day 18 (Figure 4.17). In some instances, the number of specific splenic B cells in fostamatinib-treated animals was comparable to those in animals immunised with CFA alone.

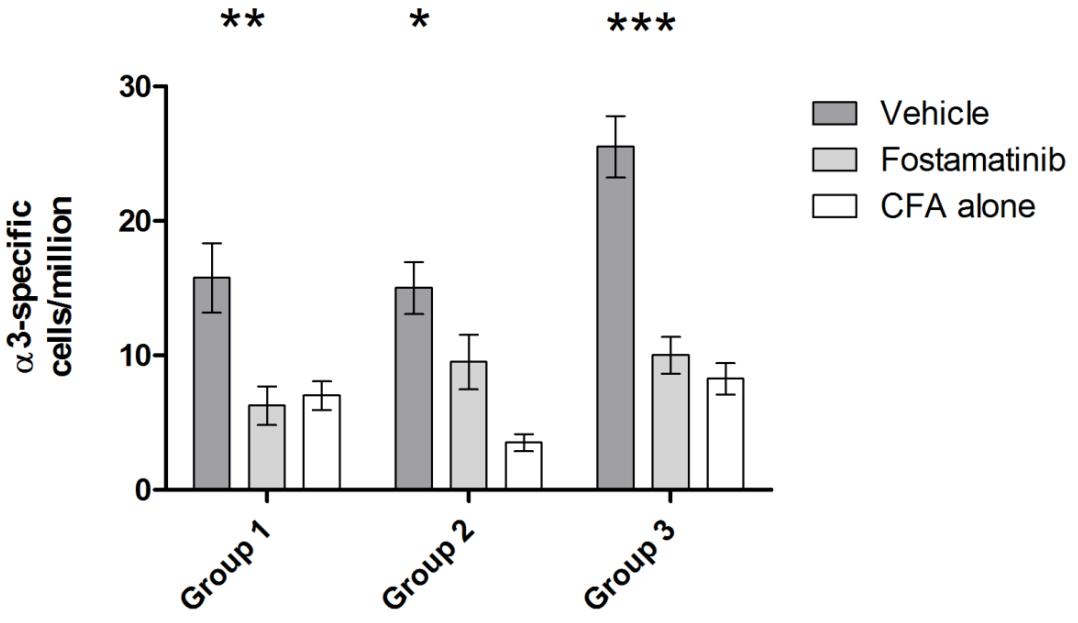

Figure 4.17: α3(IV)NC1-specific splenic B cells following fostamatinib treatment from day 0-18. Fostamatinib treatment inhibited the generation of α3(IV)NC1-specific splenic B cells. Results from three biological replicate groups are shown, each including three rats (vehicle-treated, fostamatinib-treated, and a CFA alone rat for comparison). Data shown as mean ±SEM (of ≥8 technical replicates). *p<0.05, **p<0.01, ***p<0.001, 1-way ANOVA with Bonferroni post-comparison for vehicle versus fostamatinib treatment.

In animals treated from day 18-36, once disease was established, there was no significant difference in the number of antigen-specific splenic B cells at the end of the treatment period (Figure 4.18). This supports the observation that the introduction of fostamatinib treatment at day 18 had a direct effect on antibody production by mature antigen-specific cells, since there was no ongoing antibody production during this period, despite equal numbers of antigen-specific cells being present in the spleen.

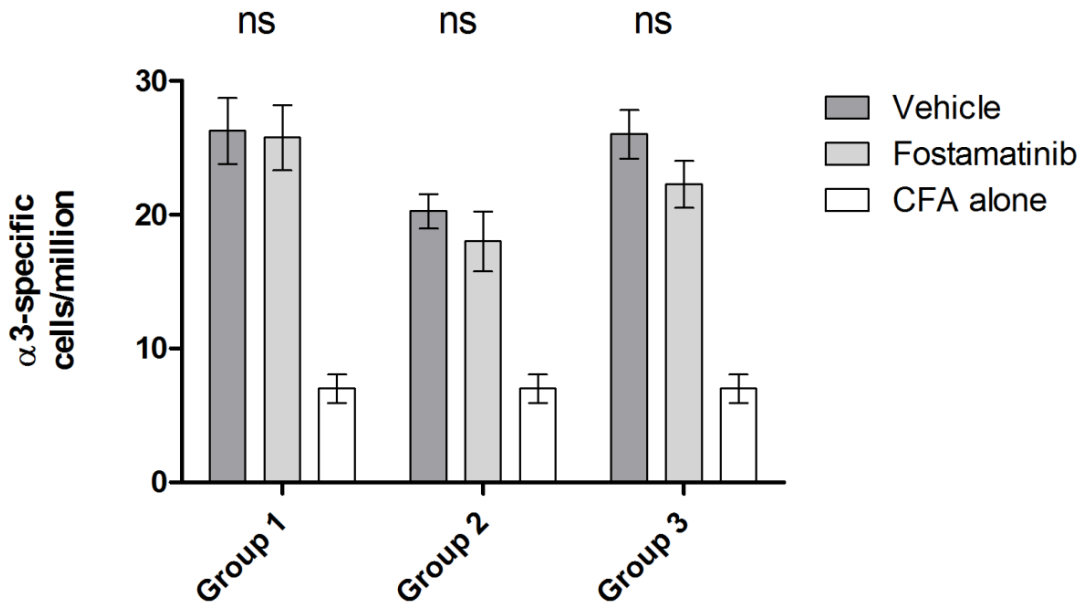

Figure 4.18: α3(IV)NC1-specific splenic B cells following fostamatinib treatment from day 18-36. Fostamatinib treatment did not significantly affect the number of α3(IV)NC1-specific splenic B cells when treatment was initiated at day 18, once clonal B cell responses were established. Results from three biological replicate groups are shown, each including three rats (vehicle-treated, fostamatinib-treated, and a CFA alone rat for comparison). Data shown as mean ±SEM (of ≥8 technical replicates). ns – not significant, 1-way ANOVA with Bonferroni post-comparison for vehicle versus fostamatinib treatment.

I also tested whether the production of anti-α3(IV)NC1 antibodies could be inhibited *in vitro* in the ELISpot assay by pre-incubating splenocytes taken from EAG rats with R406, the active metabolite of fostamatinib, before application to the ELISpot plate. An initial result suggested that there was a dose-dependent reduction in antibody production using the

approach, although subsequent assays did not confirm significant reproducibility of this observation (Figure 4.19). Since cells could not be recovered from the ELISpot plate at the end of the incubation, separate cell preparations were kept in identical conditions in standard cell culture dishes to allow cell viability counts at the end of the experiment - these did not show adverse effects on overall splenocyte survival after 48 hours' incubation with R406 at the doses used (data not shown).

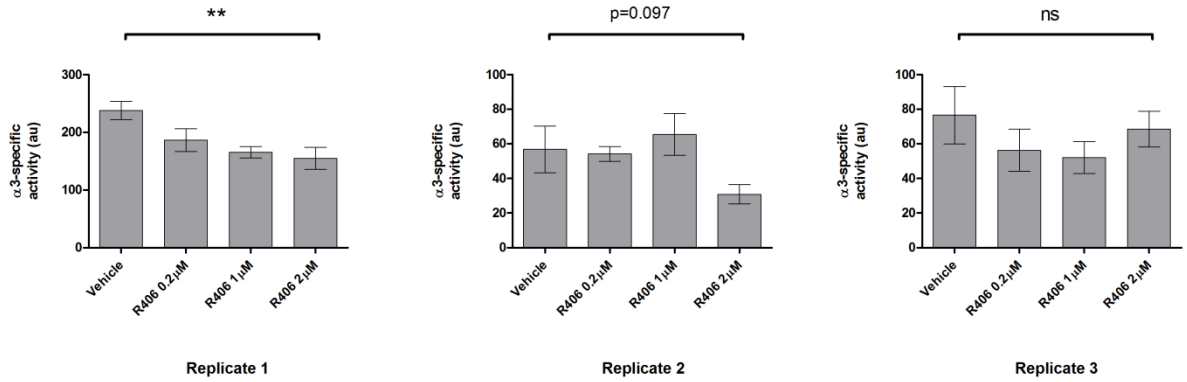

Figure 4.19: Effect of R406 on anti-α3(IV)NC1 antibody production by splenic B cells *in vitro*.
Splenocytes taken from EAG rats 28 days after disease induction were incubated with varying doses of R406, the active metabolite of fostamatinib, prior to application on the ELISpot plate and during the subsequent 48 hour assay incubation. An initial experiment (Replicate 1) suggested that R406 inhibited the production of anti-a3(IV)NC1 antibodies by splenic B cells, although this finding was not robustly reproduced (Replicates 2 & 3). a3(IV)NC1-specific 'activity' is a composite measurement of spot number, size and intensity. Overall cell viability, as assessed by trypan blue cell counting at the end of the experiment, was not affected at these concentrations of R406 (data not shown). Data from three biological replicate experiments is shown, as mean ±SEM (of ≥8 technical replicates). ns – not significant, *p<0.05, **p<0.01, 1-way ANOVA.

I analysed the overall number of CD4+, CD8+ and CD45RA+ splenocytes following treatment from days 0 to 18, in order to examine the effects of fostamatinib on overall B cell survival, and also to confirm that the relative proportions of B cells in the splenocyte preparations used for the ELISpot assays were the same. Flow cytometric analysis was performed with the assistance of Mr William Jackson and Dr Anisha Tanna. We found only modest changes in the overall proportion of CD8, CD4 and CD45RA positive splenocyte

subsets after 18 days treatment with fostamatinib (Figures 4.20). The maintenance of CD45RA positive population, in particular, suggests that B cell survival was not adversely affected by a short period of fostamatinib treatment, and again implies that the attenuation of further antibody production observed in EAG Experiment 5 was due to a direct inhibitory effect of fostamatinib on autoantibody production.

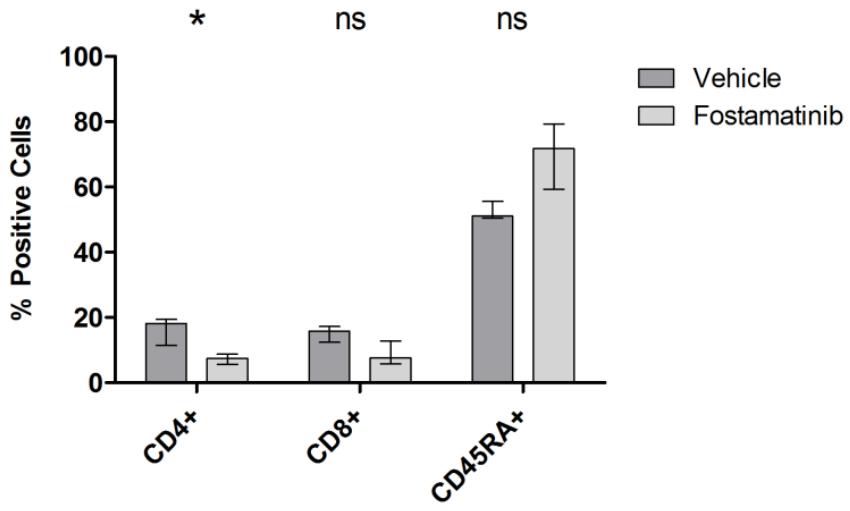

Figure 4.20: Lymphocyte subsets following fostamatinib treatment for 18 days.
The proportion of CD45RA+ splenocytes was not significantly affected by fostamatinib treatment. There was, however, a reduction in CD4+ splenocytes. Results shown from four biological replicate pairs of vehicle and fostamatinib-treated rats. Data shown as median ±IQR, ns – not significant, *p<0.05, Mann Whitney U test.

4.5 The effect of fostamatinib on antibody-dependent, FcR-mediated responses in EAG

Based on our laboratory's previous studies in NTN and my IHC findings (Section 3.6), I hypothesised that in addition to inhibiting the production of autoantibodies, fostamatinib may prevent their downstream function via inhibition of FcR-signalling. To investigate a role for SYK independent of autoantibody production in EAG, I isolated nephritic glomeruli from untreated animals 28 days after disease induction, in order to examine the effects of SYK

inhibition in diseased tissue dissociated from the systemic humoral response. When these nephritic glomeruli were incubated with R406, the active metabolite of fostamatinib, there was a dose-dependent reduction in the spontaneous production of a number of pro-inflammatory cytokines (Figure 4.21), including MCP-1, TNF-α and IL-12, each of which has been implicated in the pathogenesis of experimental glomerulonephritis[132,240,241].

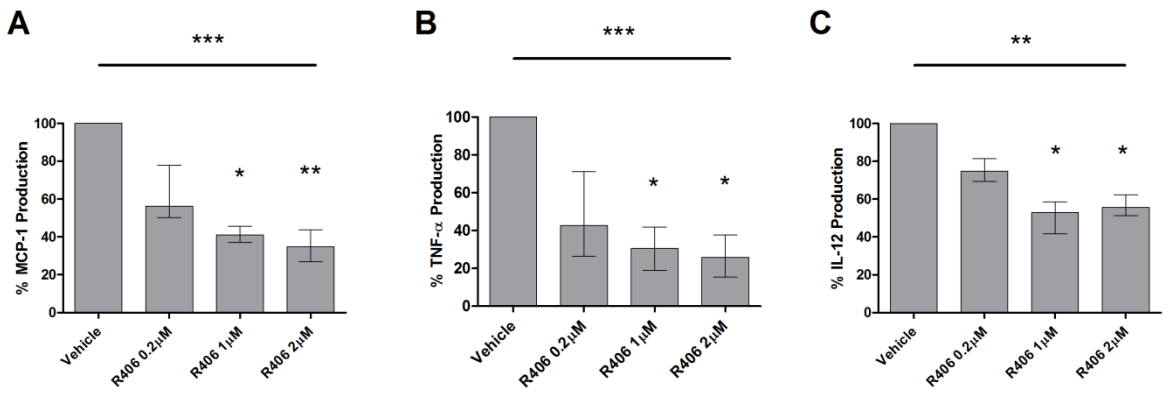

Figure 4.21: Effect of R406 on spontaneous cytokine production by nephritic glomeruli *ex vivo*.
Incubation with R406, the active metabolite of fostamatinib, inhibited the spontaneous production of pro-inflammatory cytokines, including (A) MCP-1, (B) TNFα, and (C) IL-12, by nephritic glomeruli *ex vivo* during a 48 hour incubation period. Data from four biological replicates are shown. Since the yield of sieved glomeruli was variable for each replicate, the data shown have been normalised to vehicle treatment, whilst statistical analysis has been performed on non-normalised data using Friedman repeated measures test (overall significance indicated by upper symbol) with Dunn's post-test comparison to vehicle group (significance indicated by lower symbol). *p<0.05, **p<0.01, ***p<0.001.

To examine this further, I studied the effects of R406 on cytokine production by primary bone marrow-derived macrophages (BMDM) *in vitro*, since macrophages are the predominant infiltrating leucocyte observed in this model and my immunohistochemical findings suggested significant co-localisation of phosphorylated SYK to this cell type. Heat-aggregated IgG has been used previously in our laboratory as a means to stimulate BMDM by cross-ligation of FcR[136,232]. I was first keen to confirm that this stimulus resulted in SYK activation in BMDM from WKY rats. To this end, I performed Western blot analysis for SYK and JNK phosphorylation (the latter a MAPK activated downstream of SYK) following

heat-aggregated IgG exposure (Figure 4.22). This also allowed me to demonstrate that the antibodies used for immunohistochemical staining in other parts of this project were reactive to rodent SYK.

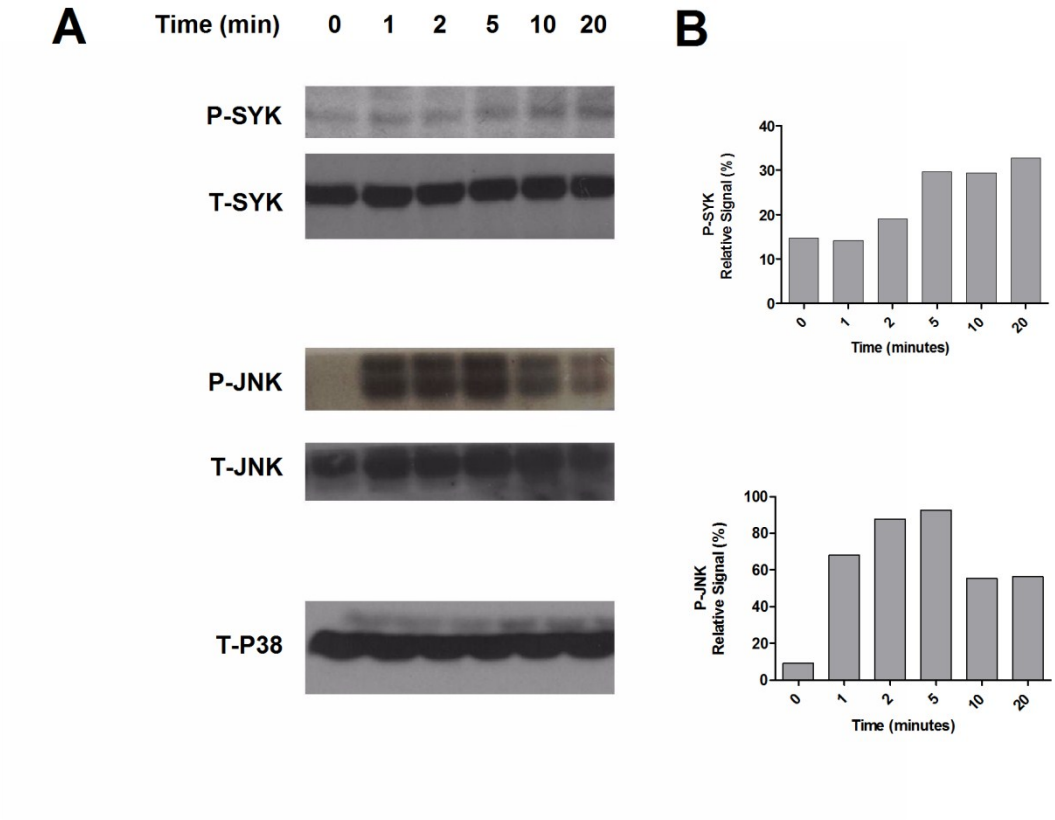

Figure 4.22: SYK and JNK activation in rat bone-marrow derived macrophages following stimulation with heat-aggregated IgG.

(A) Western blot for phosphorylated (P-) and total (T-) SYK and JNK in BMDM following cross-ligation of FcR with heat-aggregated IgG, with total-P38 loading control. No P38 phosphorylation was observed (data not shown). (B) Semi-quantitative densitometry analysis for relative P-SYK and P-JNK signals, compared to respective total protein loading controls. Representative blots from one of two biological replicate experiments are shown.

Incubation with R406 inhibited the production of MCP-1, TNFα and IL-12 by BMDM following stimulation with heat-aggregated IgG, in a similar pattern to that observed in nephritic glomeruli (Figure 4.23). Overall BMDM survival was not affected by incubation with R406 at these concentrations (data not shown). It is notable, however, that the absolute amount of IL-12 production by BMDM (in the range of 10-20pg/ml) was much less than

detected within inflamed glomeruli (median 559pg/ml), suggesting that there are sources of IL-12 other than macrophages within diseased glomeruli. This is consistent with previous reports suggesting that IL-12 production by intrinsic renal cells is important in the pathogenesis of experimental glomerulonephritis, and our laboratory's previous observation that intrinsic renal cells express SYK and may respond to SYK inhibition[242,243].

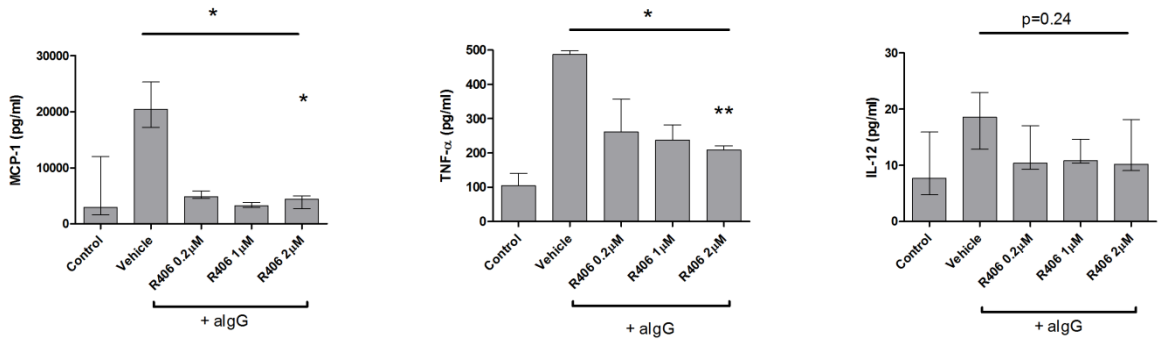

Figure 4.23: Effect of R406 on pro-inflammatory cytokine production by rat bone marrow-derived macrophages (BMDM) following stimulation with heat-aggregated IgG (aIgG).

Incubation with R406, the active metabolite of fostamatinib, inhibited the production of pro-inflammatory cytokines, including (A) MCP-1, (B) TNFα, and (C) IL-12, by BMDM stimulated with aIgG during a 24 hour incubation period. Technical replicate results from one of at least two representative experiments are shown. BMDM cell viability, as assessed by MTT assay at the end of the experiment, was not affected by R406 at these concentrations (data not shown). Data shown as median ±IQR, *p<0.05, **p<0.01, ***p<0.001, Kruskall Wallis test (overall significance shown by upper symbol) with Dunn's post-test comparison to vehicle group (significance indicated by lower symbol).

4.6 Chapter Four: Discussion of results and future work

The findings of the prevention study (EAG Experiment 4) suggest that SYK activity is an absolute requirement for the induction of autoimmunity in this model, as fostamatinib treatment completely protected from the development of any features of disease, including autoantibody production, during the initial 18 day treatment period. When treatment was withdrawn at day 18, animals subsequently developed typical features of disease, and at day 36 each of these disease parameters was comparable to those in untreated animals at day 18, suggesting that SYK 'disinhibition' by treatment withdrawal allowed the natural history of

the model to be restored. In established disease (EAG Experiment 5), SYK inhibition with fostamatinib was an effective treatment, resulting in reversal of severe glomerular pathology, preservation of renal function, and protection from lung haemorrhage.

In both *in vivo* studies I observed significant effects of SYK inhibition on the induction and progression of humoral autoimmunity. In particular, there was considerable attenuation of autoantibody production after the introduction of treatment in the second study. This finding is in contrast to previous reports in murine lupus, CIA, and spontaneous diabetes in NOD mice, where no clear-cut effects on anti-dsDNA, anti-collagen, or anti-insulin antibody levels, respectively, were observed[56,67,68]. However, the exposure period in these studies was not optimal for studying humoral responses, since treatment was initiated after maximal autoantibody responses were established, and did not continue beyond the lifetime of these pre-existing antibodies. Flow cytometric and B cell ELISpot analyses suggest that the changes in autoantibody production I observed were due to a direct inhibitory effect of fostamatinib on mature, antibody producing B cells or plasma cells, without significantly affecting overall B cell survival or causing overt bone marrow suppression. This is somewhat in contrast to previous immunotoxicity assessments in rats, where a modest fall in CD45RA+ cell proportions in bone marrow was observed following fostamatinib exposure[80]. However, these immunotoxicity studies were conducted in a different rat strain (Sprague Dawley), using higher doses of fostamatinib (100mg/kg/day) for a longer period of exposure (28 days), which may account for the differences observed. Previous studies in mice have also suggested that prolonged exposure to fostamatinib (>1-3 months) is associated with a decline in total B cell number and altered proportions of certain B cell subpopulations[56,68]. Further analysis of lymphocyte subsets, or on the effects of B cell functions *in vitro*, however, were limited by the paucity of validated lymphocyte markers in the rat.

Since constitutively SYK deficient B cells arrest at the pro-B cell stage, it has only been possible to study the role of SYK in mature cells with the advent of specific small molecule inhibitors (and potentially conditional genetic techniques[39-41]) and these novel observations suggest that SYK inhibition may prevent the production of pathogenic autoantibody, even after aberrant clonal responses have been established.

In addition to preventing the production of pathogenic autoantibodies, SYK inhibition appeared to have the potentially therapeutic second effect of inhibiting their downstream effector functions. Spontaneous pro-inflammatory cytokine production by nephritic glomeruli was inhibited by incubation with R406, the active metabolite of fostamatinib, independent of its effects on systemic humoral immunity. I observed a similar pattern of attenuated cytokine production by primary BMDM following FcR ligation, suggesting that the effect in glomeruli was mediated, at least in part, by inhibition of antibody-dependent, FcR-mediated responses in macrophages. Notably, the effect on IL-12 production by BMDM was less dramatic than that seen in whole glomerular preparations, in keeping with previous reports that IL-12 production by intrinsic renal cells is important in the pathogenesis of glomerulonephritis[241], and that resident renal cells may also respond to SYK inhibition[244].

The combined effect of SYK inhibition on antibody production and antibody-mediated effector functions, was a striking reversal of severe glomerular pathology in EAG, confirming our laboratory's previous observations in NTN, where we observed approximately 20% reduction in glomerular crescent formation when treatment was initiated in severe disease with greater than 90% established glomerular crescents[136]. The complete reversal of injury seen in this model (as opposed to the partial reversal in NTN) may be due to a number of

factors, including (1) less established disease at the initiation of treatment (approximately 90% vs 26% crescents), (2) longer duration of SYK inhibitor treatment in this study (18 days versus seven days), and (3) inhibition of pathogenic autoantibody production in this model (whereas the presence of heterologous NTS was not altered in NTN)

In the future, I am keen to study the effect of SYK inhibition in more advanced stages of EAG, which are characterised by progression to fibrocellular and fibrous crescents, interstitial fibrosis and tubular atrophy, since this may more accurately reflect the nature of disease seen clinically (and be more generally applicable to other causes of progressive glomerulosclerosis and renal scarring).

4.7 Summary of key findings

- SYK activity is an absolute requirement for the induction of autoimmunity in EAG.

- SYK inhibition is a remarkably effective treatment for established disease in EAG, resulting in reversal of necrotising and crescentic glomerulonephritis and protection from lung hemorrhage.

- The data suggests that short-term fostamatinib exposure inhibited both the generation and activity of antigen-specific antibody producing cells, without affecting overall B cell survival or causing disproportionate bone marrow suppression.

- Independent of these effects on autoantibody production, SYK inhibition with fostamatinib had a direct inhibitory effect on pro-inflammatory cytokine production

with nephritic glomeruli, most likely due to attenuation of FcR-mediated responses within infiltrating macrophages, and potentially within resident renal cells.

CHAPTER FIVE - SPLEEN TYROSINE KINASE INHIBITION IN EXPERIMENTAL AUTOIMMUNE VASCULITIS

5.1 Introduction and experiment design

As described previously (section 1.5.3), Experimental Autoimmune Vasculitis (EAV) is a model of ANCA-associated vasculitis that is induced by immunising WKY rats with the human ANCA-target antigen, myeloperoxidase (MPO). This model was historically developed in our laboratory[212], and is currently operated by Dr John McDaid and Dr Anisha Tanna. Together, we have studied the effects of SYK inhibition in this model, using their standard experimental protocols and a commercially available recombinant human MPO (hMPO) antigen (thus I have not conducted any preliminary experiments in EAV). The natural history of this model, as described previously[213], and the overall experiment design, is summarised in Figure 5.1.

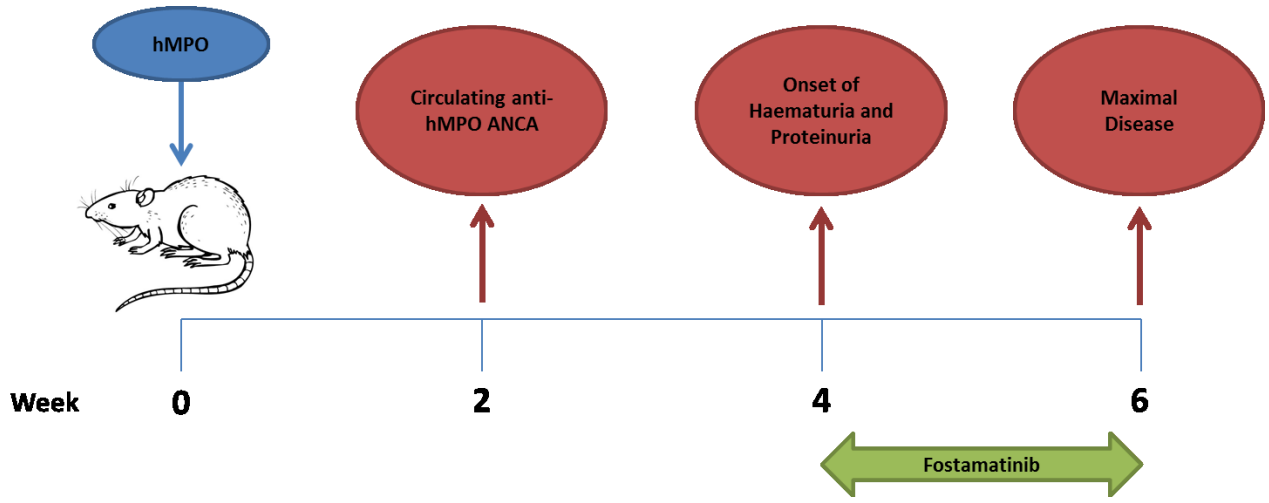

Figure 5.1: Experimental design for SYK inhibition study in EAV.
This experiment aimed to investigate the effects of SYK inhibition with fostamatinib in established EAV. Animals were treated from week 4, when the onset of disease was confirmed by the presence of haematuria and proteinuria, until week 6, when maximal disease is typically observed. hMPO, human myeloperoxidase; ANCA, anti-neutrophil cytoplasm antibody.

Following immunisation with hMPO in CFA, rats develop circulating anti-MPO ANCA that are detectable by two weeks. At approximately week four, the onset of glomerulonephritis is evidenced by the development of haematuria and mild proteinuria. By week 6, animals will have peak glomerular inflammation (as evidenced by maximal urinary findings) that typically begins to resolve by week 8. This is, in general, a model of mild renal injury compared to NTN and EAG, where fewer glomeruli (typically 10-20%) are affected with milder abnormalities (minor areas of proliferation, segmental necrosis and, less frequently, crescent formation). A significant proportion of animals, however, will also develop lung haemorrhage during the course of this model.

To determine if SYK inhibition was an effective treatment for established systemic vasculitis in EAV, we therefore treated animals (female WKY rats; aged six weeks with average body weight 118g; eight per group) from week 4 until week 6, when maximal urinary and glomerular findings should be observed. In this study, I used two doses of fostamatinib, 20mg/kg bd and 30mg/kg bd, since I wanted to establish if the dramatic therapeutic effects observed in EAG could be reproduced at a lower dose, and to account for the milder phenotype observed in this model.

5.2 Confirmation of rat anti-MPO ANCA reactivity to rat MPO

Since the ELISA method used to detect circulating anti-MPO antibodies uses the same hMPO antigen used for disease induction, I was interested to confirm that the antibodies detected are reactive to rat MPO (rMPO). To do this, I performed indirect immunofluorescence on cytospin preparations of acetone fixed rat leucocytes, using sera from historical EAV

animals, kindly provided by Dr John McDaid. This confirmed reactivity, and demonstrated a predominantly peri-nuclear pattern of fluorescence staining (Figure 5.2)

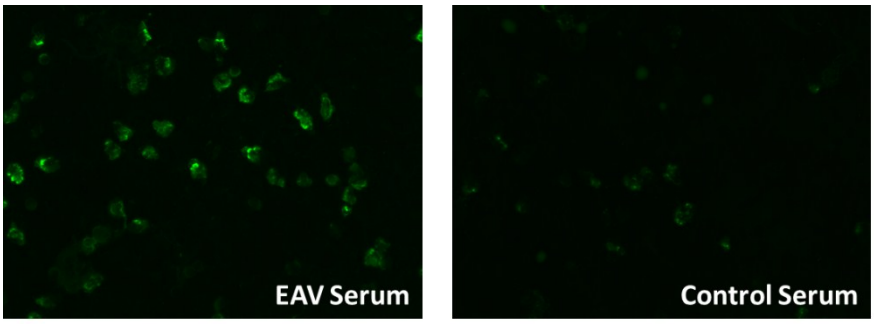

Figure 5.2: Indirect immunofluorescence on acetone-fixed rat leucocytes.
Indirect immunofluorescence using serum from historical EAV serum samples on acetone-fixed rat leucocyte preparations confirmed the presence of antibodies directed against components of neutrophil cytoplasm, with a predominantly peri-nuclear pattern of fluorescence. Control serum did not demonstrate significant reactivity. Anti-rat IgG FITC, x 200 magnification.

5.3 Confirmation of SYK expression in EAV

Using the same immunohistochemistry methods described in Chapter Three, I stained kidney sections from animals with EAV for phosphorylated SYK (P-SYK) in order to confirm that SYK is activated in this model (Figure 5.3). Staining of serial sections for ED1 suggested co-localisation to infiltrating macrophages.

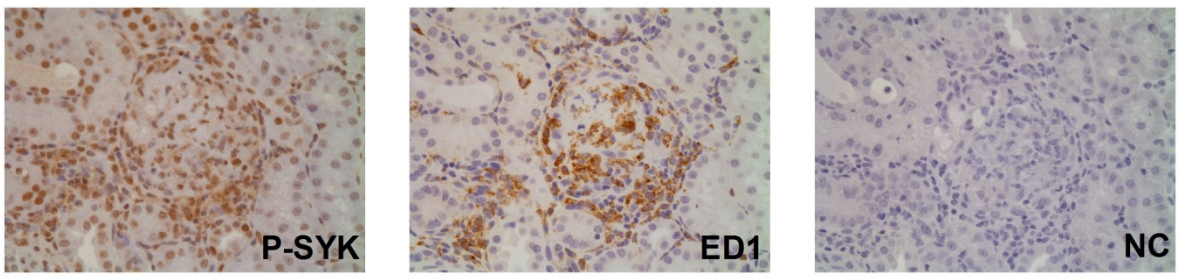

Figure 5.3: Phosphorylated SYK (P-SYK) expression in EAV.
Serial sections stained for P-SYK, ED1, and negative control (NC), as indicated, showing that P-SYK is detected in EAV, and that it appears to co-localise with ED1+ infiltrating macrophages. Immunoperoxidase stains with haematoxylin counterstain, x400 magnification.

5.4 SYK inhibition in EAV

5.4.1 Haematuria and proteinuria

Following immunisation with hMPO, all animals developed haematuria and proteinuria by week 4. Notably, haematuria is the predominant urinary abnormality observed in this model, with proteinuria being of low grade. Following the introduction of fostamatinib at week 4, these urinary abnormalities completely resolved in both treatment groups but persisted with vehicle treatment (Figure 5.4).

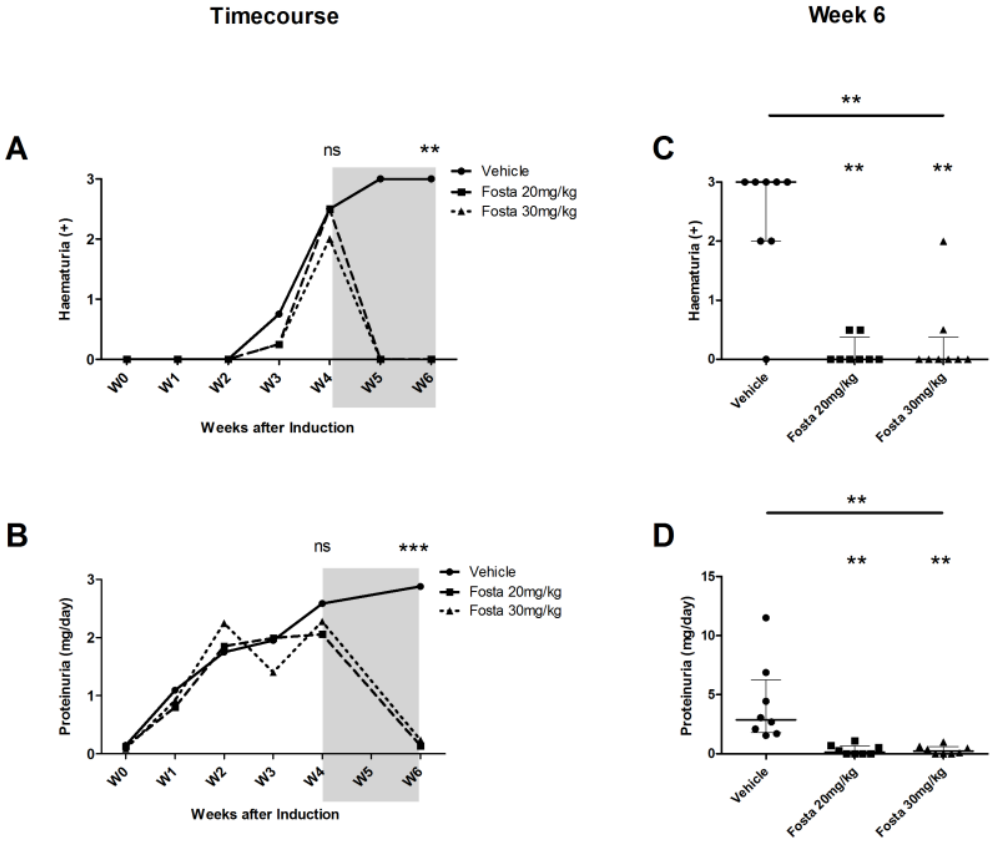

Figure 5.4: Urinary findings following SYK inhibition in EAV.

Time-course of (A) Haematuria, and (B) Proteinuria, in each treatment group, following induction at of EAV at week 0, with fostamatinib treatment period (shaded) from week 4 to week 6. Data are shown as median, without error, for clarity. (C) & (D) Week 6 measurements of haematuria and proteinuria in each of the treatment groups, with data shown as median ±IQR. ns – not significant, *p<0.05, **p<0.001, by Kruskall Wallis test (overall significance indicated by upper symbol), with Dunn's post-test comparison to Vehicle group (significance indicated by lower symbol).

5.4.2 Histological injury and infiltrating leucocytes

Histological assessment at week 6 revealed median 12% glomerular abnormalities in vehicle treated animals, in keeping with the mild renal phenotype of this model. There was a dose-dependent reduction in glomerular abnormalities following fostamatinib treatment, with completely normal glomerular architecture observed in the majority of animals in the 30mg/kg dose group (Figure 5.5). There was a similar dose-dependent reduction in ED1+ cell infiltration into glomeruli following fostamatinib treatment. Representative histology is shown in figure 5.5.

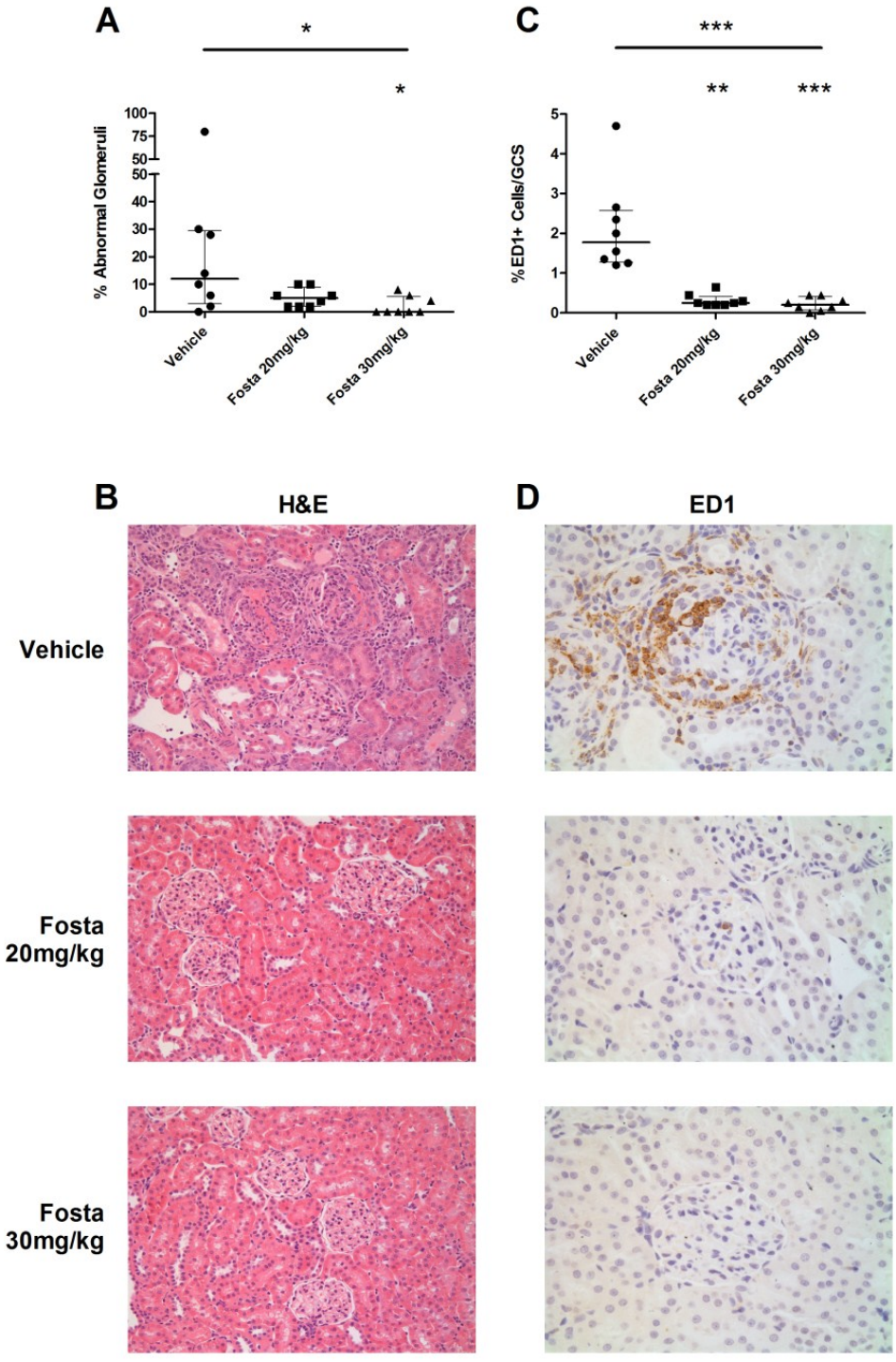

Figure 5.5: Renal histology and ED1+ cell infiltration following SYK inhibition in EAV.
Quantification of (A) glomerular abnormalities, expressed as the percentage of abnormal glomeruli, and (B) glomerular ED1+ cell infiltration, expressed as the mean percentage of ED1+ cells per glomerular cross section (GCS), in each treatment group at week 6, showing a dose-dependent reduction in both parameters. All data shown as median ±IQR. *p<0.05, **p<0.01, ***p<0.001, by Kruskall Wallis test (overall significance indicated by upper symbol) with Dunn's post-test comparison to Vehicle group (significance indicated by lower symbols) (C) Photomicrographs showing representative histology (H&E stain, x200 magnification) and ED1 immunoperoxidase staining (with haematoxylin counterstain, x400 magnification).

5.4.3 Direct immunofluorescence for IgG on kidney sections

Direct immunofluorescence for deposited IgG on frozen kidney sections from these animals confirmed a pauci-immune pattern of renal injury, consistent with previous descriptions of the model. No difference was observed between groups when this was quantified (Figure 5.6).

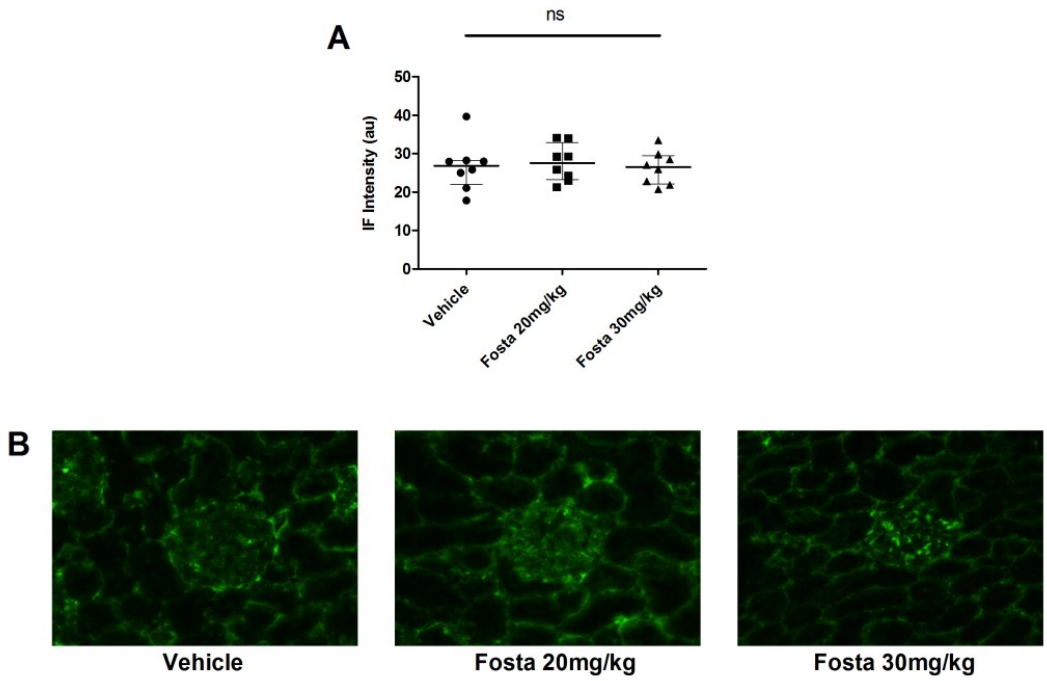

Figure 5.6: Direct immunofluorescence for deposited IgG in glomeruli following SYK inhibition in EAV. (A) Quantification of fluorescence intensity for deposited rat IgG, acquired using automated image analysis software, in each treatment group at week 6. No difference between groups was observed. Data shown as median ±IQR. ns – not significant by Kruskall Wallis test (overall significance shown). (B) Photomicrographs showing representative fluorescence images in each group. Anti-rat IgG FITC, x400 magnification.

5.4.4 Renal function

In keeping with the mild histological findings observed in this experiment, changes in measurements of renal function were also modest. No difference is serum urea concentrations was observed between treatment groups, though it is notable that several animals had serum

urea concentrations greater than the normal range defined in Chapter One, whilst having mild (if any) histological damage. I believe this reflects, as before, the difficulty in defining reliable serum markers of renal function in small rodents. It was interesting to observe that there was a modest, dose-dependent, and statistically significant, reduction in serum creatinine concentrations following fostamatinib treatment, although all values lay within the normal range defined in Chapter One (Figure 5.7).

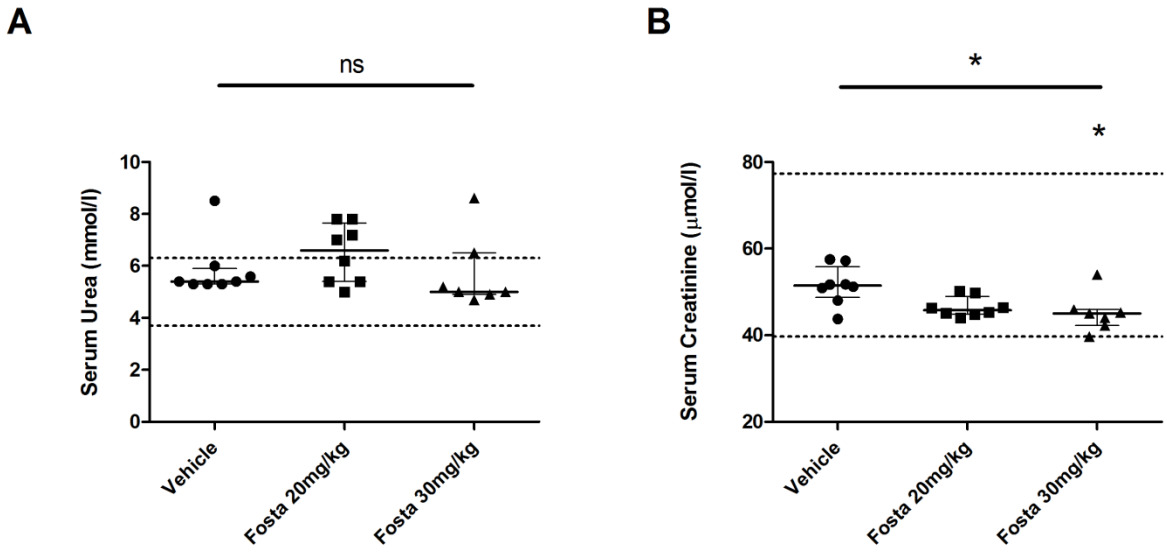

Figure 5.7: Renal function following SYK inhibition in EAV.

(A) Serum urea, and (B) Serum creatinine concentrations, in each treatment groups at week 6. No difference in serum urea concentrations was observed, whilst there was a dose-dependent reduction in serum creatinine concentrations, although all creatinine values lay within the normal range defined in Chapter One. All data shown as median ±IQR. ns – not significant, *p<0.05, by Kruskall Wallis test (overall significance indicated by upper symbol) with Dunn's post-test comparison to Vehicle group (significance indicated by lower symbol).

5.4.5 Lung haemorrhage

All vehicle treated animals had macroscopic evidence of lung haemorrhage at the time of cull (Figure 5.8). There was a dose-dependent reduction in visible lung injury following fostamatinib treatment, with no evidence of lung disease in the 30mg/kg dose group at week

6. There was a corresponding dose-dependent reduction in haemosiderin-laden cells detected within lung sections from these animals.

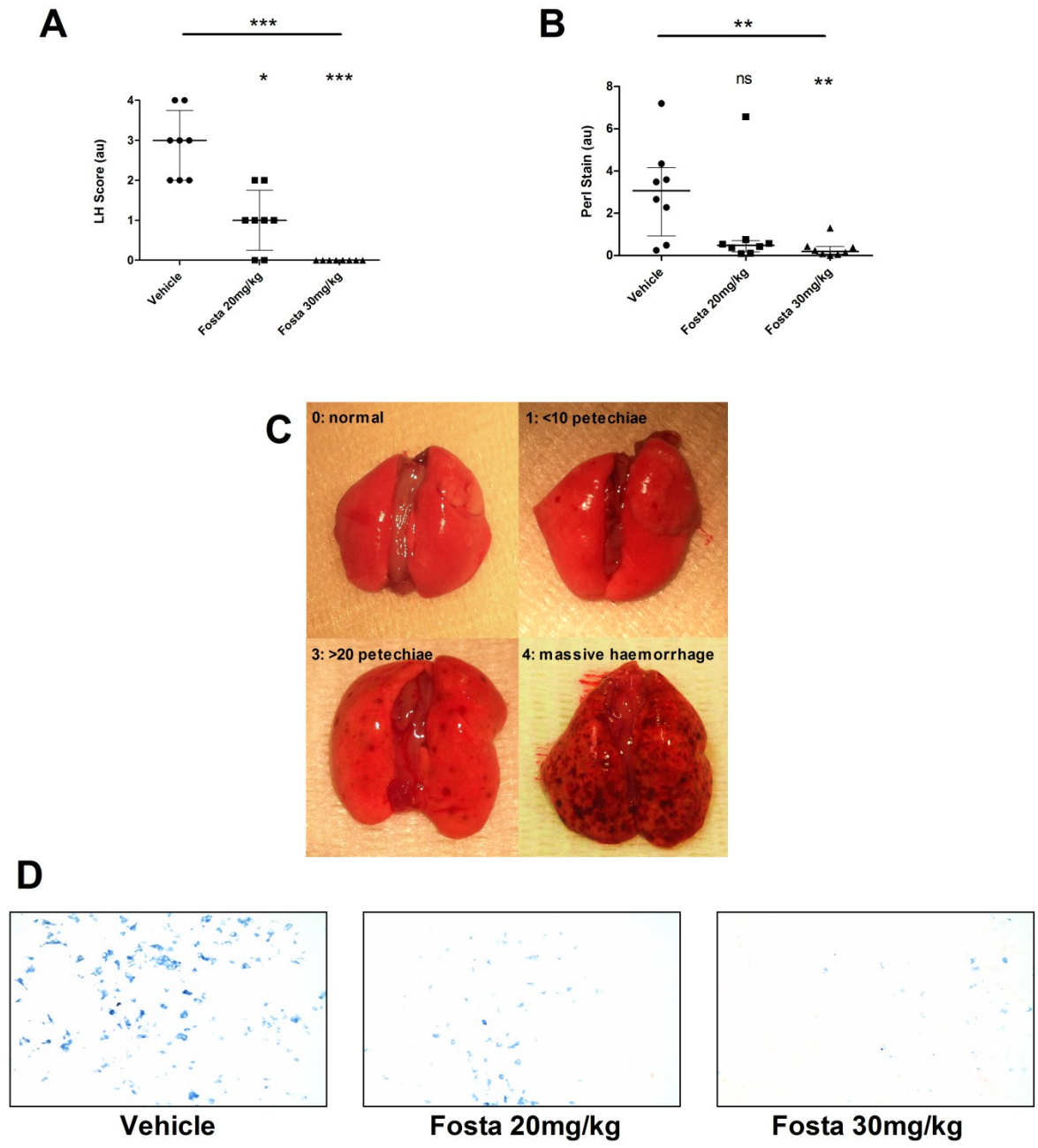

Figure 5.8: Lung haemorrhage following SYK inhibition in EAV.

(A) Macroscopic lung haemorrhage score, and (B) Quantification of haemosiderin-laden cells in lung tissue, in each of the treatment groups at week 6. A dose-dependent reduction was observed. Data shown as median ±IQR. ns – not significant, *p<0.05, **p<0.01, **p<0.001, ***p<0.0001 by Kruskall Wallis test (overall significance indicated by upper symbol) with Dunn's post-test comparison to Vehicle group (significance indicated by lower symbol). (C) Photographs showing representative examples of lung haemorrhage at week 6 (described fully in Methods section 2.5.6). (D) Photomicrographs showing representative staining for haemosiderin-laden cells in lung sections from animals in each treatment group, using Perls' Prussian Blue, without counterstain to facilitate counting, x200 magnification.

5.4.6 Measurement of circulating MPO-ANCA

No differences in circulating MPO-ANCA levels were observed between treatment groups at any of the time-points assessed (week 2, 4 and 6; Figure 5.9). At week 6, there was a trend towards lower MPO-ANCA levels in the fostamatinib groups, although this was not statistically significant. This is somewhat in contrast to my findings in EAG, although it is important to note that, in this experiment, fostamatinib treatment was not introduced until week 4, when high titre MPO-ANCA antibodies were already present. Since the half-life of these antibodies is likely to exceed the duration of the two week period of fostamatinib treatment, this experiment was unlikely to detect significant effects on ongoing MPO-ANCA production.

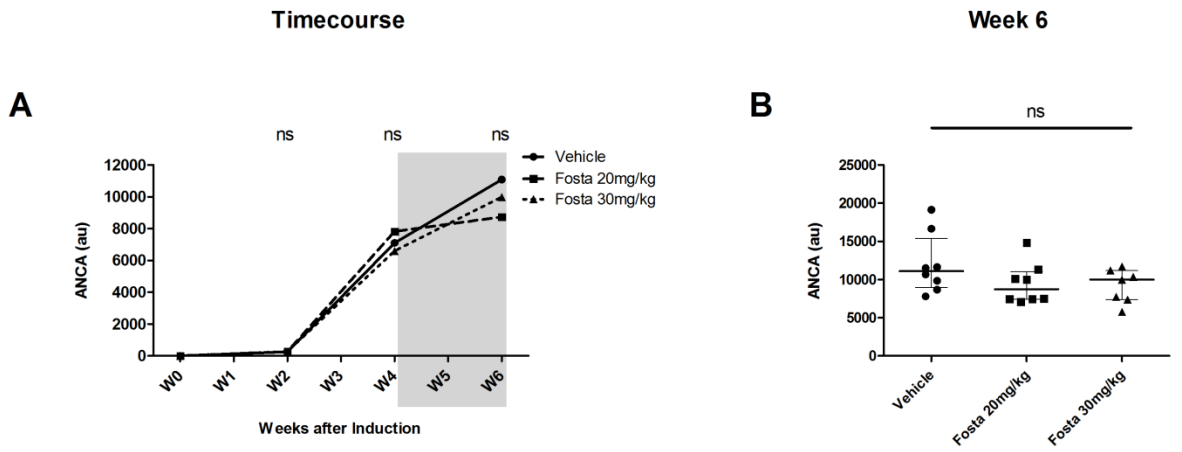

Figure 5.9: Circulating ANCA titres following SYK inhibition in EAV.
(A) Time-course of ANCA measurements in each treatment group, following disease induction at week 0 and fostamatinib treatment (shaded) from week 4 to week 6. Data shown as median, without error, for clarity. (B) ANCA measurements in each treatment group at week 6, showing a non-significant trend towards lower ANCA levels in fostamatinib-treated groups. Data shown as median ±IQR. ns – not significant, by Kruskall Wallis test (overall significance shown).

5.4.7 Haematological indices

In keeping with my findings in EAG, there was a mild reduction in peripheral blood white cell counts following fostamatinib treatment in this experiment. At these doses of fostamatinib, no changes in haemoglobin concentration were observed. A mild dose-dependent thrombocytosis was observed, similar to that seen in EAG (Figure 5.10).

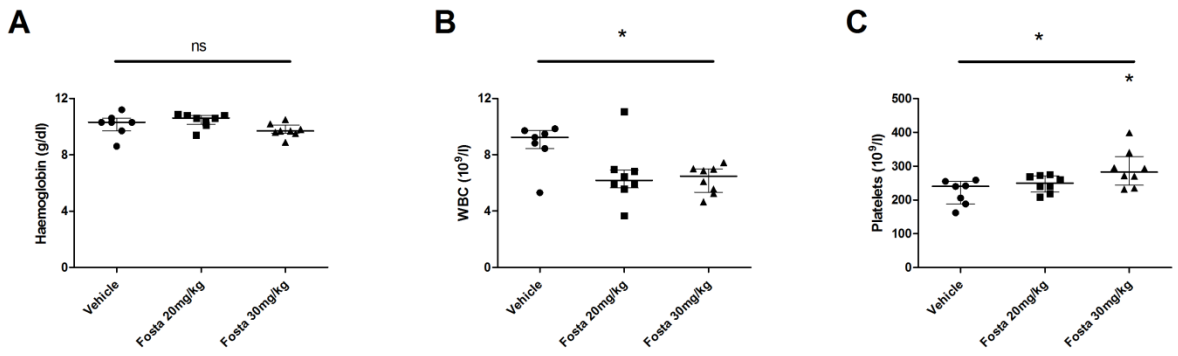

Figure 5.10: Haematological indices following SYK inhibition in EAV.
(A) Haemoglobin concentration, (B) White blood cell (WBC) count, and (C) Platelet count, in each treatment groups at week 6. Data shown as median ±IQR. ns – not significant, *p<0.05, by Kruskall Wallis test (overall significance indicated by upper symbol) with Dunn's post-test comparison to Vehicle group (significance indicated by lower symbols).

5.5 Chapter Five: Discussion of results and future work

The results presented in this chapter confirm that SYK inhibition with fostamatinib is an effective treatment for the systemic manifestations of disease in this preclinical model of AAV, and are in keeping with my previous findings in the related but distinct model of renal and lung injury, EAG. It is reassuring that a dose-response effect was observed in this study, and that there was significant attenuation of disease with fostamatinib 20mg/kg bd, since PK studies suggest that the average plasma concentrations of R406 achieved with this dose (approximately 500ng/ml) were easily achieved in clinical studies and well tolerated by

patients with non-renal diseases. As with my findings in EAG, overt bone marrow suppression was not observed with these doses of fostamatinib, although it would be desirable to perform detailed PK studies of fostamatinib in both models.

In contrast to my findings in EAG, I did not observe a significant effect on circulating antibody levels following fostamatinib treatment in this study. This may be due to differences in the time-point that fostamatinib treatment was introduced in the two experiments – in EAG, treatment was started after 18 days, when antibody levels were rapidly increasing, whereas in EAV, treatment was introduced after 28 days, when maximal antibody responses were already established. This suggests that SYK inhibition may prevent the production of new antibody, but does not affect levels of pre-existing antibody. Differences in the dose of fostamatinib used may also be relevant – the higher doses of 40mg/kg used in the EAG study may be required to inhibit antibody production. Alternatively, this discrepancy may reflect differences in response to allo- and autoantigen (*human* MPO being used for immunisation in EAV, *rat* α3(IV)NC1 in EAG). It would be of interest to repeat these studies in EAV using similar time-points and dosing regimens to the EAG studies to establish if the latter suggestion is a possibility. I could also examine differences in antibody subclass after SYK inhibitor treatment – it is thought, for example, that the IgG1 and IgG4 subclasses are more pathogenically relevant in human disease[245] and the ELISA I have used detects only total IgG. In addition, it was recently shown that MPO-ANCA epitope specificity may determine pathogenicity in humans[246], although the corresponding epitopes are not defined in the rat[247], raising possibilities for future work in this model generally, and following SYK inhibitor treatment.

Whilst no apparent effects on anti-MPO antibody levels were detected in this experiment, end-organ renal and lung damage was reduced. This would suggest that fostamatinib inhibited the effects of ANCA on their target cells, such as neutrophils. Previous studies have shown that SYK is phosphorylated in neutrophils following ANCA-induced activation, and in future studies I plan to examine the effects of fostamatinib, as R406, on myeloid cells stimulated with MPO-ANCA *in vitro.* Since glomerular endothelial cells expressing moesin have been implicated in the pathogenesis of murine anti-MPO vasculitis[183], it would also be of interest to establish if this mechanism contributes to disease in our model, and if so, whether SYK inhibition may have activity in glomerular endothelial cells.

Other areas for future work include defining the pathology of disease at week 4 when treatment was introduced in this experiment – all animals had haematuria and proteinuria, although the extent of glomerular and lung injury at this time point is not known. It would also be desirable to augment the severity of this model, as it has a mild phenotype that spontaneously resolves beyond week 6, which may limit its translation to human disease.

5.6 Summary of key findings

- SYK inhibition protects from the development of glomerulonephritis and alveolar haemorrhage in EAV.

- This effect is seen with modest doses of fostamatinib, consistent with those that can be achieved safely in clinical studies, and without overt bone marrow suppression in this model.

- SYK inhibition did not affect the levels of MPO-ANCA when treatment was started at maximal circulating antibody titre, suggesting that the therapeutic effect of fostamatinib was mediated via inhibition of ANCA-induced effector responses.

CHAPTER SIX - SPLEEN TYROSINE KINASE EXPRESSION IN HUMAN GLOMERULAR DISEASE

6.1 Introduction

Thus far, I have demonstrated that SYK is expressed and activated in two rodent models of GN, and that SYK inhibition can prevent and treat established disease in these models. It would be desirable, however, to demonstrate that SYK is expressed in human glomerular disease, and to confirm that SYK has a role in the pathogenesis of these conditions, before considering clinical application of SYK inhibition. At the outset of this project, SYK expression in human GN had not been described, although there has since been a single report of SYK expression in post-infectious GN[239].

In this chapter, I have sought to demonstrate SYK expression in a range of human glomerulonephritides and that SYK is activated (i.e. phosphorylated) in these conditions. I have used an immunohistochemistry-based approach, developed from the methods used initially on tissue from experimental models. I have optimised these methods for use on formalin-fixed paraffin-embedded tissue sections, since these are readily available following routine clinical renal biopsies, without the need for taking biopsy material surplus to diagnostic requirements or performing additional tissue preservation procedures.

6.2 Immunohistochemistry for total SYK

For total SYK (T-SYK) staining, I have used the same commercially available rabbit polyclonal antibody, directed against the N-terminus of human SYK, which was used on rodent tissue (Chapter Three). This antibody was shown previously by a colleague in our laboratory (Dr Min Jeong Kim) to be reactive to human SYK by Western blot[243]. I also used

this antibody for immunoblotting in my rodent studies, where it demonstrated cross-reactivity to, and specificity for, SYK.

I initially tested the antibody for IHC on human lymph node sections (provided by the Imperial College Healthcare NHS Trust Tissue Bank), as SYK is known to be highly expressed in cells of haematopoietic lineage. Negative control stains were performed by pre-incubating the antibody with the immunising peptide (sourced from the antibody manufacturer). Representative staining is shown in Figure 6.1. T-SYK staining localised to lymphoid follicles, consistent with an important role for SYK in the generation of adaptive immune responses.

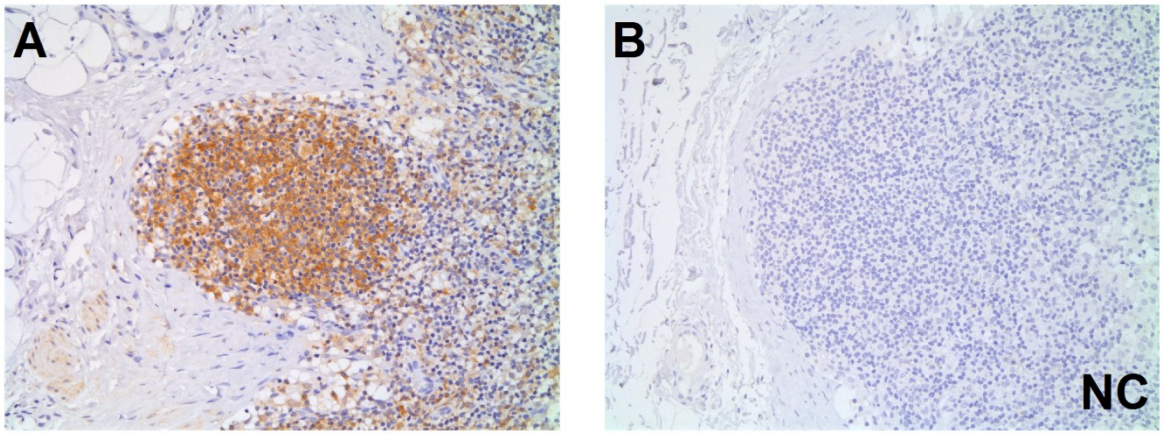

Figure 6.1: Total SYK (T-SYK) expression in human lymph node.
(A) T-SYK staining localised predominantly to a lymphoid follicle. (B) Negative control (NC) performed on a sequential section by pre-incubating primary T-SYK antibody with the relevant immunising peptide. x200 magnification.

Having established that this antibody could be used successfully to detect T-SYK in formalin-fixed paraffin-embedded human tissue sections, I wanted to establish the pattern of T-SYK expression in biological 'negative' and 'positive' control renal tissue. For negative control, or 'normal', renal tissue, I used biopsy specimens from patients with thin-basement

membrane lesion (TBM) and minimal change disease (MCD). These are non-proliferative glomerulopathies with normal light-microscopic findings and a usually benign clinical course. Truly 'normal' kidney tissue is not readily available (as there is clinical indication to perfomr renal biopsy). Normal renal tissue may be obtained from nephrectomy specimens (performed for excision of renal malignancies), although these specimens are unlikely to be processed in the same manner as diagnostic biopsies, which limits their use for developing methods to use with the latter.

The pattern of T-SYK expression in TBM is shown in Figure 6.2. Notably, there was no staining within glomeruli in these cases. I did observe, however, intermittent staining of tubular cells, likely distal tubular epithelial cells (having thin cuboidal epithelium with little brush border and open tubular lumens), the significance of which is unknown, although it is similar to that seen in normal rat tissue (section 3.6).

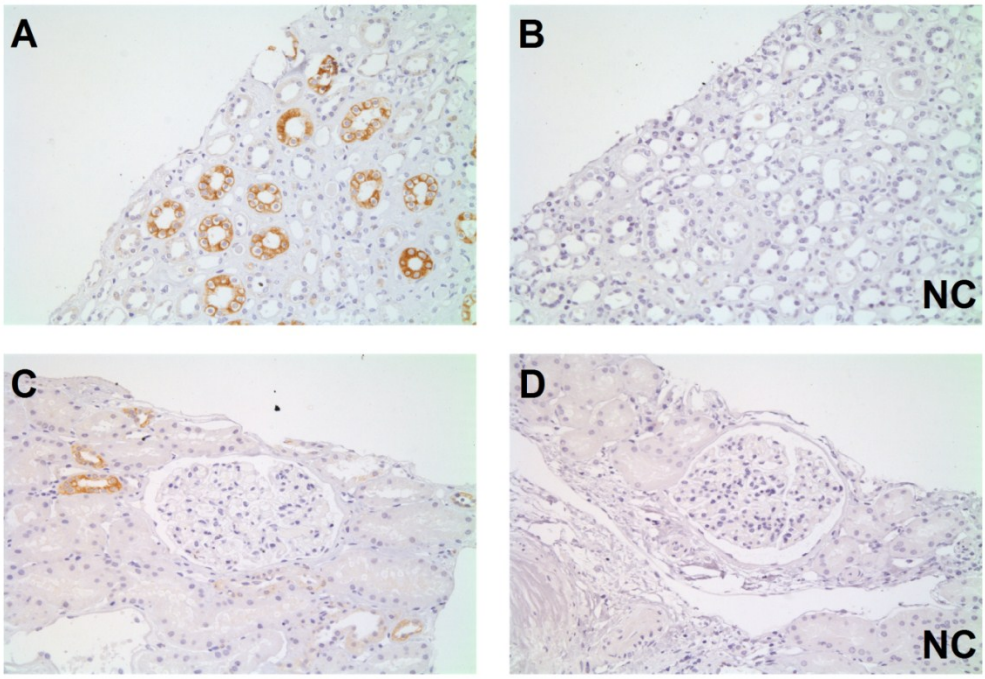

Figure 6.2: Total SYK (T-SYK) expression in thin basement membrane lesion.
(A) & (B) T-SYK staining within distal tubular epithelial cells in the renal medulla, with a sequential negative control (NC) section. (C) & (D) T-SYK staining within distal tubular epithelial cells in the renal cortex, and no glomerular staining, with sequential negative control (NC) section. x200 magnification.

For positive control, or 'nephritic', tissue, I used biopsies from patients with diffuse proliferative post-infectious glomerulonephritis (DPIGN), as I expected these specimens to have a glomerular infiltrate of leucocytes that would be positive for SYK. Representative staining is shown in Figure 6.3. As expected, there was strong staining for T-SYK within the glomerular tuft, in addition to the intermittent tubular staining that was observed in TBM.

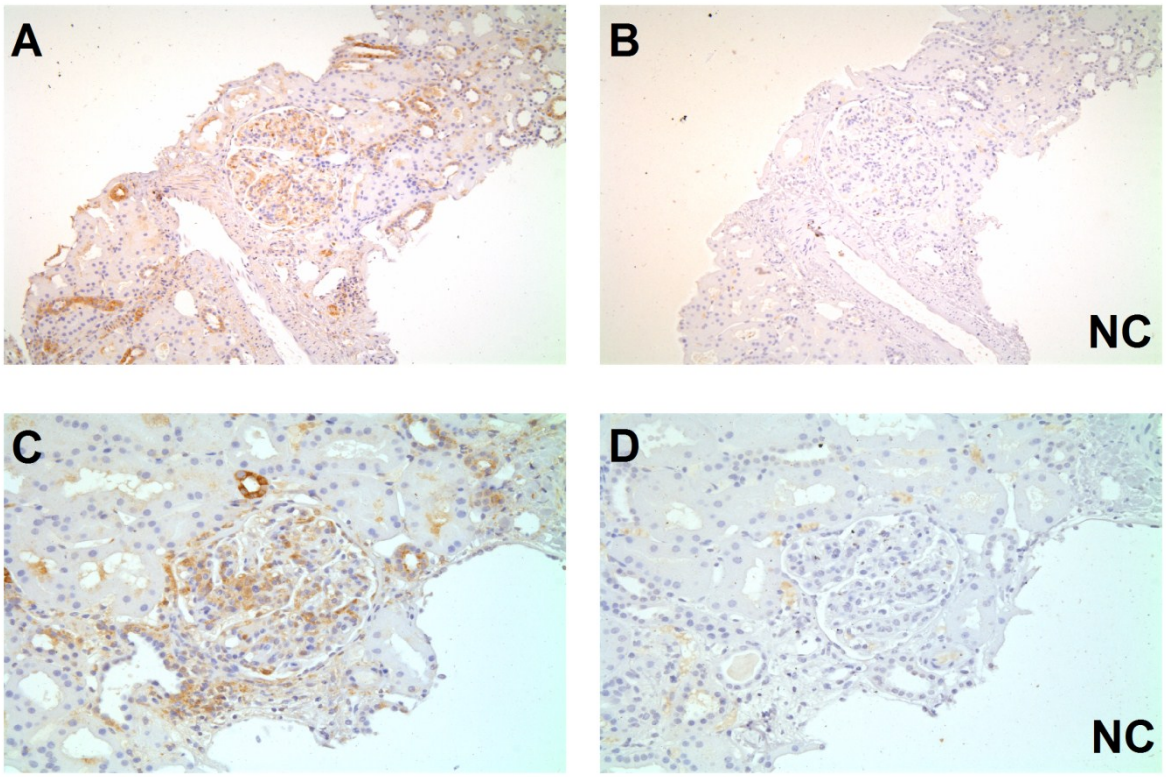

Figure 6.3: Total SYK (T-SYK) expression in diffuse proliferative post-infectious glomerulonephritis.
(A) & (B) T-SYK staining within an inflamed glomerulus and distal tubular epithelial cells, with a sequential negative control (NC) section. x100 magnification. (C) & (D) T-SYK staining within a diseased glomerulus, with a sequential negative control (NC) section. x200 magnification.

6.2.1 Total SYK expression in anti-GBM disease (12 cases)

Since EAG is a model of anti-GBM disease, this was the first GN in which I performed systematic analysis of SYK expression, using biopsies from 12 historical patients.

Morphologically, T-SYK was detected within inflamed glomeruli, localising in particular to areas of crescent formation (Figure 6.4).

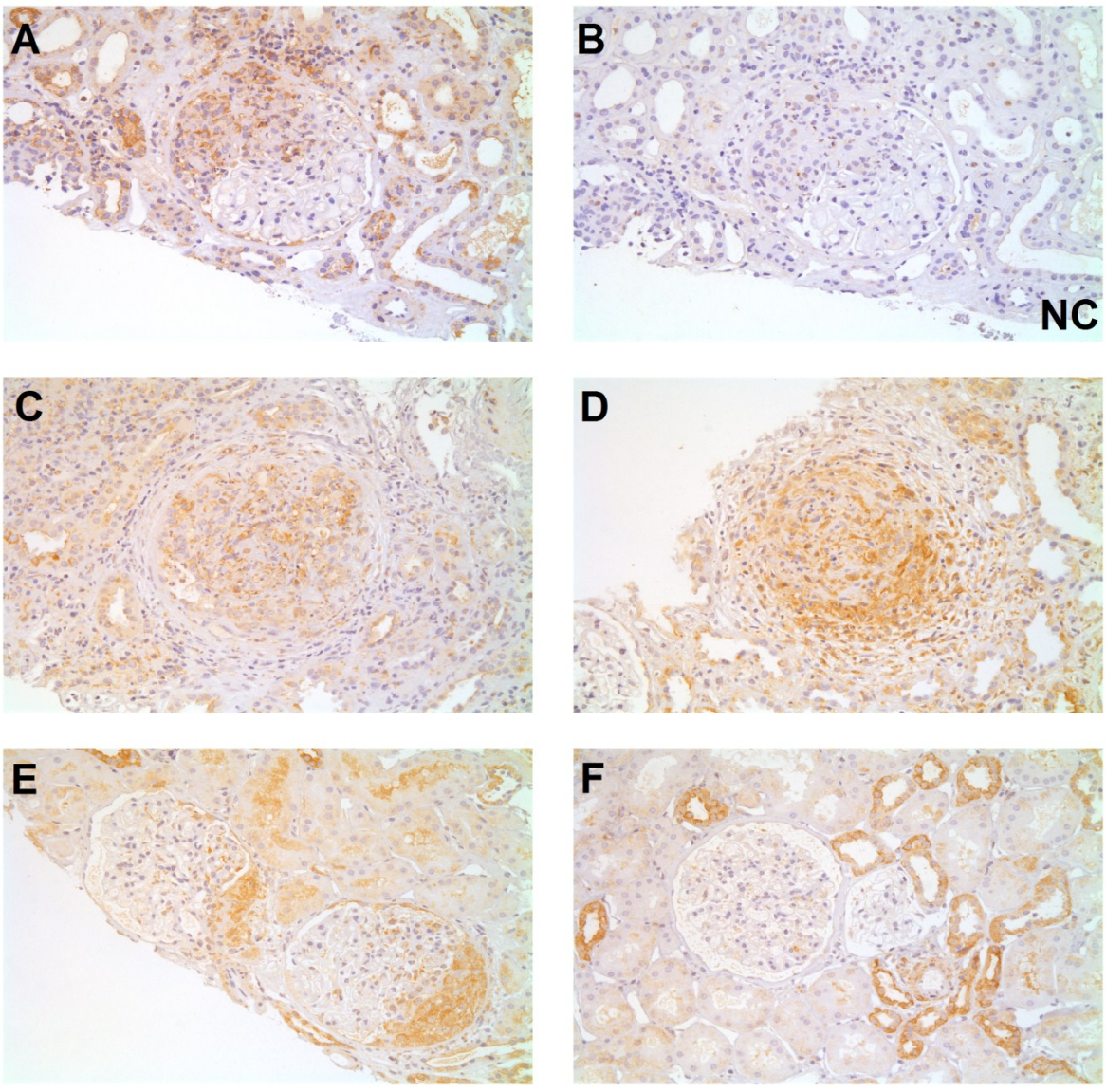

Figure 6.4: Total SYK (T-SYK) expression in anti-GBM disease.
(A) & (B) T-SYK staining localised to an area of crescent formation in anti-GBM disease, with a sequential negative control (NC) section. (C), (D) & (E) T-SYK staining within inflamed glomeruli from a further three cases of anti-GBM disease. (F) T-SYK staining in a patient with circulating anti-GBM antibodies and lung haemorrhage, but without glomerulonephritis, showing minimal glomerular staining. All x200 magnification.

Quantitative analysis using automated image analysis to calculate the mean proportion of glomerular T-SYK staining in each biopsy case showed that T-SYK expression levels were highest in patients who presented with dialysis-dependent renal failure, a marker of severe disease that confers poor prognosis (Figure 6.5A)[128]. In patients who were not dialysis-dependent at the time of biopsy, T-SYK expression levels correlated with presenting serum creatinine, in keeping with previous reports that the proportion of crescents seen on renal biopsy also correlates strongly with presenting serum creatinine (Figure 6.5B)[128,248].

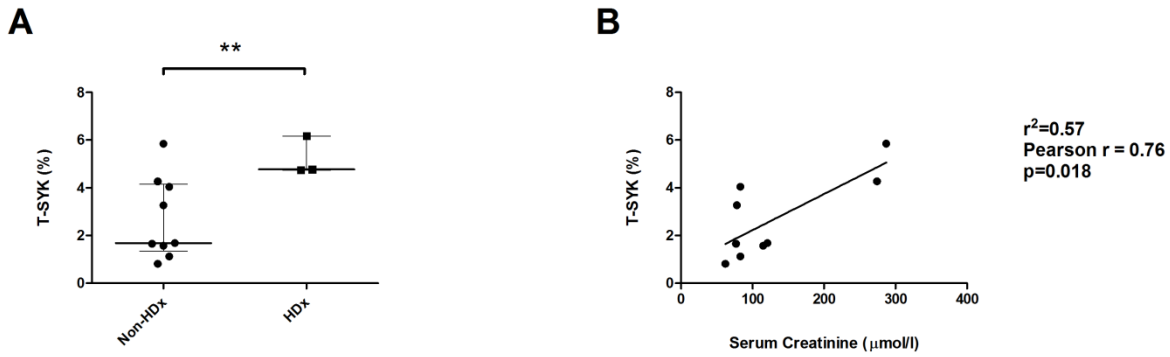

Figure 6.5: Quantification of Total SYK (T-SYK) expression in anti-GBM disease.
(A) Glomerular T-SYK expression levels were significantly higher in patients who presented with haemodialysis-dependent renal failure (HDx). Data shown as median ±IQR. **p<0.01, Mann Whitney U test. (B) In patients who were haemodialysis-independent at presentation, glomerular T-SYK expression correlated with presenting serum creatinine. Pearson correlation as indicated.

6.2.2 Total SYK expression in ANCA-associated glomerulonephritis (18 cases)

In ANCA-associated GN (AAGN), T-SYK expression localised to areas of segmental inflammation and crescent formation within diseased glomeruli, in addition to the now typically observed pattern of distal tubular staining (Figure 6.6).

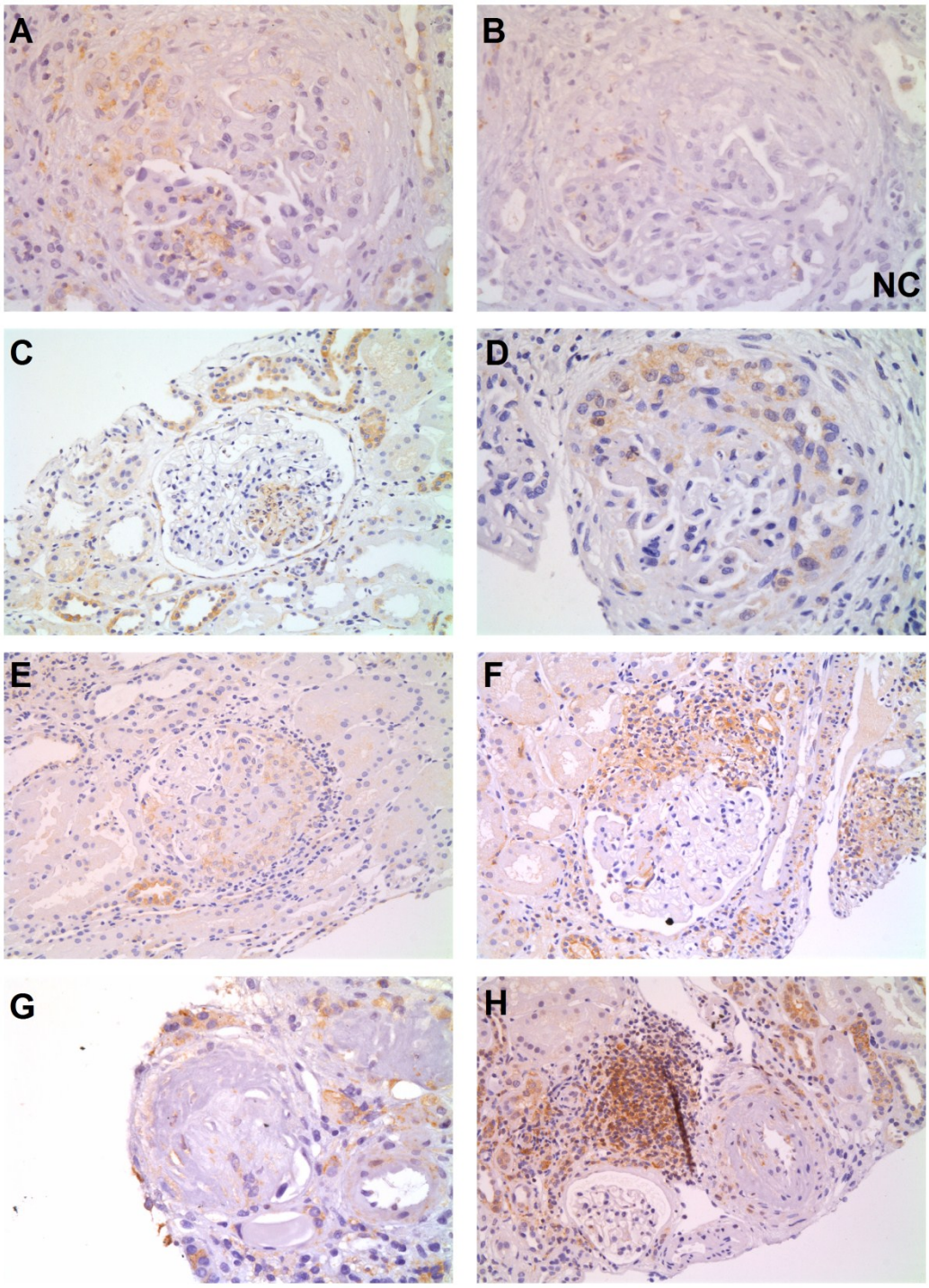

Figure 6.6: Total SYK (T-SYK) expression in ANCA-associated glomerulonephritis (AAGN).
(A) & (B) T-SYK staining in a crescentic glomerulus from a patient with AAGN, with a sequential negative control (NC) section. (C), (D), (E) & (F) T-SYK staining in additional cases of AAGN, showing SYK localisation to areas of segmental inflammation within the glomerular tuft and areas of extra-capillary crescent formation. (G) An obsolete glomerulus from a patient with 'sclerotic' class AAGN, showing minimal T-SYK staining. (H) Positive T-SYK staining within the tubulo-interstitial infiltrate in a case of AAGN with concomitant tubulo-interstitial nephritis. x200-400 magnification.

To assess the relationship with disease activity, T-SYK expression levels were correlated with histological class as defined in the recently proposed system of Burden *et al*[249]. This system describes four classes of disease: crescentic, focal, sclerotic and mixed. The first three categories are based on the predominance (>50%) of crescentic, normal and globally sclerotic glomeruli in the biopsy, respectively, whilst in mixed class disease none of these features is predominant. I found that SYK expression levels were highest in 'crescentic' class disease, and lowest in 'sclerotic' class, suggesting that SYK expression is a feature of acute disease that may respond to treatment (Figure 6.7).

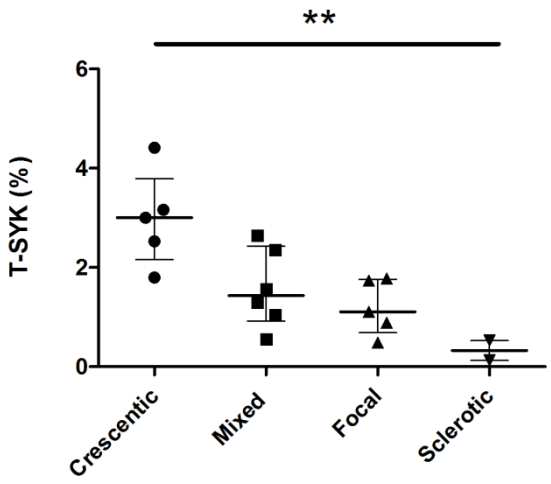

Figure 6.7: Quantification of Total SYK (T-SYK) expression in ANCA-associated glomerulonephritis (AAGN).

Glomerular SYK expression levels were significantly higher in patients with 'crescentic' class disease versus 'sclerotic' class disease, suggesting T-SYK expression is a feature of acute inflammatory disease. Data shown as median ±IQR. **P<0.01, Kruskall Wallis test (overall significance shown).

6.2.3 Total SYK expression in lupus nephritis (16 cases)

In proliferative classes of lupus nephritis (ISN/RPS Class III and IV)[250], T-SYK positive cells could be identified within capillary lumens of affected glomeruli (Figure 6.8). In non-proliferative class V disease, typical tubular epithelial cell staining was observed, however no significant T-SYK stain was observed within the glomerular tuft. Consistent with these

observations, quantified T-SYK expression levels were highest in class IV (diffuse proliferative) disease (Figure 6.9).

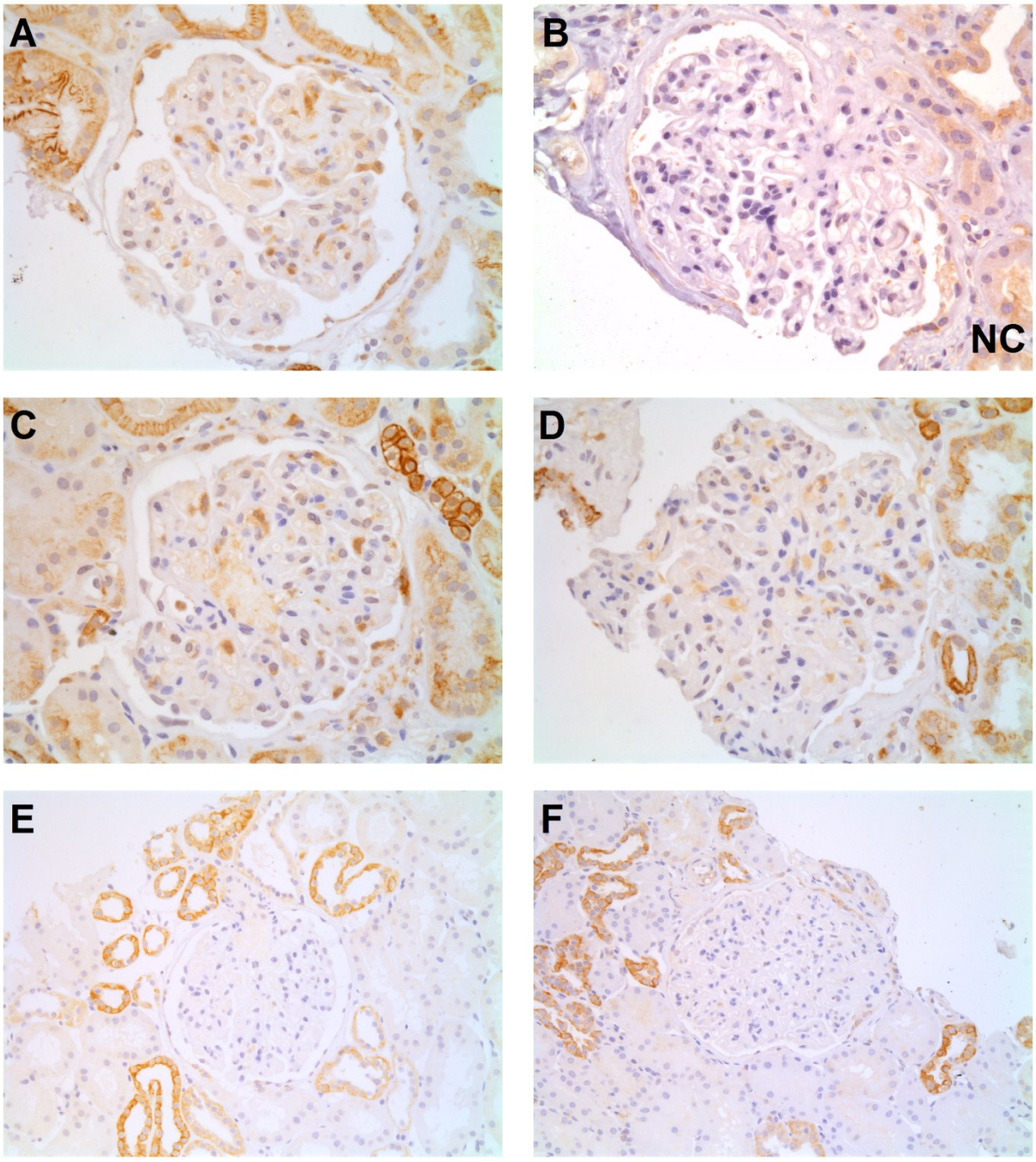

Figure 6.8: Total SYK (T-SYK) expression in lupus nephritis.
(A) & (B) T-SYK positive cells identified within glomerular capillary lumens in a patient with diffuse proliferative (class IV) lupus nephritis, with a sequential negative control (NC) section. (C) & (D) Additional examples of T-SYK positive cells within glomeruli in proliferative lupus nephritis. (E) & (F) In non-proliferative (class V) lupus nephritis, no staining for T-SYK was observed within the glomerular tuft. x200-400 magnification.

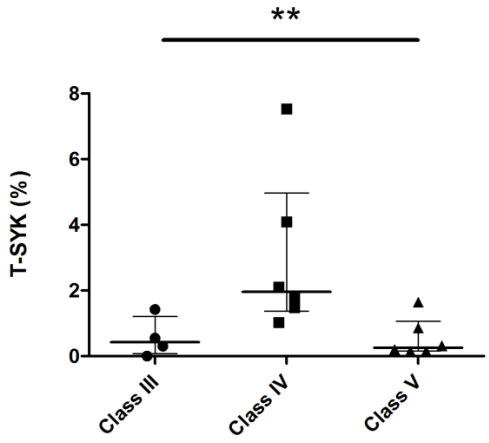

Figure 6.9: Quantification of Total SYK (T-SYK) expression in lupus nephritis.
Highest levels of T-SYK expression were seen in diffuse proliferative (class IV) lupus nephritis. Lower levels of SYK expression were observed in focal proliferative (class III) disease since a significant number of glomeruli were unaffected in these patients. Data shown as median ±IQR. **P<0.01, Kruskall Wallis test (overall significance shown).

6.2.4 Total SYK expression in IgA nephropathy (26 cases)

Consistent with the patterns of staining seen in the other forms of proliferative GN, SYK expression was observed within areas of both endocapillary and extracapillary proliferation in patients with IgA nephropathy (Figure 6.10). The Oxford Classification is a recently described system that defines the histopathological features that confer poor prognosis in IgA nephropathy[251,252]. These are (i) mesangial hypercellularity, (ii) endocapillary proliferation, (iii) segmental sclerosis, and (iv) tubular atrophy. The former two features most likely reflect active inflammatory disease and the latter two reveal chronic damage. Significant amounts of SYK expression were only observed in patients with endocapillary proliferation, rather than mesangial hypercellularity alone, suggesting that SYK expression is associated with the presence of infiltrating leucocytes in this condition (Figure 6.11).

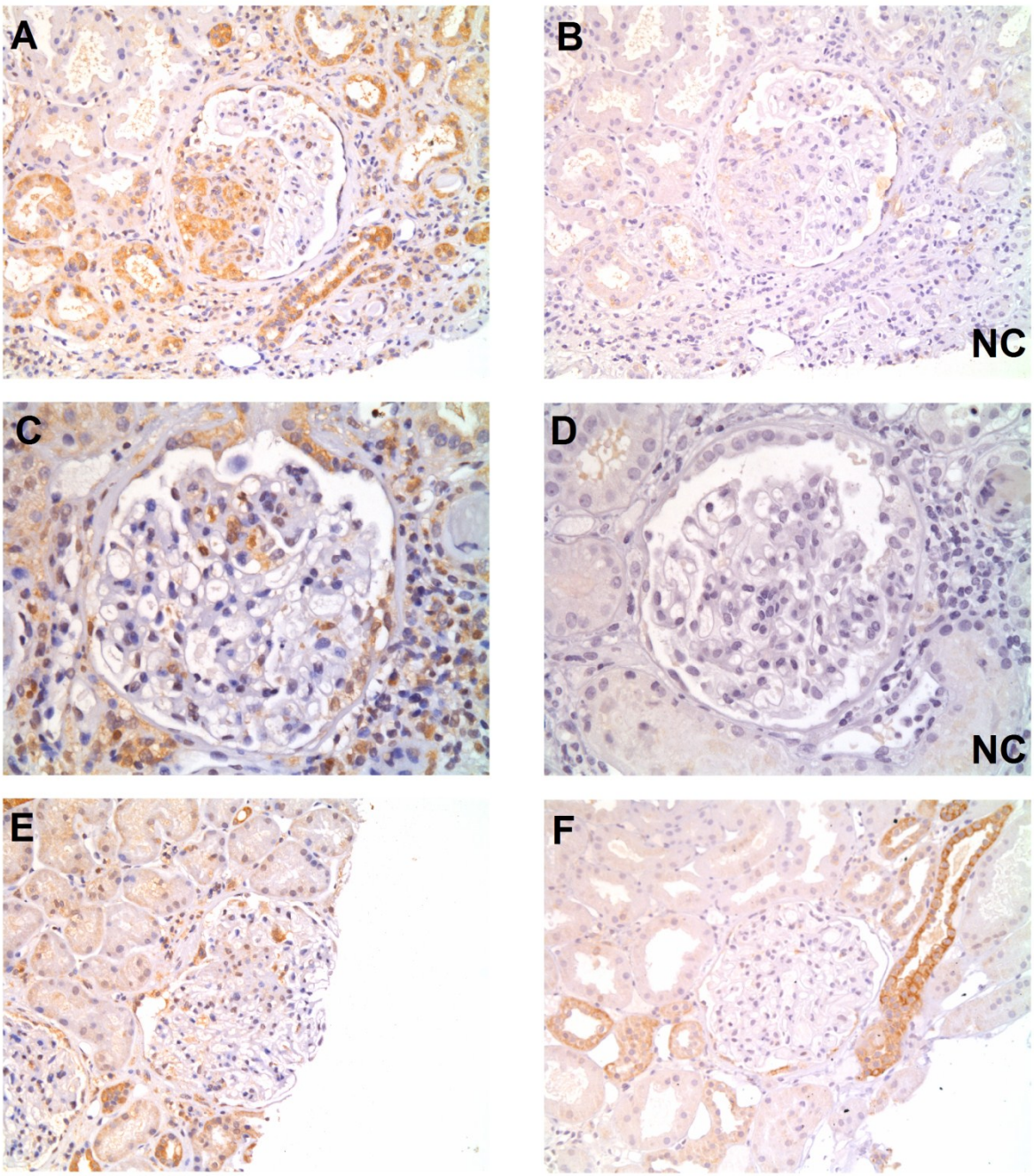

Figure 6.10: Total SYK (T-SYK) expression in IgA nephropathy.

(A) & (B) T-SYK staining within a small crescent in IgA nephropathy, with a sequential negative control (NC) section. (C) & (D) T-SYK positive cells within glomerular capillary lumens in a patient with endocapillary proliferation in IgA nephropathy, with a sequential negative control (NC) section. (E) A single T-SYK positive cell within a capillary lumen in a case of IgA nephropathy with endocapillary proliferation. (F) Negative glomerular staining for T-SYK in a patient with IgA nephropathy without mesangial or endocapillary proliferation. x200-400 magnification.

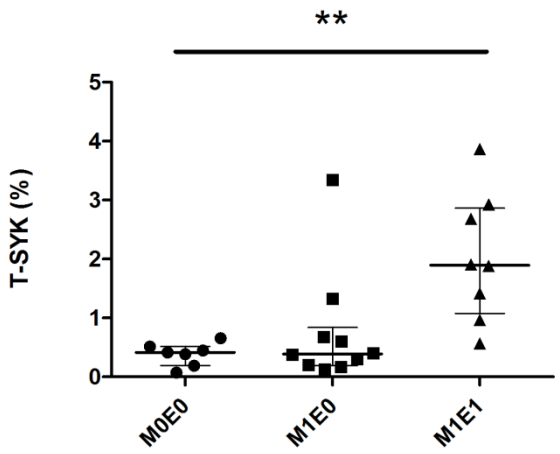

Figure 6.11: Quantification of Total SYK (T-SYK) expression in IgA nephropathy.
Minimal T-SYK staining was observed in patients with neither mesangial nor endocapillary proliferation (M0E0), or with mesangial hypercellularity alone (M1E0). Significantly higher levels of T-SYK expression were observed in patients with both mesangial and endocapillary proliferation (M1E1). Data shown as median ±IQR. **P<0.01, Kruskall Wallis test (overall significance shown).

6.2.5 Total SYK expression in idiopathic membranous nephropathy (5 cases)

Akin to the pattern of staining seen in class V lupus nephritis (which has morphologically similar findings on light microscopy), minimal glomerular staining for SYK was seen in biopsies from patients with idiopathic membranous nephropathy (Figure 6.12).

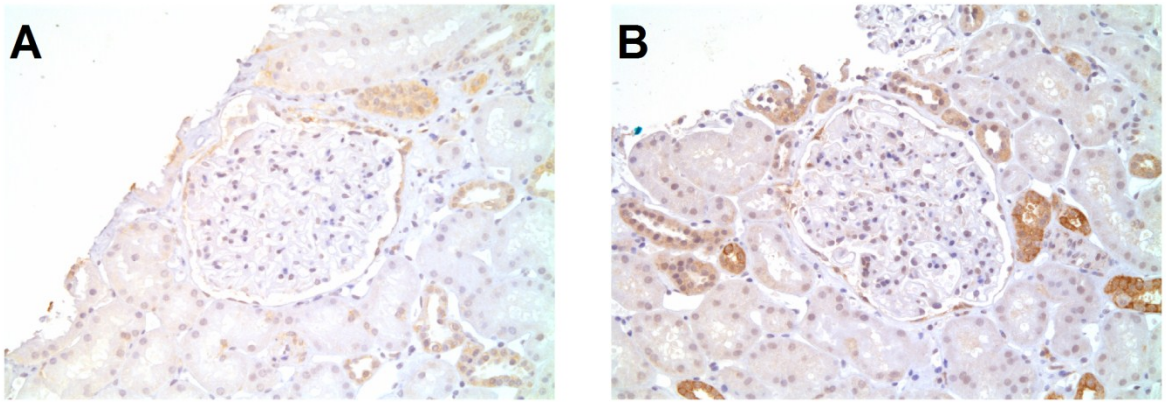

Figure 6.12: Total SYK (T-SYK) expression in idiopathic membranous nephropathy.
(A) & (B) Minimal glomerular staining for T-SYK in two cases of idiopathic membranous nephropathy, similar to that seen in class V lupus nephritis. x200 magnification.

6.2.6 Total SYK expression in the spectrum of glomerulonephritides

Figure 6.13 summarises the quantification of glomerular SYK expression in the spectrum of glomerulonephritides. In summary, significant T-SYK expression appears to be a feature of only proliferative classes of diseases, and expression levels appear to correlate broadly with disease severity, with highest levels seen in anti-GBM disease and AAGN, both of which typically present with a rapidly progressive clinical course.

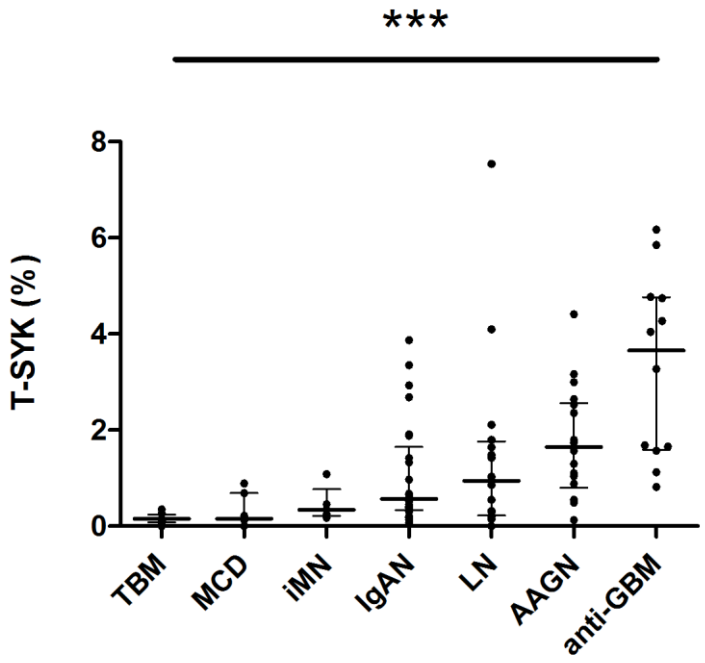

Figure 6.13: Quantification of Total SYK (T-SYK) expression in the spectrum of human glomerular diseases.

Significant T-SYK expression was observed only in proliferative forms of glomerulonephritis, and expression levels correlate broadly with the severity of disease. TBM, thin basement membrane lesion; MCD, minimal change disease; iMN, idiopathic membranous nephropathy; IgAN, IgA nephropathy; LN, lupus nephritis; AAGN, ANCA-associated glomerulonephritis; anti-GBM disease, anti-glomerular basement membrane disease. Data shown as median ±IQR. ***P<0.001, Kruskall Wallis test (overall significance shown).

6.3 Immunohistochemistry for phosphorylated SYK

For phosphorylated SYK (phospho-SYK; P-SYK) staining, I trialled a number of commercially available antibodies, directed against a variety of phosphorylated tyrosine residues in human SYK. Optimal staining on positive control tissue (human lymph node) was achieved with a rabbit polyclonal antibody to phospho-tyrosine 625/626. As with the selected T-SYK antibody, this antibody was shown to be reactive to human and rodent SYK by Western blot by myself and others in our laboratory. Tyrosine residue 625/626 is also located with the activation loop of the catalytic domain of SYK, so its phosphorylation is likely to be functionally relevant in disease pathogenesis. Representative staining on human lymph node is shown in Figure 6.14. The pattern of P-SYK detection was similar to that observed with T-SYK staining (Figure 6.1).

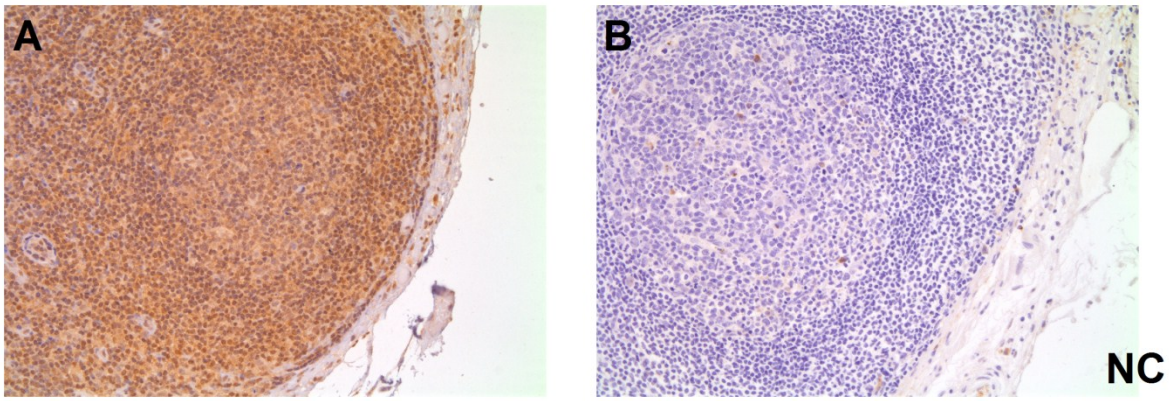

Figure 6.14: Phospho-SYK (P-SYK) detection in human lymph node.
(A) & (B) P-SYK staining localised predominantly to a lymphoid follicle, with a sequential negative control (NC) section performed by pre-incubating primary P-SYK antibody with the relevant immunising peptide. x200 magnification.

In 'normal' kidney tissue (TBM and MCD; Figures 6.15 and 6.16 respectively), minimal P-SYK expression was observed, particularly within glomeruli. There was weak staining within

tubular epithelial cells, suggesting that SYK may be expressed in this cell type, but that it not functionally active in the non-diseased state.

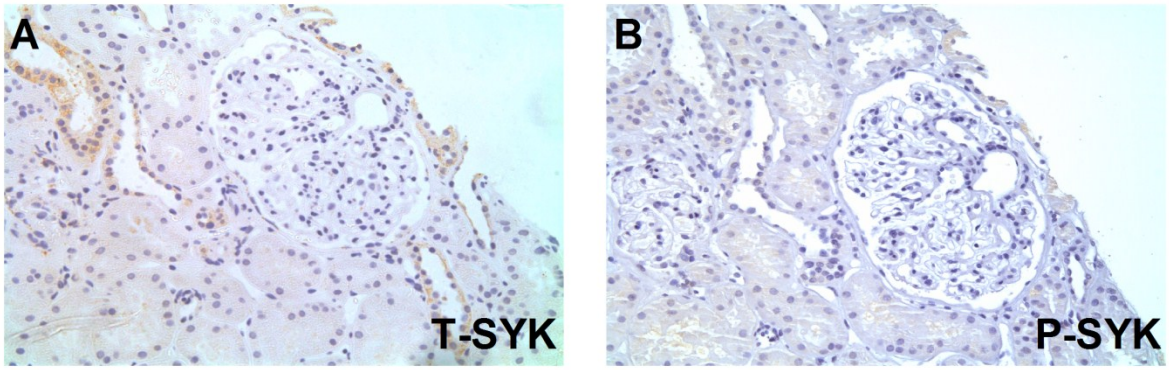

Figure 6.15: Phospho-SYK (P-SYK) detection in thin basement membrane lesion (TBM).
(A) & (B) Paired sections showing Total SYK (T-SYK) and P-SYK in TBM. SYK appears to be expressed but not functionally active (i.e. phosphorylated) in distal tubular epithelial cells. Glomeruli were negative for both T-SYK and P-SYK. x200 magnification.

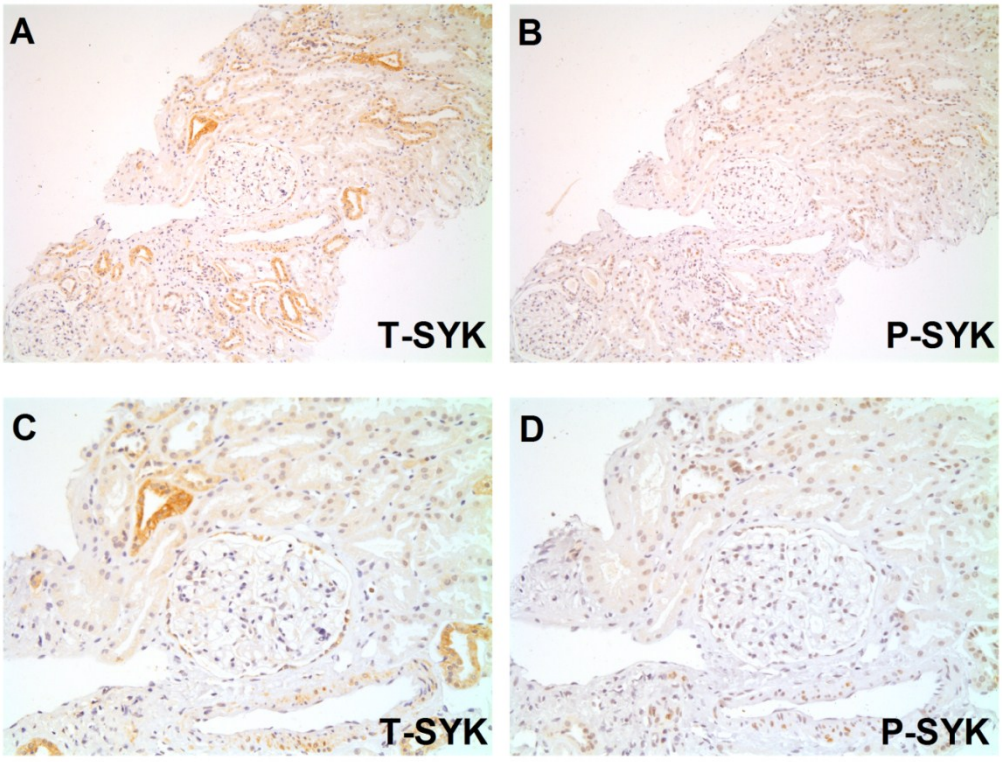

Figure 6.16: Phospho-SYK (P-SYK) detection in minimal change disease (MCD).
(A) & (B) Paired sections at low power, showing Total SYK (T-SYK) and P-SYK in MCD. SYK appears to be expressed but not functionally active (i.e. phosphorylated) in distal tubular epithelial cells. Glomeruli were negative for both T-SYK and P-SYK. x100 magnification (C) & (D) Higher power view of the same tissue sections, confirming that glomeruli are negative for both T-SYK and P-SYK. x200 magnification.

6.3.1 Phosphorylated SYK detection in anti-GBM disease

Since T-SYK expression levels were highest in anti-GBM disease, I selected these biopsies for initial staining for P-SYK. Figure 6.17 shows sequential sections of a biopsy taken from such a case. This shows positive P-SYK detection in a distribution similar to that seen for T-SYK, suggesting that SYK is functionally active (and thus pathogenically relevant) in anti-GBM disease. Notably, P-SYK had a predominantly nuclear pattern of staining. Since this staining was not present on negative control sections, and was consistently identified in a similar distribution to T-SYK within diseased glomeruli, using an antibody that was shown to be specific by immunoblotting, I believe this is genuine staining despite the somewhat atypical staining appearance. In lymphoid cells, SYK is known to reside in both nuclear and cytoplasmic locations, although little is known about how trafficking between these compartments is regulated.[253]

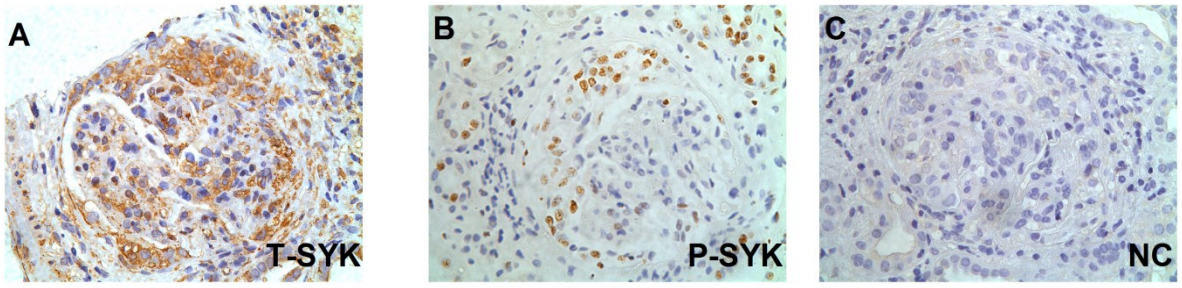

Figure 6.17: Phospho-SYK (P-SYK) detection in anti-GBM disease.
(A), (B) & (C) Sequential sections showing Total SYK (T-SYK), P-SYK and negative control (NC; for P-SYK antibody) staining in the same glomerulus from a patient with anti-GBM disease. P-SYK is detected within an area of crescent formation that is strongly positive for T-SYK, suggesting that SYK is expressed and functionally active in anti-GBM disease.

6.3.2 Phosphorylated SYK expression in other proliferative glomerulonephritides

In AAGN, staining of sequential sections showed a similar pattern of P-SYK in the distribution that was observed for T-SYK (Figure 6.18). In each case, staining for P-SYK in tubular epithelial cells was less striking than for T-SYK, again suggesting that whilst SYK may be constitutively expressed in this cell type, it is not functionally active (Figure 6.19).

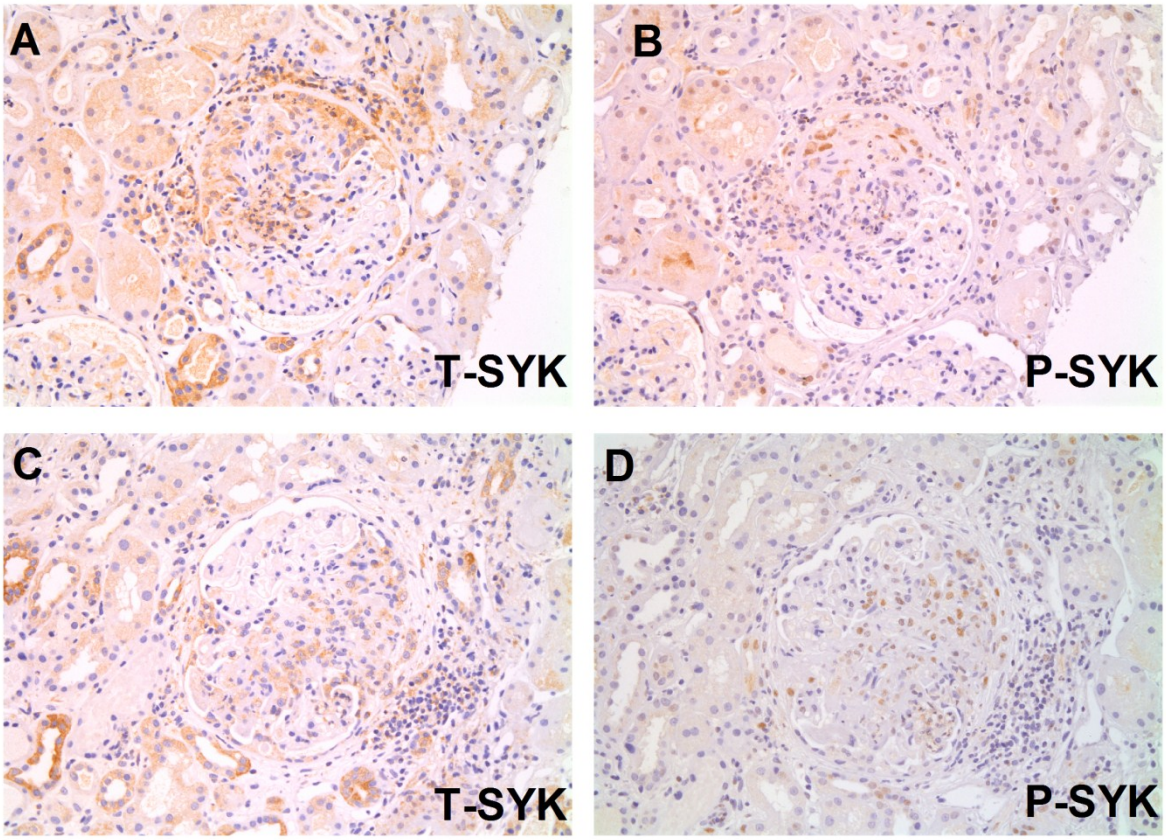

Figure 6.18: Phospho-SYK (P-SYK) detection ANCA-associated glomerulonephritis (AAGN).
(A), (B), (C) & (D) Two sets of paired sections showing total SYK (T-SYK) and P-SYK staining in two cases of AAGN. P-SYK is detected within areas of crescent formation that are strongly positive for T-SYK, suggesting that SYK is expressed and functionally active in AAGN.

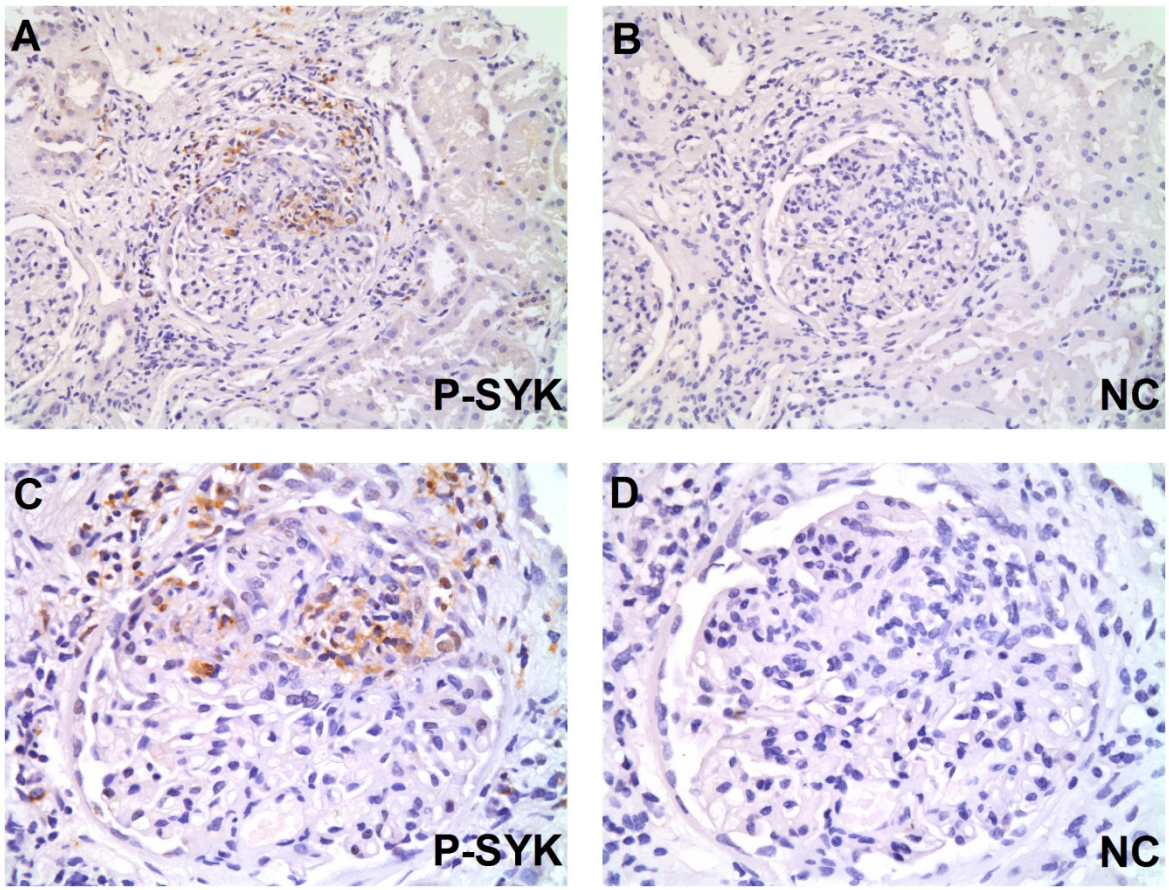

Figure 6.19: Phospho-SYK (P-SYK) detection in ANCA-associated glomerulonephritis (AAGN).
(A) & (B) P-SYK detection within a crescentic glomerulus in AAGN, within minimal staining seen in tubular epithelial cells, suggesting that SYK may be expressed but not functionally active in the latter, with sequential negative control (NC) section. x200 magnification . (C) & (D) Higher power view of the same tissue section showing glomerular P-SYK staining in more detail. x400 magnification.

A similar pattern of predominantly nuclear staining in cells within inflammatory lesions was observed in both lupus nephritis (Figure 6.20) and IgA nephropathy (Figure 6.21).

In general, P-SYK detection was less reproducible than that for T-SYK, and was sometimes inconsistent across the same tissue section. I believe this may be due to rapid de-phosphorylation of SYK prior to adequate tissue fixation, a recognised difficulty in immunostaining for phosphorylated proteins[254]. Since this study was performed on surplus sections from routine clinical biopsies that were not specifically processed for research

purposes, this problem was difficult to resolve, and hence it was not possible to reliably quantify the degree of P-SYK detection. However, the demonstration of activated SYK within abnormal glomeruli strongly implicates SYK in the pathogenesis of proliferative GN.

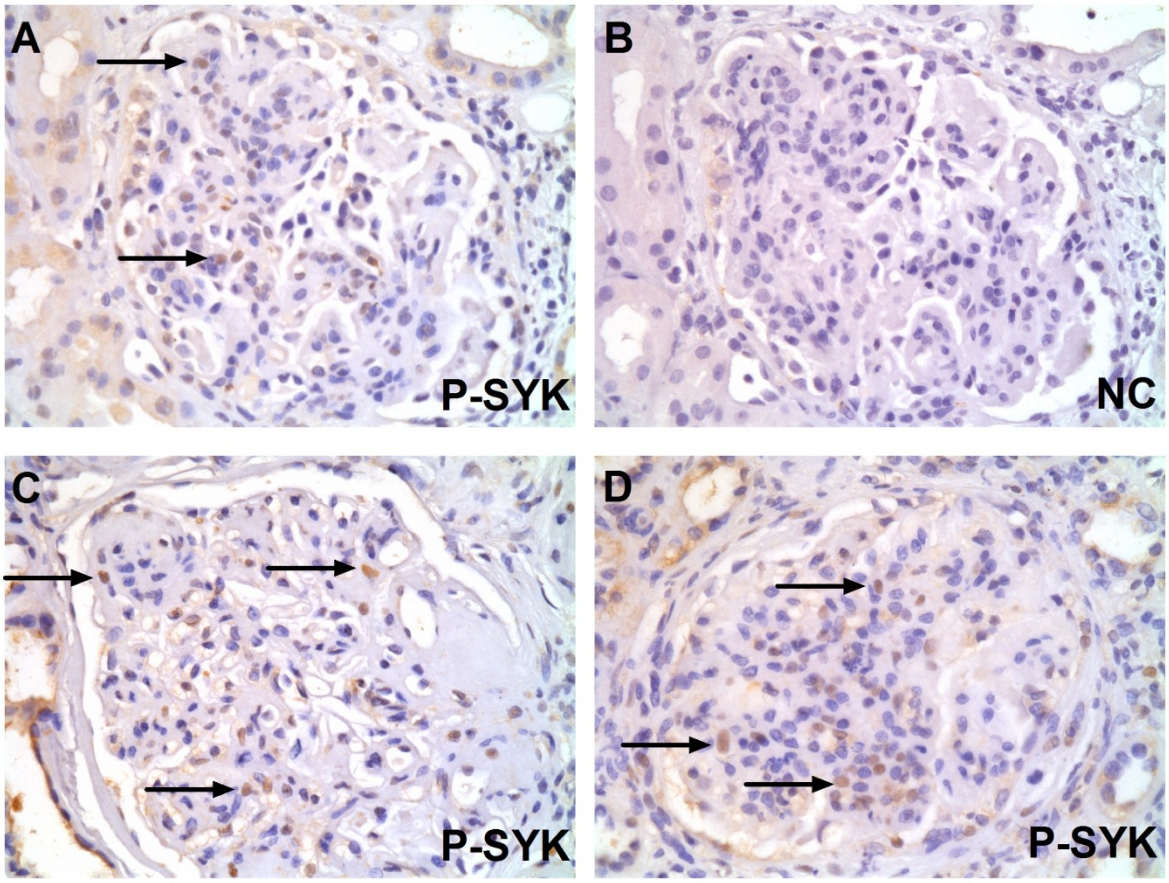

Figure 6.20: Phospho-SYK (P-SYK) detection in class IV lupus nephritis.
(A) & (B) P-SYK positive cells (with examples illustrated by arrows) within glomerular capillary lumens in proliferative lupus nephritis, with a sequential negative control (NC) section. (C) & (D) Two additional examples of P-SYK positive cells within glomerular capillary loops in proliferative lupus nephritis. x400 magnification.

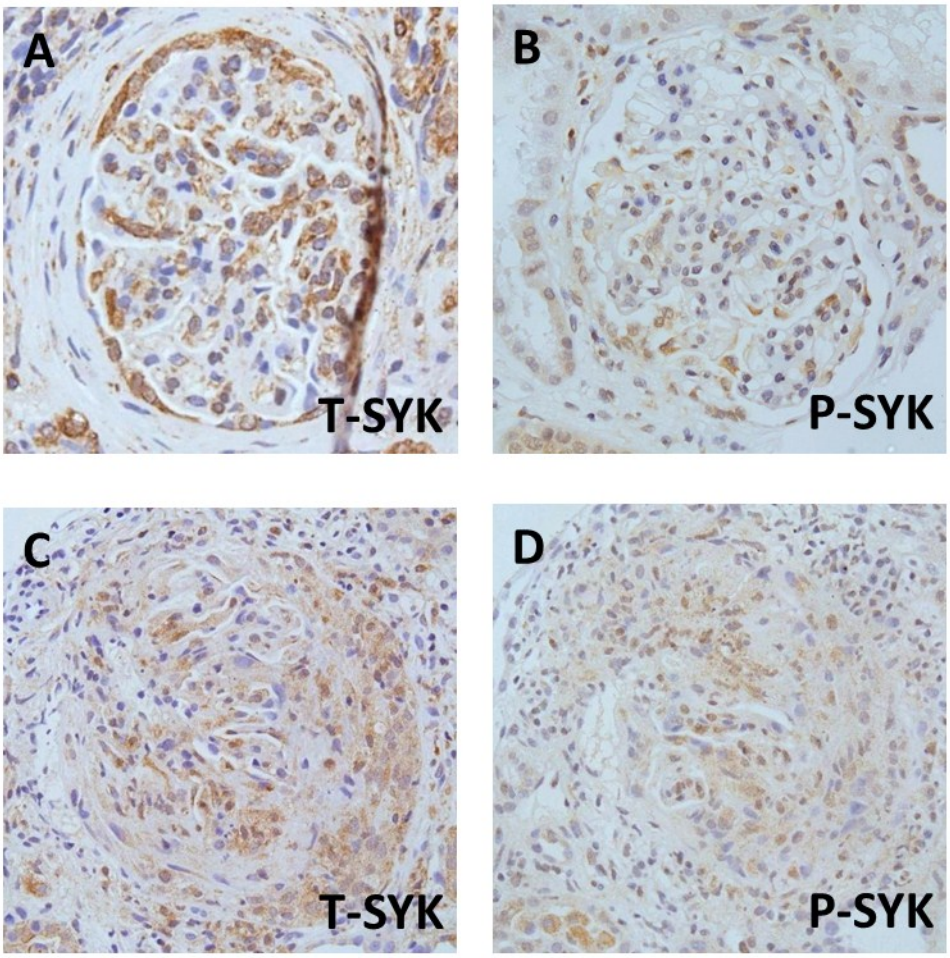

Figure 6.21: Phospho-SYK (P-SYK) detection in IgA nephropathy.
(A) & (B) Sequential sections showing Total (T-SYK) and P-SYK detection in IgA nephropathy with endocapillary proliferation. (C) & (D) Sequential sections showing T-SYK and P-SYK detection in 'crescentic' IgA nephropathy. x200-400 magnification.

6.4 Cellular localisation of SYK in proliferative glomerulonephritis

SYK expression levels were highest in proliferative GN, and SYK appeared to localise in particular to areas of endocapillary and extracapillary proliferation that contain infiltrating leucocytes. Since I observed significant co-localisation of SYK with ED1+ macrophages in the rodent models, I therefore sought to establish if SYK similarly localised to infiltrating myeloid cells in human disease.

Staining of serial sections from patients with lupus nephritis identified a small number of CD15+ cells within capillary loops in glomeruli that also contained SYK positive cells (Figure 6.22).

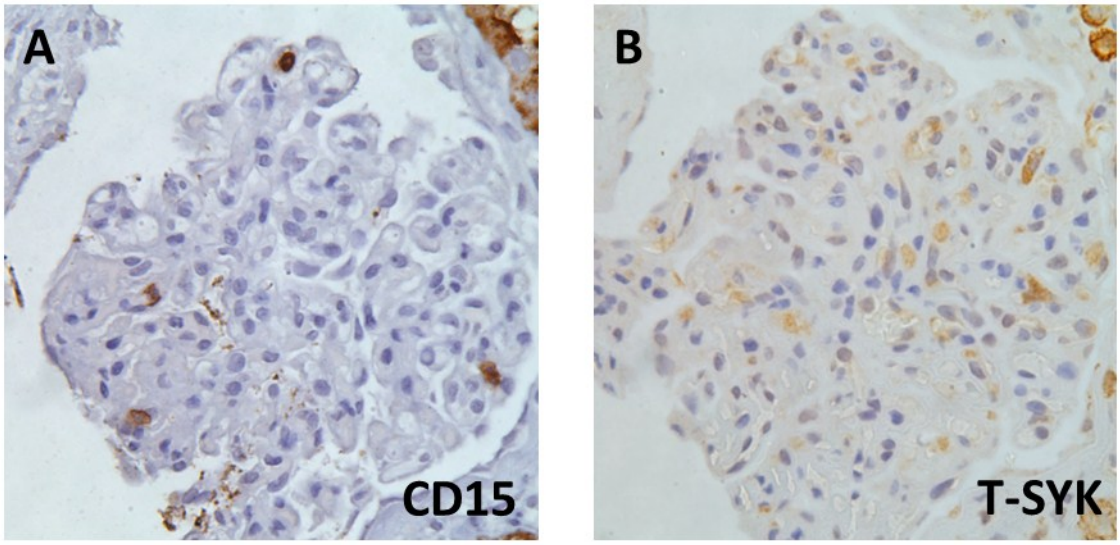

Figure 6.22: CD15 and Total SYK (T-SYK) detection in class IV lupus nephritis.
(A) & (B) Sequential sections showing CD15 (a neutrophil marker) positive cells and T-SYK positive cells within the same glomerulus from a patient with proliferative lupus nephritis. x400 magnification.

In AAGN, a larger number of CD68+ cells were identified, in a similar distribution to SYK positive cells, within glomeruli (Figure 6.23).

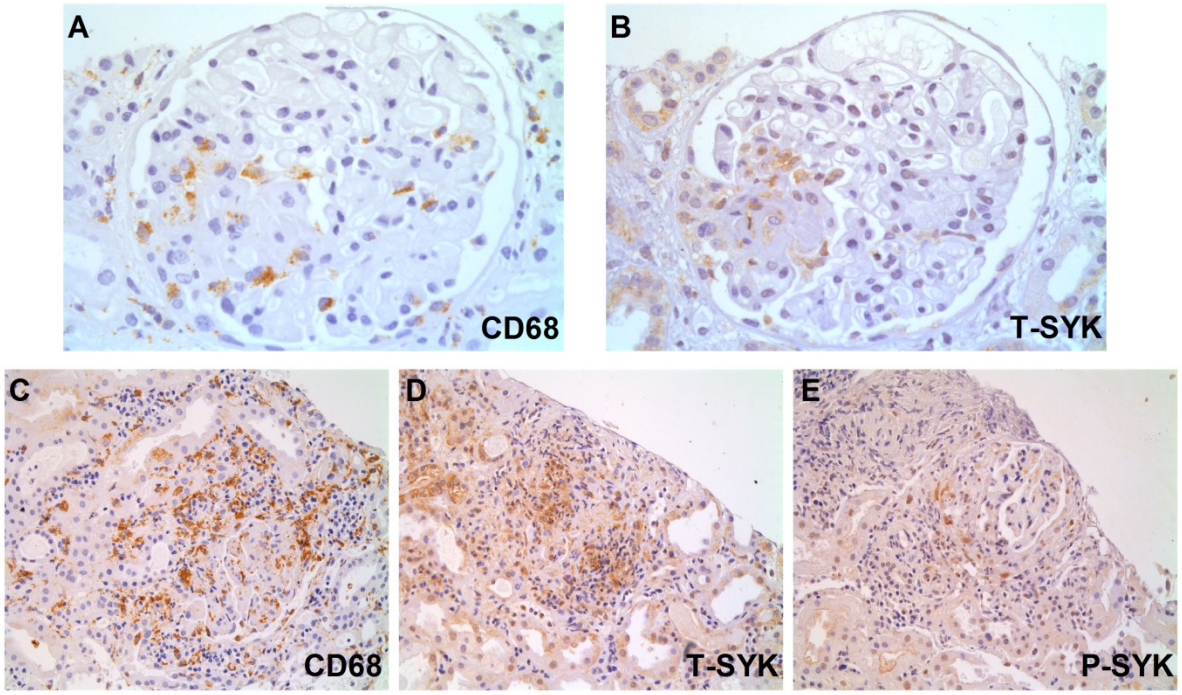

Figure 6.23: CD68 and SYK detection in ANCA-associated glomerulonephritis (AAGN).
(A) & (B) Sequential sections showing CD68 (a macrophage marker) and Total SYK (T-SYK) positive cells localised to the same area of segmental inflammation in a patient with AAGN. x400 magnification. (C), (D) & (E) Sequential sections showing CD68 positive, T-SYK positive, and Phospho-SYK (P-SYK) positive cells within the same glomerulus from a patient with 'crescentic' class AAGN. x200 magnification.

To define this more precisely, I attempted to perform double staining for CD68 and T-SYK on single tissue sections. This raised several technical problems. Firstly, subjecting the same tissue section to repeated rounds of antigen retrieval led to significant degradation in the quality of the section. In addition, the method I developed for immunophosphatase staining gave a 'blue' reaction product, meaning that a standard counterstaining with haematoxylin count not be used to delineate tissue detail. Notwithstanding, double staining of AAGN tissue suggested significant co-localisation of T-SYK to CD68+ cells (Figure 6.24). There was, however, a proportion of cells that were T-SYK positive and CD68 negative, implying that

SYK may be expressed within a number of cell types, both resident renal cells and other types of infiltrating leucocytes, in AAGN.

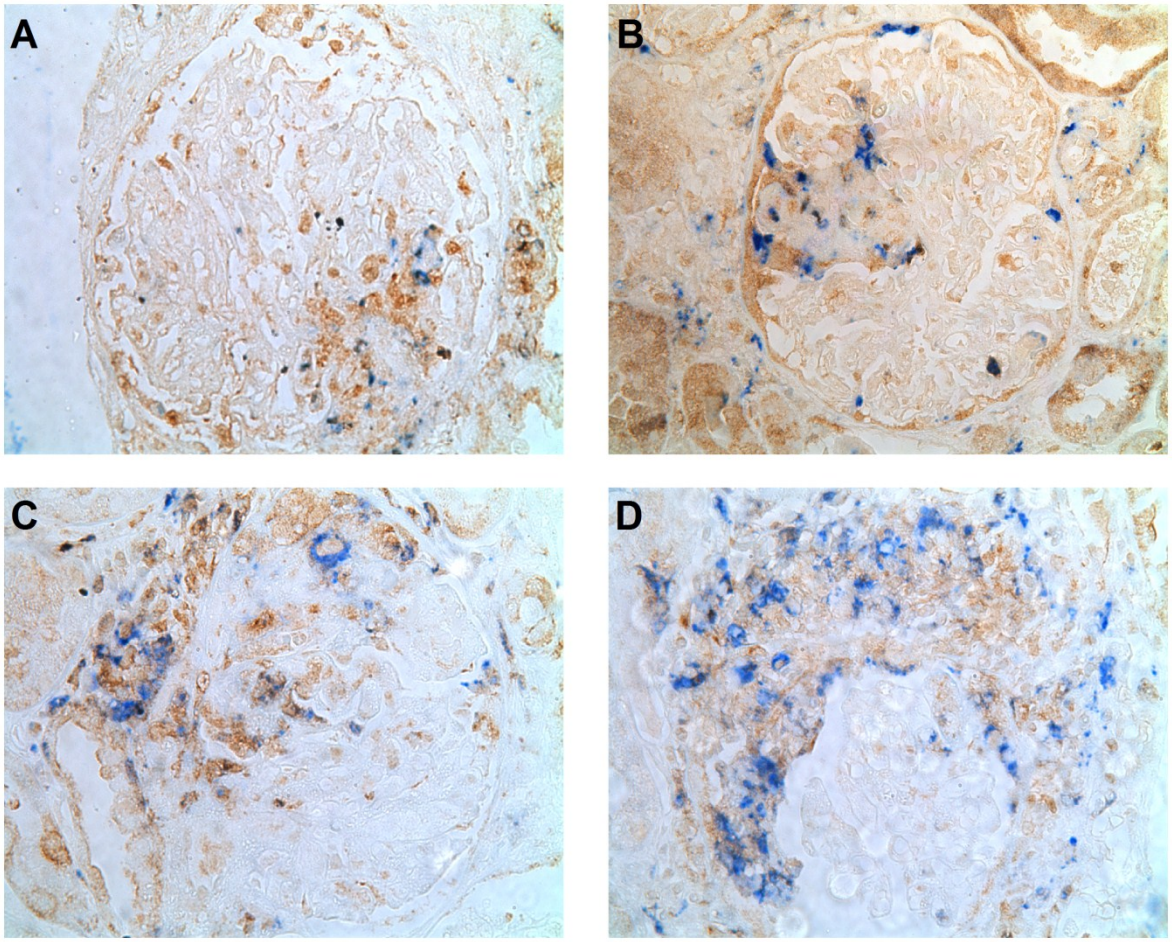

Figure 6.24: Double staining for CD68 and Total SYK (T-SYK) in ANCA-associated glomerulonephritis (AAGN).

(A), (B), (C) & (D). Double staining for CD68 (a macrophage marker; in blue) and T-SYK (in brown) in four cases of AAGN. In all cases, there is apparent co-localisation of CD68 and T-SYK to the same areas of segmental inflammation or crescent formation in diseased glomeruli. A proportion of cells, however, are T-SYK positive and CD68 negative, suggesting that cells types other than macrophages may express SYK within diseased glomeruli in AAGN.

6.5 Chapter Six: Discussion of results and future work

The work reported in this chapter is the first systematic analysis of SYK expression in glomerular disease, using biopsy specimens from a large number of patients. I have shown that SYK is expressed in a spectrum of human glomerulonephritides, that expression levels are highest in proliferative classes of GN, and that they correlate broadly with disease severity or histological class in anti-GBM disease, AAGN, lupus nephritis and IgA nephropathy. SYK appears to be phosphorylated and functionally active within diseased glomeruli, implying it has a pathogenic role in these conditions. SYK localises to infiltrating leucocytes, and in particular infiltrating macrophages, within disease glomeruli, although there are a number of other cell types, both resident and infiltrating, that may contain SYK.

The potential role of SYK in the pathogenesis of anti-GBM disease and AAV has been discussed in Chapters Four and Five. SYK has also been implicated in the pathogenesis of SLE. SYK inhibitor treatment using fostamatinib, for example, has shown efficacy in three distinct murine models[68,69]. In particular, treatment of the lupus-prone NZB/NZW and MRL/lpr mouse strains reduced kidney disease as determined by both proteinuria and renal histology. Higher levels of SYK expression and activity have been reported in T cells from SLE patients versus normal controls[58], and it was recently reported that silencing of SYK expression in SLE T cells, or forced over-expression of SYK in normal T cells, normalised their gene expression signature, or recapitulated an SLE expression signature, respectively[255]. SYK is also implicated in the pathogenesis of IgA nephropathy, the most common primary glomerulonephritis for which there is still no universally accepted treatment. Our laboratory has previously reported that IgA1 isolated from patients with IgA nephropathy induced proliferation and pro-inflammatory cytokine production by human renal mesangial cells *in*

vitro, and that this could be inhibited by pharmacological inhibition using fostamatinib, or genetic 'knock-down' using siRNA techniques[243]. Taken together, these data suggest that SYK inhibition may be a rational therapeutic target in a variety of human GN.

Whilst these data suggest that SYK is expressed within infiltrating leucocytes, I have not addressed SYK expression in resident renal cells, such as epithelial cells or mesangial cells, which may also contribute to disease pathogenesis. It would be desirable to pursue this in future work, although the paucity of validated cell markers that can used for the identification of such cells by immunohistochemistry on formalin-fixed paraffin-embedded tissue will make this challenging. The use of frozen tissue sections and immunofluorescence techniques could be explored. I also observed substantial SYK staining outwith glomeruli in tubular epithelial cells, both in normal and diseased cases. The significance of which is not clear, and thus also warrants further investigation. It would also be desirable to optimise P-SYK staining in order to allow quantification; the challenges, however, of staining for phospho-proteins have already been discussed (Section 6.3). Finally, it would be desirable to correlate SYK staining in proliferative GN with other clinical parameters such as renal function, proteinuria and patient outcomes, and to examine those patients who had serial biopsies to investigate any correlations with disease progression or response to treatment.

6.6 Summary of key findings

- SYK is expressed in the glomeruli in a spectrum of human GN

- SYK expression levels are highest in proliferative GN, and correlate broadly with disease severity in anti-GBM disease, AAGN, lupus nephritis and IgA nephropathy.

- SYK is phosphorylated and functionally active within diseased glomeruli, implying it has a pathogenic role in these conditions.

- SYK localises to infiltrating leucocytes, and in particular infiltrating macrophages, within diseased glomeruli, although there are a number of other cell types, both resident and infiltrating that may express SYK

CHAPTER SEVEN - DISCUSSION AND FUTURE WORK

7.1 Discussion

This project set out to investigate the role of SYK in the pathogenesis of GN, and to establish if it may represent a therapeutic target in clinical disease. To address these questions, I studied the effects of SYK inhibition using a pharmacological small molecule inhibitor in two distinct experimental models, and conducted an immunohistochemical survey of almost 100 clinical specimens from patients with various forms of GN.

I have reported several novel observations, including:

(i) Activation of SYK is a key requirement for the induction of experimental autoimmune glomerulonephritis.

(ii) In established experimental disease, SYK inhibition is an effective treatment for the renal and pulmonary manifestations of autoimmune glomerulonephritis and autoimmune vasculitis.

(iii) SYK inhibition attenuates the production of pathogenic anti-GBM autoantibodies in EAG, likely through direct effects on antibody-producing B cells.

(iv) SYK in expressed and activated in pathological lesions in various forms of human GN.

These observations suggest that SYK contributes significantly to the pathogenesis of inflammation in GN, and that clinical studies using SYK inhibition should be considered.

The majority of this work was undertaken in rodent models of human glomerular disease. Whilst these models have been developed to recapitulate as closely as possible the pathogenic mechanisms and phenotype that is observed clinically, *in vivo* models are well recognised to have shortcomings that may limit their translation of human disease. EAG and EAV, for example, are non-spontaneous, requiring active immunisation in the presence of potent adjuvants. EAV, whilst characterised by the presence of autoreactive ANCA, is induced by immunisation with an alloantigen, and unlike AAV, the disease it models, it has a gradual and spontaneous resolution beyond week 6, and does not replicate the relapsing-remitting course of clinical disease. In addition, the rodent and human immune systems are phylogenetically distinct, with recognised differences in both innate and adaptive elements, such that the pathogenic mechanisms (and thus responses to potentially therapeutic interventions) may not translate from one species to another[256]. This is perhaps illustrated by our laboratory's previous finding that experimental glomerulonephritis and vasculitis could be successfully attenuated by TNF-α blockade[132,214], a therapy that has shown uncertain efficacy in clinical studies in AAV[257,258].

In an attempt to identify 'conserved' and 'divergent' components of the murine and human immune systems, the Immunological Genetics (ImmGen) Consortium has compared the transcriptional profiles of mouse and human immune cell types[259]. They found conserved expression patterns for most orthologous genes, although several hundred genes showed clearly divergent expression patterns across different cell types. Interrogation of the ImmGen database reports that the *SYK* gene has a 'co-efficient of conservation' of 0.938 (range -1 to 1), suggesting that its transcriptional profile is highly conserved between species, and perhaps indicating that it has conserved function across species.

Other limitations that should be considered in the interpretation of my experimental findings include:

(i) Specificity of the inhibitor used: The available data, as described in section 1.2, suggests the R406 is highly selective for SYK, although it does have documented activity, albeit as much less potency in cell based assays, on other kinases including Flt3, Lyn and Lck. It is possible that the combined effect of low-level inhibition of these multiple kinases (or activity on other kinases not yet tested in *in vitro* assays) may have accounted for the dramatic effects observed in my *in vivo* studies. This makes it difficult to propose definite inferences about the role of SYK in disease pathogenesis, though these may be less of a concern with regards to translating my findings to the clinical arena. Indeed, the drug's therapeutic potential may be reliant on producing 'off-target' effects on multiple kinases.

(ii) Pharmacokinetics: I have not gathered any PK data in these studies. The doses of fostamatinib used were based on those used in comparable, published *in vivo* studies, including our laboratory's previous work in NTN, and on PK data from other rat strains provided by the drug manufacturer. Whether these are applicable to WKY rats (and in the presence of renal impairment and systemic inflammation) is not known. It would be of value to perform PK analyses in future studies, both to confirm that sufficient plasma R406 levels were achieved in order to inhibit cellular SYK activity, and to identify the possibility of excessive dosing resulting in increased 'off-target' drug effects.

(iii) Cellular target of SYK inhibition: My *in vitro* data suggests SYK activity in B cell and macrophages contributes to autoantibody production and inflammation in GN. However, it is difficult to delineate to role of SYK in different cell types *in vivo*, due to systemic exposure to the pharmacological agent. I have therefore not addressed the role of other cell types that express SYK and are known to contribute to the pathogenesis of experimental GN, such as neutrophils[260], mast cells[261] and dendritic cells[262].

7.2 Future work

The use of genetic approaches may overcome some of the limitations I have identified. My colleague Dr Min Jeong Kim, for example, has compared the effect of *SYK* siRNA knockdown and pharmacological SYK inhibition with R406, on cultured human mesangial cells stimulated with IgA1 from IgA nephropathy patients, and shown that both approaches have similar effects on cytokine production profile, suggesting that R406 is active against SYK, and implying a degree of specificity[243]. A similar approach could be used in my *in vitro* studies with BMDM and other cell types.

In work ongoing in the laboratory at present, I am investigating the effects of inducible *SYK* deletion in accelerated murine NTN, using the Cre-loxP system described in section 1.1.6 (using mice kindly provided by Victor Tybulewicz at the National Institute for Medical Research). Preliminary results suggests that inducible *SYK* deletion results in protection from NTN, and if confirmed, these findings raise the possibility of defining the role of SYK in specific cell types in NTN, by inducing deletion under various cell- or tissue-specific

promoters. These animals will also provide a source of SYK-deficient cells that could be used for further *in vitro* studies.

Whilst this project has focused on the role of SYK in adaptive immune responses, SYK has also been implicated in a number of other signalling pathways that may be relevant in these models, or to subsequent clinical translation of these findings, and that warrant further consideration. These include roles in integrin signalling, platelet function, bone metabolism, oncogenesis, and innate immunity.

Integrin signalling

SYK has been implicated in integrin signalling in myeloid cells[30,31,263]. Integrins are transmembrane receptors that have a critical role in cell adhesion, migration and activation, via their interaction with adhesion molecules expressed on other cells, particularly the vascular endothelium. SYK deficient myeloid cells show impaired integrin-mediated responses (such as impaired respiratory burst and cytokine release, though not impaired migration or cell recruitment) thought to be dependent on the association of integrins with ITAM-containing adaptor proteins such as FcRγ-chain and DAP12, as myeloid cells deficient in these adaptor proteins show similar defects. Inhibition of integrin-dependent responses in myeloid cells may have contributed to the attenuation of injury that was observed in my *in vivo* studies.

Platelet function

SYK has been shown to be involved in a number of platelet activation pathways, including via the glycoprotein GPVI receptor (an FcRγ chain-associated receptor that bears an ITAM motif), integrin αIIbβ3, and C-type Lectin 2 (CLEC-2; a type II membrane protein containing a single tyrosine-based motif in its cytoplasmic tail that has been termed a hemITAM)[264,265]. In addition, R406 has demonstrated inhibitory activity in these pathways[62]. However, high dose exposure to R406 did not prolong bleeding time in mice, and in phase I human studies, R406 did not inhibit collagen or ADP-induced platelet aggregation *ex vivo*[48], perhaps suggesting redundancy of SYK dependent pathways *in vivo*. Notwithstanding, the potential effect of altered platelet function in the experimental models (and particularly in murine NTN, which has a thrombotic phenotype) could be investigated, and may have obvious implications for use of SYK inhibition in clinical studies.

Bone metabolism

SYK has been shown to regulate osteoclastic bone resorption, via its association with integrin αvβ3 and ITAM bearing proteins, such as DAP12 and FcRγ chain, expressed at the osteoclast cell surface[266]. In addition, SYK has recently been implicated in the suppression of osteoblast differentiation[267]. Thus, SYK may represent a therapeutic target in disorders of bone metabolism such as osteoporosis, although potential effects of SYK inhibition on normal bone, such as osteosclerosis or increased fragility and fracture risk, have yet to be investigated *in vivo* or in clinical studies.

Oncogenesis

It has been suggested that SYK is a negative regulator of progression in various types of malignancy (including breast, gastric and melanoma) based on the observation of decreased SYK expression in these tumour types and experimental studies where SYK transfection and re-expression in tumour cell lines suggested a tumour- and metastasis- suppressive effect[268]. The molecular mechanism of this suppressive role has yet to be established. Conversely, fostamatinib has shown activity in NCI-60 (a panel of 60 diverse human cancer cell lines), although this may be due to off-target effects, rather than SYK inhibition specifically. Fostamatinib had limited anti-tumour activity in a broad multi-histology Phase II study[78].

SYK signalling through the BCR has also been implicated as an important survival signal in various lymphoid malignancies, and R406 has shown anti-proliferative and pro-apoptotic activity in B cell lymphoma and CLL lines *in vitro*[50-52]. Furthermore, R788 is highly active in animal models of NHL and CLL[63,64] and, in a Phase II clinical trial, fostamatinib showed significant clinical activity in a heterogeneous group of NHL and CLL[77]. Based on these findings, larger Phase II trials in haematological malignancy are ongoing (NCT00798096). Interestingly, some oncogenic viruses have been shown to encode ITAM-containing proteins – for example, Epstein Barr virus (EBV) latent membrane protein 2A (LMP2A) contains an ITAM motif, and has been shown to promote B cell development and survival[269]. Recently, it was shown that R406 induces cell-cycle arrest and apoptosis in EBV positive B cell lymphoma post-transplant lymphoproliferative disorder (PTLD) cell lines *in vitro*, although increased nodal tumour growth was observed in *in vivo* models[270]. More work is clearly needed to define the true nature and mechanisms of SYK involvement in these cancer pathways.

Innate immunity

SYK has recently been associated with a variety of pathogen recognition receptors (PRR), important components of the innate immune response that recognise pathogen-associated molecular patterns (PAMPs). C-type Lectins, one such class of PRR, play an important role in antifungal immunity in particular, and SYK has been implicated in the intracellular signalling cascades for these receptors[271]. Some, such as Dectin-1, contain an ITAM motif on their cytoplasmic domain, and others may associate with ITAM-containing adaptor proteins such as FcRγ chain or DAP12. Signalling via these pathways may be involved in the pathogenesis of the experimental models I have used (in particular, during the response to adjuvant) and the effects of SYK inhibition in these responses warrants further investigation. In addition, it is notable that SYK is reported to couple activation of fungal PRR to Nlrp3-inflammasome activation[272]. Our laboratory has previously shown that differences in Nlrp3-inflammaome activation may account for the distinct susceptibility of the WKY rat strain, and resistance of the Lewis strain, to experimental models of GN[273]. It would be of interest to establish if there are genetic or functional differences in SYK signalling between these two strains.

Effects on these innate immune responses raise obvious concerns for clinical use of SYK inhibition as a therapeutic strategy in autoimmune disease. The results of the preclinical toxicity assessments and host resistance models are reassuring in this respect[80] (although a host resistance model of fungal infection has not been studied), as is the absence of severe, atypical or opportunistic infection in the clinical studies thus far. Larger and longer clinical studies are, however, needed to establish the long term and cumulative effects of SYK

inhibition on innate immune responses and infection risk, particularly in patient groups who may have had extensive treatment histories with other immunosuppressant agents.

7.3 Conclusions

The findings reported in this thesis suggest that SYK inhibition using fostamatinib has the capacity to prevent, treat, and even reverse disease in experimental models of glomerulonephritis and vasculitis. My findings also implicate SYK in the pathogenesis of human glomerular disease, and support existing experimental data suggesting SYK is important in the development of lupus, IgA nephropathy and AAV. Whilst the diverse biological functions of SYK, coupled to the potential off-target effects of its inhibitors are a source of possible toxicity, the available data augurs well for future clinical use of SYK inhibition in glomerulonephritis, and potentially other systemic or organ-specific autoimmune diseases.

REFERENCES

1. Shaw C, Pruthi R, Pitcher D, Fogarty D. UK Renal Registry 15th annual report: Chapter 2 UK RRT prevalence in 2011: national and centre-speci fi c analyses. *Nephron. Clinical practice.* 2013;123 Suppl 1:29-54.

2. Collins AJ, Foley RN, Chavers B, et al. 'United States Renal Data System 2011 Annual Data Report: Atlas of chronic kidney disease & end-stage renal disease in the United States. *American journal of kidney diseases : the official journal of the National Kidney Foundation.* Jan 2012;59(1 Suppl 1):A7, e1-420.

3. Couser WG. Basic and translational concepts of immune-mediated glomerular diseases. *Journal of the American Society of Nephrology : JASN.* Mar 2012;23(3):381-399.

4. Sada K, Takano T, Yanagi S, Yamamura H. Structure and function of Syk protein-tyrosine kinase. *Journal of biochemistry.* Aug 2001;130(2):177-186.

5. Mocsai A, Ruland J, Tybulewicz VL. The SYK tyrosine kinase: a crucial player in diverse biological functions. *Nature reviews. Immunology.* Jun 2010;10(6):387-402.

6. Riccaboni M, Bianchi I, Petrillo P. Spleen tyrosine kinases: biology, therapeutic targets and drugs. *Drug Discov Today.* Jul 2010;15(13-14):517-530.

7. Zioncheck TF, Harrison ML, Geahlen RL. Purification and characterization of a protein-tyrosine kinase from bovine thymus. *The Journal of biological chemistry.* Nov 25 1986;261(33):15637-15643.

8. Kobayashi T, Nakamura S, Taniguchi T, Yamamura H. Purification and characterization of a cytosolic protein-tyrosine kinase from porcine spleen. *European journal of biochemistry / FEBS.* Mar 30 1990;188(3):535-540.

9. Taniguchi T, Kobayashi T, Kondo J, et al. Molecular cloning of a porcine gene syk that encodes a 72-kDa protein-tyrosine kinase showing high susceptibility to proteolysis. *J Biol Chem.* Aug 25 1991;266(24):15790-15796.

10. Ku G, Malissen B, Mattei MG. Chromosomal location of the Syk and ZAP-70 tyrosine kinase genes in mice and humans. *Immunogenetics.* 1994;40(4):300-302.

11. Cho P, Gelinas L, Corbett NP, et al. Association of common single-nucleotide polymorphisms in innate immune genes with differences in TLR-induced cytokine production in neonates. *Genes and immunity.* Jun 2013;14(4):199-211.

12. Zhang J, Benavente CA, McEvoy J, et al. A novel retinoblastoma therapy from genomic and epigenetic analyses. *Nature.* Jan 19 2012;481(7381):329-334.

13. Yuan Y, Mendez R, Sahin A, Dai JL. Hypermethylation leads to silencing of the SYK gene in human breast cancer. *Cancer research.* Jul 15 2001;61(14):5558-5561.

14. Furlong MT, Mahrenholz AM, Kim KH, Ashendel CL, Harrison ML, Geahlen RL. Identification of the major sites of autophosphorylation of the murine protein-tyrosine kinase Syk. *Biochim Biophys Acta.* Feb 4 1997;1355(2):177-190.

15. Au-Yeung BB, Deindl S, Hsu LY, et al. The structure, regulation, and function of ZAP-70. *Immunol Rev.* Mar 2009;228(1):41-57.

16. Deindl S, Kadlecek TA, Brdicka T, Cao X, Weiss A, Kuriyan J. Structural basis for the inhibition of tyrosine kinase activity of ZAP-70. *Cell.* May 18 2007;129(4):735-746.

17. Kulathu Y, Grothe G, Reth M. Autoinhibition and adapter function of Syk. *Immunol Rev.* Nov 2009;232(1):286-299.

18. Turner M, Schweighoffer E, Colucci F, Di Santo JP, Tybulewicz VL. Tyrosine kinase SYK: essential functions for immunoreceptor signalling. *Immunol Today.* Mar 2000;21(3):148-154.

19. Tsang E, Giannetti AM, Shaw D, et al. Molecular mechanism of the Syk activation switch. *J Biol Chem.* Nov 21 2008;283(47):32650-32659.

20. Bradshaw JM. The Src, Syk, and Tec family kinases: distinct types of molecular switches. *Cell Signal.* Aug 2010;22(8):1175-1184.

21. Latour S, Zhang J, Siraganian RP, Veillette A. A unique insert in the linker domain of Syk is necessary for its function in immunoreceptor signalling. *The EMBO journal.* May 1 1998;17(9):2584-2595.

22. Turner M, Mee PJ, Costello PS, et al. Perinatal lethality and blocked B-cell development in mice lacking the tyrosine kinase Syk. *Nature.* Nov 16 1995;378(6554):298-302.

23. Cheng AM, Rowley B, Pao W, Hayday A, Bolen JB, Pawson T. Syk tyrosine kinase required for mouse viability and B-cell development. *Nature.* Nov 16 1995;378(6554):303-306.

24. Abtahian F, Guerriero A, Sebzda E, et al. Regulation of blood and lymphatic vascular separation by signaling proteins SLP-76 and Syk. *Science.* Jan 10 2003;299(5604):247-251.

25. Geahlen RL. Syk and pTyr'd: Signaling through the B cell antigen receptor. *Biochimica et biophysica acta.* Jul 2009;1793(7):1115-1127.

26. Crowley MT, Costello PS, Fitzer-Attas CJ, et al. A critical role for Syk in signal transduction and phagocytosis mediated by Fcgamma receptors on macrophages. *The Journal of experimental medicine.* Oct 6 1997;186(7):1027-1039.

27. Kiefer F, Brumell J, Al-Alawi N, et al. The Syk protein tyrosine kinase is essential for Fcgamma receptor signaling in macrophages and neutrophils. *Molecular and cellular biology.* Jul 1998;18(7):4209-4220.

28. de Castro RO. Regulation and function of syk tyrosine kinase in mast cell signaling and beyond. *Journal of signal transduction.* 2011;2011:507291.

29. Sedlik C, Orbach D, Veron P, et al. A critical role for Syk protein tyrosine kinase in Fc receptor-mediated antigen presentation and induction of dendritic cell maturation. *J Immunol.* Jan 15 2003;170(2):846-852.

30. Mocsai A, Abram CL, Jakus Z, Hu Y, Lanier LL, Lowell CA. Integrin signaling in neutrophils and macrophages uses adaptors containing immunoreceptor tyrosine-based activation motifs. *Nat Immunol.* Dec 2006;7(12):1326-1333.

31. Mocsai A, Zhou M, Meng F, Tybulewicz VL, Lowell CA. Syk is required for integrin signaling in neutrophils. *Immunity.* Apr 2002;16(4):547-558.

32. Jakus Z, Simon E, Balazs B, Mocsai A. Genetic deficiency of Syk protects mice from autoantibody-induced arthritis. *Arthritis and rheumatism.* Jul 2010;62(7):1899-1910.

33. Matsuda M, Park JG, Wang DC, Hunter S, Chien P, Schreiber AD. Abrogation of the Fc gamma receptor IIA-mediated phagocytic signal by stem-loop Syk antisense oligonucleotides. *Mol Biol Cell.* Jul 1996;7(7):1095-1106.

34. Stenton GR, Kim MK, Nohara O, et al. Aerosolized Syk antisense suppresses Syk expression, mediator release from macrophages, and pulmonary inflammation. *J Immunol.* Apr 1 2000;164(7):3790-3797.

35. Stenton GR, Ulanova M, Dery RE, et al. Inhibition of allergic inflammation in the airways using aerosolized antisense to Syk kinase. *J Immunol.* Jul 15 2002;169(2):1028-1036.

36. White PJ, Anastasopoulos F, Pouton CW, Boyd BJ. Overcoming biological barriers to in vivo efficacy of antisense oligonucleotides. *Expert Rev Mol Med.* 2009;11:e10.

37. Lu Y, Wang W, Mao H, et al. Antibody-mediated platelet phagocytosis by human macrophages is inhibited by siRNA specific for sequences in the SH2 tyrosine kinase, Syk. *Cell Immunol.* 2011;268(1):1-3.

38. Davidson BL, McCray PB, Jr. Current prospects for RNA interference-based therapies. *Nat Rev Genet.* May 2011;12(5):329-340.

39. Ozaki N, Suzuki S, Ishida M, et al. Syk-dependent signaling pathways in neutrophils and macrophages are indispensable in the pathogenesis of anti-collagen antibody-induced arthritis. *International immunology.* Sep 2012;24(9):539-550.

40. Wex E, Bouyssou T, Duechs MJ, et al. Induced Syk deletion leads to suppressed allergic responses but has no effect on neutrophil or monocyte migration in vivo. *European journal of immunology.* Nov 2011;41(11):3208-3218.

41. Schweighoffer E, Vanes L, Nys J, et al. The BAFF receptor transduces survival signals by co-opting the B cell receptor signaling pathway. *Immunity.* Mar 21 2013;38(3):475-488.

42. Ruzza P, Biondi B, Calderan A. Therapeutic prospect of Syk inhibitors. *Expert Opin Ther Pat.* Oct 2009;19(10):1361-1376.

43. Norman P. Spleen tyrosine kinase inhibitors: a review of the patent literature 2010 - 2013. *Expert opinion on therapeutic patents.* Feb 20 2014.

44. Yamamoto N, Takeshita K, Shichijo M, et al. The orally available spleen tyrosine kinase inhibitor 2-[7-(3,4-dimethoxyphenyl)-imidazo[1,2-c]pyrimidin-5-ylamino]nicotinamide dihydrochloride (BAY 61-3606) blocks antigen-induced airway inflammation in rodents. *J Pharmacol Exp Ther.* Sep 2003;306(3):1174-1181.

45. Lin YC, Huang DY, Chu CL, Lin WW. Anti-inflammatory actions of Syk inhibitors in macrophages involve non-specific inhibition of toll-like receptors-mediated JNK signaling pathway. *Mol Immunol.* Apr 2010;47(7-8):1569-1578.

46. Mazuc E, Villoutreix BO, Malbec O, et al. A novel druglike spleen tyrosine kinase binder prevents anaphylactic shock when administered orally. *J Allergy Clin Immunol.* Jul 2008;122(1):188-194, 194 e181-183.

47. Rossi AB, Herlaar E, Braselmann S, et al. Identification of the Syk kinase inhibitor R112 by a human mast cell screen. *J Allergy Clin Immunol.* Sep 2006;118(3):749-755.

48. Braselmann S, Taylor V, Zhao H, et al. R406, an orally available spleen tyrosine kinase inhibitor blocks fc receptor signaling and reduces immune complex-mediated inflammation. *The Journal of pharmacology and experimental therapeutics.* Dec 2006;319(3):998-1008.

49. Cha HS, Boyle DL, Inoue T, et al. A novel spleen tyrosine kinase inhibitor blocks c-Jun N-terminal kinase-mediated gene expression in synoviocytes. *J Pharmacol Exp Ther.* May 2006;317(2):571-578.

50. Buchner M, Fuchs S, Prinz G, et al. Spleen tyrosine kinase is overexpressed and represents a potential therapeutic target in chronic lymphocytic leukemia. *Cancer Res.* Jul 1 2009;69(13):5424-5432.

51. Chen L, Monti S, Juszczynski P, et al. SYK-dependent tonic B-cell receptor signaling is a rational treatment target in diffuse large B-cell lymphoma. *Blood.* Feb 15 2008;111(4):2230-2237.

52. Quiroga MP, Balakrishnan K, Kurtova AV, et al. B-cell antigen receptor signaling enhances chronic lymphocytic leukemia cell migration and survival: specific targeting with a novel spleen tyrosine kinase inhibitor, R406. *Blood.* Jul 30 2009;114(5):1029-1037.

53. Buchner M, Baer C, Prinz G, et al. Spleen tyrosine kinase inhibition prevents chemokine- and integrin-mediated stromal protective effects in chronic lymphocytic leukemia. *Blood.* Jun 3 2010;115(22):4497-4506.

54. Valera I, Fernandez N, Trinidad AG, et al. Costimulation of dectin-1 and DC-SIGN triggers the arachidonic acid cascade in human monocyte-derived dendritic cells. *J Immunol.* Apr 15 2008;180(8):5727-5736.

55. Matsubara S, Koya T, Takeda K, et al. Syk activation in dendritic cells is essential for airway hyperresponsiveness and inflammation. *Am J Respir Cell Mol Biol.* Apr 2006;34(4):426-433.

56. Colonna L, Catalano G, Chew C, et al. Therapeutic targeting of Syk in autoimmune diabetes. *Journal of immunology.* Aug 1 2010;185(3):1532-1543.

57. Sanderson MP, Gelling SJ, Rippmann JF, Schnapp A. Comparison of the anti-allergic activity of Syk inhibitors with optimized Syk siRNAs in FcepsilonRI-activated RBL-2H3 basophilic cells. *Cell Immunol.* 2010;262(1):28-34.

58. Krishnan S, Juang YT, Chowdhury B, et al. Differential expression and molecular associations of Syk in systemic lupus erythematosus T cells. *Journal of immunology.* Dec 1 2008;181(11):8145-8152.

59. Liossis SN, Ding XZ, Dennis GJ, Tsokos GC. Altered pattern of TCR/CD3-mediated protein-tyrosyl phosphorylation in T cells from patients with systemic lupus erythematosus. Deficient expression of the T cell receptor zeta chain. *The Journal of clinical investigation.* Apr 1 1998;101(7):1448-1457.

60. Enyedy EJ, Nambiar MP, Liossis SN, Dennis G, Kammer GM, Tsokos GC. Fc epsilon receptor type I gamma chain replaces the deficient T cell receptor zeta chain in T cells of patients with systemic lupus erythematosus. *Arthritis and rheumatism.* May 2001;44(5):1114-1121.

61. Pine PR, Bahjat R, Chang B, Taylor V, Markovstov V, Hitoshi Y. An orally bioavailable inhibitor of FLT3 and Syk kinases prevents tumor growth in subcutaneously implanted human tumor xenografts and promotes cell death of FLT3 mutant AML cells [abstract]. *Blood.* 2005;106:243.

62. Spalton JC, Mori J, Pollitt AY, Hughes CE, Eble JA, Watson SP. The novel Syk inhibitor R406 reveals mechanistic differences in the initiation of GPVI and CLEC-2 signaling in platelets. *J Thromb Haemost.* Jul 2009;7(7):1192-1199.

63. Suljagic M, Longo PG, Bennardo S, et al. The Syk inhibitor fostamatinib disodium (R788) inhibits tumor growth in the Emu- TCL1 transgenic mouse model of CLL by blocking antigen-dependent B-cell receptor signaling. *Blood.* Dec 2 2010;116(23):4894-4905.

64. Young RM, Hardy IR, Clarke RL, et al. Mouse models of non-Hodgkin lymphoma reveal Syk as an important therapeutic target. *Blood.* Mar 12 2009;113(11):2508-2516.

65. Podolanczuk A, Lazarus AH, Crow AR, Grossbard E, Bussel JB. Of mice and men: an open-label pilot study for treatment of immune thrombocytopenic purpura by an inhibitor of Syk. *Blood.* Apr 2 2009;113(14):3154-3160.

66. Matsubara S, Li G, Takeda K, et al. Inhibition of spleen tyrosine kinase prevents mast cell activation and airway hyperresponsiveness. *Am J Respir Crit Care Med.* Jan 1 2006;173(1):56-63.

67. Pine PR, Chang B, Schoettler N, et al. Inflammation and bone erosion are suppressed in models of rheumatoid arthritis following treatment with a novel Syk inhibitor. *Clinical immunology.* Sep 2007;124(3):244-257.

68. Bahjat FR, Pine PR, Reitsma A, et al. An orally bioavailable spleen tyrosine kinase inhibitor delays disease progression and prolongs survival in murine lupus. *Arthritis and rheumatism.* May 2008;58(5):1433-1444.

69. Deng GM, Liu L, Bahjat FR, Pine PR, Tsokos GC. Suppression of skin and kidney disease by inhibition of spleen tyrosine kinase in lupus-prone mice. *Arthritis and rheumatism.* Jul 2010;62(7):2086-2092.

70. Meltzer EO, Berkowitz RB, Grossbard EB. An intranasal Syk-kinase inhibitor (R112) improves the symptoms of seasonal allergic rhinitis in a park environment. *J Allergy Clin Immunol.* Apr 2005;115(4):791-796.

71. Grossbard E, Mant T, Jurcevic S, Sterba M. A multiple dose study of an orally bioavailable inhibitor of Syk-kinase (R406) in human volunteers: safety, pharmacokinetics, and pharmacodynamics [abstract]. *Arthritis Rheum.* 2005;52(9):S690.

72. Baluom M, Grossbard EB, Mant T, Lau DT. Pharmacokinetics of fostamatinib, a spleen tyrosine kinase (SYK) inhibitor, in healthy human subjects following single and multiple oral dosing in three phase I studies. *British journal of clinical pharmacology.* Jul 2013;76(1):78-88.

73. Weinblatt ME, Kavanaugh A, Burgos-Vargas R, et al. Treatment of rheumatoid arthritis with a Syk kinase inhibitor: a twelve-week, randomized, placebo-controlled trial. *Arthritis and rheumatism.* Nov 2008;58(11):3309-3318.

74. Weinblatt ME, Kavanaugh A, Genovese MC, Musser TK, Grossbard EB, Magilavy DB. An oral spleen tyrosine kinase (Syk) inhibitor for rheumatoid arthritis. *The New England journal of medicine.* Sep 30 2010;363(14):1303-1312.

75. Weinblatt ME, Kavanaugh A, Genovese MC, et al. Effects of fostamatinib (R788), an oral spleen tyrosine kinase inhibitor, on health-related quality of life in patients with active rheumatoid arthritis: analyses of patient-reported outcomes from a randomized, double-blind, placebo-controlled trial. *The Journal of rheumatology.* Apr 2013;40(4):369-378.

76. Genovese MC, Kavanaugh A, Weinblatt ME, et al. An oral syk kinase inhibitor in the treatment of rheumatoid arthritis: A 3 month randomized placebo controlled phase 2 study in patients with active RA who had failed biologic agents. *Arthritis Rheum.* Oct 27 2010.

77. Friedberg JW, Sharman J, Sweetenham J, et al. Inhibition of Syk with fostamatinib disodium has significant clinical activity in non-Hodgkin lymphoma and chronic lymphocytic leukemia. *Blood.* Apr 1 2010;115(13):2578-2585.

78. Park SR, Speranza G, Piekarz R, et al. A multi-histology trial of fostamatinib in patients with advanced colorectal, non-small cell lung, head and neck, thyroid, and renal cell carcinomas, and pheochromocytomas. *Cancer chemotherapy and pharmacology.* Apr 2013;71(4):981-990.

79. Sweeny DJ, Li W, Clough J, et al. Metabolism of fostamatinib, the oral methylene phosphate prodrug of the spleen tyrosine kinase inhibitor R406 in humans: contribution of hepatic and gut bacterial processes to the overall biotransformation. *Drug Metab Dispos.* Jul 2010;38(7):1166-1176.

80. Zhu Y, Herlaar E, Masuda ES, et al. Immunotoxicity assessment for the novel Spleen tyrosine kinase inhibitor R406. *Toxicology and applied pharmacology.* Jun 15 2007;221(3):268-277.

81. Skinner M, Philp K, Lengel D, et al. The Contribution of Vegf Signalling to Fostamatinib-Induced Blood Pressure Elevation. *British journal of pharmacology.* Dec 16 2013.

82. Clemens GR, Schroeder RE, Magness SH, et al. Developmental toxicity associated with receptor tyrosine kinase Ret inhibition in reproductive toxicity testing. *Birth Defects Res A Clin Mol Teratol.* Feb 2009;85(2):130-136.

83. Baluom M, Samara E, Grossbard EB, Lau DT. Fostamatinib, a syk-kinase inhibitor, does not affect methotrexate pharmacokinetics in patients with rheumatoid arthritis. *J Clin Pharmacol.* Sep 2011;51(9):1310-1318.

84. Montalvao F, Garcia Z, Celli S, et al. The mechanism of anti-CD20-mediated B cell depletion revealed by intravital imaging. *The Journal of clinical investigation.* Dec 2 2013;123(12):5098-5103.

85. Jennette JC, Falk RJ, Bacon PA, et al. 2012 revised International Chapel Hill Consensus Conference Nomenclature of Vasculitides. *Arthritis and rheumatism.* Jan 2013;65(1):1-11.

86. Jennette JC. Rapidly progressive crescentic glomerulonephritis. *Kidney international.* Mar 2003;63(3):1164-1177.

87. Stanton MC, Tange JD. Goodpasture's syndrome (pulmonary haemorrhage associated with glomerulonephritis). *Australas Ann Med.* May 1958;7(2):132-144.

88. Goodpasture EW. The significance of certain pulmonary lesions in relation to the etiology of influenza. *Am J Med Sci.* 1919;158:863-870.

89. Scheer R, Grossman M. Immune aspects of the glomerulonephritis associated with pulmonary haemorrhage. *Annals of internal medicine.* 1964;60(6):1009-1021.

90. Lerner RA, Glassock RJ, Dixon FJ. The role of anti-glomerular basement membrane antibody in the pathogenesis of human glomerulonephritis. *J Exp Med.* Dec 1 1967;126(6):989-1004.

91. McPhaul JJ, Jr., Dixon FJ. The presence of anti-glomerular basement membrane antibodies in peripheral blood. *Journal of immunology.* Dec 1969;103(6):1168-1175.

92. Wilson CB, Dixon FJ. Anti-glomerular basement membrane antibody-induced glomerulonephritis. *Kidney Int.* Feb 1973;3(2):74-89.

93. Pusey CD. Anti-glomerular basement membrane disease. *Kidney international.* Oct 2003;64(4):1535-1550.

94. Donaghy M, Rees AJ. Cigarette smoking and lung haemorrhage in glomerulonephritis caused by autoantibodies to glomerular basement membrane. *Lancet.* Dec 17 1983;2(8364):1390-1393.

95. Bombassei GJ, Kaplan AA. The association between hydrocarbon exposure and anti-glomerular basement membrane antibody-mediated disease (Goodpasture's syndrome). *American journal of industrial medicine.* 1992;21(2):141-153.

96. Klassen J, Elwood C, Grossberg AL, et al. Evolution of membranous nephropathy into anti-glomerular-basement-membrane glomerulonephritis. *The New England journal of medicine.* Jun 13 1974;290(24):1340-1344.

97. Weber MF, Andrassy K, Pullig O, Koderisch J, Netzer K. Antineutrophil-cytoplasmic antibodies and antiglomerular basement membrane antibodies in Goodpasture's

syndrome and in Wegener's granulomatosis. *Journal of the American Society of Nephrology : JASN.* Jan 1992;2(7):1227-1234.

98. Guerin V, Rabian C, Noel LH, et al. Anti-glomerular-basement-membrane disease after lithotripsy. *Lancet.* Apr 7 1990;335(8693):856-857.

99. Umekawa T, Kohri K, Iguchi M, Yoshioka K, Kurita T. Glomerular-basement-membrane antibody and extracorporeal shock wave lithotripsy. *Lancet.* Feb 27 1993;341(8844):556.

100. Xenocostas A, Jothy S, Collins B, Loertscher R, Levy M. Anti-glomerular basement membrane glomerulonephritis after extracorporeal shock wave lithotripsy. *American journal of kidney diseases : the official journal of the National Kidney Foundation.* Jan 1999;33(1):128-132.

101. Zhou XJ, Lv JC, Zhao MH, Zhang H. Advances in the genetics of anti-glomerular basement membrane disease. *Am J Nephrol.* 2010;32(5):482-490.

102. Fisher M, Pusey CD, Vaughan RW, Rees AJ. Susceptibility to anti-glomerular basement membrane disease is strongly associated with HLA-DRB1 genes. *Kidney Int.* Jan 1997;51(1):222-229.

103. Saus J, Wieslander J, Langeveld JP, Quinones S, Hudson BG. Identification of the Goodpasture antigen as the alpha 3(IV) chain of collagen IV. *J Biol Chem.* Sep 15 1988;263(26):13374-13380.

104. Pedchenko V, Bondar O, Fogo AB, et al. Molecular architecture of the Goodpasture autoantigen in anti-GBM nephritis. *N Engl J Med.* Jul 22 2010;363(4):343-354.

105. Turner N, Mason PJ, Brown R, et al. Molecular cloning of the human Goodpasture antigen demonstrates it to be the alpha 3 chain of type IV collagen. *J Clin Invest.* Feb 1992;89(2):592-601.

106. Cashman SJ, Pusey CD, Evans DJ. Extraglomerular distribution of immunoreactive Goodpasture antigen. *J Pathol.* May 1988;155(1):61-70.

107. Hudson BG, Reeders ST, Tryggvason K. Type IV collagen: structure, gene organization, and role in human diseases. Molecular basis of Goodpasture and Alport syndromes and diffuse leiomyomatosis. *J Biol Chem.* Dec 15 1993;268(35):26033-26036.

108. Hudson BG, Tryggvason K, Sundaramoorthy M, Neilson EG. Alport's syndrome, Goodpasture's syndrome, and type IV collagen. *N Engl J Med.* Jun 19 2003;348(25):2543-2556.

109. Netzer KO, Leinonen A, Boutaud A, et al. The goodpasture autoantigen. Mapping the major conformational epitope(s) of alpha3(IV) collagen to residues 17-31 and 127-141 of the NC1 domain. *J Biol Chem.* Apr 16 1999;274(16):11267-11274.

110. Zhao J, Yan Y, Cui Z, Yang R, Zhao MH. The immunoglobulin G subclass distribution of anti-GBM autoantibodies against rHalpha3(IV)NC1 is associated with disease severity. *Human immunology.* Jun 2009;70(6):425-429.

111. Segelmark M, Butkowski R, Wieslander J. Antigen restriction and IgG subclasses among anti-GBM autoantibodies. *Nephrology, dialysis, transplantation : official publication of the European Dialysis and Transplant Association - European Renal Association.* 1990;5(12):991-996.

112. Cui Z, Zhao MH. Avidity of anti-glomerular basement membrane autoantibodies was associated with disease severity. *Clinical immunology.* Jul 2005;116(1):77-82.

113. Savage CO, Pusey CD, Bowman C, Rees AJ, Lockwood CM. Antiglomerular basement membrane antibody mediated disease in the British Isles 1980-4. *British medical journal.* Feb 1 1986;292(6516):301-304.

114. Johnson JP, Moore J, Jr., Austin HA, 3rd, Balow JE, Antonovych TT, Wilson CB. Therapy of anti-glomerular basement membrane antibody disease: analysis of prognostic significance of clinical, pathologic and treatment factors. *Medicine (Baltimore).* Jul 1985;64(4):219-227.

115. Zhou XJ, Lv JC, Bu DF, et al. Copy number variation of FCGR3A rather than FCGR3B and FCGR2B is associated with susceptibility to anti-GBM disease. *International immunology.* Jan 2010;22(1):45-51.

116. Zhou XJ, Lv JC, Yu L, et al. FCGR2B gene polymorphism rather than FCGR2A, FCGR3A and FCGR3B is associated with anti-GBM disease in Chinese. *Nephrology, dialysis, transplantation : official publication of the European Dialysis and Transplant Association - European Renal Association.* Jan 2010;25(1):97-101.

117. Cui Z, Zhao MH, Segelmark M, Hellmark T. Natural autoantibodies to myeloperoxidase, proteinase 3, and the glomerular basement membrane are present in normal individuals. *Kidney Int.* Sep 2010;78(6):590-597.

118. Olson SW, Arbogast CB, Baker TP, et al. Asymptomatic autoantibodies associate with future anti-glomerular basement membrane disease. *J Am Soc Nephrol.* Oct 2011;22(10):1946-1952.

119. Derry CJ, Ross CN, Lombardi G, et al. Analysis of T cell responses to the autoantigen in Goodpasture's disease. *Clinical and experimental immunology.* May 1995;100(2):262-268.

120. Zou J, Hannier S, Cairns LS, et al. Healthy individuals have Goodpasture autoantigen-reactive T cells. *Journal of the American Society of Nephrology : JASN.* Feb 2008;19(2):396-404.

121. Salama AD, Chaudhry AN, Ryan JJ, et al. In Goodpasture's disease, CD4(+) T cells escape thymic deletion and are reactive with the autoantigen alpha3(IV)NC1. *Journal of the American Society of Nephrology : JASN.* Sep 2001;12(9):1908-1915.

122. Wong D, Phelps RG, Turner AN. The Goodpasture antigen is expressed in the human thymus. *Kidney international.* Nov 2001;60(5):1777-1783.

123. Zou J, Henderson L, Thomas V, Swan P, Turner AN, Phelps RG. Presentation of the Goodpasture autoantigen requires proteolytic unlocking steps that destroy prominent T cell epitopes. *J Am Soc Nephrol.* Mar 2007;18(3):771-779.

124. Salama AD, Chaudhry AN, Holthaus KA, et al. Regulation by CD25+ lymphocytes of autoantigen-specific T-cell responses in Goodpasture's (anti-GBM) disease. *Kidney Int.* Nov 2003;64(5):1685-1694.

125. Ang C, Savige J, Dawborn J, et al. Anti-glomerular basement membrane (GBM)-antibody-mediated disease with normal renal function. *Nephrology, dialysis, transplantation : official publication of the European Dialysis and Transplant Association - European Renal Association.* Apr 1998;13(4):935-939.

126. Salama AD, Dougan T, Levy JB, et al. Goodpasture's disease in the absence of circulating anti-glomerular basement membrane antibodies as detected by standard techniques. *American journal of kidney diseases : the official journal of the National Kidney Foundation.* Jun 2002;39(6):1162-1167.

127. Lockwood CM, Rees AJ, Pearson TA, Evans DJ, Peters DK, Wilson CB. Immunosuppression and plasma-exchange in the treatment of Goodpasture's syndrome. *Lancet.* Apr 3 1976;1(7962):711-715.

128. Levy JB, Turner AN, Rees AJ, Pusey CD. Long-term outcome of anti-glomerular basement membrane antibody disease treated with plasma exchange and immunosuppression. *Annals of internal medicine.* Jun 5 2001;134(11):1033-1042.

129. Lindemann W. Sur le mode d'action de certains poisons renaux. *Annales de l'Institut Pasteur.* 1900;14:49-60.

130. Tam FW, Smith J, Morel D, et al. Development of scarring and renal failure in a rat model of crescentic glomerulonephritis. *Nephrology, dialysis, transplantation : official publication of the European Dialysis and Transplant Association - European Renal Association.* Jul 1999;14(7):1658-1666.

131. Kitching AR, Holdsworth SR, Tipping PG. Crescentic glomerulonephritis--a manifestation of a nephritogenic Th1 response? *Histol Histopathol.* Jul 2000;15(3):993-1003.

132. Khan SB, Cook HT, Bhangal G, Smith J, Tam FW, Pusey CD. Antibody blockade of TNF-alpha reduces inflammation and scarring in experimental crescentic glomerulonephritis. *Kidney international.* May 2005;67(5):1812-1820.

133. Tam FW, Smith J, Karkar AM, Pusey CD, Rees AJ. Interleukin-4 ameliorates experimental glomerulonephritis and up-regulates glomerular gene expression of IL-1 decoy receptor. *Kidney Int.* Nov 1997;52(5):1224-1231.

134. Lai PC, Cook HT, Smith J, Keith JC, Jr., Pusey CD, Tam FW. Interleukin-11 attenuates nephrotoxic nephritis in Wistar Kyoto rats. *J Am Soc Nephrol.* Nov 2001;12(11):2310-2320.

135. Sheryanna A, Bhangal G, McDaid J, et al. Inhibition of p38 mitogen-activated protein kinase is effective in the treatment of experimental crescentic glomerulonephritis and suppresses monocyte chemoattractant protein-1 but not IL-1beta or IL-6. *Journal of the American Society of Nephrology : JASN.* Apr 2007;18(4):1167-1179.

136. Smith J, McDaid JP, Bhangal G, et al. A spleen tyrosine kinase inhibitor reduces the severity of established glomerulonephritis. *Journal of the American Society of Nephrology : JASN.* Feb 2010;21(2):231-236.

137. Tipping PG, Huang XR, Qi M, Van GY, Tang WW. Crescentic glomerulonephritis in CD4- and CD8-deficient mice. Requirement for CD4 but not CD8 cells. *Am J Pathol.* Jun 1998;152(6):1541-1548.

138. Li S, Holdsworth SR, Tipping PG. Antibody independent crescentic glomerulonephritis in mu chain deficient mice. *Kidney Int.* Mar 1997;51(3):672-678.

139. Ruth AJ, Kitching AR, Semple TJ, Tipping PG, Holdsworth SR. Intrinsic renal cell expression of CD40 directs Th1 effectors inducing experimental crescentic glomerulonephritis. *J Am Soc Nephrol.* Nov 2003;14(11):2813-2822.

140. Wolf D, Hochegger K, Wolf AM, et al. CD4+CD25+ regulatory T cells inhibit experimental anti-glomerular basement membrane glomerulonephritis in mice. *J Am Soc Nephrol.* May 2005;16(5):1360-1370.

141. Timoshanko JR, Holdsworth SR, Kitching AR, Tipping PG. IFN-gamma production by intrinsic renal cells and bone marrow-derived cells is required for full expression of crescentic glomerulonephritis in mice. *J Immunol.* Apr 15 2002;168(8):4135-4141.

142. Timoshanko JR, Sedgwick JD, Holdsworth SR, Tipping PG. Intrinsic renal cells are the major source of tumor necrosis factor contributing to renal injury in murine crescentic glomerulonephritis. *J Am Soc Nephrol.* Jul 2003;14(7):1785-1793.

143. Paust HJ, Turner JE, Steinmetz OM, et al. The IL-23/Th17 axis contributes to renal injury in experimental glomerulonephritis. *J Am Soc Nephrol.* May 2009;20(5):969-979.

144. Tarzi RM, Davies KA, Robson MG, et al. Nephrotoxic nephritis is mediated by Fcgamma receptors on circulating leukocytes and not intrinsic renal cells. *Kidney Int.* Dec 2002;62(6):2087-2096.

145. Tarzi RM, Davies KA, Claassens JW, Verbeek JS, Walport MJ, Cook HT. Both Fcgamma receptor I and Fcgamma receptor III mediate disease in accelerated nephrotoxic nephritis. *Am J Pathol.* May 2003;162(5):1677-1683.

146. Giorgini A, Brown HJ, Sacks SH, Robson MG. Toll-like receptor 4 stimulation triggers crescentic glomerulonephritis by multiple mechanisms including a direct effect on renal cells. *Am J Pathol.* Aug 2010;177(2):644-653.

147. Chavele KM, Martinez-Pomares L, Domin J, et al. Mannose receptor interacts with Fc receptors and is critical for the development of crescentic glomerulonephritis in mice. *J Clin Invest.* May 3 2010;120(5):1469-1478.

148. Steblay RW. Glomerulonephritis induced in sheep by injections of heterologous glomerular basement membrane and Freund's complete adjuvant. *J Exp Med.* Aug 1 1962;116:253-272.

149. Sado Y, Naito I, Okigaki T. Transfer of anti-glomerular basement membrane antibody-induced glomerulonephritis in inbred rats with isologous antibodies from the urine of nephritic rats. *J Pathol.* Aug 1989;158(4):325-332.

150. Reynolds J, Albouainain A, Duda MA, Evans DJ, Pusey CD. Strain susceptibility to active induction and passive transfer of experimental autoimmune glomerulonephritis in the rat. *Nephrol Dial Transplant.* Dec 2006;21(12):3398-3408.

151. Reynolds J, Sallie BA, Syrganis C, Pusey CD. The role of T-helper lymphocytes in priming for experimental autoimmune glomerulonephritis in the BN rat. *J Autoimmun.* Oct 1993;6(5):571-585.

152. Wu J, Hicks J, Borillo J, Glass WF, 2nd, Lou YH. CD4(+) T cells specific to a glomerular basement membrane antigen mediate glomerulonephritis. *J Clin Invest.* Feb 2002;109(4):517-524.

153. Reynolds J, Cashman SJ, Evans DJ, Pusey CD. Cyclosporin A in the prevention and treatment of experimental autoimmune glomerulonephritis in the brown Norway rat. *Clin Exp Immunol.* Jul 1991;85(1):28-32.

154. Reynolds J, Pusey CD. In vivo treatment with a monoclonal antibody to T helper cells in experimental autoimmune glomerulonephritis in the BN rat. *Clin Exp Immunol.* Jan 1994;95(1):122-127.

155. Reynolds J, Norgan VA, Bhambra U, Smith J, Cook HT, Pusey CD. Anti-CD8 monoclonal antibody therapy is effective in the prevention and treatment of experimental autoimmune glomerulonephritis. *J Am Soc Nephrol.* Feb 2002;13(2):359-369.

156. Reynolds J, Khan SB, Allen AR, Benjamin CD, Pusey CD. Blockade of the CD154-CD40 costimulatory pathway prevents the development of experimental autoimmune glomerulonephritis. *Kidney Int.* Oct 2004;66(4):1444-1452.

157. Reynolds J, Tam FW, Chandraker A, et al. CD28-B7 blockade prevents the development of experimental autoimmune glomerulonephritis. *J Clin Invest.* Mar 2000;105(5):643-651.

158. Reynolds J, Abbott DS, Karegli J, Evans DJ, Pusey CD. Mucosal tolerance induced by an immunodominant peptide from rat alpha3(IV)NC1 in established experimental autoimmune glomerulonephritis. *The American journal of pathology.* Jun 2009;174(6):2202-2210.

159. Kalluri R, Danoff TM, Okada H, Neilson EG. Susceptibility to anti-glomerular basement membrane disease and Goodpasture syndrome is linked to MHC class II genes and the emergence of T cell-mediated immunity in mice. *J Clin Invest.* Nov 1 1997;100(9):2263-2275.

160. Hopfer H, Maron R, Butzmann U, Helmchen U, Weiner HL, Kalluri R. The importance of cell-mediated immunity in the course and severity of autoimmune anti-glomerular basement membrane disease in mice. *FASEB J.* May 2003;17(8):860-868.

161. Nakamura A, Yuasa T, Ujike A, et al. Fcgamma receptor IIB-deficient mice develop Goodpasture's syndrome upon immunization with type IV collagen: a novel murine model for autoimmune glomerular basement membrane disease. *J Exp Med.* Mar 6 2000;191(5):899-906.

162. van der Woude FJ, Rasmussen N, Lobatto S, et al. Autoantibodies against neutrophils and monocytes: tool for diagnosis and marker of disease activity in Wegener's granulomatosis. *Lancet.* Feb 23 1985;1(8426):425-429.

163. Falk RJ, Jennette JC. Anti-neutrophil cytoplasmic autoantibodies with specificity for myeloperoxidase in patients with systemic vasculitis and idiopathic necrotizing and crescentic glomerulonephritis. *N Engl J Med.* Jun 23 1988;318(25):1651-1657.

164. Niles JL, McCluskey RT, Ahmad MF, Arnaout MA. Wegener's granulomatosis autoantigen is a novel neutrophil serine proteinase. *Blood.* Nov 1 1989;74(6):1888-1893.

165. Jennette JC, Hoidal JR, Falk RJ. Specificity of anti-neutrophil cytoplasmic autoantibodies for proteinase 3. *Blood.* Jun 1 1990;75(11):2263-2264.

166. Jennette JC, Falk RJ, Andrassy K, et al. Nomenclature of systemic vasculitides. Proposal of an international consensus conference. *Arthritis and rheumatism.* Feb 1994;37(2):187-192.

167. Hagen EC, Daha MR, Hermans J, et al. Diagnostic value of standardized assays for anti-neutrophil cytoplasmic antibodies in idiopathic systemic vasculitis. EC/BCR Project for ANCA Assay Standardization. *Kidney international.* Mar 1998;53(3):743-753.

168. Boomsma MM, Stegeman CA, van der Leij MJ, et al. Prediction of relapses in Wegener's granulomatosis by measurement of antineutrophil cytoplasmic antibody levels: a prospective study. *Arthritis and rheumatism.* Sep 2000;43(9):2025-2033.

169. Joshi L, Lightman SL, Salama AD, Shirodkar AL, Pusey CD, Taylor SR. Rituximab in refractory ophthalmic Wegener's granulomatosis: PR3 titers may predict relapse, but repeat treatment can be effective. *Ophthalmology.* Dec 2011;118(12):2498-2503.

170. Han WK, Choi HK, Roth RM, McCluskey RT, Niles JL. Serial ANCA titers: useful tool for prevention of relapses in ANCA-associated vasculitis. *Kidney international.* Mar 2003;63(3):1079-1085.

171. Jayne DR, Gaskin G, Pusey CD, Lockwood CM. ANCA and predicting relapse in systemic vasculitis. *QJM : monthly journal of the Association of Physicians.* Feb 1995;88(2):127-133.

172. Bansal PJ, Tobin MC. Neonatal microscopic polyangiitis secondary to transfer of maternal myeloperoxidase-antineutrophil cytoplasmic antibody resulting in neonatal pulmonary hemorrhage and renal involvement. *Annals of allergy, asthma & immunology : official publication of the American College of Allergy, Asthma, & Immunology.* Oct 2004;93(4):398-401.

173. Schlieben DJ, Korbet SM, Kimura RE, Schwartz MM, Lewis EJ. Pulmonary-renal syndrome in a newborn with placental transmission of ANCAs. *American journal of*

kidney diseases : the official journal of the National Kidney Foundation. Apr 2005;45(4):758-761.

174. Jayne DR, Gaskin G, Rasmussen N, et al. Randomized trial of plasma exchange or high-dosage methylprednisolone as adjunctive therapy for severe renal vasculitis. *Journal of the American Society of Nephrology : JASN.* Jul 2007;18(7):2180-2188.

175. Stone JH, Merkel PA, Spiera R, et al. Rituximab versus cyclophosphamide for ANCA-associated vasculitis. *The New England journal of medicine.* Jul 15 2010;363(3):221-232.

176. Jones RB, Tervaert JW, Hauser T, et al. Rituximab versus cyclophosphamide in ANCA-associated renal vasculitis. *The New England journal of medicine.* Jul 15 2010;363(3):211-220.

177. Lyons PA, Rayner TF, Trivedi S, et al. Genetically distinct subsets within ANCA-associated vasculitis. *The New England journal of medicine.* Jul 19 2012;367(3):214-223.

178. Ewert BH, Jennette JC, Falk RJ. Anti-myeloperoxidase antibodies stimulate neutrophils to damage human endothelial cells. *Kidney Int.* Feb 1992;41(2):375-383.

179. Savage CO, Pottinger BE, Gaskin G, Pusey CD, Pearson JD. Autoantibodies developing to myeloperoxidase and proteinase 3 in systemic vasculitis stimulate neutrophil cytotoxicity toward cultured endothelial cells. *Am J Pathol.* Aug 1992;141(2):335-342.

180. Radford DJ, Savage CO, Nash GB. Treatment of rolling neutrophils with antineutrophil cytoplasmic antibodies causes conversion to firm integrin-mediated adhesion. *Arthritis Rheum.* Jun 2000;43(6):1337-1345.

181. Radford DJ, Luu NT, Hewins P, Nash GB, Savage CO. Antineutrophil cytoplasmic antibodies stabilize adhesion and promote migration of flowing neutrophils on endothelial cells. *Arthritis Rheum.* Dec 2001;44(12):2851-2861.

182. Hewins P, Williams JM, Wakelam MJ, Savage CO. Activation of Syk in neutrophils by antineutrophil cytoplasm antibodies occurs via Fcgamma receptors and CD18. *Journal of the American Society of Nephrology : JASN.* Mar 2004;15(3):796-808.

183. Nagao T, Suzuki K, Utsunomiya K, et al. Direct activation of glomerular endothelial cells by anti-moesin activity of anti-myeloperoxidase antibody. *Nephrology, dialysis, transplantation : official publication of the European Dialysis and Transplant Association - European Renal Association.* Sep 2011;26(9):2752-2760.

184. Brinkmann V, Reichard U, Goosmann C, et al. Neutrophil extracellular traps kill bacteria. *Science.* Mar 5 2004;303(5663):1532-1535.

185. Fuchs TA, Abed U, Goosmann C, et al. Novel cell death program leads to neutrophil extracellular traps. *The Journal of cell biology.* Jan 15 2007;176(2):231-241.

186. Kessenbrock K, Krumbholz M, Schonermarck U, et al. Netting neutrophils in autoimmune small-vessel vasculitis. *Nature medicine.* Jun 2009;15(6):623-625.

187. Nakazawa D, Shida H, Tomaru U, et al. Enhanced Formation and Disordered Regulation of NETs in Myeloperoxidase-ANCA-Associated Microscopic Polyangiitis. *Journal of the American Society of Nephrology : JASN.* Jan 2 2014.

188. Rihova Z, Maixnerova D, Jancova E, et al. Silica and asbestos exposure in ANCA-associated vasculitis with pulmonary involvement. *Renal failure.* 2005;27(5):605-608.

189. Hogan SL, Cooper GS, Savitz DA, et al. Association of silica exposure with anti-neutrophil cytoplasmic autoantibody small-vessel vasculitis: a population-based, case-control study. *Clinical journal of the American Society of Nephrology : CJASN.* Mar 2007;2(2):290-299.

190. Csernok E, Lamprecht P, Gross WL. Clinical and immunological features of drug-induced and infection-induced proteinase 3-antineutrophil cytoplasmic antibodies and myeloperoxidase-antineutrophil cytoplasmic antibodies and vasculitis. *Current opinion in rheumatology.* Jan 2010;22(1):43-48.

191. Tervaert JW, Popa ER, Bos NA. The role of superantigens in vasculitis. *Current opinion in rheumatology.* Jan 1999;11(1):24-33.

192. Kain R, Matsui K, Exner M, et al. A novel class of autoantigens of anti-neutrophil cytoplasmic antibodies in necrotizing and crescentic glomerulonephritis: the lysosomal membrane glycoprotein h-lamp-2 in neutrophil granulocytes and a related membrane protein in glomerular endothelial cells. *The Journal of experimental medicine.* Feb 1 1995;181(2):585-597.

193. Kain R, Exner M, Brandes R, et al. Molecular mimicry in pauci-immune focal necrotizing glomerulonephritis. *Nature medicine.* Oct 2008;14(10):1088-1096.

194. Roth AJ, Brown MC, Smith RN, et al. Anti-LAMP-2 antibodies are not prevalent in patients with antineutrophil cytoplasmic autoantibody glomerulonephritis. *Journal of the American Society of Nephrology : JASN.* Mar 2012;23(3):545-555.

195. Kain R. L29. Relevance of anti-LAMP-2 in vasculitis: why the controversy. *Presse medicale.* Apr 2013;42(4 Pt 2):584-588.

196. Pendergraft WF, 3rd, Preston GA, Shah RR, et al. Autoimmunity is triggered by cPR-3(105-201), a protein complementary to human autoantigen proteinase-3. *Nature medicine.* Jan 2004;10(1):72-79.

197. Yang J, Bautz DJ, Lionaki S, et al. ANCA patients have T cells responsive to complementary PR-3 antigen. *Kidney international.* Nov 2008;74(9):1159-1169.

198. Stegeman CA, Tervaert JW, Sluiter WJ, Manson WL, de Jong PE, Kallenberg CG. Association of chronic nasal carriage of Staphylococcus aureus and higher relapse rates in Wegener granulomatosis. *Annals of internal medicine.* Jan 1 1994;120(1):12-17.

199. Stegeman CA, Tervaert JW, de Jong PE, Kallenberg CG. Trimethoprim-sulfamethoxazole (co-trimoxazole) for the prevention of relapses of Wegener's granulomatosis. Dutch Co-Trimoxazole Wegener Study Group. *The New England journal of medicine.* Jul 4 1996;335(1):16-20.

200. Zycinska K, Wardyn KA, Zielonka TM, Krupa R, Lukas W. Co-trimoxazole and prevention of relapses of PR3-ANCA positive vasculitis with pulmonary involvement. *European journal of medical research.* Dec 7 2009;14 Suppl 4:265-267.

201. Morgan MD, Day CJ, Piper KP, et al. Patients with Wegener's granulomatosis demonstrate a relative deficiency and functional impairment of T-regulatory cells. *Immunology.* May 2010;130(1):64-73.

202. Chavele KM, Shukla D, Keteepe-Arachi T, et al. Regulation of myeloperoxidase-specific T cell responses during disease remission in antineutrophil cytoplasmic antibody-associated vasculitis: the role of Treg cells and tryptophan degradation. *Arthritis and rheumatism.* May 2010;62(5):1539-1548.

203. Free ME, Bunch DO, McGregor JA, et al. Patients with antineutrophil cytoplasmic antibody-associated vasculitis have defective Treg cell function exacerbated by the presence of a suppression-resistant effector cell population. *Arthritis and rheumatism.* Jul 2013;65(7):1922-1933.

204. Nogueira E, Hamour S, Sawant D, et al. Serum IL-17 and IL-23 levels and autoantigen-specific Th17 cells are elevated in patients with ANCA-associated vasculitis. *Nephrology, dialysis, transplantation : official publication of the European Dialysis and Transplant Association - European Renal Association.* Jul 2010;25(7):2209-2217.

205. Bunch DO, McGregor JG, Khandoobhai NB, et al. Decreased CD5(+) B cells in active ANCA vasculitis and relapse after rituximab. *Clinical journal of the American Society of Nephrology : CJASN.* Mar 2013;8(3):382-391.

206. Todd SK, Pepper RJ, Draibe J, et al. Regulatory B cells are numerically but not functionally deficient in anti-neutrophil cytoplasm antibody-associated vasculitis. *Rheumatology.* Apr 11 2014.

207. Xiao H, Heeringa P, Hu P, et al. Antineutrophil cytoplasmic autoantibodies specific for myeloperoxidase cause glomerulonephritis and vasculitis in mice. *J Clin Invest.* Oct 2002;110(7):955-963.

208. Xiao H, Schreiber A, Heeringa P, Falk RJ, Jennette JC. Alternative complement pathway in the pathogenesis of disease mediated by anti-neutrophil cytoplasmic autoantibodies. *Am J Pathol.* Jan 2007;170(1):52-64.

209. Huugen D, Xiao H, van Esch A, et al. Aggravation of anti-myeloperoxidase antibody-induced glomerulonephritis by bacterial lipopolysaccharide: role of tumor necrosis factor-alpha. *Am J Pathol.* Jul 2005;167(1):47-58.

210. Xiao H, Heeringa P, Liu Z, et al. The role of neutrophils in the induction of glomerulonephritis by anti-myeloperoxidase antibodies. *Am J Pathol.* Jul 2005;167(1):39-45.

211. Schreiber A, Xiao H, Falk RJ, Jennette JC. Bone marrow-derived cells are sufficient and necessary targets to mediate glomerulonephritis and vasculitis induced by anti-myeloperoxidase antibodies. *J Am Soc Nephrol.* Dec 2006;17(12):3355-3364.

212. Little MA, Smyth CL, Yadav R, et al. Antineutrophil cytoplasm antibodies directed against myeloperoxidase augment leukocyte-microvascular interactions in vivo. *Blood.* Sep 15 2005;106(6):2050-2058.

213. Little MA, Smyth L, Salama AD, et al. Experimental autoimmune vasculitis: an animal model of anti-neutrophil cytoplasmic autoantibody-associated systemic vasculitis. *The American journal of pathology.* Apr 2009;174(4):1212-1220.

214. Little MA, Bhangal G, Smyth CL, et al. Therapeutic effect of anti-TNF-alpha antibodies in an experimental model of anti-neutrophil cytoplasm antibody-associated systemic vasculitis. *Journal of the American Society of Nephrology : JASN.* Jan 2006;17(1):160-169.

215. Pfister H, Ollert M, Frohlich LF, et al. Antineutrophil cytoplasmic autoantibodies against the murine homolog of proteinase 3 (Wegener autoantigen) are pathogenic in vivo. *Blood.* Sep 1 2004;104(5):1411-1418.

216. van der Geld YM, Hellmark T, Selga D, et al. Rats and mice immunised with chimeric human/mouse proteinase 3 produce autoantibodies to mouse Pr3 and rat granulocytes. *Annals of the rheumatic diseases.* Dec 2007;66(12):1679-1682.

217. Primo VC, Marusic S, Franklin CC, et al. Anti-PR3 immune responses induce segmental and necrotizing glomerulonephritis. *Clinical and experimental immunology.* Mar 2010;159(3):327-337.

218. Little MA, Al-Ani B, Ren S, et al. Anti-proteinase 3 anti-neutrophil cytoplasm autoantibodies recapitulate systemic vasculitis in mice with a humanized immune system. *PloS one.* 2012;7(1):e28626.

219. Hellmich B, Flossmann O, Gross WL, et al. EULAR recommendations for conducting clinical studies and/or clinical trials in systemic vasculitis: focus on anti-neutrophil cytoplasm antibody-associated vasculitis. *Annals of the rheumatic diseases.* May 2007;66(5):605-617.

220. Mukhtyar C, Guillevin L, Cid MC, et al. EULAR recommendations for the management of primary small and medium vessel vasculitis. *Annals of the rheumatic diseases.* Mar 2009;68(3):310-317.

221. Specks U, Merkel PA, Seo P, et al. Efficacy of remission-induction regimens for ANCA-associated vasculitis. *The New England journal of medicine.* Aug 1 2013;369(5):417-427.

222. Pendergraft WF, 3rd, Cortazar FB, Wenger J, et al. Long-term maintenance therapy using rituximab-induced continuous B-cell depletion in patients with ANCA vasculitis. *Clinical journal of the American Society of Nephrology : CJASN.* Apr 2014;9(4):736-744.

223. McAdoo SP, Pusey CD. Should Rituximab Be Used to Prevent Relapse in Patients with ANCA-Associated Vasculitis? *Clinical journal of the American Society of Nephrology : CJASN.* Mar 13 2014.

224. Little MA, Nightingale P, Verburgh CA, et al. Early mortality in systemic vasculitis: relative contribution of adverse events and active vasculitis. *Annals of the rheumatic diseases.* Jun 2010;69(6):1036-1043.

225. Ryan JJ, Reynolds J, Norgan VA, Pusey CD. Expression and characterization of recombinant rat alpha 3(IV)NC1 and its use in induction of experimental autoimmune glomerulonephritis. *Nephrol Dial Transplant*

Feb 2001;16(2):253-261.

226. Reynolds J, Moss J, Duda MA, et al. The evolution of crescentic nephritis and alveolar haemorrhage following induction of autoimmunity to glomerular basement membrane in an experimental model of Goodpasture's disease. *The Journal of pathology.* May 2003;200(1):118-129.

227. Davies J, Jimenez A. A new selective agent for eukaryotic cloning vectors. *The American journal of tropical medicine and hygiene.* Sep 1980;29(5 Suppl):1089-1092.

228. Krakower CA, Greenspon SA. Localization of the nephrotoxic antigen within the isolated renal glomerulus. *A.M.A. archives of pathology.* Jun 1951;51(6):629-639.

229. Tam FW, Smith J, Cashman SJ, Wang Y, Thompson EM, Rees AJ. Glomerular expression of interleukin-1 receptor antagonist and interleukin-1 beta genes in antibody-mediated glomerulonephritis. *The American journal of pathology.* Jul 1994;145(1):126-136.

230. Boltz-Nitulescu G, Wiltschke C, Holzinger C, et al. Differentiation of rat bone marrow cells into macrophages under the influence of mouse L929 cell supernatant. *Journal of leukocyte biology.* Jan 1987;41(1):83-91.

231. Hora K, Satriano JA, Santiago A, et al. Receptors for IgG complexes activate synthesis of monocyte chemoattractant peptide 1 and colony-stimulating factor 1. *Proceedings of the National Academy of Sciences of the United States of America.* Mar 1 1992;89(5):1745-1749.

232. Smith J, Lai PC, Behmoaras J, et al. Genes expressed by both mesangial cells and bone marrow-derived cells underlie genetic susceptibility to crescentic glomerulonephritis in the rat. *Journal of the American Society of Nephrology : JASN.* Jun 2007;18(6):1816-1823.

233. Mosmann T. Rapid colorimetric assay for cellular growth and survival: application to proliferation and cytotoxicity assays. *Journal of immunological methods.* Dec 16 1983;65(1-2):55-63.

234. D'Souza Z, McAdoo SP, Smith J, et al. Experimental crescentic glomerulonephritis: a new bicongenic rat model. *Disease models & mechanisms.* Nov 2013;6(6):1477-1486.

235. Lupher ML, Jr., Rao N, Lill NL, et al. Cbl-mediated negative regulation of the Syk tyrosine kinase. A critical role for Cbl phosphotyrosine-binding domain binding to Syk phosphotyrosine 323. *The Journal of biological chemistry.* Dec 25 1998;273(52):35273-35281.

236. Yankee TM, Keshvara LM, Sawasdikosol S, Harrison ML, Geahlen RL. Inhibition of signaling through the B cell antigen receptor by the protooncogene product, c-Cbl, requires Syk tyrosine 317 and the c-Cbl phosphotyrosine-binding domain. *Journal of immunology.* Dec 1 1999;163(11):5827-5835.

237. Sada K, Zhang J, Siraganian RP. Point mutation of a tyrosine in the linker region of Syk results in a gain of function. *Journal of immunology.* Jan 1 2000;164(1):338-344.

238. Pamuk ON, Lapchak PH, Rani P, Pine P, Dalle Lucca JJ, Tsokos GC. Spleen tyrosine kinase inhibition prevents tissue damage after ischemia-reperfusion. *American journal of physiology. Gastrointestinal and liver physiology.* Aug 2010;299(2):G391-399.

239. Ryan J, Ma FY, Kanellis J, Delgado M, Blease K, Nikolic-Paterson DJ. Spleen tyrosine kinase promotes acute neutrophil-mediated glomerular injury via activation of JNK and p38 MAPK in rat nephrotoxic serum nephritis. *Laboratory investigation; a journal of technical methods and pathology.* Dec 2011;91(12):1727-1738.

240. Lloyd CM, Minto AW, Dorf ME, et al. RANTES and monocyte chemoattractant protein-1 (MCP-1) play an important role in the inflammatory phase of crescentic nephritis, but only MCP-1 is involved in crescent formation and interstitial fibrosis. *The Journal of experimental medicine.* Apr 7 1997;185(7):1371-1380.

241. Kitching AR, Tipping PG, Holdsworth SR. IL-12 directs severe renal injury, crescent formation and Th1 responses in murine glomerulonephritis. *European journal of immunology.* Jan 1999;29(1):1-10.

242. Timoshanko JR, Kitching AR, Holdsworth SR, Tipping PG. Interleukin-12 from intrinsic cells is an effector of renal injury in crescentic glomerulonephritis. *Journal of the American Society of Nephrology : JASN.* Mar 2001;12(3):464-471.

243. Kim MJ, McDaid JP, McAdoo SP, et al. Spleen tyrosine kinase is important in the production of proinflammatory cytokines and cell proliferation in human mesangial cells following stimulation with IgA1 isolated from IgA nephropathy patients. *Journal of immunology.* Oct 1 2012;189(7):3751-3758.

244. Kim MJ, McDaid JP, McAdoo SP, et al. Spleen Tyrosine Kinase Is Important in the Production of Proinflammatory Cytokines and Cell Proliferation in Human Mesangial Cells following Stimulation with IgA1 Isolated from IgA Nephropathy Patients. *Journal of immunology.* Oct 1 2012;189(7):3751-3758.

245. Segelmark M, Wieslander J. IgG subclasses of antineutrophil cytoplasm autoantibodies (ANCA). *Nephrology, dialysis, transplantation : official publication of the European Dialysis and Transplant Association - European Renal Association.* 1993;8(8):696-702.

246. Roth AJ, Ooi JD, Hess JJ, et al. Epitope specificity determines pathogenicity and detectability in ANCA-associated vasculitis. *The Journal of clinical investigation.* Apr 1 2013;123(4):1773-1783.

247. Patry YC, Nachman PH, Audrain MA, Falk RJ, Meflah K, Esnault VL. Difference in antigenic determinant profiles between human and rat myeloperoxidase. *Clinical and experimental immunology.* Jun 2003;132(3):505-508.

248. Fischer EG, Lager DJ. Anti-glomerular basement membrane glomerulonephritis: a morphologic study of 80 cases. *American journal of clinical pathology.* Mar 2006;125(3):445-450.

249. Berden AE, Ferrario F, Hagen EC, et al. Histopathologic classification of ANCA-associated glomerulonephritis. *Journal of the American Society of Nephrology : JASN.* Oct 2010;21(10):1628-1636.

250. Weening JJ, D'Agati VD, Schwartz MM, et al. The classification of glomerulonephritis in systemic lupus erythematosus revisited. *Journal of the American Society of Nephrology : JASN.* Feb 2004;15(2):241-250.

251. Working Group of the International Ig ANN, the Renal Pathology S, Cattran DC, et al. The Oxford classification of IgA nephropathy: rationale, clinicopathological correlations, and classification. *Kidney international.* Sep 2009;76(5):534-545.

252. Working Group of the International Ig ANN, the Renal Pathology S, Roberts IS, et al. The Oxford classification of IgA nephropathy: pathology definitions, correlations, and reproducibility. *Kidney international.* Sep 2009;76(5):546-556.

253. Zhou F, Hu J, Ma H, Harrison ML, Geahlen RL. Nucleocytoplasmic trafficking of the Syk protein tyrosine kinase. *Molecular and cellular biology.* May 2006;26(9):3478-3491.

254. Holzer TR, Fulford AD, Arkins AM, et al. Ischemic time impacts biological integrity of phospho-proteins in PI3K/Akt, Erk/MAPK, and p38 MAPK signaling networks. *Anticancer research.* Jun 2011;31(6):2073-2081.

255. Grammatikos AP, Ghosh D, Devlin A, Kyttaris VC, Tsokos GC. Spleen tyrosine kinase (Syk) regulates systemic lupus erythematosus (SLE) T cell signaling. *PloS one.* 2013;8(8):e74550.

256. Mestas J, Hughes CC. Of mice and not men: differences between mouse and human immunology. *Journal of immunology.* Mar 1 2004;172(5):2731-2738.

257. Wegener's Granulomatosis Etanercept Trial Research G. Etanercept plus standard therapy for Wegener's granulomatosis. *The New England journal of medicine.* Jan 27 2005;352(4):351-361.

258. Booth A, Harper L, Hammad T, et al. Prospective study of TNFalpha blockade with infliximab in anti-neutrophil cytoplasmic antibody-associated systemic vasculitis. *Journal of the American Society of Nephrology : JASN.* Mar 2004;15(3):717-721.

259. Shay T, Jojic V, Zuk O, et al. Conservation and divergence in the transcriptional programs of the human and mouse immune systems. *Proceedings of the National Academy of Sciences of the United States of America.* Feb 19 2013;110(8):2946-2951.

260. Mayadas TN, Rosetti F, Ernandez T, Sethi S. Neutrophils: game changers in glomerulonephritis? *Trends in molecular medicine.* Aug 2010;16(8):368-378.

261. Holdsworth SR, Summers SA. Role of mast cells in progressive renal diseases. *Journal of the American Society of Nephrology : JASN.* Dec 2008;19(12):2254-2261.

262. Hochheiser K, Engel DR, Hammerich L, et al. Kidney Dendritic Cells Become Pathogenic during Crescentic Glomerulonephritis with Proteinuria. *Journal of the American Society of Nephrology : JASN.* Feb 2011;22(2):306-316.

263. Van Ziffle JA, Lowell CA. Neutrophil-specific deletion of Syk kinase results in reduced host defense to bacterial infection. *Blood.* Nov 26 2009;114(23):4871-4882.

264. Watson SP, Auger JM, McCarty OJ, Pearce AC. GPVI and integrin alphaIIb beta3 signaling in platelets. *J Thromb Haemost.* Aug 2005;3(8):1752-1762.

265. Watson SP, Herbert JM, Pollitt AY. GPVI and CLEC-2 in hemostasis and vascular integrity. *J Thromb Haemost.* Jul 2010;8(7):1456-1467.

266. Zou W, Kitaura H, Reeve J, et al. Syk, c-Src, the alphavbeta3 integrin, and ITAM immunoreceptors, in concert, regulate osteoclastic bone resorption. *J Cell Biol.* Mar 12 2007;176(6):877-888.

267. Yoshida K, Higuchi C, Nakura A, Yoshikawa H. Spleen tyrosine kinase suppresses osteoblastic differentiation through MAPK and PKCalpha. *Biochem Biophys Res Commun.* Jul 18 2011.

268. Coopman PJ, Mueller SC. The Syk tyrosine kinase: a new negative regulator in tumor growth and progression. *Cancer Lett.* Sep 28 2006;241(2):159-173.

269. Caldwell RG, Wilson JB, Anderson SJ, Longnecker R. Epstein-Barr virus LMP2A drives B cell development and survival in the absence of normal B cell receptor signals. *Immunity.* Sep 1998;9(3):405-411.

270. Hatton O, Lambert SL, Phillips LK, et al. Syk-induced phosphatidylinositol-3-kinase activation in Epstein-Barr virus posttransplant lymphoproliferative disorder. *American*

journal of transplantation : official journal of the American Society of Transplantation and the American Society of Transplant Surgeons. Apr 2013;13(4):883-890.

271. Drummond RA, Saijo S, Iwakura Y, Brown GD. The role of Syk/CARD9 coupled C-type lectins in antifungal immunity. *Eur J Immunol.* Feb 2011;41(2):276-281.

272. Gross O, Poeck H, Bscheider M, et al. Syk kinase signalling couples to the Nlrp3 inflammasome for anti-fungal host defence. *Nature.* May 21 2009;459(7245):433-436.

273. Deplano S, Cook HT, Russell R, et al. P2X7 receptor-mediated Nlrp3-inflammasome activation is a genetic determinant of macrophage-dependent crescentic glomerulonephritis. *Journal of leukocyte biology.* Jan 2013;93(1):127-134.